UNIVERSITÀ
DEGLI STUDI
DI PADOVA

University of Padua
Department of Biology

PhD COURSE IN BIOSCIENCES
CURRICULUM: BIOCHEMISTRY AND BIOTECHNOLOGY
SERIES XXXII

Mitochondrial localization of proteins and organelle membrane interactions: two key elements in neurodegeneration explored by new splitGFP tools

Coordinator: Ch.mo Prof. Ildikò Szabò

Supervisore: Ch.mo Prof. Marisa Brini

PhD Student: Cristina Catoni

"La Vita è un'esperienza meravigliosa"

Vanessa, 21.01.2019

Index

Summary

Mutations in the mitochondrial serine–threonine kinase PINK1 are associated with familial forms of Parkinson's disease and mitochondrial Ca^{2+} overload. The targeting of PKA to mitochondria and its activation rescue functional defects observed in PINK1 deficient neurons and mitochondrial Ca^{2+} overload due to the loss of PINK1 function. PINK1 and PKA have been proposed to cooperate at the mitochondria level to prevent neurodegeneration, and we have found that PINK1 was able to reduce mitochondrial Ca^{2+} accumulation. Sustained Ca^{2+} accumulation into the mitochondrial matrix has been shown to correlate with increases of cAMP levels in the same compartment. If the localization and the action of PKA at the OMM (OMM) are well recognized, its presence and, consequently, its role in the mitochondrial matrix and in the intramembrane space (IMS) is still amply debated.

In order to investigate that, we developed a probe based on the splitGFP system and Bimolecular Fluorescence Complementation (BiFC) to monitor PKA distribution at sub-mitochondrial level in living cells. The non-fluorescent GFP_{1-10} fragment was targeted to the OMM, the IMS and the mitochondrial matrix by the addition of targeting sequences. The β_{11} fragment, necessary to reconstitute GFP fluorescence, was fused to two PKA regulatory subunits (RIα and RIIβ) and to PKA catalytic subunit (CATα).

The co-transfection of the plasmids encoding the targeted GFP_{1-10} fragments and the β11-CATα or the β11-RIα or the β11-RIIβ in Hela cells revealed the presence of all these subunits at the OMM. Interestingly, strong GFP fluorescence emission in the presence of GFP_{1-10} fragment targeted to the IMS and mitochondrial matrix was observed in the case of β11-CATα co-expression, but not of β11-RIα and β11-RIIβ, suggesting the presence of PKA CAT-α in these compartments. Then, we evaluated the interference of regulatory subunits with mitochondrial CATα localization, co-transfecting the GFP_{1-10} fragment targeted to OMM, IMS and mitochondrial matrix with CATα and RIα or RIIβ. In these conditions we still observed fluorescence reconstitution at the OMM and IMS, but not in the mitochondrial matrix when CATα was co-expressed together with RIIβ. In the presence of co-expressed RIα subunit the green fluorescent signal was also detect in the mitochondrial matrix. Then, we analyzed the effect of CATα overexpression on mitochondrial Ca^{2+} transients, which are strongly decreased compared to the control. This reduction is almost abolished when CATα is co-expressed with RIIβ subunit, but not with RIα suggesting that the modulation of the effects of CATα on Ca^{2+} transients is dependent on the regulatory subunit in an isoform specific manner. Targeting CATα to the mitochondrial matrix (mtCATα), we have found

that the selective expression of mtCATα specifically reduced mitochondrial Ca^{2+} transients, suggesting the existence of mitochondrial targets for PKA action inside the mitochondria. All together these results reveal that CATα may translocate to this compartment only upon activation and release from RIIβ subunit.

In addition to the work on PKA, during my PhD program, I carried out another project based on a different application of the splitGFP tool. The communication between organelles is important to favour different pathways and its dysregulation are present in a number of different diseases, including neurodegenerative disease. In particular, this methodology was used to characterize the ER-plasma membrane (PM) contact sites.

The close contacts between the ER and the PM are required for the mechanism of store-operated Ca^{2+} entry (SOCE), a process induced as a consequence of the Ca^{2+} depletion of the ER store and dependent on the dynamic interaction between the ER resident protein stromal interaction molecule 1 that acts as Ca^{2+} sensor (STIM1) and Orai1, the protein forming the channel in the PM that permits Ca^{2+} entry from the extracellular ambient. To visualize the ER-PM junctions, we generated a YFP_{1-10} fragment targeted to the PM and β11 strand was targeted to the ER. We generated a construct where the PM-YFP_{1-10} and the ER_S-β11 or ER_L-β11 are cloned in the same bicistronic expression vector ($SPLICS_{S/L}$ ER-PM probes).

In a first set of experiments these SPLICS probes detected two types of interactions: long and short ER-PM interactions. Then, we investigated whether and how genetic and pharmacological manipulations could impact on ER-PM interface. We analysed the response of $SPLICS_{S/L}$ ER-PM probes to STIM1/Orai1 downregulation and ER Ca^{2+} depletion. To this purpose, STIM1/Orai1 proteins were silenced by ShRNA or ER Ca^{2+} depletion was induced by the incubation with 2,5-tert-butylhydroquinone (THBQ) or thapsigargin inhibitors of the sarcoplasmic/endoplasmic reticulum Ca2+-ATPase and with histamine. We have found that $SPLICS_S$ signal (monitoring ER-PM short interactions below 10 nm) decreased when we downregulated STIM1 or Orai1 proteins and strongly increased upon ER Ca^{2+} depletion. We have also detected the ER-PM long interactions under the same conditions and found that upon STIM1 or Orai1 downregulation the number of the long contacts decreased in respect with the control cells. All together, these data reveal that the SPLICS methodology is able to monitor short and long ranges ER-PM interactions and their changes upon pharmacological/genetic manipulations.

Introduction

1.1. Mitochondrial dysfunction in Neurodegenerative Disorders

Neurodegenerative diseases are a heterogenous group of disabling disorders of the central nervous system (CNS), characterized by the progressive and selective degeneration of neuronal subtypes. They share critical features such as the presence of misfolded and/or aggregated proteins, neuroinflammation, impairment of autophagy, oxidative stress and mitochondrial abnormalities (Figure 1). Mitochondria play a pivotal role in many functional processes of neurons, from bioenergetics to cell death. Neurons have high energy requirements to maintain important processes, such as membrane excitability, neurotransmission and plasticity and this characteristic makes them more prone to injury and death after mitochondrial dysfunction (Filosto et al., 2011). The characterisation of the involvement of mitochondrial dysfunction in pathogenesis of neurodegenerative disease, including Alzheimer's disease (AD), Parkinson's disease (PD), Huntington's disease (HD), and amyotrophic lateral sclerosis (ALS), is essential to define important hallmarks and eventually find potential novel therapeutic target for their treatments (Lin and Beal, 2006).

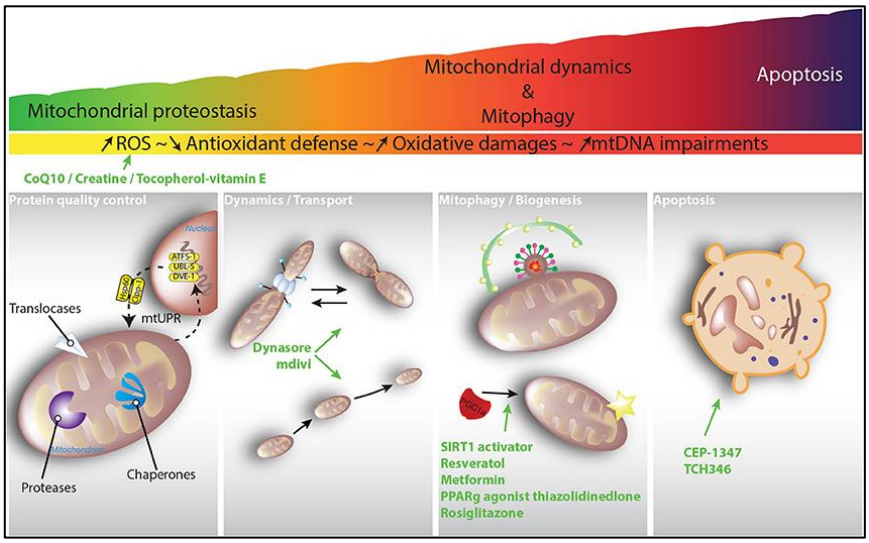

Figure 1 *Schematic representation of a hypothesized scenario responsible for mitochondrial dysfunction in neurodegeneration* (Sandra Franco-Iborra *et al.*, 2018).

Mitochondria are the "powerhouses of the cell": they are the site where the process of oxidative phosphorylation (OXPHOS) occurs and where the large majority of ATP amount necessary for cell function is produced. In addition to this, they are responsible for different metabolic pathways including the biosynthesis of amino acids and steroids, β-oxidation of fatty acids, and the regulation of cytosolic calcium homeostasis and for the release of proapoptotic factors. A myriad of factors can contribute to mitochondrial perturbations

ranging from defects in mitochondrial dynamics, in OXPHOS, in the protein quality control and in the degradation of misfolded and damaged proteins to excessive reactive oxygen species (ROS) production and calcium signalling. The post-mitotic nature of neurons, which does not permit their replacement, contributes to the accumulation of mitochondria damage that can lead to cell death (Abramov et al., 2017).

1.1.1. Mitochondrial Dynamics

Mitochondria have a double membrane system. The outer mitochondrial membrane (OMM) faces the cytosol, and the inner mitochondrial membrane (IMM) protrudes into the mitochondrial matrix and contains the respiratory complexes. The compartment delimited by the IMM and the OMM is referred as the intermembrane space (IMS).

Mitochondria undergo continuous dynamic processes that are in place to maintain their functionality. The structure and the distribution of mitochondria are maintained by two important and opposite pathways: mitochondrial fusion and fission, that represent the main quality control system of these organelles (Van der Bliek *et al.*, 2013). The importance of mitochondrial dynamics in the pathogenesis of neurodegenerative diseases has been increasingly revealed after the molecular identification of key proteins that act as regulators of the fusion and fission processed. In mammal fusion is mediated by the optic atrophy 1 (OPA1) protein and the mitofusins 1 and 2 (Mfn1 and Mfn2), which control the mitochondrial inner membrane and outer membrane fusion, respectively. Fission is facilitated by the mitochondrial fission 1 (Fis1) protein that acts as adaptor for the dynamin-related protein 1 (Drp1), a cytosolic protein with GTPase activity that is recruited at the mitochondrial outer membranes where forms oligomers and promote mitochondrial membrane constriction (QIN et al., 2018). It is now well recognized that ER was also required for the initial step of mitochondrial division. Indeed, oligomeric forms of Drp1 accumulate at ER-sites where the pre-constriction of the membrane has been initiated: high-resolution and 3D reconstructed images acquired using EM and tomography have shown that not only ER tubules make contact with mitochondria but they can also wrap around them leading to mitochondrial constriction (Friedman et al., 2011).

The balance between fusion and fission is important for mitochondrial length and distribution. Unbalance fusion or fission leads to mitochondrial elongation or to excessive mitochondrial fragmentation, respectively, and these changes in mitochondrial structure are linked with cell death and mitochondrial dysfunction (QIN et al., 2018). The clearance of defective organelles prevents the accumulation of damaged mitochondria.

Numerous studies revealed that mutations in proteins involved in familial forms of PD, such as α-synuclein, LRRK2, PINK1, Parkin and DJ-1, have been shown to affect mitochondrial dynamics by interfering with Drp1 expression and activity (Yang et al., 2008). For instance, pathogenic mutations or knockdown of Parkin lead to increased Drp1 levels and aberrant mitochondrial fission (Deng et al., 2008). Furthermore, LRRK2 protein regulates mitochondrial dynamics by increasing Drp1 (Wang et al., 2012). Kamp and co-workers have demonstrated that α-synuclein can induce mitochondrial fragmentation by directly binding to the OMM and inhibiting mitochondrial fusion. This inhibition is not due to the direct interaction of α-synuclein with proteins involved in mitochondrial fusion, but it is due to its property to interact with membrane phospholipids. α-synuclein-induced mitochondrial fragmentation can be rescued by the co-expression of PINK1, Parkin or DJ-1.

In addition to processes that guarantee mitochondrial network remodelling, mitochondria are highly dynamic since they can be actively transported to sites with high bioenergetics requirements. The trafficking of mitochondria to specific cellular locations is regulated by bidirectional (anterograde and retrograde) movements that involve microtubules for fast movement and actin filaments for slow movement via different motor-adaptor complexes (Frederick and Shaw, 2007). Moreover, mitochondria can be transported between different cell type upon cell damage: neurons can release damaged mitochondria and transfer them to astrocytes for degradation and astrocytes can release functional mitochondria to neurons (Hayakawa et al., 2016).

1.1.2. Mitochondrial OXPHOS

Several studies reported that dysfunctions of electron transport chain (ETC) complexes are implicated in neurodegenerative diseases. The ETC complexes consist of four multisubunit complexes (I-IV) and two electron carriers (coenzyme Q and cytochrome c) that transfer electrons and generate a proton gradient across the mitochondrial inner membrane, which in turn is used by the ATP synthase (complex V) to generate ATP. It has been demonstrated that the hyperphosphorylation of proteins, such as the microtubule-associated protein tau, β-amyloid and the presynaptic neuronal α-synuclein protein, whose mutations are related to neurodegenerative diseases, can promote their accumulation in misfolded or aggregated forms that failed to be degraded by the proteasome multiproteic complex for protein degradation and thus leads to an impairment of the mitochondrial respiratory chain complexes activity (Beal, 2005). The ETC complexes are main site in which the electrons are released and react with oxygen inducing ROS production and consequently oxidative

stress (Andreazza et al., 2010). For instance, the ROS production by complex II leads to deleterious or beneficial effects depending on the (patho)physiological condition: this ambivalent aspect can be explained by the diverse role of complex II on mitochondrial ROS production, which can be a producer or modulator of them depending on substrates and the activities of the other complexes and the Krebs cycle enzymes (Dröse, 2013). In healthy conditions, low concentration of ROS is involved in the regulation of processes, such immune response, inflammation, synaptic plasticity, learning and memory (Kishida & Klann, 2006). However, during aging or during mitochondrial damage, the excessive ROS production could lead to dangerous oxidative modifications of cell macromolecules and damage cell component, including mitochondrial structure (Rego and Oliveira, 2003). This imbalance could be further exacerbated by a reduction in the efficiency of antioxidant defences.

1.1.3. Misfolded/aggregated proteins in mitochondrial homeostasis

Mutations in α-synuclein, amyloid precursor, tau proteins are known to be a cause of self-protein aggregation and produce oligomers and fibrils that can generate extra- or intracellular deposits. These inclusions have been shown to affect mitochondrial dynamics (morphology and trafficking) and bioenergetics and interfere with the quality control pathways or promote mitochondria-dependent cell death (Figure 2).

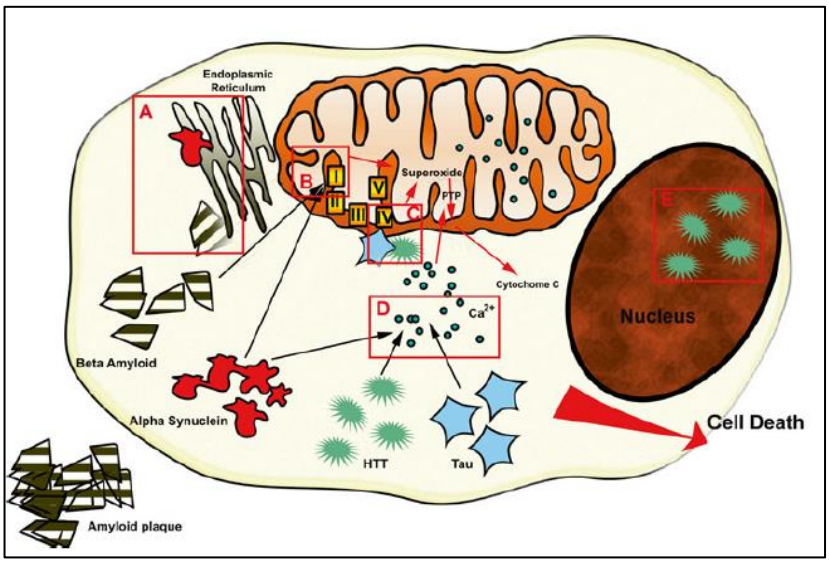

Figure 2 *Neurotoxic effects of alpha-synuclein, tau, β-amyloid* (Aβ), *and huntingtin proteins*. **A**) Both Aβ and α-Syn interact with the endoplasmic reticulum (ER) resulting in ER stress and altered mitochondria-associated membrane interaction. **B-C**) α-Syn (in PD), Huntingtin (Htt) (in HD) and Aβ (in AD) interact with complexes of the electron transport chain. **D**) Dysregulation of calcium homeostasis can be induced by protein inclusions. **E**) Htt can also interact with the nucleus itself (Marthe H. R. Ludtmann *et al.*, 2018).

Extracellular plaques of β-amyloid (Aβ) and intracellular tangles of tau proteins are the major hallmarks in AD brain and their accumulation has a direct consequence in mitochondrial functions: no direct link between Aβ and mitochondrial dysfunction was identified until 2004, when Lustbader and co-workers showed that Aβ localized to mitochondria and in the mitochondria of AD patients and transgenic mice induced toxicity upon binding to alcohol dehydrogenase (Lustbader et al., 2004). More recently, it has been suggested that Aβ is also generated intracellularly and that the contact sites between the OMM and the ER membrane are the site where enhanced Aβ production was observed. Considering that these sites are crucial for ER-mitochondrial Ca^{2+} transfer, as discussed later, the Aβ accumulation may be responsible for impaired Ca^{2+} handling and bioenergetics and represent one key step in the cascade of events eventually leading to neurodegeneration in AD (Schreiner et al., 2015).

It has been described that hyperphosphorylated and truncated forms of tau generate an impairment in mitochondrial trafficking (Amadoro et al., 2014). These pathological forms also generate an increase of mitochondrial length, a decrease in fission proteins expression and Drp1 mis-localization. Interestingly, tau phosphorylation has also been shown to increase ER-mitochondria contacts by promoting a close interaction between tau, DRP1, and ER. On the other hand, C-terminal caspase-cleaved tau form has been shown to induce mitochondrial fragmentation through the reduction of the Opa1 expression (Amadoro et al., 2014). Similarly that for Aβ, several studies have reported that a fraction of cytosolic α-synuclein, can be found associated with mitochondria, where it causes cytochrome c release, increase in mitochondrial Ca^{2+} and nitric oxide and oxidative damage (Parihar et al., 2008). Moreover, it has been observed that α-synuclein accumulation decreases complex I activity and increases ROS production in human foetal dopaminergic primary neuronal cultures. Overexpression of PD-related α-synuclein mutants accelerated these effects (Devi et al., 2008). Evidence that α-synuclein is directly involved on the modulation of Ca^{2+} signalling is obtained in the laboratory where I accrued out my PhD project and will be discussed in the *Paragraph 1.3*.

One key question, that was one of the aims of my studies, was whether these proteins, that are different for distribution and function, could interfere with mitochondrial functionality because they can localize at the mitochondrial level under specific conditions or upon their mutation. In particular, the question was to identify whether wildtype and mutant forms could differently distribute in the three different mitochondrial sub-compartments, i.e., the OMM, the IMS and the mitochondrial matrix.

1.2. Mitochondrial Ca^{2+} signalling

1.2.1. Role of mitochondrial Ca^{2+} signalling in the regulation of cell metabolism and survival

Over the past 60 years, it has clearly established the role of mitochondria in the regulation of cellular calcium ion (Ca^{2+}) homeostasis. Ca^{2+} is one of the most important second messenger in eukaryotic cells that translates information from extracellular and intracellular signals into an intracellular effect. Under resting condition, the cytosolic concentration, $[Ca^{2+}]_{Cyt}$, is very low, around 100-200 nM, however, due to the high step gradient between the extracellular ambient and the intracellular stores, it can rapidly increase to reach values in the low micromolar range. This increase relies on two main sources: the extracellular environment and the intracellular stores where the $[Ca^{2+}]$ reached values around 1-2 mM. The most important Ca^{2+} store in the cell is the ER, even if recent works demonstrated that also other organelles, such as Golgi apparatus, endosome and lysosome are able to contribute to Ca^{2+} release at significant amount (Hao et al., 2009).

Cells are endowed with different mechanisms to mobilize Ca^{2+} from the extracellular ambient and from the stores and these pathways are not mutually exclusive, but cells can to combine them. A well-known pathway is the activation of the plasma membrane-associated phospholipase C (PLC), that triggers to the production of inositol-1,4,5-trisphosphate (IP_3) and diacylglycerol (DAG) from membrane phospholipids. IP_3 interacts with the Ca^{2+} releasing channels of the ER and Golgi apparatus, causing their opening and the release of Ca^{2+} into the cytosol. Once Ca^{2+} has carried out its cell functions, the signal has to be rapidly turned off to avoid excessive and dangerous stimulation. The main mechanisms that are involved in maintaining low intracellular $[Ca^{2+}]$ are: the extrusion from the cytosol into the extracellular space, the compartmentalization into intracellular Ca^{2+} stores and the binding to buffering proteins (Berridge, 2009). In the cytosol different Ca^{2+} binding proteins are present, capable to shape the signal and to translate the increase of cytosolic $[Ca^{2+}]$ activating different biological processes. These proteins usually contain conserved EF-hands domains for Ca^{2+} binding and they act as buffering proteins, such as Parvalbumin, Calbindin and Calretinin, or as Ca^{2+} sensors, such as Calmodulin (CaM) (Hoeflich and Ikura, 2002). The distribution and the concentration of these Ca^{2+}-binding proteins are cell-type specific and it has been reported that the selective susceptibility to cell death of the specific neuronal population could be related to the low abundance of these proteins (Zallo et al., 2018).

In the generation and propagation of cytosolic Ca^{2+} signal is necessary to consider also the contribute of organelles, such as mitochondria. The ability of mitochondria to take up Ca^{2+} was firstly documented more than 50 years ago by two important papers that described for the first time the ability of energized mitochondria to accumulate large amount of Ca^{2} (DeLuca & Engstrom, 1961; Vasington & Murphy, 1962). It has to be remembered that mitochondria are endowed with two functionally and structurally different membranes: the OMM, essentially permeable to solutes and ions, and the IMM, characterized by invaginations called *cristae* which enclose the mitochondrial matrix, which is highly selective. The proton pumping by the respiratory chain complexes from the matrix to the IMS generates an electrochemical gradient ($\Delta\psi$) across the IMM, which is negative inside the matrix (-180 mV) and is utilized by the F1/F0 ATPase to convert the energy of NADH and $FADH_2$ into ATP. The proton electrochemical gradient generated by the respiratory chain is also the driving force that permits the uptake of Ca^{2+} into the mitochondrial matrix across the ions impermeable IMM. The Ca^{2+} transport is mediated by a high capacity but low affinity mechanism, the complex of the mitochondrial Ca^{2+} uniporter (MCU), whose activity was characterized in the 70s in isolated mitochondria, but the molecular identity remained unknown until 2010 (see below). Mitochondrial Ca^{2+} concentration does not reach the equilibrium inside the matrix, because of the existence of Ca^{2+} efflux mechanisms in the inner mitochondrial membrane, such the antiporters that exchange Ca^{2+} with Na^{+} or with H^{+} (see below) (De Stefani et al., 2016).

The first direct evidence that mitochondria can rapidly accumulate Ca^{2+} in intact cells were obtained in 1992 when the Ca^{2+} sensitive photoprotein aequorin was targeted to the mitochondrial matrix and employed to measure mitochondrial Ca^{2+} transients induced by cell stimulation (Rizzuto et al., 1992). The apparent divergence between the rapid accumulation of mitochondrial Ca^{2+} inside the matrix and the low Ca^{2+} affinity of the MCU was solved by the high $[Ca^{2+}]$ microdomains theory: mitochondria that are located close to the mouth of the ER release Ca^{2+} channels such as the inositol-1,4,5-trisphosphate-sensitive channels (IP_3R) (Rizzuto et al., 1993) and the ryanodine sensitive channels (RYRs) (Csordás et al., 2001) or the Ca^{2+} channels on the plasma membrane (PM), such as voltage-operated channels and store operated channels (Glitsch et al., 2002) are exposed to local microdomains where the Ca^{2+} concentration is higher than that measured in the bulk cytoplasm.

Mitochondrial Ca^{2+} uptake exerts a complex regulatory role: it is able to increase ATP production by activating three key enzymes of the Kreb's cycle, i.e., the pyruvate dehydrogenase (PDH), the isocitrate dehydrogenase (ICDH) and the α-ketoglutarate dehydrogenase (OGDH) (McCormack *et al.*, 1990). Activation of dehydrogenase results in stimulation of electron flow in the respiratory chain and in increase of ATP production, consequently.

Instead to sustain metabolism, when the mitochondrial Ca^{2+} accumulation become excessive the mitochondrial Ca^{2+} overload triggers apoptosis through the opening of the high-conductance permeability transition pore (PTP) (Rasola and Bernardi, 2011). The voltage dependent anion channel VDAC, a beta barrel porin present on the OMM, has been reported to contribute to selectively transfer apoptotic Ca^{2+} signal to mitochondria, through a physical interaction with IP_3R via Grp75 that is enhanced by apoptotic stimuli (De Stefani et al., 2012). PTP opening permits the release of cytochrome c and caspase activation that leads to apoptosis (Giorgi et al., 2012).

A different cell death pathway, i.e. necrosis pathway, can be also dependent from mitochondria since when the ATP depletion causes an impairment of the ATP-dependent Ca^{2+} transporters, such as PMCA and SERCA and indirectly the Na^+/Ca^{2+} exchanger, the cytosolic $[Ca^{2+}]$ increase and, consequently, also the mitochondrial Ca^{2+} accumulation was enhanced leading to the swelling of mitochondria, and the necrosis of the cell (Pivovarova and Andrews, 2010).

Since mitochondrial Ca^{2+} signalling can greatly influence cell functions and survival, it is evident that it must finely regulated. As mentioned, the coordinated action of different pathways for mitochondrial Ca^{2+} uptake and efflux is in place to guarantee the maintenance of mitochondrial Ca^{2+} homeostasis (see the next paragraph).

1.2.2. Molecular components of Ca^{2+} uptake and release of mitochondria

The regulation of mitochondrial Ca^{2+} transport is controlled by channels and exchangers located in the outer and inner mitochondrial membrane (Figure 3). In recent years, the identification of the molecular machinery regulating mitochondrial Ca^{2+} fluxes has been important to understand physiological and pathological conditions that rely on mitochondrial Ca^{2+} homeostasis.

1.2.2.1. Mitochondrial Ca^{2+} entry

To reach the mitochondrial matrix, cytosolic Ca^{2+} has to cross the OMM and IMM. The first barrier, the OMM, is highly permeable to ions (Ca^{2+}), nucleotides (ADP and/or ATP) and

other metabolites up to 5 kDa (e.g. acetylcholine, dopamine glutamate and ATP), and this permeability is guaranteed by the abundant expression of the voltage-dependent anion-selective channel proteins (VDACs). They represent the first molecular interface between mitochondria and Ca^{2+} stores (ER and/or SR and the extracellular space). There are three known isoforms of VDACs (VDAC1, VDAC2 and VDAC3), which are expressed ubiquitously, and each of them has a molecular mass of about 30 KDa. VDACs can assume different structural conformations and the transition between open and close states occurs in a voltage-dependent manner (Hodge and Colombini, 1997). The states differ in their ability to pass non-electrolytes and to conduct ions: a membrane potential higher than 25 mV promotes lower conductance and the assumed conformations become impermeable to ATP and ADP, but still allow the flow of small cations, including Ca^{2+}. Recent studies have highlighted the key role of VDACs in facilitating Ca^{2+} entry into the IMS and its accumulation inside the matrix. The Ca^{2+} transport from ER to mitochondria shows the involvement of supra-molecular complexes including the IP_3R, the sigma 1 receptor (Sig1R, a reticular chaperone), binding immunoglobulin protein (BiP), the ER HSP70 chaperone and glucose-regulated protein 75 (GRP75). IP_3 activates the IP_3R in the ER to release Ca^{2+} that is directly transferred to the IMS via VDAC1.

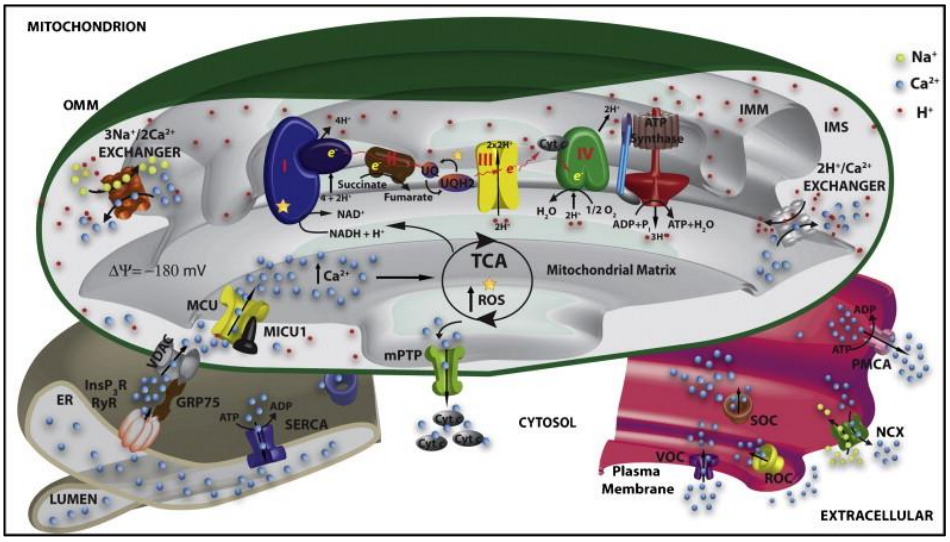

Figure 3 The main components that regulate mitochondrial Ca^{2+} transport. (Calì *et al.*, 2012)

After reaching the IMS, Ca^{2+} ions pass the IMM mainly through the mitochondrial Ca^{2+} uniporter (MCU) complex. It has been well established that the uniporter exists in a macromolecular complex composed by the MCU (De Stefani et al. 2011; Baughman et al. 2011), its paralog MCUb (Raffaello et al., 2013) and the regulators MICU1 (Perocchi et al., 2010), MICU2 and MICU3 (Plovanich et al., 2013) (Figure 4). The pore forming subunit is

composed by MCU and MCUb dominant negative isoform, an additional protein, EMRE, is necessary to structurally assemble the channel but it is not a pore forming subunit (Mammucari et al., 2016).

MCU is a 40 kDa protein that presents two transmembrane domains (TMDs) critical for Ca^{2+} transport, two coiled-coil domains and a short loop of acidic residues between the two TMDs. Overexpression of MCU increases the rate of mitochondrial Ca^{2+} influx in both intact and permeabilized cells, causing a significant decrease in cytosolic [Ca^{2+}] transients in intact cells (De Stefani et al., 2011). MCUb is a 33 kDa protein that shares 50% similarity to MCU.

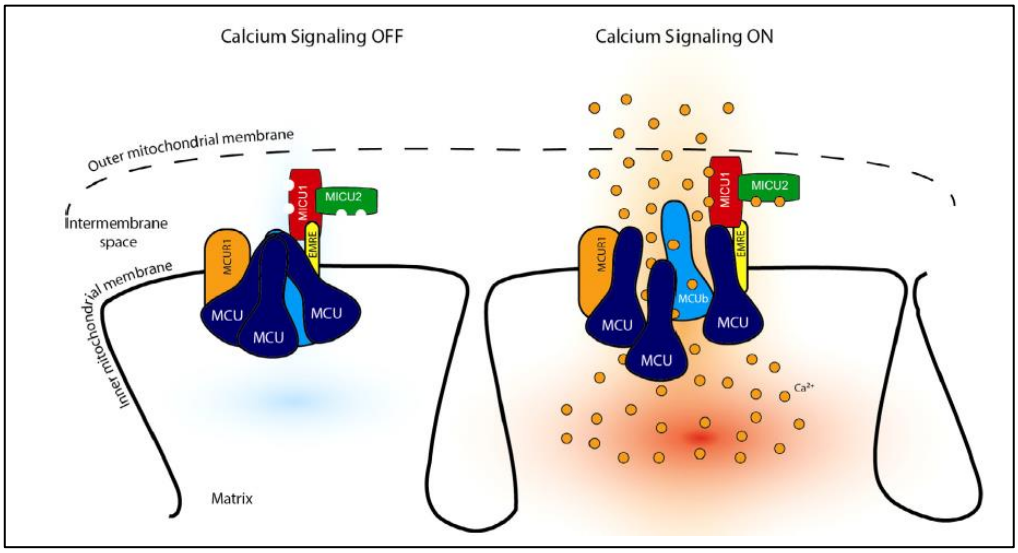

Figure 4 Schematic representation of MCU complex. (De Stefani and Rizzuto, 2014)

MCUb is able to form hetero-oligomers with MCU and strongly affects the Ca^{2+} entry through the channel: MCUb overexpression induces a significant decrease in mitochondrial Ca^{2+} uptake, while its silencing increases the mitochondrial Ca^{2+} entry (Raffaello et al., 2013), suggesting that MCUb acts as an endogenous dominant-negative subunit of the MCU pore. It has been demonstrated that the MCU complex is a highly selective and low affinity Ca^{2+} channel: the opening of MCU is modulated by extra-mitochondrial Ca^{2+} and by the MICU protein family, that includes three isoforms named MICU1, MICU2 and MICU3, containing the two EF-hand domains (Patron et al., 2014). While MICU1 and MICU2 are expressed ubiquitously, MICU3 appears to be mostly present in the brain, suggesting a tissue-specific function of this isoform. MICU1 (and also MICU2 and MICU3) is a soluble protein that interacts with MCU and is generally recognized to be in the IMS (Csordás et al., 2013). At low cytosolic [Ca^{2+}] (<500 nM), the inhibitory role of MICU2 keeps the channel closed, ensuring minimal Ca^{2+} transfer despite in presence of a huge driving force for its accumulation inside the matrix. The increase of cytosolic [Ca^{2+}] causes conformational

changes of the MICU1-MICU2 dimer, releasing MICU2-dependent inhibition of the channel and thus triggering the activation of MCU by MICU1 to favour extensive Ca^{2+} entry, aerobic metabolism and increasing ATP production (Patron et al., 2014). Recently, it has been proposed a model in which the conserved acidic residues in the matrix-localized carboxyl tail of EMRE sense matrix [Ca^{2+}] and, together with MICU1 and MICU2, ensure the inhibition of uniporter activity under normal conditions (Vais et al., 2016). However, the role of EMRE in the regulation of MCU channel activity is more debated: purified MCU is sufficient to give rise to Ca^{2+} currents in a planar lipid bilayer (De Stefani et al., 2011).

1.2.2.2. Mitochondrial Ca^{2+} efflux.

When Ca^{2+} has carried out its functions in the mitochondria, it is necessary to rapidly extrude it to restablish the resting balance into mitochondria. Ca^{2+} efflux from mitochondrial matrix is finely regulated by two systems: the mitochondrial Na^+/Ca^{2+} exchanger (mNCX) and the mitochondrial H^+/Ca^{2+} exchanger (mHCX) (Bernardi 1999). The transport stoichiometry of mNCX is defined as electrogenic with three Na^+ for one Ca^{2+} (Dash and Beard, 2008), while the exchange ratio of mHCX is electroneutral (two H^+ for one Ca^{2+})(Gunter et al., 1991). In 2010 the mNCX function was assigned to NCLX, an isoform of a plasma membrane NCX (Palty et al., 2010), which localizes to mitochondria and mediates not only Ca^{2+} exchange with Na^+, but also Li^+-dependent Ca^{2+} transport. Moreover, it has been observed that NCLX is inhibited by the selective and classical inhibitor of mitochondrial Na^+/Ca^{2+} exchanger, benzothiazepine CGP-37157, and its loss in multiple cell types alters mitochondrial Ca^{2+} efflux (Luongo et al., 2017). New structural information of NCLX shed light into the mechanism and stoichiometry of Na^+/Ca^{2+} exchanger superfamily: NCLX is an IMM protein containing 13 transmembrane domains with four ion-binding sites, three for Na^+ and one for Ca^{2+} within the translocation region.

Finally, it has also been suggested that the mitochondrial permeability transition pore (mPTP) might represent an alternative Ca^{2+} efflux pathway. This hypothesis has been questioned because inhibition of the PTP component cyclophilin D (CYPD) by cyclosporin A has little or no effect on mitochondrial Ca^{2+} uptake in living cells. Nevertheless, waves of membrane depolarization, which are signals for PTP opening, cause the release of Ca^{2+} from mitochondria. More recently, it has been provided further evidence for a role of PTP in Ca^{2+} efflux: cyclophilin D-deficient mice display high $[Ca^{2+}]_{mt}$ in heart (Elrod et al., 2010). In addition, oxidative stress in cyclophilin D-deficient neurons causes a smaller Ca^{2+} release from mitochondria than in wild-type cells (Barsukova et al., 2011)

1.3. Mitochondrial Ca^{2+} signalling in the pathogenesis of Parkinson's Disease

1.3.1. Parkinson's Disease (PD)

1.3.1.1. General overview

Dysregulation of Ca^{2+} handling has been found both in aging and neurodegeneration (Pchitskaya et al., 2018), in particular its involvement in the pathogenesis of PD has been proposed by several groups (Calì et al., 2014; Surmeier et al., 2017).

PD is the second most common neurodegenerative disease in the world (after Alzheimer's disease). It is a debilitating disease characterized by motor symptoms, such as progressive bradykinesia, resting tremor, movement impairment and postural rigidity occurring at a later stage. Non-motor symptoms can be present, including autonomic dysfunction, pain, fatigue, sleep disorders and cognitive and psychiatric disturbances, and they also have a significant impact on the patient's quality of life. The pathological hallmarks of PD are the progressive loss of dopaminergic neurons of *Substantia nigra pars compacta* (SNc) and the presence of cytoplasmic aggregates within the survived neurons. These inclusions are called Lewy bodies (LBs) and are mainly enriched in α-synuclein that aggregates into soluble oligomers and protofibers that become insoluble (Spillantini et al., 1997). In addition to α-synuclein, they also include a number of proteins, such as ubiquitin, parkin, heat shock proteins, cytoskeletal proteins, oxidized proteins, proteasomal and lysosomal components (Xia, 2008). Mitochondrial dysfunction, abnormal protein clearance and neuroinflammation are additional common elements associated with PD, but whether they are the cause, or the consequence of neurodegeneration is still unclear.

PD is a multifactorial disorder whose aetiology is associated to many risk factors, including aging and both genetic and environmental factors. Aging represents the major risk factor and since the average life expectancy is increasing, the incidence of PD will rise significantly in the next future. It has been estimated that about the 3-5% of the population over the 85 years has developed PD. Evidence suggests that a high risk of PD is associated with the exposure to mitochondrial toxins: in the eighties the MPP^+ (1-methyl-4-phenylpyridinium) metabolite of 1-methyl-4-phenyl-1,2,3,6-tetrahydropyridine (MPTP) was first discovered to cause parkinsonism with nigrostriatal degeneration in drug addicted people (Langston et al., 1983). The MPP^+ has been proven to work as mitochondrial complex I inhibitor and, later on, other substances such Paraquat, a herbicide structurally similar to MPP^+ and rotenone (a pesticide) were shown to induce loss of dopaminergic neurons in animal model of PD (Betarbet et al.,

2000). Heavy metal exposure (iron, copper, aluminium and zinc) has also been suggested to represent a risk for developing PD.

Even if the 95% of PD cases have a sporadic origin , there is a number of cases that have hereditary nature (10-15%), among which about 5% display Mendelian inheritance (Domingo and Klein, 2018). The "*PARK*" acronym following by a number increasing according to the order of identification has been assigned to the genes found to be associated to Young-Onset PD (YOPD): the mutations in *PARK* genes may have both autosomal dominant and autosomal recessive inheritance. Familial autosomal dominant PD are linked to mutations in the genes encoding α -synuclein, leucine-rich repeat kinase 2 (LRRK2) and VPS35 proteins (Bogaerts et al., 2008). Three other proteins whose mutations are linked to autosomal recessive parkinsonism are Parkin, PINK1 and DJ-1 (Farrer, 2006). Since sporadic and familial forms of PD share clinical, pathological and biochemical features, cellular and animal models harbouring gene mutations associated to PD have been widely investigated and have revealed that the function of many proteins encoded by the mutated genes are clearly related to the maintenance of mitochondrial homeostasis. One example is the involvement of PINK1 and Parkin in the process that regulates the clearance of dysfunctional mitochondria, called mitophagy: loss-of-function mutations of these genes impair mitochondrial quality control (Pickrell and Youle, 2015). Moreover, it is well characterized that α-synuclein also interfere with mitochondrial functions: it has been observed that prefibrillar α-synuclein oligomers decrease the mitochondrial Ca^{2+} uptake, alter membrane potential and electron flow through complex I leading to an enhanced cytochrome c release (Luth et al., 2014) (for more details see below).

1.3.1.2. Selective vulnerability of *Substantia nigra pars compacta*: the "Ca^{2+} hypothesis".

As mentioned, multiple factors are involved in the mechanisms of neuronal loss in PD and mitochondria seem to play an important key role for both familial and sporadic forms of PD. In the last decades, it has been strongly emerged the importance of Ca^{2+} ions in the regionally selective nature of neuronal loss in PD pathogenesis. Unlike Na^+ and K^+ ions, which have 10-30-fold differences in ion concentration on two sides of PM, Ca^{2+} ions have a 20,000-fold lower concentration in the cytoplasm compared to extracellular space (Surmeier and Schumacker, 2013). These gradients allow neurons to use Ca^{2+} as a potent intracellular signal to temporarily or permanent change physiological functions. In polarized neurons Ca^{2+} signalling affects all aspect of neuronal cell biology and for this reason this ion must be tightly regulated to avoid uncontrolled responses, which could lead to pathological condition

and cell death. A study from Surmeier's laboratory showed that dopaminergic neurons in the SNc exhibit autonomous rhythmic pacemaking activity that exposes them to continual Ca^{2+} influx. This action is essential to maintain regular release of dopamine (DA) to the striatum (Chan et al., 2007). The release of DA is important for voluntary movement and it is strictly linked to Ca^{2+}.

The electrical activity of dopaminergic neurons relies on several different types of voltage- and ligand-gated ion channels, permeable to Na^+, K^+, Cl^- and Ca^{2+}. In particular, L-type voltage-gate Ca^{2+} channels of the Ca_V1 family, i.e. $Ca_V1.2$ and $Ca_V1.3$, are present in dopaminergic neurons and their opening is responsible for the pacemaking activity also in the absence of synaptic stimuli. The increased susceptibility of dopaminergic neurons of SNc in respect with other neuronal types is associated to the expression of these specific Cav1 channels and is supported by the fact that the dopaminergic neurons of ventral tegmental area, which do not express the Cav1.3 channels, are less susceptible to cell death (Hurley et al., 2013). The importance of these channels in PD pathogenesis has been also underline by experiments where cultured neurons were pre-treated with Isradipine, a dihydropyridine blocker of the L-type voltage-gated Ca^{2+} channel, and then exposed to α-synuclein pre-formed fibrils (PFF) or to MPP^+ (Chan et al., 2007). In addition to the activity of these channels that exposes dopaminergic neurons to a constant Ca^{2+} influx, their low level of Ca^{2+} buffering proteins, such as calbindins and parvalbumin (Damier et al., 1999), further exacerbate the exposure to Ca^{2+} overload. As demonstrated by Surmeier and co-workers, the elevated Ca^{2+} load in dopaminergic neurons of SNc leads to the accumulation of Ca^{2+} in the mitochondria and the generation of oxidant stress which was specific to vulnerable SNc dopaminergic neurons. The oxidant stress engaged defences that induced transient, mild mitochondrial depolarization or uncoupling. The presence of mutations in PD-associated genes or the exposure to environmental factors may exacerbate this stress, which compromises mitochondrial functions (James Surmeier et al., 2012).

1.3.2. Parkinson's Disease-related proteins and mitochondrial Ca^{2+} signalling

Despite of α-synuclein, LRRK2, DJ-1, PINK1 and Parkin proteins have different function in the cell, their mutations have been reported to compromise mitochondrial function and Ca^{2+} handling, but the molecular mechanisms are not completely elucidated (Figure 5).

Under physiological conditions α-synuclein plays an important role in synaptic vesicle release interacting with members of SNARE family (Burré et al., 2010). It is 140 amino acids in length and a helically folded tetramer. In pathological condition, such us PD, it

adopts a β-sheet-rich amyloid-like structure that is prone to aggregate, and form oligomers and fibrils and intracellular deposits called Lewy bodies. This progressive accumulation of the protein has been proposed to lead neuronal toxicity by different mechanisms (Lashuel et al., 2002), among which some of them suggest the interference of α-synuclein with Ca^{2+} homeostasis (Duda et al., 2016). The presence of fibrillar α-synuclein aggregates has been shown to increase plasma membrane permeability to Ca^{2+}. One possible mechanism proposed is the formation of permeabilizing pores (Schmidt et al., 2012), enhanced by pathogenic point mutations of α-synuclein protein, A53T and A30P. Indeed mutant α-synuclein has been reported to have a higher tendency to form protofibrils and to associate with cellular membranes than the wild type (Furukawa et al., 2006). Other reports have revealed that α-synuclein can be secreted into the extracellular space and alter membrane fluidity, or that it can increase Ca^{2+} entry by modulating the activity of the voltage-gated or other types of Ca^{2+} influx channels of the PM. Application of voltage-operated Ca^{2+} channel blockers or Ca^{2+} chelators abolishes α-synuclein-mediated toxicity (Emmanouilidou et al., 2010). It has also been shown that α-synuclein causes a redistribution of $Ca_V2.2$ channels from lipid rafts to cholesterol-poor domains, changing the activity of Ca^{2+} channels via the reorganization of membrane microdomains (Ronzitti et al., 2014). Work from our laboratory has shown that α-synuclein is able to enhance ER- mitochondrial Ca^{2+} transfer by favouring ER-mitochondria tethering (for more details see *Chapter* 5) (Calì et al., 2012a). Later, it has been shown that α-synuclein can be found in the mitochondrial associate ER membranes fraction (MAM) and that PD-related mutations lead to a reduction in this association by increasing mitochondrial fragmentation and autophagy (Guardia-Laguarta et al., 2014).

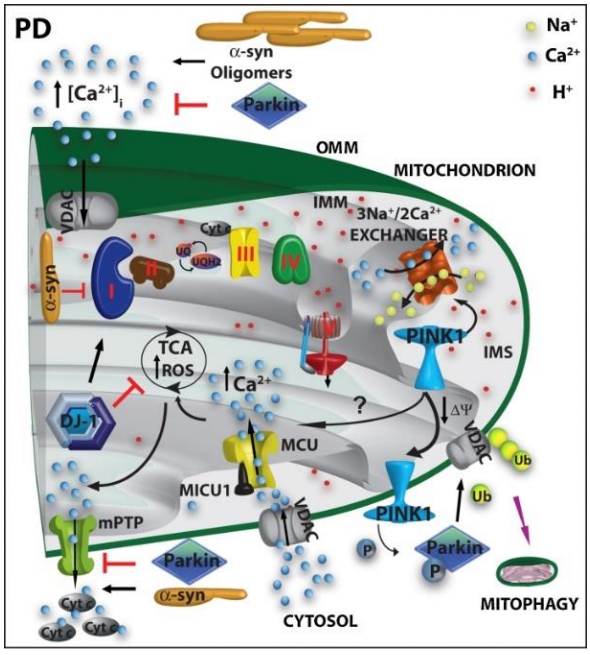

Figure 5 PD-related proteins and mitochondrial Ca^{2+} impairment. (Calì et al., 2012)

Moreover, It has been shown that the interaction of post-translationally modified α-synuclein with TOM20, a translocase of the outer mitochondrial membrane, impairs mitochondrial proteins import and this may explain the defects in oxidative phosphorylation proteins observed both in vitro and in post-mortem brains of PD patients (Di Maio et al., 2016).

Another PD-related protein whose function has been associated to mitochondrial Ca^{2+} handling is DJ-1. DJ-1 is a multifunctional protein and its main function is exerted in the protection against oxidative stress. It is localized in the cytosol and nucleus, but during oxidative stress it has been observed its translocation to the OMM in order to maintain health mitochondria (Junn et al., 2009). It is also involved in the regulation of mitochondria dynamics, even though the precise molecular mechanism under its protective function is still unknown. Several mutations in the DJ-1 gene are associated with autosomal recessive early-onset parkinsonism (van der Merwe et al., 2015). Recently, it has been observed that DJ-1 overexpression increased mitochondrial Ca^{2+} uptake, while reduced levels of DJ-1 caused mitochondrial fragmentation and decreased mitochondrial Ca^{2+} uptake. Moreover, in overexpressing DJ-1 cells an increase in contact sites between ER and mitochondria, that favours the Ca^{2+} transfer between these two organelles, was detected (Ottolini et al., 2013).

It is well established that PINK1 plays important neuroprotective roles against mitochondrial dysfunctions by phosphorylating and recruiting Parkin to facilitate the elimination of damaged mitochondria via autophagy-lysosomal pathway, named mitophagy (Pickrell and Youle, 2015). More details about this pathway will be discussed in the following paragraph (*Paragraph* 1.4). PINK1 loss of function has been associated to mitochondrial Ca^{2+} overload, which renders dopaminergic neurons particularly vulnerable to injury (Gandhi et al., 2009a; Marongiu et al., 2009). Important observation indicates that blocking MCU-dependent mitochondrial Ca^{2+} influx with ruthenium red completely restores the alterations in mitochondrial structure and neurite outgrowth observed in neuroblastoma cells co-expressing both mutant PINK1 and α-synuclein (Marongiu et al, 2009). However, a different interpretation has been done by others to explain mitochondrial Ca^{2+} impairment: mitochondrial Ca^{2+} overload observed in PINK1 KO MEF cells and in PINK1-silenced neuroblastoma cells is due to a defect in mitochondrial Ca^{2+} efflux by NCLX (Gandhi et al., 2009a; Kostic et al., 2015). Recently, it has also been shown that PINK1-dependent phosphorylation of LETM1, an inner mitochondrial membrane K^+/H^+ exchanger (Huang et al., 2017) which may act as a mitochondrial Ca^{2+}/H^+ antiporter, was able to control

mitochondrial Ca^{2+} handling, as well as, that inhibition of mitochondrial Ca^{2+} uniporter rescues dopaminergic neuronal cell loss in PINK1 KO zebrafish (Soman et al., 2017).

As for the involvement of Parkin in the control of Ca^{2+} homeostasis our laboratory has importantly contributed showing that, similarly to α-synuclein and DJ-1, also parkin overexpression was able to modulate ER-mitochondria tethering enhancing them and thus sustaining ER-mitochondria Ca2+ transfer and ATP production (Calì et al., 2013). In addition to this it has also been shown that Parkin exerts an important role in the regulation of the MCU complex component MICU1, thus directly acting in the control of the mitochondrial Ca^{2+} uptake machinery (Matteucci et al., 2018)

1.4. PINK1 and PKA: Are they two neuroprotective (mitochondrial) kinases?

1.4.1. PTEN-induced putative kinase (PINK1): structure, processing and function

Mutations in the mitochondrial serine-threonine kinase PINK1 are associated with autosomal recessive forms of PD (Valente et al., 2004). The PINK1 gene encodes a 581 amino acids protein ubiquitously expressed at high levels in the brain, heart, testis and skeletal muscle (d'Amora et al., 2011). The protein is composed by an N-terminal mitochondrial targeting sequence (MTS) of 98 amino acids, 21 amino acids long alpha-helix transmembrane domain (TM), a highly conserved serine/threonine kinase domain of 357 amino acids and C-terminal autoregulatory region of 69 amino acids. Its kinase activity is regulated by autophosphorylation on three residues (Ser228, Thr257, and Ser402) in the kinase domain (Aerts et al., 2015). So far, more than 70 missense mutations, mostly localized in the kinase domain, have been described in autosomal recessive familial PD patients (Bonifati, 2014).

Under basal conditions, PINK1 is imported into healthy mitochondria through the translocase complexes of the OMM (TOM20, TOM22, TOM70) and the IMM (TIM23). Positive charged MTS is recognized by TOM20 cooperating with TOM22 and delivers PINK1 into the TOM40 channel and transferred to the translocase TIM23 complex in the IMM. This translocation is energetically driven by mitochondrial membrane potential ($\Delta\Psi m$). Once in the mitochondrial matrix, the N-terminal MTS was cleaved by the mitochondrial protein peptidase MPP giving origin to the mature full-length form of PINK1. The full-length PINK1 (PINK1-FL,63 kDa) is inserted into the IMM with the transmembrane domain and undergoes to further cleavage by the presenilin-associated rhomboid-like protease (PARL protease), which removes the first 111 N-terminal amino acids. This PINK1 cleaved isoform of 52 kDa is released into the cytosol (Greene et al., 2012), where could be either stabilized through the interaction with molecular chaperones or degraded by the N-end rule pathway through the Ub/proteasome system. This complex processing of the endogenous PINK1 is essential to maintain PINK1 protein at very low levels in cells with healthy mitochondria (Yamano and Youle, 2013). As mentioned above, the import of PINK1 into mitochondria requires mitochondrial membrane potential, indeed when proton gradient is inhibited by incubation with uncoupler agents, such us CCCP (Carbonyl cyanide m-chlorophenyl hydrazine) (Narendra et al., 2010a), depolarized

mitochondria fail to process PINK1 that accumulates at the OMM. At the OMM PINK1-FL undergoes dimerization and auto-phosphorylation, a step that is required for the activation of its kinase activity (Okatsu et al., 2012). Upon activation, through a process that requires ubiquitin protein phosphorylation, PINK1 recruits the E3 ubiquitin ligase Parkin at the OMM which in turn ubiquitinates OMM resident proteins and activate the selective elimination of damaged mitochondria through the mitophagy process (see paragraph 1.4.1.2; Narendra, Jin, et al., 2010). A selective accumulation of PINK1-FL at the OMM is also observed following misfolded protein accumulation in the mitochondrial matrix, treatment with OXPHOS inhibitors and PD-related toxins (Jin and Youle, 2013). How PINK1 is stabilized on damage mitochondria is still not clear: on one side, it has been proposed that it depends on the inactivation of IMM proteases due to the dissipation of membrane potential (Jin et al., 2010); on the other, it has been reported that in depolarized mitochondria, endogenous PINK1 was stacked in a 700 kDa complex with the TOM complex and failed to be imported in the IMM (Lazarou et al., 2012). The TOM complex is considered to provide a location for the activation of PINK1 kinase activity by facilitating the correct orientation of dimeric PINK1 to allow auto-phosphorylation (Okatsu et al., 2013). If it is recognized that PINK1 plays important neuroprotective roles against mitochondrial dysfunction, the role of PINK1/parkin pathway in healthy mitochondria is far to be elucidated. Recently, the possibility that they may act independently from each other in regulating mitochondrial function starts to emerge as a novel concept (Voigt et al., 2016).

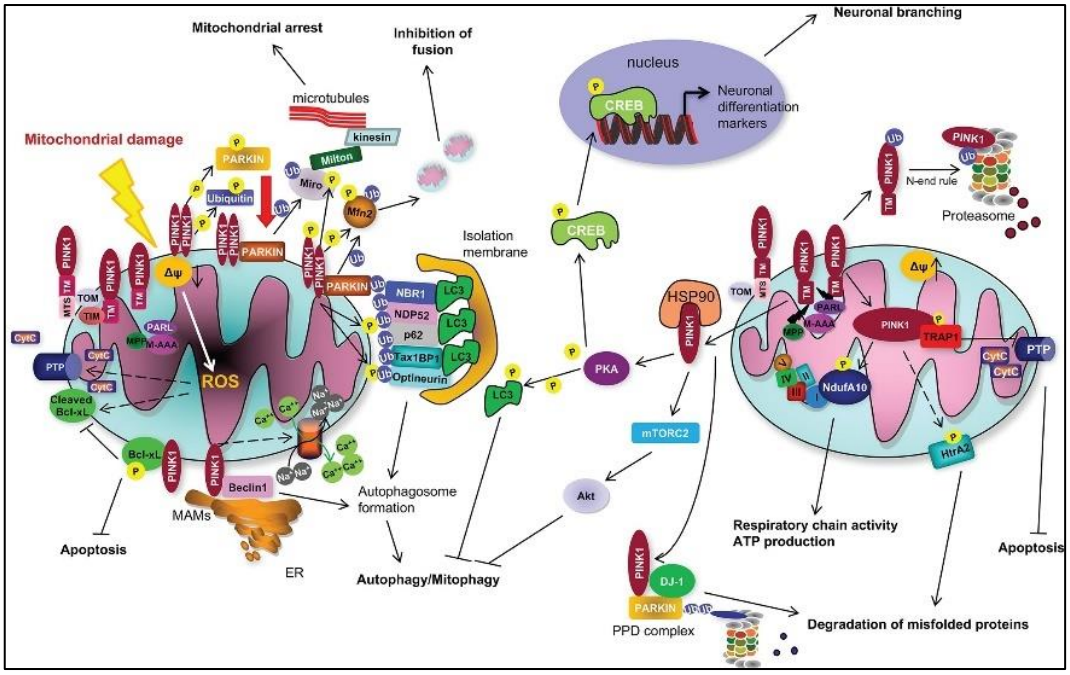

Figure 6 Schematic pathways in which PINK1 protein is involved (Arena and Valente, 2016).

Considering the sophisticated mechanism for PINK1 processing in mitochondria, it is tempting to hypothesize that relevant mitochondrial targets could exist and that PINK1 action is not limited to mitophagy (Figure 6). In this respect emerging evidence is appearing in the literature and are discussed in the next paragraph.

1.4.1.1. PINK1 functions outside and inside mitochondria.

Cytosolic PINK1-FL. As mentioned before, a pool of cleaved PINK1 is exported into the cytosol and degraded in a proteasome-dependent manner or stabilized with molecular chaperones. In the cytoplasm PINK1 was shown to activate mTORC2/Akt pathway, which is known to be involved in neuronal survival: mTORC2 phosphorylation by PINK1 leads to activation of Akt protein, crucial for the protection of neuronal cells from various cytotoxic agents (Murata et al., 2011). Interestingly, it has been observed that the overexpression of a PINK1 form lacking its MTS was able to enhance neurites and dendrites lengths in mouse cortical neurons by a mechanism that stimulated mitochondria anterograde transport from the soma to periphery and that required the activity of another kinase, the protein kinase A (PKA). Indeed, in the presence of pharmacological inhibitor of PKA protein, PINK1-mediated dendritic branching is abolished thus suggesting functional interaction between PINK1 and PKA in neuronal differentiation and neurites maintenance (Dagda et al., 2014). It has also been reported that in the cytosol, PINK1, by forming a complex with parkin and DJ-1 (PPD complex), participates to the ubiquitination and proteasomal degradation of misfolded/damaged proteins (Xiong et al., 2009).

Intramitochondrial PINK1. The possible action of PINK1 inside the mitochondria has been suggested by the pioneering observation that PINK1-depleted cells showed impaired electron transport chain activity, reduced oxygen consumption and increased ROS amount as well as increased sensitivity to complex I inhibitors with respect to their wt counterpart (Morais et al., 2009). Later on, it has been shown that in healthy cells, the IMM processed PINK1 is able to sustain respiratory chain activity and ATP production by phosphorylating the NADH dehydrogenase ubiquinone 1 alpha subunit 10 (NdufA10) of complex I of the respiratory chain (Morais et al., 2014) and, in *Dropsophila*, it is also able to regulate OMM targeting (and translation) of nuclear mRNAs encoding respiratory chain components (among which the complex I subunits C-I 30 and ND75) via TOM complex translocase (Gehrke et al., 2015).

Two additional intramitochondrial targets for PINK1 kinase activity have been described: the mitochondrial chaperone TRAP1 and the serine protease HtrA2, both involved in stress resistance mechanisms. PINK1-mediated phosphorylation of TRAP1 protects against oxidative stress-induced apoptosis and the ability of PINK1 to promote cell survival is impaired by the presence of PD-linked mutations in its kinase domain (Pridgeon et al., 2007). Phosphorylation of HtrA2 and activation of its proteolytic activity increase protection against mitochondrial stress by removing damaged mitochondrial proteins: reduced levels of phospho-HtrA2 were observed in the brains of PINK1-mutated PD patients (Moisoi et al., 2009).

PINK1-FL in the OMM. As mentioned before, PINK1 plays an important role in the elimination of damaged mitochondria. This process is of particular relevance for cell function since the network of healthy mitochondria undergoes to continuous process of fission and fusion and damaged mitochondria need to be excluded from these dynamics to keep only healthy organelles in the network (Twig et al., 2008). The participation of PINK1 in the process of the mitochondrial quality control requires Parkin, a cytosolic E3-ubiquitin ligase whose mutations are also linked to autosomal recessive form of familial PD (Kitada et al., 1998).

1.4.1.2. PINK1 and mitochondrial quality control.

Increases in mitochondrial DNA mutations, ROS production and misfolded proteins accumulation represent a common event during ageing and are associated to neurodegeneration. All of them cause a reduction in $\Delta\Psi_m$, leading to the accumulation of PINK1-FL at the OMM. Seminal genetic studies on PINK1 loss of function *Drosophila melanogaster* mutants have established that PINK1 and Parkin work in the same pathway: PINK1 knockout phenotype is rescued by overexpression of Parkin, but PINK1 overexpression is not able to rescue the Parkin-knockout phenotype, demonstrating that PINK1 acts upstream of Parkin (Clark et al., 2006). In 2010 Youle and co-workers reported that the recruitment of Parkin to impaired mitochondria required PINK1 expression and its kinase activity (Narendra et al., 2010b). In the last 10 years, our knowledge on the mechanisms and the molecular targets of PINK1/Parkin cooperative activity has impressively increased (Figure 7). The TOM complex guarantees the correct positioning of dimeric PINK1 which become actives upon auto-phosphorylation on Ser228 residue. Activated PINK1 phosphorylates ubiquitin tethered to OMM proteins, and phosphorylated

ubiquitin triggers the recruitment of parkin from the cytosol to mitochondria and its activation by inducing conformational changes (Bayne and Trempe, 2019).

PINK1 also phosphorylates Parkin ubiquitin-like domain stabilizing it in an active state (Shiba-Fukushima et al., 2012). Parkin acts as an enhancer of this signaling through ubiquitination of several mitochondrial proteins (Mfn2, VDAC, Miro etc.) that in turn recruit autophagy receptors to initiate autophagosome formation (Lazarou et al., 2015). The ubiquitinated mitochondrial substrates are in turn also phosphorylated by PINK1, creating a positive feedback amplification cycle on damaged mitochondria (Yamano et al., 2016). Most of the poly-ubiquitinated proteins can be extracted from the membrane and degraded by the proteasome system (Tanaka et al., 2010), the others associate to the ubiquitin-binding domain of autophagy receptors and lead to the formation of the autophagosomes than undergo fusion with lysosomes and then with damaged mitochondria (Lazarou et al., 2015). Very recently, Valente and collaborators observed that PINK1 is able to activate mitophagy pathway in a Parkin-independent manner (Gelmetti et al., 2017): they found that under starvation-induced autophagy, PINK1 selectively accumulates to contact sites between ER and mitochondria (MAMs) and recruits Beclin1 (BECN1), a key component of the class III phosphatidylinositol 3-kinase (PtdIns3K) complex, that is required to initiate autophagosome formation. They also reported that upon mitochondria depolarization, PINK1 interacts and phosphorylates serine 62 of Bcl-xL (Arena et al., 2013), an anti-apoptotic protein that inhibits autophagy through its binding to Beclin-1. However, in basal conditions, there is no evidence that these two endogenous proteins interact each other: the interaction was observed only upon cells treatment with the mitochondrial uncoupler CCCP suggesting a specific role for this interaction in depolarized mitochondria when PINK1 accumulates at the OMM. The phosphorylation of Bcl-xL by PINK1 at serine 62 affects its cleavage, thus maintaining Bcl-xL in the full-length form that can exert its anti-apoptotic function. This process represents another mechanism by which PINK1 could carry out its neuroprotective role.

A hallmark of model cells for PINK1 loss of function is mitochondrial Ca^{2+} overload (Gandhi et al., 2009b; Marongiu et al., 2009): this dysregulation together with low Ca^{2+} buffering capacity and continuous Ca^{2+} entry to sustain their pacemaking activity renders dopaminergic neurons particularly vulnerable to injury (Surmeier, 2018). In this contest, a few studies have directly investigated the possibility that PINK1 could have an important role in the regulation of mitochondrial Ca^{2+} handling, and despite of promising information

is emerged, many aspects are still controversial. Pioneering observation indicated that alterations in mitochondrial structure and neurite outgrowth observed in neurons co-expressing mutant PINK1 and a-syn were completely restored by blocking mitochondrial Ca^{2+} influx (Marongiu et al., 2009). Later on, it has been shown that mitochondrial Ca^{2+} overload observed in PINK1 KO cells likely relates to impairment in mitochondrial Ca^{2+} efflux (Gandhi et al., 2009a) and can be prevented by PKA-mediated activation of the mitochondrial Na+/Ca^{2+} exchanger (NCLX), implying a neuroprotective role for PKA inside the mitochondria (Kostic et al., 2015). Furthermore, more recently, PINK1 has been proposed to control mitochondrial Ca^{2+} handling by phosphorylating LETM1, an inner mitochondrial membrane K+/H+ exchanger (Huang et al., 2017) which may act as a mitochondrial Ca^{2+}/H+ antiporter (Jiang et al., 2009).

Furthermore, Heeman and collaborators showed instead that PINK1 depletion induced mitochondrial membrane depolarization and consequently a reduction of Ca^{2+} uptake (Heeman et al., 2011). Basal mitochondrial Ca^{2+} levels do not significantly differ between control and PINK1-KO cells, but upon stimulation of Ca^{2+} release from the intracellular stores, PINK1-deficient cells show impaired mitochondrial Ca^{2+} uptake and decreased mitochondrial ATP synthesis, that in turn affected cytosolic ATP-dependent Ca^{2+} extrusion, leading to decreased rate of cytosolic Ca^{2+} removal.

In this contest, in the laboratory where I carried out my PhD project, preliminary evidence was obtained that rather indicates that PINK1 could interfere with the MCU complex activity and modulate the mitochondrial Ca^{2+} uptake. Pilot experiments in Hela cells have shown that the overexpression of PINK1 wildtype (but not of kinase dead or PD-pathogenic mutants) resulted in a reduction of mitochondrial Ca^{2+} transients induced by cell stimulation. Furthermore, PINK1 co-expression with the MCU pore subunit or with its activator MICU1 was able to counteract the exaggerated mitochondrial Ca^{2+} transient generated upon cell stimulation in cells overexpressing MCU or MICU1 alone. In line with these findings, PINK1-KO MEF cells display both higher basal and stimulated mitochondrial Ca^{2+} levels than the MEF wildtype counterpart. Interestingly, we have also found that both MCU and MICU1 co-immunoprecipitated with PINK1, thus suggesting that the possible PINK1 modulatory role on MCU complex requires their physical interaction (unpublished results). These data permit to hypothesize that PINK1 could have a direct role in the control of mitochondrial Ca^{2+} uptake and open a very challenging opportunity to investigate the molecular mechanism at the basis of PINK1 action on mitochondrial Ca^{2+}.

1.4.2. PINK1 and PKA interplay in the regulation of mitochondrial functions.

A large amount of evidence supports that phosphorylation and dephosphorylation of mitochondrial proteins influence mitochondrial function. Intriguingly, a phosphoproteome analysis performed on functional mitochondria from human skeletal muscle in resting conditions showed there are 155 phosphorylation sites in 77 mitochondrial proteins including inner membrane respiratory complexes subunits and enzymes, as well as, in the component of the mitochondrial contact site and cristae organizing system (MICOS) in the insulin-stimulated state (Zhao et al., 2011, 2014). Although the detailed functions of these kinases/phosphatases in mitochondria are still unclear, there is evidence that the translocated mitochondrial kinases/phosphatases may be seen in mitochondria in several mitochondrial compartments: among them PINK1, as described above, is certainly well recognized to localize at mitochondrial levels, and others, including PKA, suffer for the appearance of more contradictory reports on their mitochondrial distribution.

1.4.2.1. cAMP-dependent protein kinase A (PKA).

Protein kinase A (PKA) is a member of a family of enzymes that is functionally dependent on the levels of cyclic AMP (cAMP) (Figure 7). It is a tetrameric enzyme consisting of two catalytic (CAT) and two regulatory subunits (R). In mammals, there are three known isoforms of catalytic subunits (CATα, CATβ, CATγ) and four isoforms of regulatory subunits (RIα, RIβ, RII α, RIIβ) (Taylor et al., 2017). cAMP binds to regulatory subunits and induces the release of active catalytic subunits, which are able to phosphorylate key substrates. cAMP is generated from ATP via adenylyl cyclases (ACs) and degraded via phosphodiesterases (PDEs). In mammals, there are two types of class III ACs: membrane bound (tmAC) and soluble s(AC). TmACs are regulated by heterotrimeric G proteins and

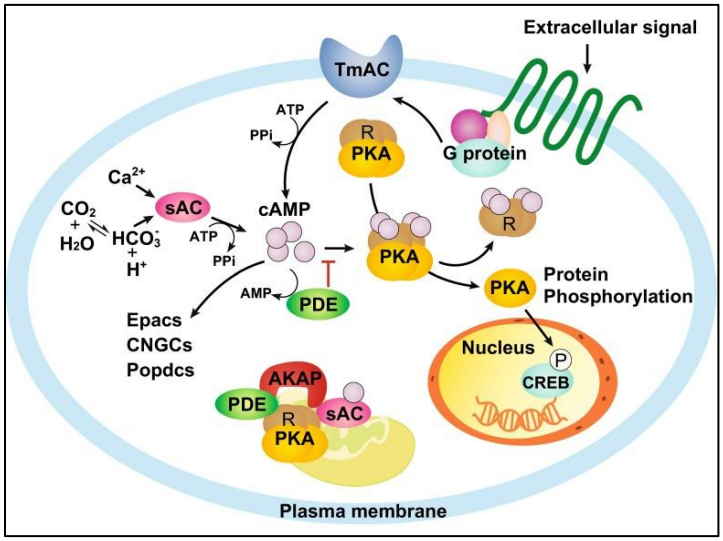

Figure 7 Intracellular cAMP/PKA signaling pathways (Zhang *et al*., 2016)

the pharmacological activator forskolin, whereas sACs are directly regulated by calcium, physiological changes in ATP, and bicarbonate. The cAMP generated by ACs is tightly regulated by PDE, which catabolize cAMP into AMP.

cAMP can also bind and activate other two main effector protein: the cyclic nucleotide regulated channels (CNG), including cyclic nucleotide-gated channels (cNGC) and hyperpolarization-activated cyclic nucleotide- gated (HCN) channels (Kaupp and Seifert, 2002), and a family of guanine-nucleotide exchange factors (GEFs) called exchange proteins activated by cAMP (EPAC) (Kawasaki et al., 1998).

Protein phosphorylation/dephosphorylation is the most important posttranslational modification of cellular proteins that is in place to modulate their function. To this end cells are equipped with many protein kinases and phosphates. Their activation in the right place and at the right moment inside cells is fundamental to guarantee specific and optimal modulation of signaling pathways. In recent years, the concept of spatial micro-compartmentation of the signal has emerged as a general cellular strategy to ensure fine regulation of many biological processes. In the case of PKA, given its ubiquitous presence in mammalian cells and its widespread involvement in numerous parallel signaling cascades this specificity is achieved, at least in part, through the compartmentation of PKA at discrete subcellular locations through interaction with a family of proteins called A kinase anchoring proteins (AKAPs) that directs PKA in proximity to its target. In addition to tethering PKA to particular subcellular location, AKAPs also act as scaffolds for PKA's substrates, ACs, PDEs, and protein phosphatases, overall facilitating the regulation by the cAMP cascade. In respect with possible PKA mitochondrial localization, the existence of a PKA pool at the OMM is now well recognized, however, despite PKA has been shown to phosphorylate a few inner mitochondrial membrane and matrix proteins, its localization in these two mitochondrial sub-compartments has not been definitely proven.

The anchoring of PKA at the OMM is mediated by three different AKAPs, AKAP1, Rab32 and AKAP2 (Lefkimmiatis and Zaccolo, 2014), that associate with the regulatory subunit type II. Cytosolic cAMP increase activates PKA tethered to the OMM by releasing it from the regulatory subunit. A novel AKAP called sphingosine kinase interacting protein (SKIP) has been recently described to bind preferentially type I regulatory subunits at the IMS (Means et al., 2011). PKA at the IMS has been shown to phosphorylate ChChd3, a scaffold protein of the MICOS complex involved in the maintaining of cristae junctions (Kozjak-Pavlovic, 2017).

1.4.2.2. PINK1 and PKA protein interaction.

An interesting observation that pointed out on a possible interplay between PKA and PINK1 at mitochondrial level was that the targeting of PKA to mitochondria was able to rescue functional defects observed in PINK1 deficient neurons. It has been observed that pharmacological and molecular modulation of the activity (and localization) of PKA in PINK1-deficient cell lines was effective in reverting several mitochondrial parameters that were compromised by the absence of PINK1 function (Dagda et al., 2011). Dagda and collaborators also investigated whether the effect of mitochondrially targeting of PKA influences the regulation of the mitochondrial fission protein Dynamin-related protein-1 (Drp1): the overexpression of a mitochondrially targeted PKA (OMM-PKA) as well as the stabilization of endogenous PKA to the OMM via AKAP1 both resulted in PKA-mediated phosphorylation and inhibition of Drp1 that in turn led to mitochondrial elongation and reverted cell death in PINK1-deficient cells. These findings were followed by the observation that PINK1 also enhanced dendrite morphogenesis and arborization through the activation of PKA-regulated signaling pathways, thus supporting the involvement of PINK1 and PKA in the same pro-survival axis to counteract neurodegenerative processes (Dagda et al., 2014). Functional interaction with PKA represents a novel neurite regulatory function for the OMM-tethered PINK1 form distinct from that in mitophagy. Interestingly, the rescue of defects in dendritic arborization in PINK1-deficient neurons was also observed when the cytosolic form of PINK1 was re-introduced, suggesting that soluble PINK1 is not exclusively a terminal degradation product of PINK1.

The absence of PINK1 is not only associated with an impairment of neurite morphogenesis, but also with a decrease of PKA signaling: PINK1 is required for cAMP-induced neurite extension and promotes PKA activation, but the mechanisms by which PINK1 activates downstream PKA signaling has to be elucidated. Given that PKA distribution is regulated by AKAPs, which confer selectively to its action at distinct subcellular sites, and that PINK1 induces an increase in the levels of the microtubule associated protein MAP2, a neuronal specific AKAP, it is possible that the tether between PKA and MAP2 is also increased at the dendrites to promote dendritic outgrowth (Matenia and Mandelkow, 2014). Another possibility is that cytosolic PINK1 may promote phosphorylation of the RIIβ subunit and, consequently, the release and activation of catalytic subunits of PKA holoenzyme. In line with this possibility, more recently, Dagda and co-workers elucidated the molecular mechanism by which PINK1 and PKA interact at the mitochondrial level to regulate dendrite

remodeling, outgrowth and trafficking (Das Banerjee et al., 2017). They have found that PINK1 enhances the association of the regulatory subunit RIIβ with AKAP1 and increases the autocatalytic-mediated phosphorylation of PKA/RIIβ to prime PKA holoenzyme for activation by cAMP. Impaired mitochondrial trafficking in PINK1-deficient neurons was reverted upon PKA activation and through the phosphorylation of the OMM protein Miro2, that together Miro1, regulates bidirectional trafficking of mitochondria in neurites by interacting with kinesin and dynein motors and the TRAK-family adaptor proteins (Birsa et al., 2013).

The connection between PINK1 and PKA axis in the control of mitochondrial function has been strongly reinforced by Akabane *et al*. and by Pryde *et al*. that have reported that PKA and PINK1 negatively regulate each other. On one hand PKA affects PINK1 stability and Parkin recruitment to damaged mitochondria by phosphorylating MIC60, an inner membrane protein of the mitochondrial contact site and cristae organizing system (MICOS) complex (Akabane et al., 2016) thus resulting in mitophagy inhibition and on the other, OMM-localized PINK1 disables the anti-fission machinery by displacing PKA from AKAP only in damaged mitochondria network, keeping intact and perfectly working the unaffected portion (Pryde et al., 2016). These data are apparently in contrast, but it has to be considered that PINK1 could play a dual role: it maintains dendrite and mitochondrial homeostasis under basal condition but upon mitochondrial damage it facilitates mitophagy activation by uncoupling mitochondrial PKA signaling. This double action has neuroprotective effects. Another neuroprotective effect for PKA has been described to occur during the early phase of ER stress through the modulation of the mitochondrial pro-fission Drp1 protein: the activation of PKA protein leads to phosphorylation and translocation of Drp1 to the ER that, in this way in addition to inhibit mitochondrial fission, it also promotes remodeling of the ER morphology and consequently of the ER-mitochondria interface that results in enhanced ER to mitochondria Ca^{2+} transfer and mitochondrial metabolism (Bravo-Sagua et al., 2018).

In summary, a number of reports suggest that PINK1 and PKA may cooperate to prevent neurodegeneration but the possibility that their functional interaction may occur inside the mitochondria and not exclusively at the OMM level is still unexplored and the investigation in this direction appears very intriguing.

1.4.3. Does PKA protein localize into mitochondrial matrix?

As described above, at the OMM PKA has emerged as an essential regulator of different aspects of mitochondrial biology including mitochondrial morphology, dynamics, and turnover. OMM PKA has been long associated with mitochondria through its interaction with the splice variants of the gene *AKAP-1*, AKAP84, AKAP121 and AKAP149 (Chen et al., 1997). This interaction is important to regulate the subcellular localization of PKA and the PKA-dependent phosphorylation processes.

The role of PKA at the cytoplasmic surface of the OMM is now well established. OMM PKA was first linked to the organelle dynamics through phosphorylating OMM-localized dynamin-related protein 1 (Drp1). Phosphorylation of S637-Drp1 by OMM PKA slows its GTPase activity and inhibits mitochondrial fission, and results in elongated mitochondria (Dagda et al., 2011). Moreover, it could be crucial to mitochondrial transport in neurons, as well as, mitochondrial integration at synapses (Merrill et al., 2011).

As well known, OPA1 together with Mitofusin 1/2 (Mfn1/2) controls fusion of IMMs and OMMs, respectively, between two adjacent mitochondria (Schrepfer and Scorrano, 2016). Phosphorylation of Mfn-2 by PKA leads to cell growth arrest in vascular smooth muscle cells (VSMCs) (Zhou et al., 2010). OPA1 also acts as a A-kinase anchoring protein associated with lipid droplets: it composes a supramolecular complex containing PKA and perilipin, that controls access of lipases to lipid droplets (Pidoux et al., 2011). OPA1 targets PKA to lipid droplets, which is necessary for control of perilipin phosphorylation and lipolysis.

PKA activity on the OMM has been shown to influence the stability of PINK1 via the mitochondrial contact site and organizing system (MICOS), a multiprotein complex involved in the formation and maintenance of mitochondrial cristae (Akabane et al., 2016). MIC60 and MIC19, two components of MICOS complex, were identified as a target of PKA-mediated phosphorylation in response to forskolin treatment. Increasing PKA mitochondrial activity was found to phosphorylate MIC60 on Ser528 destabilizing PINK1 in the OMM, and MIC19 on Thr11 impairing Parkin recruitment to depolarized mitochondria. These results suggest that PKA is involved in the regulation of mitophagy.

Furthermore, it has been described to promote cell survival impairing apoptosis (Kumar et al., 2009). Upon cell death stimuli, the pro-apoptotic protein Bad inhibits anti-apoptotic Bcl-2 family members, triggering two other pro-apoptotic proteins Bax and Bak to aggregate on

mitochondria (Elmore, 2007). OMM PKA has several apoptosis-related proteins as substrates. The phosphorylation of Bad on Ser 112 and on Ser155 alleviates the inhibitory effects of Bad on anti-apoptotic proteins Bcl-2 and Bcl-xL, inhibiting release of cytochrome c from mitochondria and protecting cells from apoptosis (Affaitati et al., 2003). However, PKA activity is also showed to be linked to apoptosis through the phosphorylation and stabilization of Bim on Ser83 (Moujalled et al., 2011). However, phosphorylation of Bax on Ser60 promotes Bax translocation to mitochondria, leads to mitochondrial ROS formation and triggers cytochrome c release (Arokium et al., 2007).

PKA activity can increases the import of proteins by promoting interactions with chaperones like Hsp70, anyway it can phosphorylate protein transports on the mitochondrial surface and impairs their functions (Schmidt et al., 2011). It phosphorylates TOM22 on Thr76 and TOM40 on Ser125, preventing transport of proteins into mitochondria (Gerbeth et al., 2013; Rao et al., 2012). The mitochondrial import receptor subunit TOM70 was described to be phosphorylated on Ser174 by PKA on the OMM (Lucero et al., 2019).

The possibility that PKA could also operate in the intramembrane space or in the mitochondrial matrix is still amply debated, but few indications suggest that PKA could specifically act also at these sub-mitochondrial compartments.

First of all, pioneering data by Acin-Perez *et al.* have suggested the existence of soluble adenylyl cyclase (sAC) inside the mitochondrial matrix that is responsible for the generation of mitochondrial cAMP. It is well demonstrated that sAC is insensitive to heterotrimeric G protein regulation or forskolin, instead it is stimulated by bicarbonate and is sensitive to ATP and Ca^{2+} levels (Chen et al., 2000; Litvin et al., 2003). Acin-Perez *et al* have found that when nutrients are available to cell, the TCA cycle generates CO_2 which levels increase and carbonic anhydrases (CA) convert CO_2 into bicarbonate, stimulating sAC activity and activating cAMP/PKA pathway. They have also shown that its activation was specifically dependent by the metabolically generated carbon dioxide thus suggesting the existence of a CO_2-HCO^{3-}-sAC-cAMP-PKA signaling cascade wholly contained within mitochondria, which serves as a metabolic sensor modulating ATP generation and ROS production in response to nutrient availability. Indeed, they were also able to show that the modulation of intramitochondrial sAC regulated ATP production by phosphorylation of mitochondrial proteins, including subunits of cytochrome c oxidase (Acin-Perez et al., 2009; Di Benedetto et al., 2014; Lefkimmiatis et al., 2013).

Later, making use of a FRET-based cAMP sensor selectively localized to the mitochondrial matrix, Di Benedetto *et al.* directly demonstrated, in living cells that cytosolic cAMP does not diffuse from cytosol into the organelle but, instead, consistent with the suggestion of Acin-Perez *et al.*, it is generated in the matrix by sAC. More importantly, they also showed that cAMP increases within the mitochondrial matrix not only in response to bicarbonate, but also in response to mitochondrial matrix Ca^{2+} increase (Di Benedetto et al., 2013), thus suggesting an interesting interplay between cAMP and Ca^{2+}-mediated signaling.

Other components of cAMP signaling cascade have also been identified in the matrix, such as PDE2A2, an isoform of PDE which is found to localize in the matrix (Acin-Perez et al., 2011a). This protein is identified as a novel regulator of cAMP signals in the matrix: cGMP binds a GAF domain in its regulatory portion and activates the enzyme which is assigned to degrade cAMP. Moreover, when a non-selective PDE inhibited 3-isobutyl-1-methylxanthin (IBMX) was used, mitochondrial PDE activity was only partially suppressed, suggesting the existence of additional PDE isoforms in the matrix (Acin-Perez et al., 2011a).

All together these observations open the possibility that the cAMP effectors, among which PKA is the main candidate, could be present or translocate inside the mitochondria and participate in the regulation of mitochondrial functions.
However, no cAMP-dependent PKA activity could have been detected inside the matrix since Lefkimmiatis *et al.* did not detect the endogenous PKA activity in this compartment using a mitochondrial matrix localized FRET-based PKA activity sensor (Lefkimmiatis et al., 2013). They stimulated the production of cAMP in the matrix via HCO_3^-/CO_2 and monitored the PKA activity using the sensor: as expected, bicarbonate induced the increase of cAMP pool in the matrix, but surprisingly there was no increase in PKA activity. They also used a potent activator of PKA that rapidly reached the mitochondrial matrix [8-(4-chloro-phenylthio)-adenosine-3'-5'-cyclic monophosphate, 8CPT-cAMP] and they did not detect PKA activity. They also generated a OMM-localized FRET-based PKA activity sensor and the PKA activity was detected when cytosolic cAMP pool was generated by forskolin. Their data indicate that there is an high PKA activity at the OMM involved in the maintenance of the phosphorylation state, for example, of Drp1 and BAD, but it is not present in the matrix or its activity is so low to detect (Lefkimmiatis et al., 2013).

Despite this, some papers have appeared describing candidates for PKA phosphorylation that are clearly resident in the inner mitochondrial membrane or presented PKA consensus sites exposed to the matrix, thus reinforcing earlier data obtained by several independent

groups using biochemical, pharmacological, and immunological methods, including immunoelectron microscopy, that have documented the presence of PKA in the mitochondrial matrix (Livigni et al., 2006; Prabu et al., 2006; Ryu et al., 2005; Schwoch et al., 1990).

More specifically, PKA has been suggested to be localized in the inner membrane where it phosphorylates the 18 KDa NDUFS4 subunit of complex I in cultured myoblast and promotes oxidative phosphorylation (Rasmo et al., 2010). Recent experiments have pointed out on the possibility NDUFS4 was phosphorylated outside rather than inside the mitochondria and that its phosphorylation was necessary to facilitate its interaction with the chaperone Hsp70 and its import within mitochondria (De Rasmo et al., 2008). However, it has been suggested that the involvement of the intramitochondrial cAMP/PKA signalling was related to the regulation of the stability of complex I by inhibiting mitochondrial proteases: inhibition of sAC reduced complex I subunits amount and the treatment with cell-permanent cAMP analogue 8-Br-cAMP, but not with isoproterenol (which activates membrane associated adenylate cyclase and promoted elevation in cytosolic cAMP) only in the cytosol, was able to rescue the reduction (De Rasmo et al., 2015).

The hypothesis that PKA could be present or translocate into mitochondrial matrix is reinforced by the evidence that it has been found that cyclic AMP response element-binding protein (CREB), a widely expressed transcription factor, is present in the mitochondrial matrix of neurons and that it binds directly to cyclic AMP response elements (CREs) found within the mitochondrial genome (Lee et al., 2005). Disruption of CREB activity in the mitochondria decreases the expression of a subset of mitochondrial genes, including the ND5 subunit of complex I, and down-regulates complex I-dependent mitochondrial respiration. This suggests that the dysregulation of mitochondrial gene expression by reduced mitochondrial CREB activity could contribute to the mitochondrial dysfunction and neuronal loss associated with neurodegenerative disorder. Furthermore, CREB has been also shown to regulate the expression of other mitochondrial components of the electron transport chain inside mitochondria, such as ND1, ND6, and COXIII/ATP6 (De Rasmo et al., 2009) and activate a master regulator of mitochondrial biogenesis, PGC1α, upon the activation of PKA resident in the mitochondrial matrix (Fernandez-Marcos and Auwerx, 2011).

Another specific residue (Ser58) localized at the matrix side of cytochrome oxidase subunit IV-1 (COXIV-1) was identified as one of the targets of the intramitochondrial sAC-PKA pathway (Acin-Perez et al., 2009). Ser58 site is involved in binding ATP at the allosteric site

for the regulation of COX activity. PKA phosphorylates this site preventing the inhibition of COX activity (Acin-Perez et al., 2011b).

PKA seems to be involved also in the regulation of complex V by the phosphorylation of ATPase inhibitory factor AIF1 on Ser39, which prevents its bindings to complex V and its inhibitory effect on ATP synthase (García-Bermúdez et al., 2015). However, also in this case it has been claimed that the phosphorylation event may occur before the entry of the protein in the mitochondrial membrane, because it was shown that upon the incubation with the tmACs activator forskolin the phosphorylation of AIF1 also increases. It has been suggested that intramitochondrial cAMP/PKA signaling was rather involved in the modulation of the activity of complex V by controlling its turnover mitochondrial proteases (De Rasmo et al., 2016).

An additional mitochondrial protein that has been demonstrated to be phosphorylated (at least in vitro) by PKA is the mitochondrial Na^+/ Ca^{2+} exchanger (NCLX) that, as mentioned above describing mitochondrial Ca^{2+} handling, represents the main Ca^{2+} extrusion pathway from the mitochondria (Figure 8).

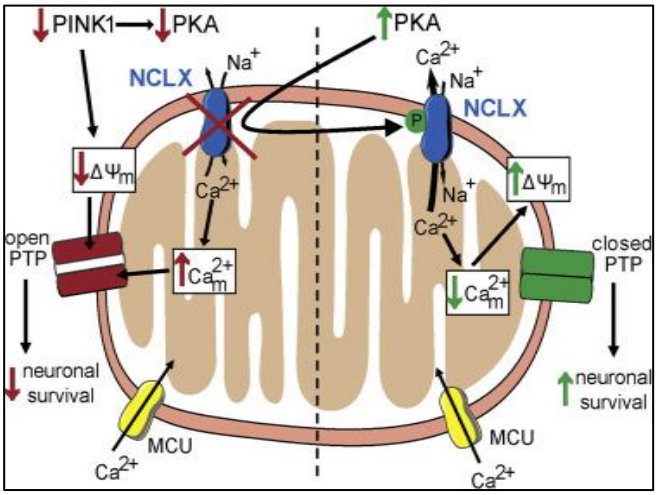

Figure 8 In PINK1 deficient neurons NCLX activity is fully rescued by activation of the protein kinase A (PKA) pathway **(**Kostic *et al*., 2015).

By applying bioinformatics tools, Kostic and coworkers have screened NCLX sequence for the presence of RRXSY PKA phosphorylation consensus site and identified at high score for Ser258. To validate the possibility that NCLX could be phosphorylated directly by PKA at this site they have performed a mass spectrometry analysis on cells overexpressing c-*myc*-tagged NCLX treated with forskolin, with or without H89 inhibitor of PKA activity and found *in vitro* phosphorylation of purified NCLX preparation on Ser258 residue. This phosphorylation site is located within hydrophilic loop of the exchanger on the matrix side,

suggesting a possible intramitochondrial localization of PKA protein (Kostic et al., 2015). As mentioned above, this finding is particular relevance since they have also observed that PKA is able to rescue mitochondrial defects such as mitochondrial depolarization and mitochondrial Ca^{2+} overload due to PINK1 deficiency. They have observed that the application of forskolin enhances the rate of mitochondrial Ca^{2+} efflux and fully recovered the loss of mitochondrial membrane potential in PINK KO cells supporting a role of PKA in the regulation of NCLX. However, the question whether in living cells this regulation may occur and whether the reversible phosphorylation of NCLX may occur at the level of the mitochondrial matrix has to be proven and opens again the issue on PKA localization inside the mitochondrial compartments.

2.4. ER/Mitochondria and ER/Plasma Membrane contact sites: a hub for calcium and membrane lipids transfer

The compartmentalization of cellular signals is an essential mechanism of regulation for cellular pathways. In eukaryotic cells, this compartmentalization is achieved because the existence of a variety of organelles with unique function, which are spatially confined by membranes. However, it is clearly emerging that communication between the organelles is also important and they can do this by exchanging molecules, ions but also because they can come in close proximity. Thus, organelles can communicate between each other creating microdomains called "membrane contact site" (MCS). This communication is important to favour different signaling and metabolic pathways (Eisenberg-Bord et al., 2016) and recent studies have discovered that dysregulation in MCS are present in a number of different diseases, including neurodegenerative disease, inflammation, cancer, type 2 diabetes and infections.

2.4.1. ER/Mitochondria contact sites

The best characterized membrane contacts are the sites of apposition between mitochondria and the ER, termed MERCs (mitochondria-ER contacts). Following initial studies where ER/mitochondria contact sites have been investigated by subcellular fractionation and electron microscopy (Mannella et al., 1998; Meier et al., 1981; Shore and Tata, 1977), more recently they were also investigated in living cells by electron tomography technique that have revealed that their apposition resides in a range of around 10 and 50 nm (Csordás et al., 2006) and by a splitGFP based tool. Latter has permitted to document the existence of narrow (8-10 nm) and wide (40-50 nm) juxtapositions in human cells that responded differently to starvation, ER stress, mitochondrial shape modifications, and changes in the levels of modulators of ER-mitochondria juxtaposition (Cieri et al., 2018).

Several proteins located on mitochondria and ER membranes are identified to be important for MERC formation and physical tethering of organelles, including ERMES complex in yeast and Mfn1/2, Fis1-Bap31, VAPB-PTPIP51 and IP3R-Grp75-VDAC1 tripartite complex in mammals (Filadi et al., 2018; Scorrano et al., 2019) (Figure 9). A part the molecular characterization of the component of these contact sites that is the subject of intense investigation and originates some controversial issues among different laboratories, the functional study of these contact sites become more and more important because they are involved in many processes critical for cell survival and death, such us phospholipid

synthesis and exchange, regulation of mitochondrial fission and trafficking, energy metabolism, protein folding, apoptosis and Ca^{2+} transfer (Giorgi et al., 2015).

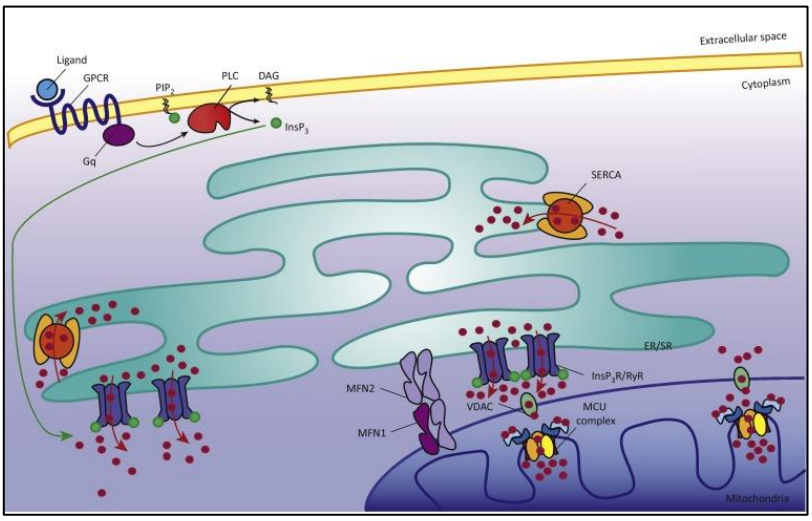

Figure 9 ER-mitochondria contact sites (Raffaello *et al.*, 2016).

In particular, as mentioned above in the section discussing mitochondrial Ca^{2+} homeostasis, Rizzuto and co-workers have demonstrated that the contact sites between the two organelles are important for the formation of high concentration Ca^{2+} hotspots that can be sensed by the low affinity mitochondrial Ca^{2+} uniporter (Rizzuto et al., 1993) (Rizzuto et al., 1998).

Alterations in ER-mitochondria associations are involved in the impairment of a variety of intracellular processes, many of them are perturbed in neurodegenerative diseases, including PD. Interestingly, some of the PD-related proteins have been found to localize at MERCs and to be involved in the regulation of ER-mitochondria signaling, among them α-synuclein is the most investigated. Until now, three different groups demonstrated that α-synuclein is involved in the regulation of ER-mitochondria associations (Calì et al., 2012a; Guardia-Laguarta et al., 2014; Paillusson et al., 2017). A study performed in the laboratory where I carried out my PhD project has demonstrated that mild overexpression of wild-type α-synuclein has a beneficial effect, since by favouring the ER-mitochondria contact sites formation it enhanced mitochondrial Ca^{2+} transfer from ER upon cell stimulation thus sustaining bioenergetics metabolism. Interestingly, a dose-dependent impairment was proposed to perturb mitochondria-ER contacts and Ca^{2+} handling: when the cells were loaded with high amounts of α-synuclein, a redistribution of the protein to cytoplasmic foci was observed and a reduction in mitochondrial Ca^{2+} uptake that correlated with reduced ER-mitochondria tethering were monitored (Calì et al., 2012a). Later on, it has been showed that α-synuclein was enriched at the mitochondria associated membranes (MAMs) fraction and that the presence of familial PD-related mutations in the α-synuclein sequence reduced its

association with the MAMs (Guardia-Laguarta et al., 2014). This is associated with a decrease in MERCs functions in cells overexpressing mutant α-synuclein. The possibility that α-synuclein behaviour at MERCs is dependent on its expression levels is also observed by Pailluson and collaborators that, moreover, showed that α-synuclein is able to interact with the ER-vesicle associated membrane proteinassociated protein B (VAPB), perturbing their association with PTPIP51 proteins and thus their mitochondria-ER association (Paillusson et al., 2017). However, the mechanism by which α-synuclein impairs functionally the MERCs is still unclear.

In addition to α-synuclein, also PINK1 and Parkin seem to be involved in the regulation of ER-mitochondria interactions. As mentioned before, while PINK1 distribution to MAMs is necessary for the recruitment of the autophagic machinery, Parkin translocation to ER-mitochondria contact sites was observed upon glutamate-induced excitotoxicity in rat primary cortical neurons suggesting a specific role in the communication between the two organelles. Under these conditions the concomitant Parkin translocation to mitochondria did not resulted in the activation of mitophagy process, unless ROS inhibition was induced by treatment with antioxidant (Van Laar et al., 2015). The role of Parkin on ER-mitochondria cross-talk and the consequences of its modulatory effect were investigated in the laboratory where I carried out my PhD by overexpressing it and monitoring Ca^{2+} homeostasis and ATP production (Calì et al., 2013). Parkin overexpression led to an increase in ER-mitochondria contacts favouring Ca^{2+} transfer from the ER to the mitochondria upon cell stimulation and Ca^{2+} release from ER. On the opposite, Parkin silencing caused mitochondrial fragmentation, reduced ER-mitochondria tethering and impairment of mitochondrial Ca^{2+} handling.

Considering this scenario a deep characterization of ER-mitochondria crosstalk and of its modulation by proteins involved in neurodegenerative pathways appears very challenging and for these reasons we have decided to better explore the role of α-synuclein and its mutants and we have also considered another aggregate-prone protein, tau, an interesting protein that could have a role in the modulation of this crosstalk. The results that we have obtained are published in two research articles that I have included in my PhD thesis and therefore they will not be further discussed in the Results and Discussion sessions (Calì et al., 2019;Vicario *et al*., 2019 under revision).

2.4.2. ER/Plasma Membrane interactions

In addition to ER/mitochondria interface, another crucial site for Ca^{2+} signalling and lipids transfer is represented by the region contacts between ER membrane and the plasma membrane (PM). ER-PM junctions have been first described by electron microscopy in the 1950s in muscle (Porter & Palade, 1957) and they were also observed in neurons (Rosenbluth, 1962;Metuzals, Chang, Hammar, & Reese, 1997; Spacek & Harris, 1997). Then it has become clear that they are represent in all eukaryotic cells, from unicellular organisms to specialized mammalian cells (Friedman and Voeltz, 2011; Pérez-Sancho et al., 2016). ER-PM contacts are contact sites where the distance between these two membrane compartments is below 40 nm.

ER-PM are important to mediate Ca^{2+} influx from extracellular space responsible for cellular depolarization and contraction in muscle cells and for the refilling of the intracellular Ca^{2+} stores also in non-excitable cells. Because ER is a limited Ca^{2+} store, cells have developed a sophisticated influx mechanism called SOCE (Store-Operated Ca^{2+} Entry) to refurnish it upon depletion (Figure 10).

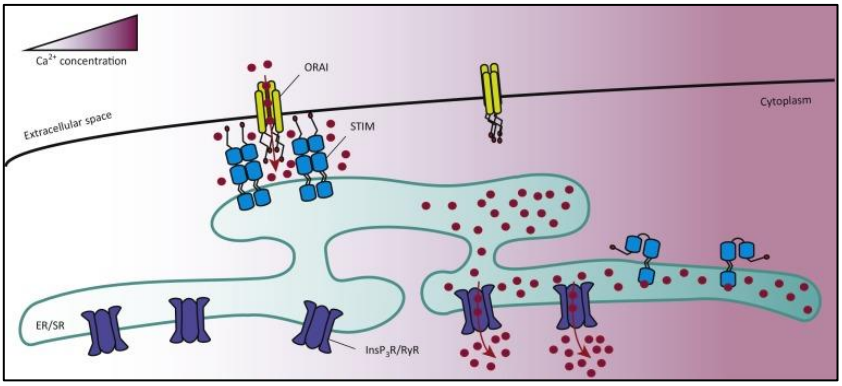

Figure 10 Schematic representation of store operated Ca^{2+} entry (SOCE). **(**Raffaello *et al.*, 2016)

This process is dependent on the dynamic interaction between the ER resident protein stromal interaction molecule 1 (STIM1), that acts as Ca^{2+} sensor, and Orai1, the protein forming the channel in the PM that permits Ca^{2+} entry from the extracellular ambient (Nwokonko and Gill, 2012). Depletion of Ca^{2+} in the ER lumen leads to dissociation of this ion from the luminal Ca^{2+}-binding EF hand of STIM1 and to the oligomerization of STIM1 protein that accumulates at ER-PM contact sites, where it binds and activates the Orai1 channel whose opening induces Ca^{2+} influx from the extracellular space. This process has been widely studied and the contact sites involving STIM1 and Orai have been well characterised. More recently, another family of proteins has been described to participate to ER-PM tethering and to regulate it dynamically during the process of replenishment of PM

with phosphatidylinositol 4,5-bisphosphate (PIP2) after receptor-induced hydrolysis to generate signalling molecules such as diacylglycerol and inositol 1,4,5 thrisphosphate, which increases cytosolic Ca^{2+} concentration.

The proteins involved are ER anchored extended Synaptotagmins (E-Syt) which interact with their cytosolic C2C domain with PIP_2. Interestingly, in the case of E-Syt1the interaction is also regulated by the increase of cytosolic Ca^{2+} levels. At high cytosolic Ca^{2+} levels, the binding of Ca^{2+} to the C2C domain leads to the translocation to ER-PM junctions and increases PIP_2 binding at PM. This translocation reduces the distance between the ER and PM making their interaction dynamic (Chang et al., 2013a).

An important question is whether the two types of tethers participate in the formation of the same junctions. A number of studies suggests that all or at least the majority of ER–PM junctions are STIM1 dependent (Chang et al., 2013b; Dingsdale et al., 2013; Várnai et al., 2007), others, mainly based on electron microscopy techniques, indicate that junctions formed by STIM1 and its interacting partners in the PM are structurally different from E-Syt-formed junctions (Fernández-Busnadiego et al., 2015). They also suggested that different tethers can be present in the same cell and in the same moment to participate in the formation of different ER-PM contact sites.

One of the difficulties in studying these junctions is the availability of techniques used to reveal them. Cryo-electron tomography is certainly one of the most sophisticated and has been used to reveal the 3D architecture of ER–PM contact sites at molecular resolution (Fernández-Busnadiego et al., 2015). Another technique was introduced by P. Varnai and colleagues that have developed a probe based on rapamycin-inducible bridge formation between two fluorescent markers for ER and PM proteins (Várnai et al., 2007). The modulation of the length of the linkers forming the bridge has allowed to estimate the distances between the two membranes in the junctions, which has been calculated to be larger than 8–9 nm but smaller than 12–14 nm (Lur et al., 2009). The development of another probe, termed MAPPER, has resolved one of the major issue of the recombinant probes to reveal the junctions, that, once expressed in the cells, usually are responsible for the tethering of ER and PM and thus resulted in a modification of the real junctions (Chang et al., 2013a). MAPPER probe was created by fusing the signal peptide and the transmembrane domain of STIM1 at the N and C termini of the GFP protein, respectively. This fusion protein was localized to the ER and did not modified the density of the junctions. The rapamycin binding domain (FRB) was added after the TM domain, a polybasic motif that binds to

phosphoinositides of the PM was added at the C-terminus and flexible and helical linkers were added to cytosolic portion of the marker to ensure that its expression did not alter the gap distance of ER-PM junctions.

In this contest, in the laboratory where I'm working it has been decided to develop a new probe with the same strategy it has been employed before for the probe SPLICS to monitor ER-mitochondria contact sites in the short- (8-10 nm) and long-range (40-50 nm) (Cieri et al., 2018). The characterization of this probe has been part of my PhD project and will be discussed in details in the section of the result.

Results

3.1. Investigating PKA protein localization and role at mitochondrial compartments

3.1.1. Construction and validation of splitGFP-based probes to monitor mitochondrial distribution of PKA protein

Considering that PINK1 and PKA interplay is emerging as potential site of modulation to counteract neurodegeneration, we have considered the possibility that they may act on common pathways. Before to explore the possibility that PKA and PINK1 could exert their action on specific mitochondrial targets, we decided to develop an approach that could permit to investigate PKA distribution in the mitochondria and that could permit us to establish whether PKA could be localized not only at the OMM (OMM), but also in the inter membrane space (IMS) e in the mitochondrial matrix.

The question whether PKA could be present in the mitochondrial compartments to exert its action is still open and debated and conflictual reports have appeared during the years on this matter. To shed light on these aspects, we decided to employ a new experimental approach, not based on canonical cell sub-fractionation or immunocytochemistry analysis, but on a new molecular tool generated using the splitGFP protein and BiFC (Bimolecular Fluorescence Complementation).

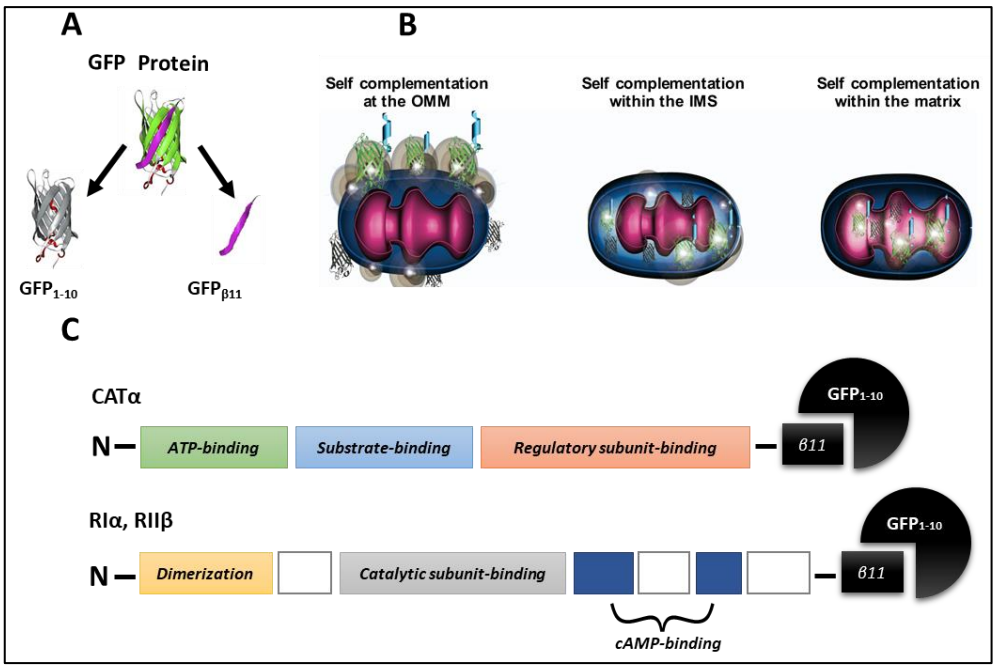

Figure 11 A) *splitGFP system and Bimolecular Fluorescence Complementation (BiFC).* GFP protein was split in two non-fluorescent portions, GFP_{1-10} and β11 fragment. **B**) Schematic representation of targeted splitGFP chimeras that complement at the OMM, within the IMS and in the mitochondrial matrix. **C**) *Schematic representation of β11-PKA constructs*. β11 fragment is fused to the C-terminal region of CATα, RIα and RIIβ.

The splitGFP is an artificial mutant of the GFP protein that has been split in two non-fluorescent portions (GFP_{1-10} and β11 beta strand) that emit fluorescence only when the two GFP fragments are close enough to properly interact (Figure 11A). This means that when GFP_{1-10} is targeted to specific mitochondrial compartment, OMM, IMS or mitochondrial matrix, the reconstitution of GFP protein occurs when β11 strand is located in the same compartment, as shown in the cartoon (Figure 11B).

The constructs of targeted GFP_{1-10} portion to the OMM and the mitochondrial matrix (mt) have been previously developed in our laboratory (Calì et al., 2015). The GFP_{1-10} portion targeted to the IMS has been developed to follow the intramitochondrial distribution of tau protein (Cieri et al., 2018). In brief, the strategy followed to target the GFP_{1-10} portion to each sub mitochondrial compartments was the generation of GFP_{1-10} chimera fused to amino acidic targeting sequences from different proteins well known resident in the specific mitochondrial sub-compartments. For the targeting to the OMM the first 33 amino acids of the TOM20 N-terminal tail (N33) were fused at the N-terminal of the GFP_{1-10} protein (Kanaji et al., 2000); for IMS the 68 amino acid leader sequence of the native IMS serine beta-lactamase-like protein LACTB (Polianskyte et al., 2009) was employed and the pre-sequence of the human subunit VIII of the cytochrome c oxidase was added to GFP_{1-10} to drive its import in the mitochondrial matrix(Rizzuto et al., 1989). A construct for the expression of the GFP_{1-10} fragment in the cytoplasm was also generated and employed as control. All the cDNAs were cloned in the mammalian expression vector pcDNA3 under the control of the cytomegalovirus (CMV) promoter. Figure 11C shows the fusion constructs between the PKA protein and the β11 fragment: specifically, the β11 fragment has been fused to the C-terminus of the sequences encoding the mouse catalytic PKA α subunit, CATα, and two different PKA regulatory subunits, the human Iα and the rat IIβ isoforms (RIα and RIIβ). All the cDNAs were cloned in the mammalian expression vector pcDNA3 under the control of the cytomegalovirus (CMV) promoter.

Several control experiments have been performed to validate the proper targeting of the probes. First, we have checked the correct localization of untargeted, OMM, IMS and mitochondrial matrix targeted GFP_{1-10} constructs by immunocytochemistry analysis performed by the incubation with a polyclonal primary antibody against the GFP protein probed with an Alexa633 conjugated secondary antibody. The coverslip with the transfected cells were observed upon excitation both at 488nm and 633nm. No green fluorescent signal was detected upon illumination at 488nm for all the four constructs (Figure 12A), as expected considering that the GFP_{1-10} fragment is not fluorescent in the absence of the

complementing β11 fragment. Upon illumination at 633nm the red fluorescent signal revealed a good level of expression for each GFP_{1-10} constructs, a diffuse cytosolic signal for the untargeted GFP_{1-10} fragment and the correct mitochondrial targeting for the OMM, IMS and mt GFP_{1-10} fusion proteins (Figure 12A). To verify that our GFP_{1-10} fusion proteins were still able to complement, and that complementation only occurs when the two non-fluorescent portions are in the same compartment, first we have co-expressed the cytosolic mKATe2 protein fused to β11 fragment with the OMM, IMS and mitochondrial matrix targeted GFP_{1-10} constructs. As shown in Figure 12B, the cytosolic mKATe2 protein complements at the OMM (top left panel) but not in the IMS and mitochondrial matrix. The red fluorescence acquired upon excitation at 594 nm wavelength is indicative of the expression of mKATE2 protein and its cytosolic distribution. Then, we verified whether GFP complementation could efficiently occur in each mitochondrial sub-compartment we have considered. To do this, the OMM, IMS and mitochondrial matrix targeted GFP_{1-10} fragments were co-expressed together with three different proteins fused to β11 artificially targeted or naturally resident at the same mitochondrial sub compartment. To test complementation at the OMM a β11 fused cytosolic α-synuclein was employed; a β11 fused cytochrome c and a β11α-synuclein targeted to the mitochondrial matrix were instead used to verify complementation in the IMS and the mitochondrial matrix, respectively. The correct GFP complementation was detected for all the three constructs as documented by the appearance of a green signal upon excitation at 488 nm wavelength which colocalized with the red fluorescence of the mitochondrial marker Mitotracker (Figure 12C). In the case of complementation with β11 cytosolic α-synuclein the pattern is mitochondrial indicating that only the pool of α-synuclein molecules close to the OMM are able to complement with the OMM GFP_{1-10} fragment.

Similarly, control experiments were performed to verify the expression of the three PKA subunits fused to the β11 fragment. Hela cells were transiently transfected with CATα and regulatory subunits Iα and IIβ and processed for immunocytochemistry analysis with specific CATα and Iα or IIβ primary antibodies. Upon incubation with secondary antibodies, anti-PKA antibodies revealed a diffuse cytosolic signal in PKA-CATα, PKA-Iα and PKA-IIβ isoforms overexpressing cells. Mitochondrial morphology and distribution were detected using an anti TOM20 antibody (probed with an Alexa594 conjugated secondary antibody). No major differences were detected upon the overexpression of CATα or regulatory subunits (Figure 12D**)**.

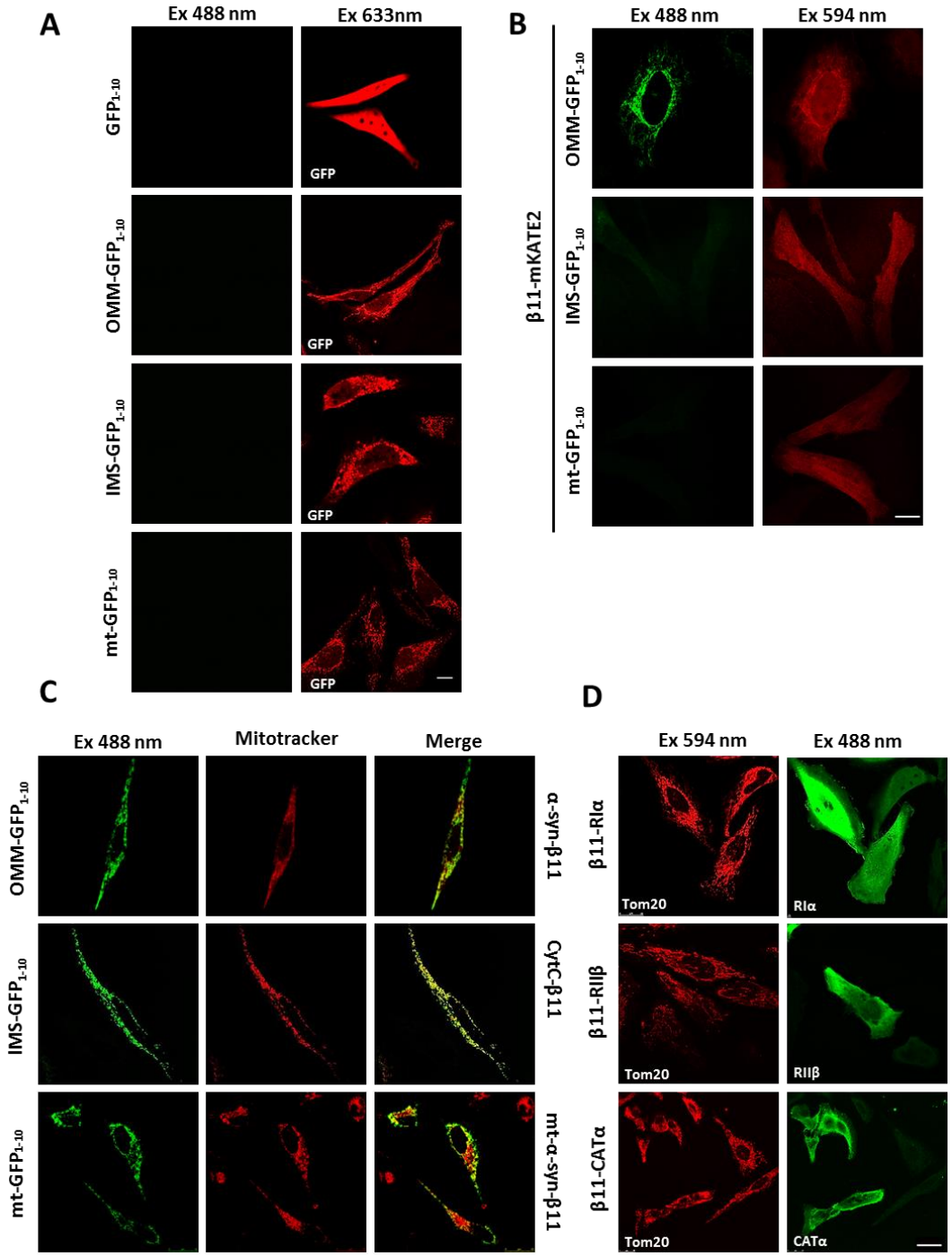

Figure 12 A) *Expression and subcellular localization of the untargeted, OMM, IMS and mitochondrial matrix targeted GFP$_{1-10}$ constructs*. HeLa cells were transfected with the indicated constructs and incubated with an anti-GFP antibody and probed with an Alexa 633 conjugated secondary antibody. Confocal images were acquired at 488 nm and 633 nm excitation wavelength. **B**) *Complementation between targeted GFP$_{1-10}$ constructs and cytosolic red fluorescent protein mKATE2 fused to β11*. Confocal images were acquired at 488 nm and 594 nm excitation wavelength from HeLa cells co-expressing GFP$_{1-10}$ constructs targeted to OMM, IMS and mitochondrial matrix with β11-mKATE2 protein. **C**) *Validation of splitGFP Bimolecular Complementation of targeted GFP1-10 constructs*. The OMM, IMS and mitochondrial matrix targeted GFP$_{1-10}$ fragments were co-expressed together with three different β11 tagged proteins artificially targeted or resident at the same mitochondrial sub compartments, i.e., α-synuclein (α-syn), cytochrome c or α-syn targeted to the mitochondrial matrix. Mitotracker was loaded as mitochondrial marker. Complementation of the GFP probes was revealed by fluorescent acquisition upon excitation at 488 nm wavelength. **D**) *Expression and cellular localization of the β11-PKA constructs.* PKA subunits were detected using a primary antibody specific for each subunit and probed with an Alexa 488 conjugated secondary antibody. Mitochondria were stained using an anti TOM20 antibody and probed with an Alexa 594 conjugated secondary antibody. Confocal images were acquired upon excitation at 488 and 594 nm wavelength. Scale bar 25 μm.

These control experiments have demonstrated the efficiency and the specificity of the splitGFP method as a tool to investigate protein localization at mitochondrial levels. Considering these results, we were confident that this methodology should permit to reveal whether and how a pool of PKA protein could be resident or translocate to any mitochondrial sub-compartments.

3.1.2. Investigating PKA localization at sub-mitochondrial level using splitGFP-based PKA chimera

To investigate the possible presence of PKA in the IMS and in the mitochondrial matrix HeLa cells were co-transfected with GFP_{1-10} constructs targeted to OMM, IMS and mitochondrial matrix and PKA CATα, RIα and RIIβ subunits fused to the β11 fragment. Confocal images acquired upon excitation at 488 nm have revealed a strong green fluorescent signal that colocalizes with mitochondrial distribution in the case of each PKA subunits (Figure 13A-C, upper panels), indicating the existence of cytosolic PKA pools located in proximity of the OMM, as previously documented by others with different approaches. This result is in line with the existence of OMM AKAP anchoring PKA regulatory subunits at the cytosolic side of the OMM. At difference from the OMM-GFP_{1-10} construct, when the IMS- an mt- GFP_{1-10} were cotransfected with the three different PKA subunits the appearance of reconstituted GFP fluorescence was detected only in the case of the CATα subunit which shows a clear green fluorescent signal in both compartments (Figure 13C, middle and lower panels, respectively). The RIα and RIIβ regulatory subunits, instead, do not display any localization at the IMS and in the matrix (Figure 13A-B, middle and lower panels, respectively). This evidence suggests that, at least, a pool of CATα molecules resides in the IMS and in mitochondrial matrix in resting condition and upon overexpression, instead, under the same conditions, the regulatory subunits are prevented to reach these compartments. The colocalization of the green fluorescence signal with the mitochondria network was confirmed by the immunostaining with anti TOM20 primary antibody (in red) or by the overexpression of a red fluorescent protein selectively targeted to the mitochondrial matrix (mtRFP) (Figure 13A-C, right panels). Interestingly, the merge panels show that, at least in the case of the CATα subunit at the level of the mitochondrial matrix, the colocalization does not occur for the entire mitochondrial network (being visible some red area in the merging). The possibility that mitochondrial targeting of the CATα may

not occur homogenously in the entire mitochondria population, but it is rather confined to a portion of them, is very intriguing and certainly demands further investigations,

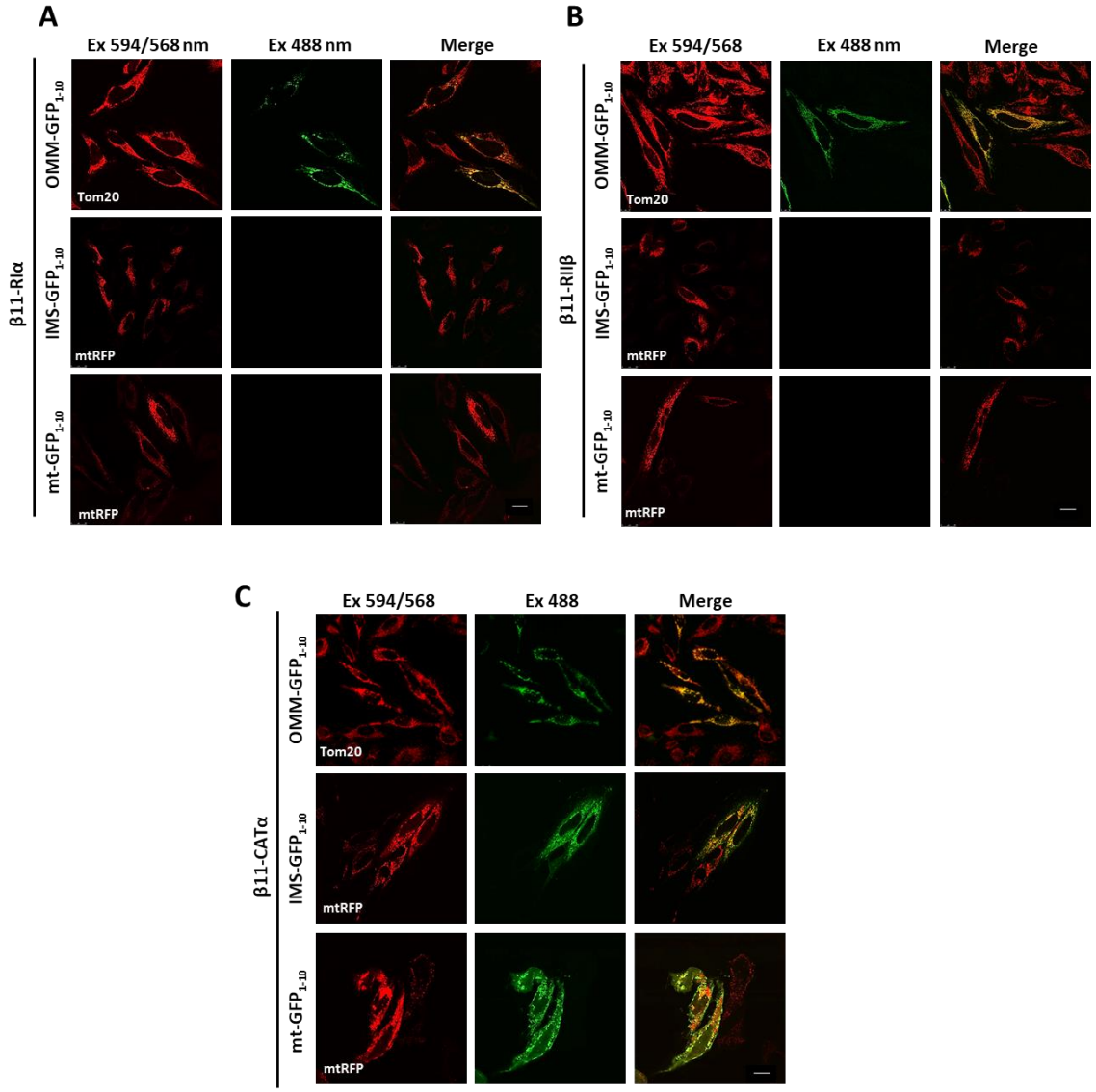

Figure 13 *Sub-mitochondrial localization of PKA subunits*. GFP_{1-10} constructs targeted to the OMM, IMS and mitochondrial matrix, and RIα (**A**), RIIβ (**B**) and CATα (**C**) fused to β11 fragment were transiently co-transfected in HeLa cells. Confocal images were acquired upon excitation at 488 and 594/568 nm wavelength. Where indicated, transfected cells were incubated with an anti TOM20 primary antibody and stained with an Alexa 594 conjugated secondary antibody or mtRFP protein is co-expressed as mitochondrial marker. Complementation of the GFP probes was revealed by fluorescent acquisition upon excitation at 488 nm wavelength. Scale bar, 25 μm.

The same experiment was performed in order to be sure that the absence of GFP reconstituted signal in the case of co-transfection of the IMS- and mt- GFP_{1-10} moieties and the RIα or the RIIβ subunits could depend on their low level of expression, we verified the expression of PKA subunits using specific antibodies. Immunocytochemistry analysis performed with RIα, RIIβ and CATα subunits-specific antibodies revealed a diffuse cytosolic pattern for all of them (Figure 14A-C, in red left panels).

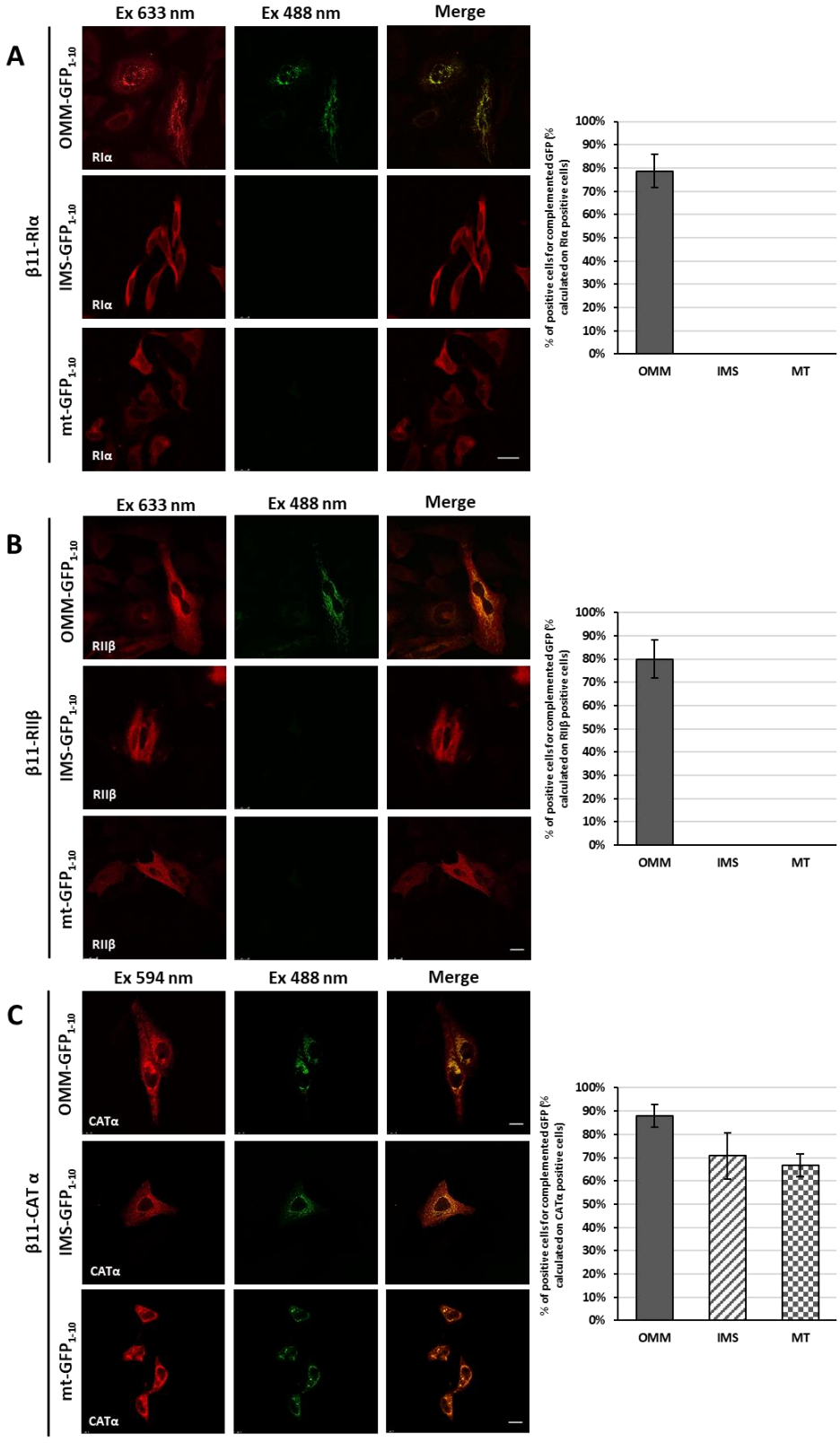

Figure 14 Targeted splitGFP chimeras complement with **A**) β11-RIα and **B**) β11-RIIβ at the OMM, **C**) β11-CATα at the OMM, in the IMS and in the mitochondrial matrix. Sub-mitochondrial localization of PKA subunits was analyzed by the co-expression of the OMM, IMS and mitochondrial matrix targeted GFP_{1-10} non-fluorescent and of the β11-PKA subunits. Confocal images were acquired upon excitation at 488 and 594/633 nm wavelength. Transfected cells were incubated with a primary antibody specific for each subunit and stained with an Alexa 594/633 conjugated secondary antibody. Scale bar 25 μm. Histograms on the right represent the quantitative analysis of positive cells for complemented GFP protein calculated on positive cells for PKA subunit overexpression.

To evaluate the possibility that not all the cells overexpressing RIα, RIIβ and CATα subunits displayed their mitochondrial distribution, we have also performed a quantitative analysis in which we have calculated the number of cells in which we have detected mitochondrial signal over the number of cells positive for the expression of RIα, RIIβ and CATα subunits. The histograms on the right of the panels of Figure 14 show the percentage of positive cells for complemented GFP protein at OMM, IMS and in the matrix calculated on positive cells for PKA RIα, RIIβ and CATα subunits overexpression. The quantification analysis revealed that about 80-90% of the cells that are positive for PKA RIα, RIIβ and CATα also display a OMM distribution of these subunits, and that about 65-70% of CATα positive cells shows also CATα in the IMS and in the mitochondrial matrix.

We have unequivocally demonstrated that the most abundant fraction of mitochondrially located PKA is present at the OMM level, as expected, where we have found both the CATα and the two regulatory subunits, RIα and RIIβ. Interestingly we have also found that a detectable fraction of overexpressed CATα subunit also resides in the IMS and in the mitochondrial matrix, but that, under the same conditions, the regulatory subunits, RIα and RIIβ, are not present in these two sub-mitochondrial compartments. Moreover, we have noticed that not all the cells that display CATα overexpression also show its presence in the IMS and in the mitochondrial matrix.

3.1.3. Could the regulatory subunits interfere with the entry of CATα subunit in the mitochondrial matrix?

At this point, we decided to address whether the co-expression of the regulatory subunits could interfere with the localization of the CATα subunit in the mitochondrial matrix. HeLa cells were co-transfected with GFP_{1-10} fragment targeted to mitochondrial matrix, the CATα subunit fused to β11 strand and the RIIβ subunit (Figure 15, upper panels). The confocal analysis of the triple transfected cells did not reveal the reconstitution of GFP protein, suggesting that the overexpressed RIIβ subunit could interfere with the entry of CATα subunit in the mitochondrial matrix. The same experiment was performed by co-expressing the RIα subunit instead of the RIIβ subunit: interestingly, when CATα is co-expressed with the RIα subunit we detected the signal for GFP complementation in the mitochondrial matrix (Figure 15, lower panels). It has to be noted that, in the case of CATα and RIα subunit co-transfected cells the percentage of positive cells for complemented GFP protein in the mitochondrial matrix is 52% ± 0.076 of the CATα subunit positive cells. This percentage is slightly lower in respect with the percentage calculated for cells transfected with CATα alone

that was around 67%, but the two values are not statistically different. The expression of the three PKA subunits was verified by the incubation with an anti-CAT antibody (probed with an Alexa405 conjugated secondary antibody, left panels in blue), by anti-RIIβ antibody (probed with an Alexa633 conjugated secondary antibody, middle upper panels in red) and by anti-RIα antibody (probed with an Alexa633 conjugated secondary antibody, middle lower panels in red).

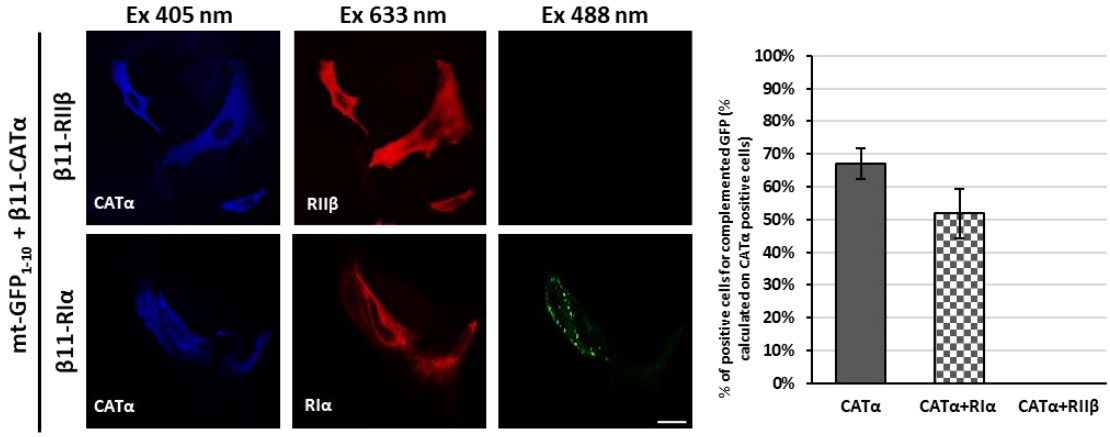

Figure 15 Co-expression of β11-CATα subunit with β11-RIIβ (upper panels) or β11-RIα (lower panels). Confocal images were acquired at 405, 633 and 488 nm excitation wavelength. Transfected cells were incubated with a primary antibody specific for each subunit and stained with an Alexa 405 conjugated secondary antibody for CATα subunit and Alexa 633 conjugated secondary antibody for RIIβ and RIα. Complementation of the GFP probes was revealed by fluorescent acquisition at 488 nm excitation wavelength. Scale bar 25μm. Histograms on the right represent the quantitative analysis of positive cells for complemented GFP protein calculated on PKA subunit positive cells in CATα overexpressing cells and in CATα and RIα or RIIβ co-expressing cells.

A positive signal was detected in all the cases, thus excluding he possibility that the absence of complementation could be due to the low expression of the GFP_{1-10} completing β11 fragment. These observations suggest that the RIα subunit is not able to prevent the localization of CATα subunit in the mitochondrial matrix.

To exclude the possibility that the absence of the GFP complementation signal in the mitochondrial matrix upon co-expression of the CATα and the RIIβ subunits could depend on lower amount of CATα in respect with the cells that express it alone, a Western blotting analysis was performed on cellular fractions obtained by HeLa cells single or double transfected. Figure 16 shows the results: the membranes were incubated with anti-CATα, anti-RIα and anti-RIIβ primary antibodies, respectively; an anti-GAPDH primary antibody was used as a marker for equal loading of total proteins. The anti-CATα antibody revealed a faint band at about 40 kDa in the control cells which represents the endogenous amount of CATα. A slightly higher band of about 45 kDa (due to the fusion with the β11 fragment) was visible in the lanes corresponding to HeLa cells transfected with CATα subunit alone or

together with the RIα and RIIβ subunits. In all the three cases, CATα is significatively overexpressed. The amount of CATα subunit is higher when it is co-expressed with RIIβ or RIα subunits than when it was overexpressed alone, as shown by the histograms on the right. These results suggest that in the double transfected cells the CATα subunit is more stable (Figure 16A).

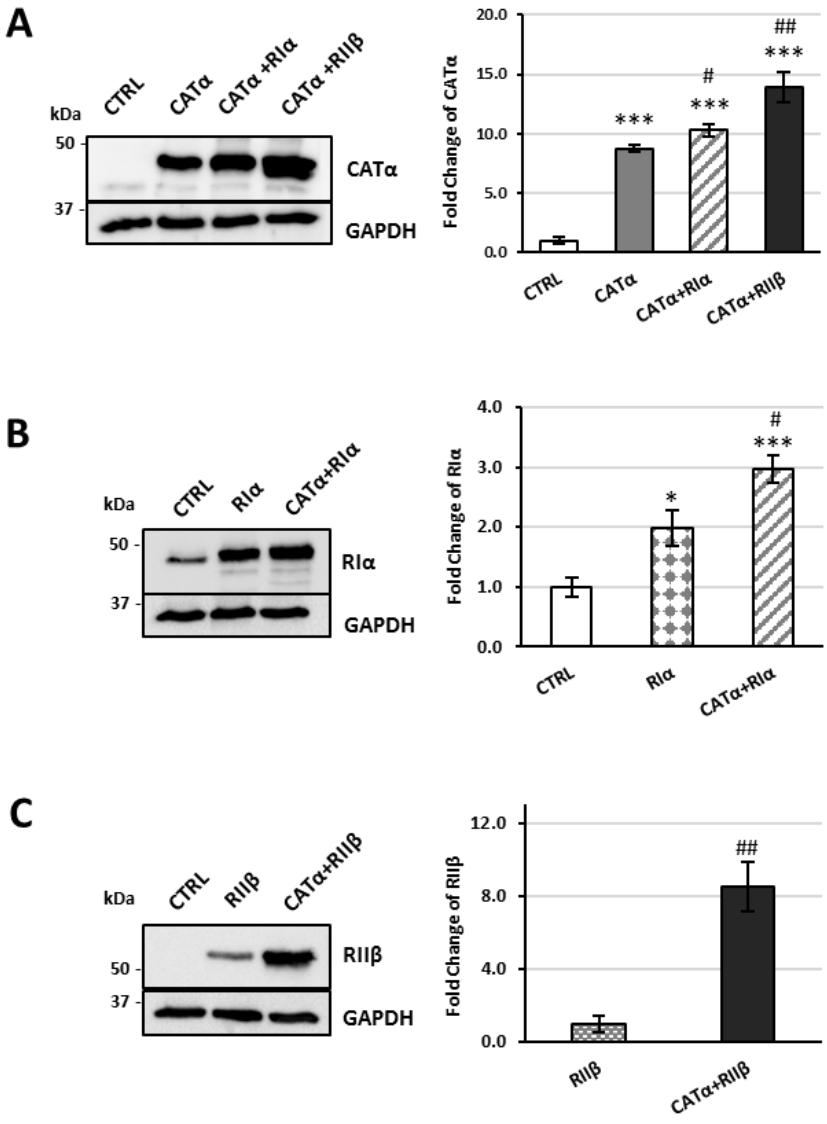

Figure 16 . *Expression levels of overexpressed PKA subunits in HeLa cells*. HeLa cells were transfected with **A**) CATα, CATα and RIα, CATα and RIIβ expression plasmids and analyzed by Western blotting with an anti-CATα antibody, **B**) RIα, CATα and RIα expression plasmids and analyzed by Western blotting with an anti RIα antibody, **C**) RIIβ, CATα and RIIβ expression plasmids and analyzed by Western blotting with an anti RIIβ antibody. Equal loading was verified by probing the membrane with an anti GAPDH antibody. Histograms on the right are relative to the quantification analysis of the expression levels of PKA subunits. (# $p \leq 0.05$ vs single transfection; ## $p \leq 0.01$ (CATα in panel A or RIα in panel B or RIIβ in panel C); * $p \leq 0.05$ vs control; ** $p \leq 0.01$ vs control; *** $p \leq 0.001$ vs control).

Similarly, when we develop the membranes with anti-RIα (Figure 16B) or anti-RIIβ (Figure 16C) primary antibodies, we detected specific bands with the correct molecular weight (about 47 kDa for the band relative to RIα; and about 52 kDa for the band relative to RIIβ). No endogenous RIIβ band was present in HeLa cells. The histograms on the right show that also the levels of the RIIβ or RIα subunits are higher when they are co-expressed with CATα subunit than when expressed alone. These results exclude the possibility that the absence of mt-GFP_{1-10}/β11-CATα reconstitution in the presence of co-expressed RIIβ subunit could depend on low expression levels of CATα.

3.1.4. CATα modulates mitochondrial and cytosolic Ca^{2+} handling

As previously documented by another group, the pharmacological activation of PKA by forskolin is able to rescue impairment in mitochondrial Ca^{2+} efflux in PINK1 KO cells by activating NCLX (Kostic et al., 2015). Considering this aspect and the localization of CATα in the mitochondrial matrix that we have observed using the splitGFP methodology, we decided to directly investigate the effect of CATα overexpression on mitochondrial Ca^{2+} handling. We directly monitored Ca^{2+} transients generated upon cell stimulation by the recombinant photoprotein Ca^{2+} sensitive aequorin targeted to the mitochondrial matrix (mtAEQ) or untargeted and expressed in the cytoplasm (cytAEQ) (Ottolini et al., 2014).
Figure 17A shows the monitoring of mitochondrial Ca^{2+} concentration upon stimulation with the IP_3-generating agonist histamine (100 μM) in HeLa cells transfected with mtAEQ. Upon histamine application, mitochondria accumulate Ca^{2+} inside the matrix through the activation of the MCU complex. The Ca^{2+} transient reaches a peak and then rapidly declines to basal levels thanks to the action of NCLX mediated efflux.

In the case of CATα overexpressing cells we observed a strong reduction in mitochondrial Ca^{2+} transients in respect with control cells. The average peak values were 51.83 ± 1.368 μM, n = 46 for control cells and 19.02 ± 1.185 μM, n = 28 for CATα overexpressing cells ($p < 0.001$). To verify whether this effect was specific for mitochondrial Ca^{2+} transients we also monitored cytosolic Ca^{2+} transients upon CATα overexpression and histamine stimulation. A reduction in the peak amplitude of the Ca^{2+} transients was observed in CATα overexpressing cells upon stimulation in respect with control cells (Figure 17B). The average peak values were 2.5 ± 0.052 μM, n = 22 for control cells and 1.434 ± 0.058 μM, n = 9 for CATα overexpressing cells ($p < 0.001$).

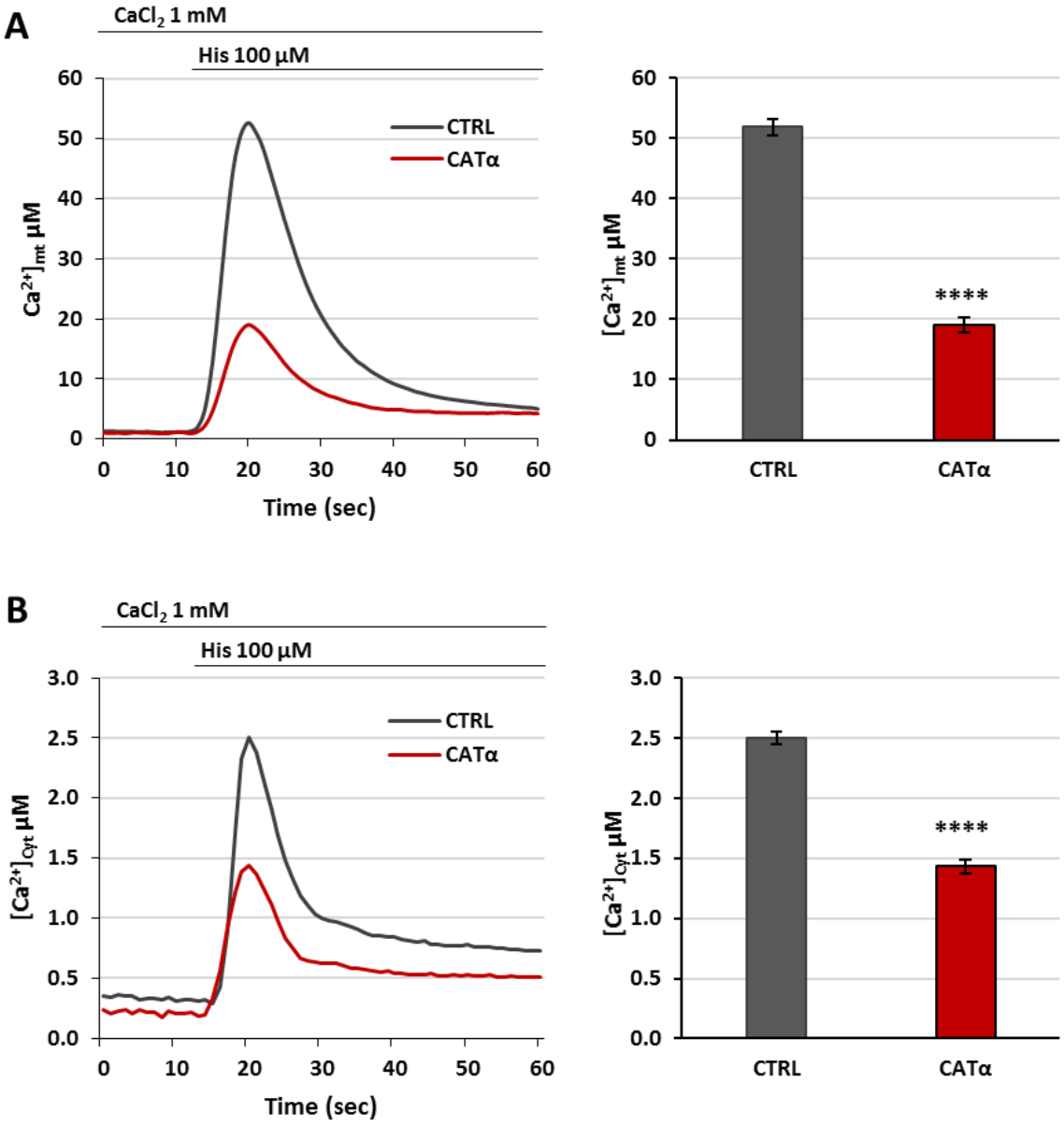

Figure 17 *CATα subunit reduces mitochondrial and cytosolic Ca^{2+} transients.* **A**) Mitochondrial $[Ca^{2+}]_{mt}$, **B**) cytosolic $[Ca^{2+}]_{Cyt}$ Ca^{2+} transients in control (CTRL) HeLa cells or overexpressing CATα are shown. Cells were transfected with AEQ (either mitochondrial or cytosolic) in control cells or co-transfected with AEQ and CATα. The traces are the media of at least 9 independent measurements obtained from 3 independent transfections. The histograms on the right represent the quantification of the average peak values of $[Ca^{2+}]_{mt}$ and $[Ca^{2+}]_{Cyt}$ in control or in cells overexpressing CATα ($[Ca^{2+}]_{mt}$ µM: 51.83 ± 1.37 n=46 for control cells; 19.02 ± 1.19 n=28 for CATα, $p <$ 0.001 vs control; $[Ca^{2+}]_{Cyt}$ µM: 2.50 ± 0.052 n=22 for control cells; 1.43 ± 0.058 n=9 for CATα, **** $p < 0.00001$ vs control.

To investigate whether the effects of CATα overexpression on mitochondrial Ca^{2+} transients could be attributed, at least partially, to the amount of CATα resident in the mitochondrial matrix we decided to selectively express it inside the matrix by using a construct that has been developed by Prof. K. Lefkimmiatis (Institute of Neurosciences, CNR, Venetian Institute of Molecular Medicine, Padua) (Lefkimmiatis et al., 2013), in which the CATα

subunit was fused to the mitochondrial pre-sequence of the subunit VIII of the human cytochrome c oxidase at the N-terminal and to the red fluorescent protein mCherry at the C-terminal (mito-PKACat-mCherry, referred as mtCATα).

The expression and the mitochondrial localization of mtCATα were evaluated by confocal and Western blotting analysis. Figure 18A shows on the left panel the mitochondrial distribution of the red fluorescence relative to mCherry emission and on the right the blot incubated with anti CATα primary antibody. In the first lane the level of the endogenous CATα is appreciable, in the second lane two bands are visible: the lower is relative to endogenous CATα and the higher, of about 70 kDa corresponds to the molecular weight of the fusion protein CATα-mCherry.

Once we had verified that mtCATα was correctly expressed in our HeLa cells, we monitored the effects of its overexpression on mitochondrial Ca^{2+} transients. Interestingly, we have found that the selective expression of CATα in the matrix is able to reduce the mitochondrial Ca^{2+} transients (Figure 18B). The average peak values were 51.83 ± 1.368 µM, n = 46 for control cells and 30.08 ± 1.017 µM, n = 21 for mtCATα overexpressing cells ($p < 0.001$). No differences were instead detected in cytosolic Ca^{2+} transients between mtCATα overexpressing and control cells (Figure 18C**;** $[Ca^{2+}]_{Cyt}$: 2.5 ± 0.052 µM, n = 22 for control cells and 2.356 ± 0.046, n = 10 for mtCATα overexpressing cells. These findings are very intriguing since they suggest that the action of CATα inside the mitochondrial matrix has a specific effect on mitochondrial Ca^{2+} transients, being cytosolic Ca^{2+} levels unaffected by its overexpression.

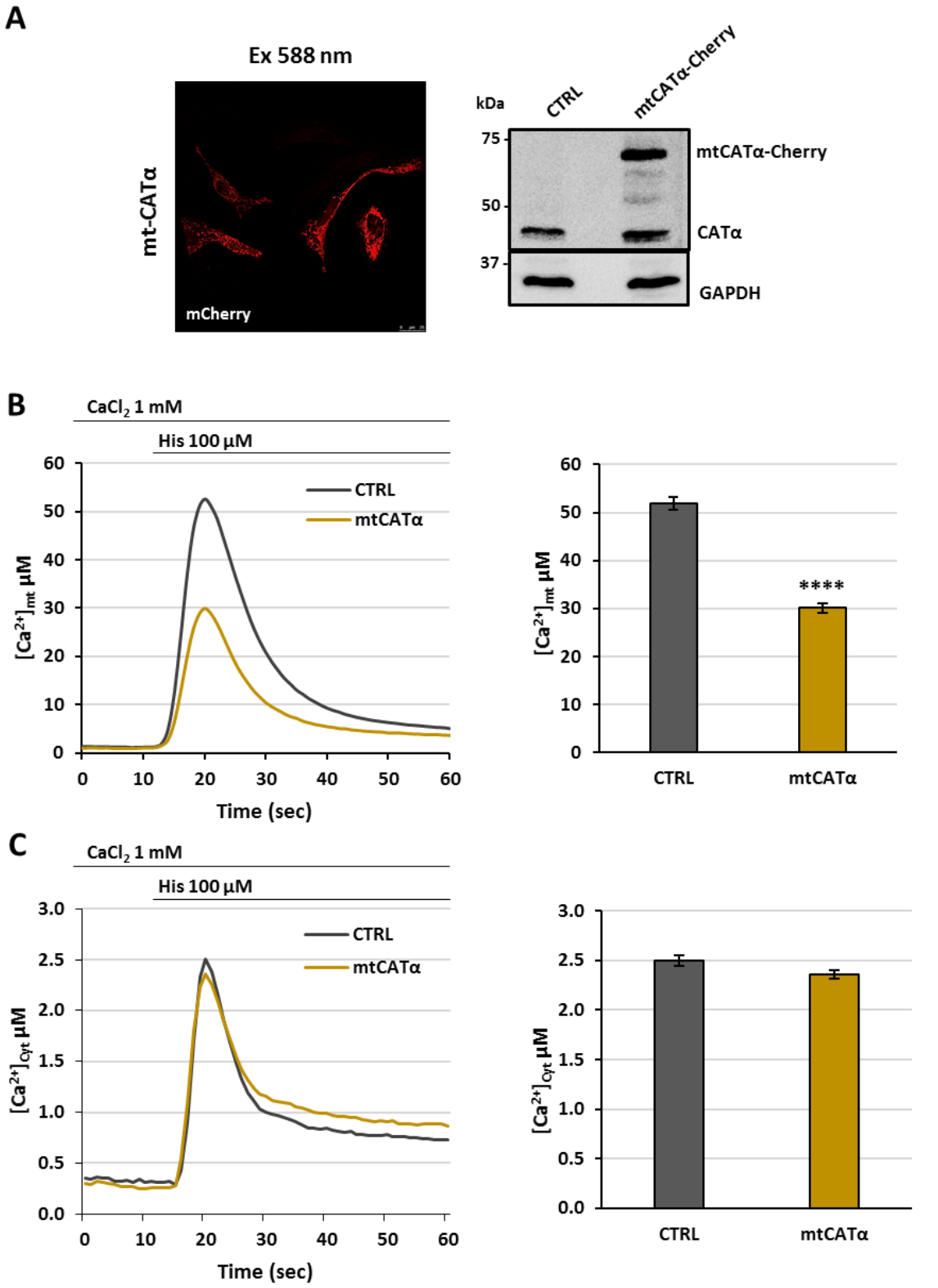

Figure 18 A) Mitochondrial localization and expression level of mtCATα-mCherry were evaluated by confocal and western blotting analysis. **B-C**) *The artificial targeting of CATα (mtCATα) subunit to the mitochondrial matrix reduces mitochondrial but not cytosolic Ca^{2+} transients.* A) Mitochondrial $[Ca^{2+}]_{mt}$, B) cytosolic $[Ca^{2+}]_{Cyt}$ Ca^{2+} transients in control (CTRL) HeLa cells or overexpressing mtCATα are shown. Cells were transfected with AEQ (either mitochondrial or cytosolic) in control cells or co-transfected with AEQ and mtCATα. The traces are the media of at least 10 independent measurements obtained from 3 independent transfections. Quantification of $[Ca^{2+}]_{mt}$ and $[Ca^{2+}]_{Cyt}$ in control cells or overexpressing mtCATα ($[Ca^{2+}]_{mt}$ µM: 51.83 ± 1.37 n=46 for control cells; 30.08 ± 1.017 n=21 for mtCATα, **** $p < 0.0001$ vs control; $[Ca^{2+}]_{Cyt}$ µM: 2.50 ± 0.052 n=22 for control cells; 2.356 ± 0.046 n=10 for mtCATα, **** $p < 0.00001$ vs control).

The experiments shown above suggest that the mitochondrial Ca^{2+} uptake is modulated by the presence of CATα in the matrix. Since we have observed that the co-expression of RIIβ prevented CATα to reach the mitochondrial matrix, we evaluated the mitochondrial Ca^{2+} uptake when CATα subunit is co-expressed with the RIIβ subunit. Interestingly, the effect of CATα overexpression on mitochondrial Ca^{2+} transients was almost completely abolished in presence of RIIβ subunit (Figure 19A; Average peak values 19.02 ± 1.185 µM, n = 28 for CATα overexpressing cells; 43.76 ± 2.013 µM, n = 24 for CATα and RIIβ co-expressing cells; $p < 0.0001$).

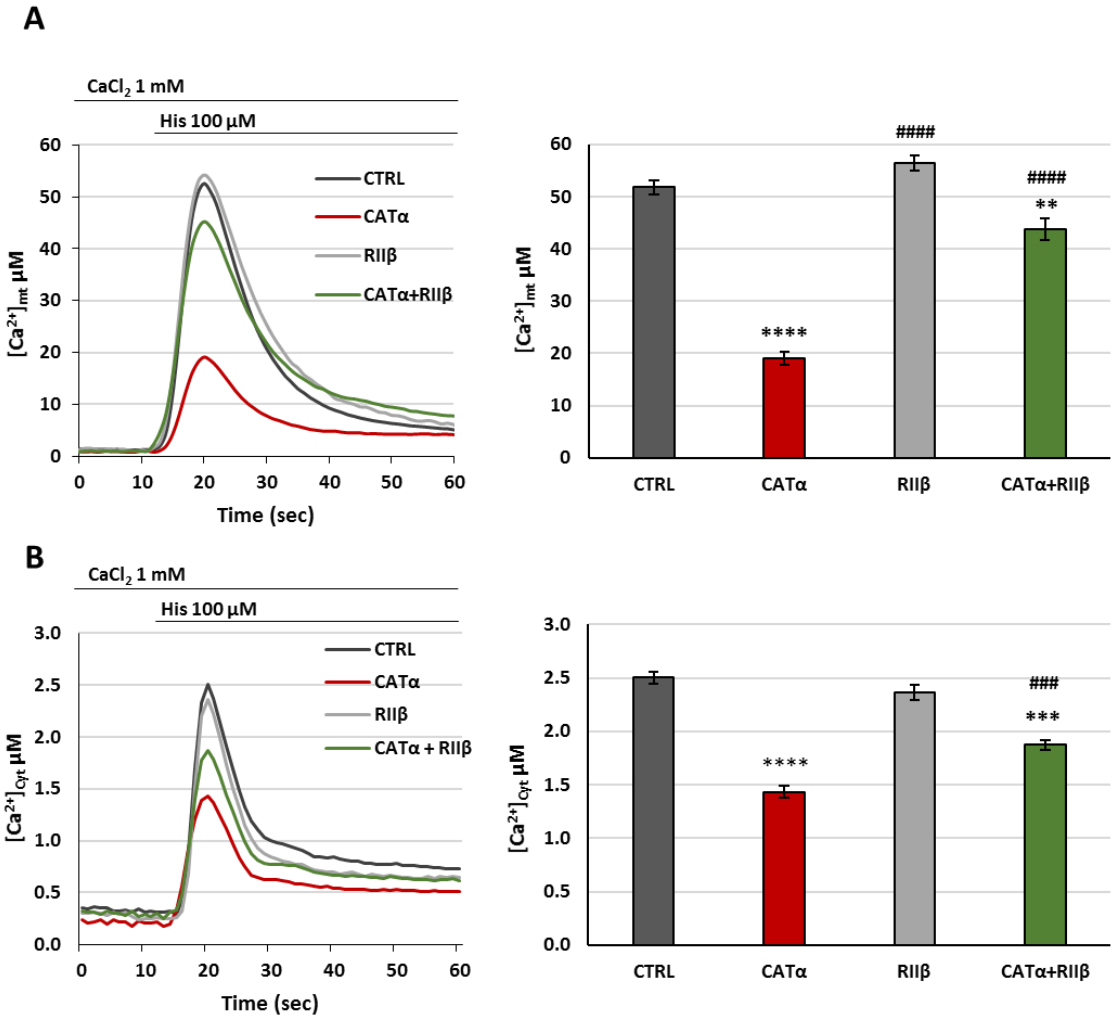

Figure 19 *RIIβ subunit almost abolishes CATα-induced reduction of mitochondrial and cytosolic Ca^{2+} transients.* **A**) Mitochondrial $[Ca^{2+}]_{mt}$, **B**) cytosolic $[Ca^{2+}]_{Cyt}$ Ca^{2+} transients in control (CTRL) HeLa cells or in cells overexpressing CATα or RIIβ alone or co-expressing CATα and RIIβ are shown. Cells were transfected with AEQ (either mitochondrial or cytosolic) in control or co-transfected with AEQ and the indicated constructs for PKA subunits expression. The traces are the media of at least 8 independent measurements obtained from 3 independent transfections. Quantification of $[Ca^{2+}]_{mt}$ and $[Ca^{2+}]_{Cyt}$ in control cells or overexpressing CATα or RIIβ alone or co-expressing CATα and RIIβ ($[Ca^{2+}]_{mt}$ µM: 51.83 ± 1.37 n=46 for control cells; 19.02 ± 1.19 µM n = 28 for CATα overexpressing cells; 56.47 ± 1.47µM n= 8 for RIIβ overexpressing cells; 43.76 ± 2.013 µM n=24 for CATα and RIIβ co-expressing cells; $[Ca^{2+}]_{Cyt}$ µM: 2.50 ± 0.052 n=22 for control cells; 2.363 ± 0.067 n=11 for RIIβ; 1.43 ± 0.058 n=9 for CATα, 2.356 ± 0.046 µM n=12 for CATα and RIIβ co-expressing cells; ** $p \leq 0.001$ vs control; *** $p < 0.0001$ vs control; **** $p < 0.00001$ vs control; ### $p < 0.0001$ *vs* overexpressed CATα; #### $p < 0.00001$ vs overexpressed CATα).

The same effect was obtained on cytosolic Ca^{2+} transients (Figure 19B**;** Average peak values 1.434 ± 0.058 µM, n = 9 for CATα overexpressing cells; 2.356 ± 0.046 µM, n = 12 for CATα and RIIβ co-expressing cells; $p < 0.0001$). Figure 19 also shows the mitochondrial and cytosolic Ca2+ transients measured in control cells and in cells transfected only with the RIIβ subunits. The overexpression of RIIβ subunit did not affect mitochondrial and cytosolic Ca2+ transients.

At this point, we evaluated whether the ability of the RIIβ subunit was isoform specific and we monitored the mitochondrial Ca^{2+} transients in cells co-expressing CATα together with the regulatory subunit RIα. The results are shown in Figure 20**:** no effect was observed on the reduction of mitochondrial Ca^{2+} transients induced by the CATα upon RIα co-expression (19.018 ± 1.185 µM, n = 28 for CATα overexpressing cells; 16.961 ± 1.724 µM, n = 7 for CATα and RIα co-expressing cells).

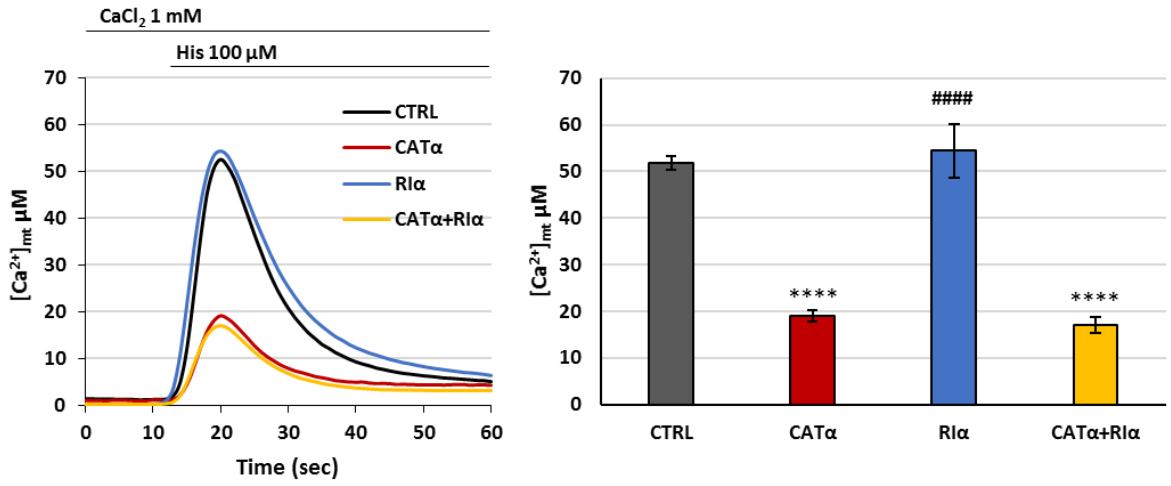

Figure 20 *RIα subunit does not abolish CATα-induced reduction of mitochondrial and cytosolic Ca^{2+} transients.* Mitochondrial $[Ca^{2+}]_{mt}$, Ca^{2+} transients in control (CTRL) HeLa cells or in cells overexpressing CATα or RIα alone or co-expressing CATα and RIα are shown. Cells were transfected with AEQ in control cells or co-transfected with AEQ and the indicated constructs. The traces are the media of at least 5 independent measurements obtained from 3 independent transfections. Quantification of $[Ca^{2+}]_{mt}$ control cells or overexpressing CATα or RIα alone or co-expressing CATα and RIα ($[Ca^{2+}]_{mt}$ µM: 51.83 ± 1.37 n=46 for control cells; 19.02 ± 1.19 µM n = 28 for CATα overexpressing cells; 54.40 ± 5.79 µM n= 8 for RIα overexpressing cells; 16.96 ± 1.72 µM n=7 for CATα and RIα co-expressing cells; **** $p < 0.00001$ vs control; #### $p < 0.00001$ vs overexpressed CATα).

By following the same approach, we decided to test whether the co-expression of the RIIβ subunit was also able to abrogate the effect of the CATα subunit selectively targeted to the mitochondrial on mitochondrial Ca^{2+} transients. Unexpectedly, the reduction of mitochondrial Ca^{2+} transients upon mtCATα overexpression was completely abolished in cells co-expressing mtCATα and RIIβ (Figure 21A; Average peak values: 30.08 ± 4.981

µM, n = 21 for mtCATα overexpressing cells; 56.343 ± 2.740 µM, n = 9 for mtCATα and RIIβ co-expressing cells; $p < 0.0001$).

Figure 21A also shows the mitochondrial Ca^{2+} transients measured in control cells and in cells transfected only with the RIIβ subunits. The average peak values between control cells and mtCATα and RIIβ co-expressing cells are not statistically different, i.e. 51.83 ± 1.368 µM, n = 46 for control cells vs 30.08 ± 4.981 µM, n = 21 for mtCATα overexpressing cells.

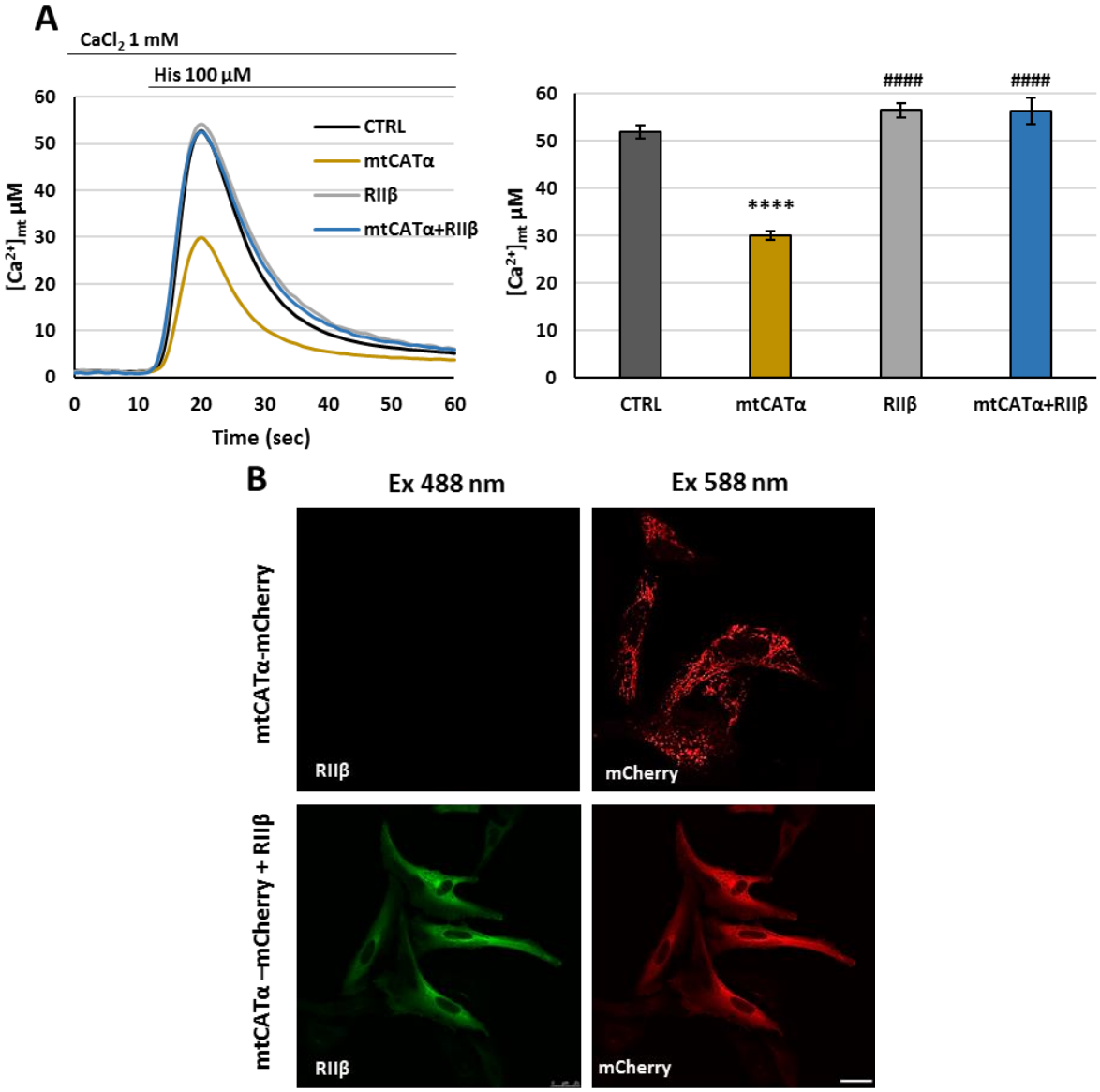

Figure 21 *RIIβ subunit totally abolishes mtCATα-induced reduction of mitochondrial Ca^{2+} transients.* **A**) Mitochondrial $[Ca^{2+}]_{mt}$ Ca^{2+} transients in control (CTRL) HeLa cells or in cells overexpressing mtCATα or RIIβ alone or co-expressing mtCATα and RIIβ cells are shown. Cells were transfected with AEQ or co-transfected with AEQ and the indicated constructs. The traces are the media of at least 8 independent measurements obtained from 3 independent transfections. Quantification of $[Ca^{2+}]_{mt}$ in control cells or overexpressing mtCATα or RIIβ alone or co-expressing mtCATα and RIIβ ($[Ca^{2+}]_{mt}$ µM: 51.83 ± 1.37 n=46 for control cells; 30.08 ± 1.017 n=21 for mtCATα; 56.47 ± 1.47µM n= 8 for RIIβ overexpressing cells; 56.34 ± 2.74 µM n=9 for mtCATα and RIIβ co-expressing cells; **** $p < 0.00001$ vs control; #### $p < 0.00001$ vs overexpressed mtCATα). **B**) Distribution of mtCATα when it is expressed alone (upper panel) and when it is co-expressed with RIIβ subunit (lower panel). The co-expression of RIIβ subunit is shown in green. Scale bare 25 µm.

To explain this unexpected result, we performed an immunocytochemistry analysis on HeLa cells transfected with the mtCATα and the RIIβ subunit and checked for mitochondrial distribution of mtCATα. Figure 21B shows a direct comparison between the distribution of mtCATα expressed alone (upper panel) with mtCATα co-expressed with RIIβ (lower panel). The co-expression of RIIβ subunit has been revealed by the incubation with Alexa 488 secondary antibody and shown in green. By the representative confocal images shown in Figure 11B it is quite evident that mitochondrial distribution of mtCATα is completely prevented in the cells co-expressing the RIIβ despite of the presence of exogenous mitochondrial targeting sequence. The mtCATα displays a clear cytosolic distribution in the lower right panel. These results gain further insights into the specificity of RIIβ subunit to regulate the activity and the localization of CATα at the mitochondrial levels: CATα subunit exerts its action on the mitochondrial Ca^{2+} handling acting inside the matrix and it can get in only when it is not engaged with the RIIβ subunit.

3.1.5. Possible mitochondrial targets for PKA protein action on mitochondrial Ca^{2+} handling

To investigate whether the effects of CATα overexpression on mitochondrial Ca^{2+} transients were due to the modulation of the Ca2+ uptake or the Ca^{2+} efflux mechanisms we have performed preliminary experiments in which these two pathways were pharmacologically or genetically manipulated (Figure 22). In Figure 22A we monitored mitochondrial Ca^{2+} transients in cells treated with the specific inhibitor CGP37157 of the NCLX. As expected, when control cells are treated with CGP37157, the amplitude of the mitochondrial Ca2+ transients was increased because of the inhibition of the main mitochondrial Ca^{2+} efflux pathway. When CGP37157 was incubated in mtCATα overexpressing cells, the mtCATα-mediated reduction of mitochondrial Ca^{2+} transients was still observed (compare the pale grey and the green histograms on Figure 12A) suggesting that either mtCATα could overcome pharmacological inhibition of NCLX or the target of its action could be different from the NCLX (Average peak values: 66.606 ± 5.664 μM, n = 8 for control cells; 98,919 ± 4.517 μM, n = 5 for CGP37157 treated control cells and 67.314 ± 1.299 μM, n = 6 for CGP37157 treated mtCATα overexpressing cells; $p < 0.0001$ treated control cells vs. control and treated control cells vs treated mtCATα overexpressing cells).

Then, we evaluated mitochondrial Ca^{2+} transients upon the overexpression of the MCU pore forming subunit in the absence or in the presence of co-expressed mtCATα (Figure 22B).

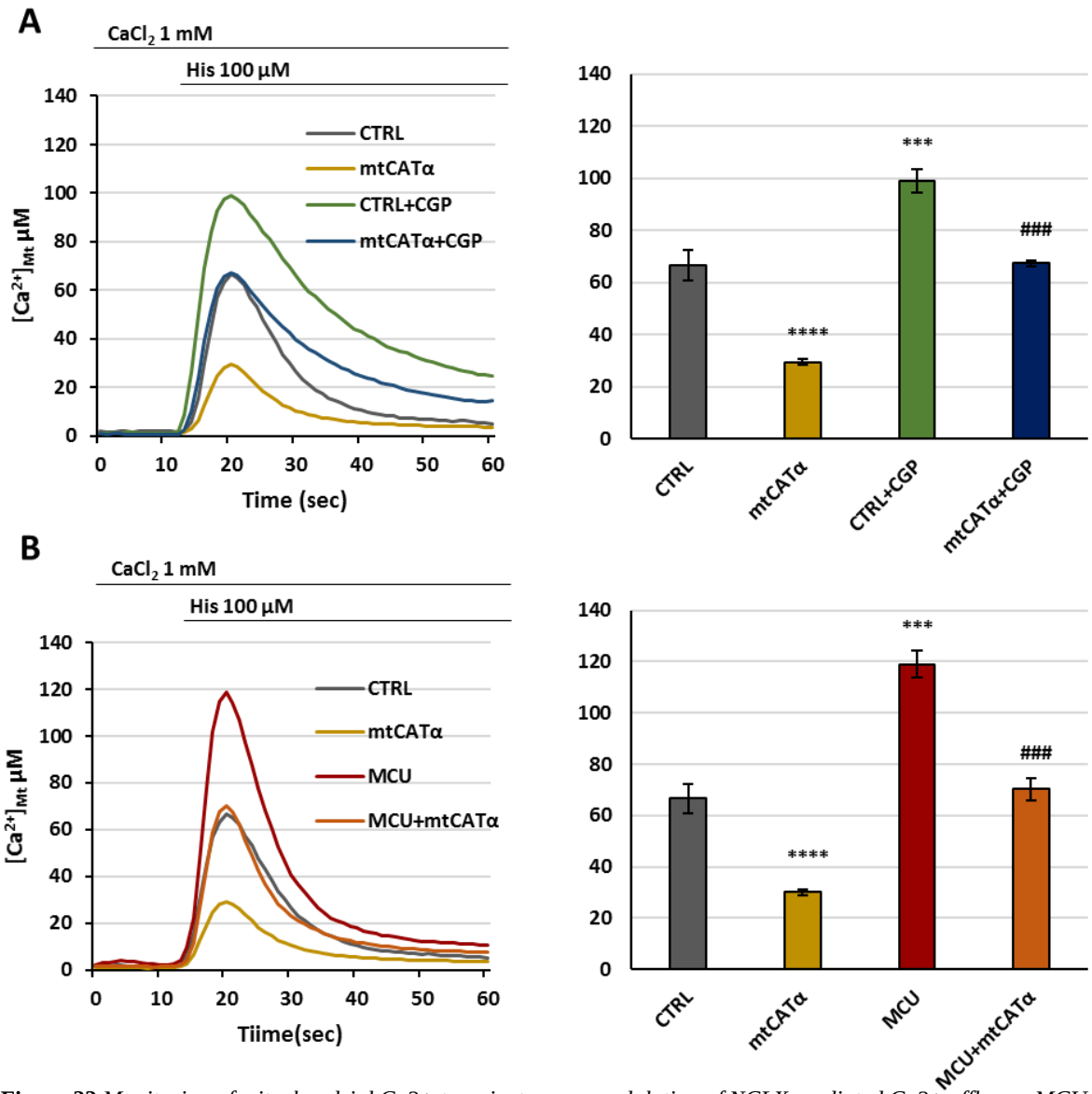

Figure 22 *Monitoring of mitochondrial Ca2+ transients upon modulation of NCLX-mediated Ca2+ efflux or MCU-mediated Ca2+ uptake in cells overexpressing* mtCATα. Mitochondrial $[Ca^{2+}]_{mt}$ Ca^{2+} transients in A) untreated and CGP37157 treated control (CTRL) or in CGP37157 treated overexpressing mtCATα overexpressing cells, and in B) control cells (CTRL) or in cells overexpressing MCU alone or along with mtCATα. The traces are the media of at least 7 independent measurements obtained from 3 independent transfections ($[Ca^{2+}]_{mt}$ µM: 66.61 ± 5.66 n=8 for control cells; 98.92 ± 4.52 n=5 for CGP treated control cells; 67.31 ± 1.30 for CGP treated mtCATα; 118.98 ± 5.15 µM n= 7 for MCU overexpressing cells; 70.20 ± 4.28 µM n=9 for mtCATα and MCU co-expressing cells; ** $p <$ 0.001 vs control; *** $p <$0.0001 vs control; **** $p <$0.00001 vs control; ### $p <$ 0.0001 vs CGP treated control cells or overexpressed MCU).

As expected, the overexpression of MCU enhanced mitochondrial Ca^{2+} uptake (compare the violet histogram with the black one). Interestingly, in the case of MCU and mtCATα co-expression, we observed that the mitochondrial Ca^{2+} transients are similar to those monitored in control cells (Average peak values: 66.606 ± 5.664 µM, n = 8 for control cells; 118.98 ±

5.146 µM, n = 7 for MCU co-expressing cells; 70.196 ± 4.275 µM, n = 6 for mtCATα + MCU overexpressing cells, p < 0.0001 MCU vs. control, and MCU vs mtCATα + MCU). These results indicate that mtCATα overexpression abolishes the effect of MCU overexpression on mitochondrial Ca^{2+} transients. Further experiments are necessary to better understand these results.

In the end, having in mind that a neuroprotective role for PKA protein has been proposed in model cell for PINK1 loss of function, we decided to carry out pilot experiments to explore a possible interplay between PKA and PINK1. In this case we took advantage from the characterization in terms of mitochondrial Ca2+ levels that we have done in PINK1 loss of function model cells. Indeed, we have evaluated mitochondrial Ca^{2+} levels in resting condition (Figure 23A) and upon cell stimulation with histamine (Figure 23B) in embryonic mouse fibroblast obtained from PINK1 knock out mice and PINK1 KO MEF cells and found that they are both elevated in respect with the levels measured in control PINK1 WT MEF (see the histograms in Figure 23A and B for the quantification). Mitochondrial Ca2+ levels in resting condition were measured by transfecting the ratiometric mitochondrial Ca^{2+} indicator 2mtGCaMP (Vicario and Calì, 2019); mitochondrial Ca^{2+} levels upon cell stimulation were measured by mtAEQ. Panel A also shows that when PINK1 WT protein was reintroduced in PINK1KO MEF cells it can counteract mitochondrial Ca^{2+} overload observed in the absence of PINK1.

At this point, we decided to challenge our splitGFP tool to monitor PKA distribution in the mitochondrial matrix in PINK WT and KO MEF cells. MEF cells were co-transfected with mt-GFP_{1-10} and CATα tagged with the β11 strand and observed at the confocal microscope (Figure 23C). We observed that complementation of the splitGFP occurred in the mitochondrial matrix of both the cell batches, confirming our previous findings obtained in HeLa cells and showing the presence of CATα in the mitochondrial matrix. Interestingly, upon quantification of the cells displaying mitochondrial CATα distribution we have found that the percentage of cells showing CATα in the mitochondrial matrix is higher in PINK1 KO MEF cells than in control WT MEF (35.86% ± 0.021 for PINK1 WT MEF cells vs. 52.37% ± 0.031 for PINK1 KO MEF cells; $p < 0.01$). The overexpression of CATα was verified by immunostaining with anti- CATα antibody and revealed in red by the Alexa 594 secondary antibody.

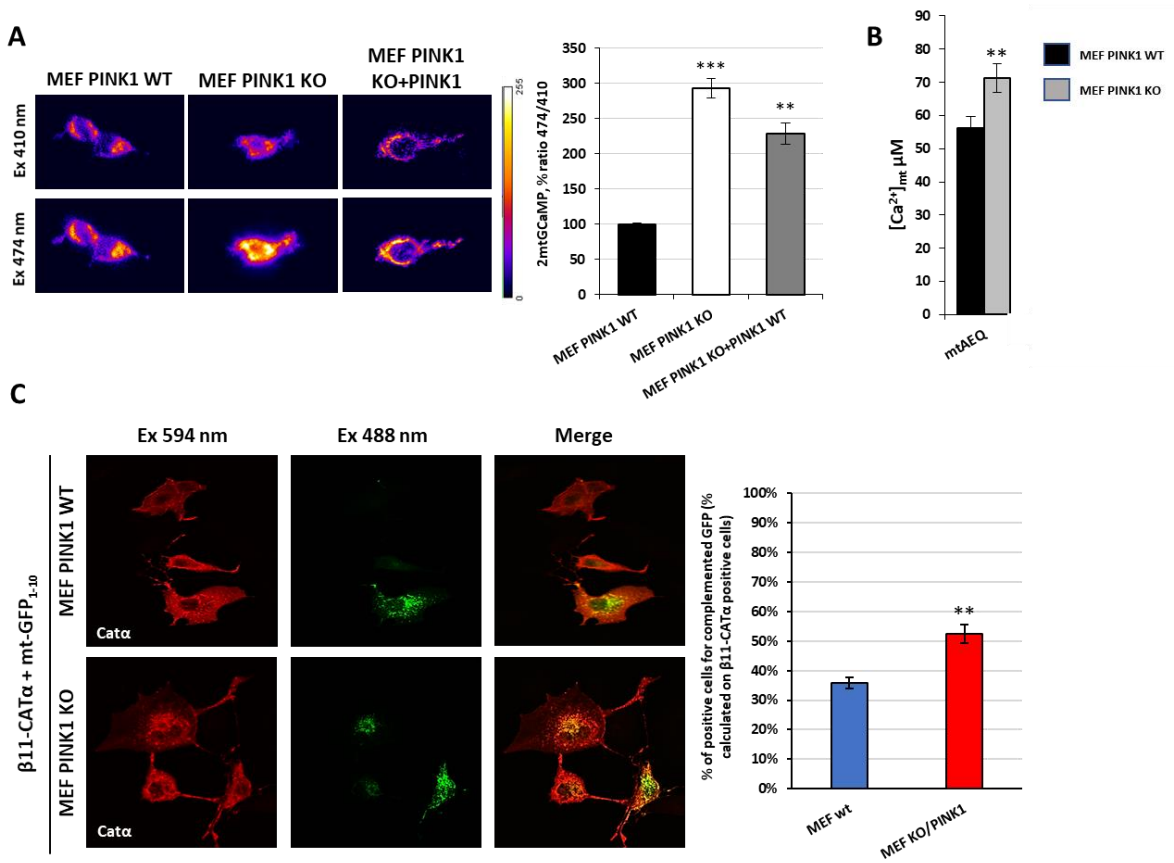

Figure 23 *Monitoring mitochondrial Ca2+ levels and PKA mitochondrial distribution in model cells for PINK1 loss of function.* Mitochondrial $[Ca2+]_{mt}$ Ca^{2+} levels in **A**) resting condition and **B**) upon cell stimulation. Average peak values 56.18 ± 3.46 n=20 for PINK1WT MEF; 71.20 ± 4.33 n=20 for PINK1 KO MEF). **C**) PKA localization in PINK1 WT MEF cells (upper panels) and in PINK1 KO MEF cells (lower panels). Sub-mitochondrial localization of PKA subunits was analyzed by the co-expression of the mitochondrial matrix targeted GFP_{1-10} non-fluorescent and of the β11-CATα subunit. Confocal images were acquired upon excitation at 488 and 594 nm wavelength. Transfected cells were incubated with an anti-CATα primary antibody and stained with an Alexa 594 conjugated secondary antibody. Complementation of the GFP probes was revealed by fluorescent acquisition at 488 nm excitation wavelength. Scale bar 25 µm. Histograms on the right represent a quantification analysis on percentage of positive cells for complemented GFP protein calculated on CATα subunit positive PINK1 WT MEF cells and PINK1 KO MEF cells (35.86% ± 0.021 for PINK1 WT MEF cells vs. 52.37% ± 0.031 for PINK1 KO MEF cells; ** $p < 0.01$ PINK1 WT MEF cells vs PINK1 KO MEF cells).

3.2. New SPLICS probes to detect ER-PM contact sites

3.2.1. Construction and validation of new probes based on the splitGFP System to detect ER-PM contact sites

Endoplasmic reticulum (ER) and plasma membrane (PM) junctions are involved in several processes critical for cell survival and death and the interest in their investigation from the structural and functional point of view is increased in the last years and it is demanding the development of new probes to study them dynamically.

In this contest, we decided to develop a new tool starting from the split-GFP contact site sensor (SPLICS) that has been originally developed to monitor ER/mitochondria contact sites. We applied a similar strategy to monitor ER-PM contact sites. We have taken in advantage the fact that the mutations responsible for the shift from the green fluorescence emission of the GFP to the yellow fluorescence of the YFP were present in the 1-10 beta barrel portion and that the S11 beta strand was able to complement with this portion to generate a probe of a different color. YFP protein was split into two non-fluorescent portions, the YFP_{1-10} moiety and the β11 strand. The coding sequence of the YFP_{1-10} fragment was fused at its N terminal region with a sequence of 35 amino acids which represents the minimal targeting sequence for the PM of the Synaptosomal-associated protein 25 (SNAP25) and the β11 strand is targeted to the ER by adding at its N terminal the minimal ER targeting sequence of Sac1, an ER membrane resident phosphatidylinositide phosphatase.

The sequences of the two tagged YFP fragments were cloned in the mammalian expression vector under the control of cytomegalovirus promoter. Since the average distance for the majority of contact sites between ER and PM was estimated by electron microscopy studies to be in the range of 40 nm, we have decided to develop two kinds of probe: one to monitor short contact sites, i.e., those that occurred at the distance of ≈8–10 nm, and another to monitor contact sites at a long-range distance, i.e., those occurring at a distance of ≈40–50 nm. The two constructs were created by introducing a spacer of different length between the ER targeting sequence and the β11 strand and were named respectively short fragment ER_S-β11 (with a 29 aa spacer) and long fragment ER_L-β11 (with a 146 aa spacer). These constructs, where the two YFP moieties were cloned in two different plasmids were used to verify that the strategy we have chosen for the targeting of the two YFP moiety was adequate. Then, to monitor ER-PM contact sites we further improve our probe in respect with the first version, since we developed a new construct to optimize the expression of the two YFP

portion. Indeed, we generated a construct where the PM-YFP$_{1-10}$ and the ER$_S$-β11 or ER$_L$-β11 were cloned in the same bicistronic expression vector, that guarantees the production of equimolar amount of the two YFP fragments. (Figure 24A). The ER$_{S/L}$-β11 and PM-YFP$_{1-10}$ coding sequences were respectively cloned upstream and downstream of a viral 2A peptide sequence (P2A), previously reported to be a skipping site for ribosome (Donnelly et al., 2001). These constructs will be hereafter named SPLICS$_S$ or SPLICS$_L$.

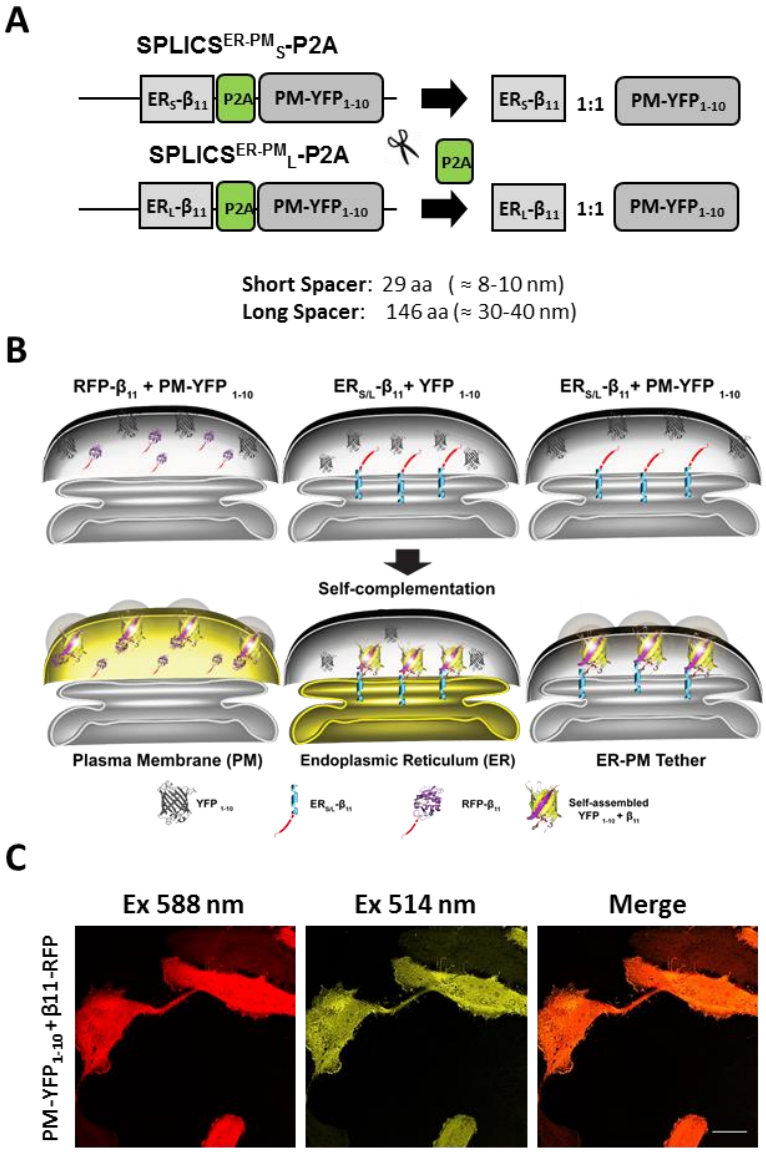

Figure 24 *Characterization of the SPLICS probes*. **A**) A schematic representation of SPLICS$_S$ (upper) and SPLICS$_L$ (lower) expression plasmids. The ER$_{S/L}$-β11 and PM-YFP$_{1-10}$ coding sequences are respectively cloned upstream and downstream of a viral 2A peptide sequence (P2A). ER$_S$-β11 and ER$_L$-β11 have a short 29 aa and a long 146 aa spacer, respectively, placed between the ER targeting sequence and the β11 strand. They were designed to monitor ER-PM tethering occurring at different membranes distance. **B**) The cartoon shows the general approach used to validate the proper targeting to the PM and the ER membrane of the YFP$_{1-10}$ and the β11 moieties and their ability to reconstitute the fluorescent signal upon reconstitution. **C**) Experimental controls showing the correct targeting of the PM (PM-YFP$_{1–10}$) by complementation with the cytosolic β11-RFP protein. Confocal images were acquired upon excitation at 588 and 514 nm wavelength for β11-RFP and YFP reconstitution, respectively. The correct targeting of the ER$_S$-β11 and ER$_L$- β11have been previously verified (Cieri et al., 2018). Scale bar 25 µm.

The strategy that we have applied to validate the targeting of the PM-YFP_{1-10} and the $ER_{S/L}$-β11 fragments is based on the co-expression of the PM-$YFP_{1–10}$ construct along with a plasmid encoding a β11-tagged cytosolic Red Fluorescent Protein (RFP, Kate) (Figure 24B, left panel) and of the $ER_{S/L}$-β11 constructs along with a cytosolic $YFP_{1–10}$ plasmid (Figure 24B, middle panel) and of the PM-$YFP_{1–10}$ along with the $ER_{S/L}$-β11 expression vectors (Figure 24B, right panel), respectively. By observing the appearance of fluorescent signal and its distribution in the three batches of co- transfected HeLa cells we expected to reveal the PM or the ER network, and the ER–PM contact sites as illustrate in the cartoon.

Here we show the results of the validation of the YFP_{1-10} delivery to the PM and its ability to reconstitute YFP fluorescence upon complementation with the β11 strand of the GFP. The complementation of the PM-$YFP_{1–10}$ fragment with the cytosolic β11-RFP protein (Figure 24C) revealed a clear PM network in yellow. Red signal is relative to RFP emission. The correct targeting of the $ER_{S/L}$-β11 constructs have been previously verified as indicated in Figure 24B and by the colocalization with ER resident proteins (Cieri et al., 2018).

Once established that the PM-$YFP_{1–10}$ protein was properly expressed and was able to complement, we employed the bicistronic probes to monitor ER-PM contact sites. $SPLICS_{S/L}$ were over-expressed in HeLa cells and 36 hours from transfection the coverslips with the cells were fixed and observed at the confocal microscope. Figure 25 shows representative confocal images illustrating our results. Upon excitation at 514 nm a clear yellow fluorescent dotted pattern appeared both in the case of the $SPLICS_S$ and the $SPLICS_L$ transfected cells (see left images in Figure 25).

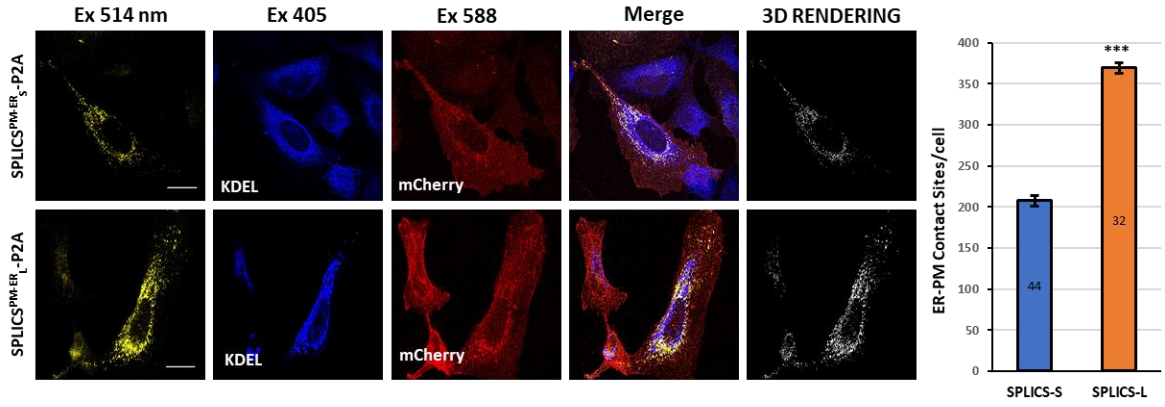

Figure 25 *Co-localization of $SPLICS_{S/L}$ fluorescent dots with PM (mCherry) and ER (KDEL) markers and their quantification.* Representative confocal pictures of HeLa cells expressing the $SPLICS_{S/L}$ probe and red fluorescent protein (mCherry) targeted to the PM. Transfected cells were incubated with an anti KDEL primary antibody as ER marker and stained with an Alexa 405 conjugated secondary antibody. Confocal images were acquired upon excitation at 405, 514 and 588 nm excitation wavelength. Scale bar 25 µm. Quantification of $SPLICS_{S/L}$ contacts by 3D rendering of complete z-stacks. Mean ± SEM: $SPLICS_S$ 208 ± 6, n = 44 cells; $SPLICS_L$ 369 ± 7, n = 32 cells. Data shown are the result of 3 independent experiments. *** $P \leq 0.001$.

Interestingly, dots quantification in the 3D rendering of a complete Z-stack for 3 independent experiments has revealed that the long and short ER-PM interactions appeared different for their number (right image Figure 25). We observed that in the cells overexpressing the $SPLICS_L$ probes the number of dots is higher than in those overexpressing the $SPLICS_S$ probes (Mean ± SEM: $SPLICS_L$ 369 ± 7, n = 32 cells vs $SPLICS_S$ 208 ± 6, n = 44 cells). Figure 25 also shows an immunocytochemistry analysis performed with an antibody against an endogenous marker of ER (KDEL, in blue) and the co-localization with an overexpressed mCherry protein targeted to the PM (in red) (left image Figure 25). By this approach we wanted to verify whether SPLICS reconstituted fluorescence colocalized with the area of ER-PM interactions. As shown in the merge panels of Figure 25, there are area of colocalization that appeared in white, but the ER and PM networks were not completely engaged in the formation of the ER–PM contacts reported by the SPLICS, suggesting that these probes are monitoring the ER-PM interactions occurring at a given moment.

3.2.2. Modulation of ER-PM contact sites inducing ER Ca^{2+} depletion and STIM1/ORA1 silencing

We next decided to verify whether our SPLICS probes were a good tool to monitor changes occurring in the ER-PM interactions upon the modulation of specific cellular pathways in which these kinds of interaction are of particular relevance. We considered the machinery that mediates Ca^{2+} influx from the extracellular ambient, the so-called Store-Operated Ca^{2+} Entry (SOCE). This process is induced as a consequence of Ca^{2+} depletion from the ER Ca^{2+} stores and it is dependent on the dynamic interaction between two proteins, the ER resident protein stromal interaction molecule 1 (STIM1), that acts as Ca^{2+} sensor, and Orai1, the protein forming the channel in the PM that permits Ca^{2+} entry from the extracellular ambient (Nwokonko & Gill, 2012). A representative scheme of the SOCE process is shown in the cartoon of Figure 26. ER Ca^{2+} depletion leads to oligomerization of STIM1 protein and its accumulation on ER-PM junctions. STIM1 activation induces conformational changes in Orai1 that lead to the opening of the channel and permit Ca^{2+} influx from extracellular space. Considering that the molecular details of the SOCE process are well established, we decided to genetically and pharmacologically manipulate it in order to investigate the behavior of our $SPLIC_{S/L}$ reporter upon changes in the ER-PM interface. First, we have analyzed the dots fluorescence revealed by $SPLICS_{S/L}$ upon induction of ER Ca^{2+} depletion in HeLa cells by the application of the ER Ca^{2}+ release inducing agonist histamine in the presence of the sarcoplasmic/endoplasmic reticulum Ca^{2+}-ATPase (SERCA pumps) inhibitor 2,5-tert-

butylhydroquinone (THBQ) to maximize ER Ca^{2+} depletion and avoid Ca^{2+} reuptake in the ER.

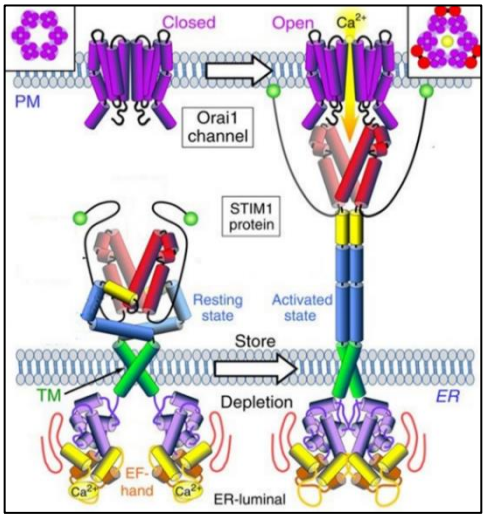

Figure 26 *Store-Operated Ca^{2+} Entry (SOCE).* The cartoon represents the Store-Operated Ca^{2+} Entry (SOCE) pathway and the action of two proteins involved in its activation: the ER resident protein stromal interaction molecule 1 (STIM1), that acts as Ca^{2+} sensor, and Orai1, the protein forming the channel in the PM that permits Ca^{2+} entry from the extracellular ambient. Adapted from Zhou Y. *et al.*, 2015.

Figure 27 shows the histograms representing the quantitative analysis: both short and long ER-PM contact sites significantly increased upon SOCE activation being the increase more evident in the case of the short contacts suggesting that they are mainly involved during the modulation of this pathway.

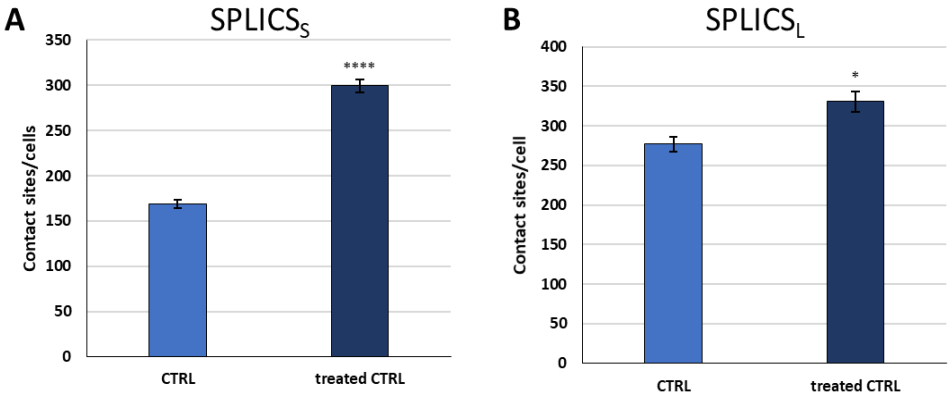

Figure 27 *Effect ER Ca^{2+} depletion on short* **A**) *and long* **B**) *range between ER and PM*. The short and long ER-PM contact sites were analysed upon SOCE activation using histamine agonist and SERCA pumps inhibitor 2,5-tert-butylhydroquinone. Quantification of SPLICS$_{S/L}$ contacts by 3D rendering of complete z-stacks: **A**) Mean ± SEM: SPLICS$_S$ (CTRL) 169 ± 4, n = 14 cells; SPLICS$_S$ (treated CTRL) 300 ± 7, n = 14 cells; **B**) SPLICS$_L$ (CTRL) 277 ± 9, n = 11 cells; SPLICS$_L$ (treated CTRL) 331 ± 13, n = 13 cells. *p < 0.01, ****p < 0.00001.

Then, to investigate whether the ER-PM contacts revealed by our SPLICS$_{S/L}$ in resting conditions are dependent by STIM1 or ORAI1 proteins, we decided to downregulate them by ShRNA silencing. Hela cells were co-transfected with shRNA STIM1 or ORAi1 plasmids

and $SPLIC_{S/L}$ constructs and the level of downregulation was evaluated by Western blotting analysis (Figure 28A).

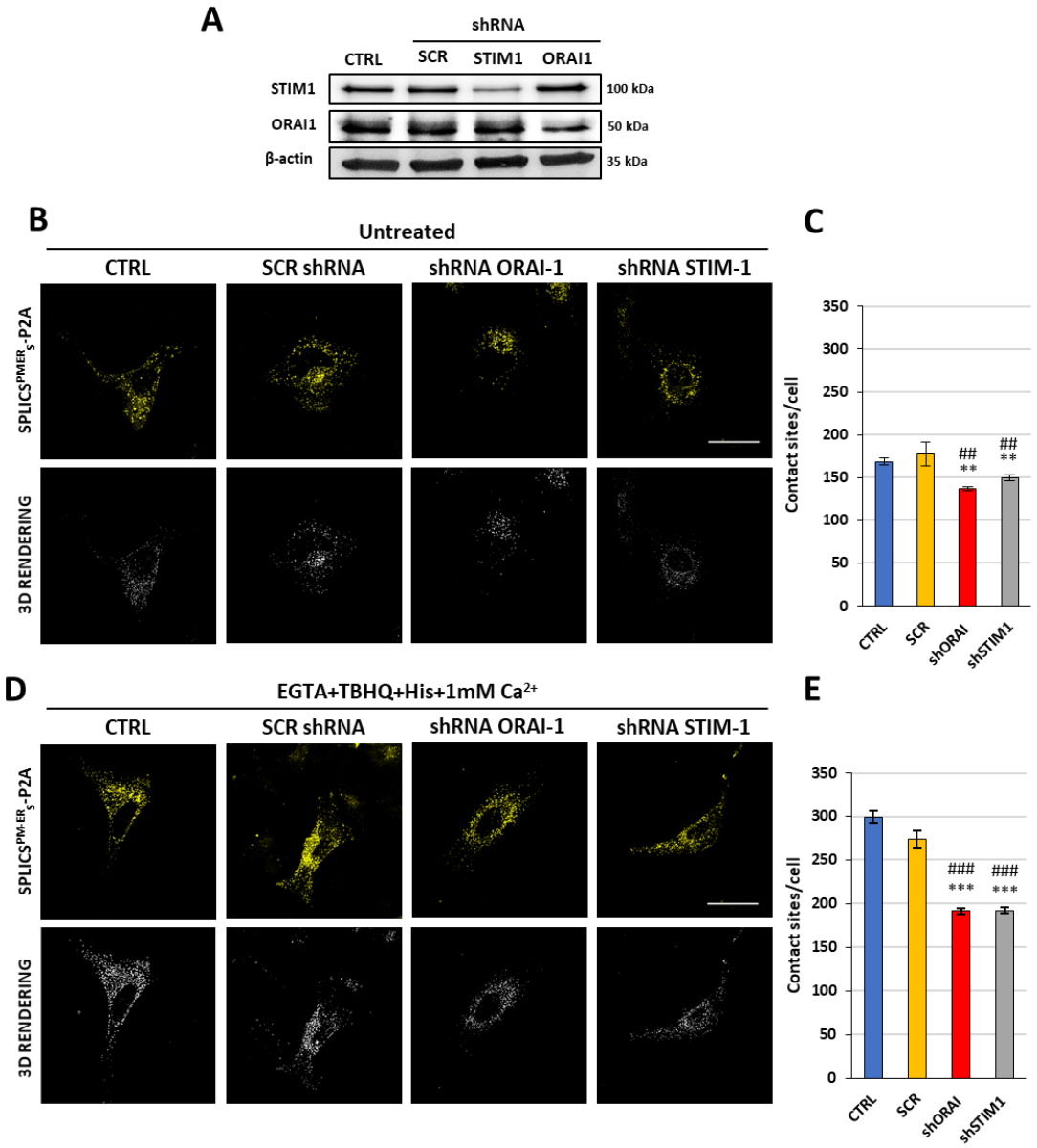

Figure 28 *Effect of STIM1/ORAI1 silencing and ER Ca^{2+} depletion on short range between ER and PM.* **A**) Western blotting analysis of silenced proteins, STIM1 and ORAI1. After silencing the expression levels of proteins was analyzed by Western blotting with an anti STIM1 or ORAI1 antibody. Equal loading was verified by probing the membrane with an anti β-actin antibody. **B**) Representative confocal pictures of untreated HeLa cells expressing the $SPLICS_S$ probe acquired upon excitation at 514 nm wavelength. **C**) Quantification of $SPLICS_S$ contacts by 3D rendering of complete z-stacks. Mean ± SEM: $SPLICS_S$ (CTRL) 169 ± 4, n = 14 cells; shRNA SCR 177 ± 13, n = 5 cells; shRNA STIM1 150 ± 4, n = 27 cells; shRNA ORAI1 137 ± 3, n = 34 cells. **D**) Representative confocal pictures of treated HeLa cells expressing the $SPLICS_S$ probe acquired upon excitation at 514 nm wavelength. **E**) Quantification of $SPLICS_S$ contacts by 3D rendering of complete z-stacks. Mean ± SEM: $SPLICS_S$ (CTRL) 300 ± 7, n = 14 cells; shRNA SCR 274 ± 10, n = 5 cells; shRNA STIM1 192 ± 4, n = 36 cells; shRNA ORAI1 192 ± 3, n = 55 cells. Data shown are the result of three independent experiments. **$p \leq 0.01$ vs control, ***$p \leq 0.001$ vs control. ## $p \leq 0.01$ vs scramble, ### $p \leq 0.001$ vs scramble.

Scramble ShRNA was co-transfected with $SPLIC_{S/L}$ constructs as control. A strong downregulation of both the STIM1 and the Orai1 relative bands is appreciable, even if both the proteins are still detectable. However, it has to be said that considering that under transient transfections the efficiency approaches is 25%, the reduction in STIM1 and Orai1 could be higher in the transfected cells. Single cell imaging analysis in positive cells revealed that $SPLICS_S$ signal was slightly decreased in the cells where STIM1 or Orai1 expression level was reduced in comparison with control untreated cells and with shRNA scramble treated cells (Mean ± SEM: $SPLICS_S$ (CTRL) 169 ± 4, n = 14 cells; shRNA SCR 177 ± 13, n = 5 cells; shRNA STIM1 150 ± 4, n = 27 cells; shRNA ORAI1 137 ± 3, n = 34 cells; Figure 28B-C**)**. The representative images are also shown. Interestingly, when in a STIM1 or ORAi1 downregulation background we induced SOCE and monitored the ER-PM interactions in the short range, the number of the contact sites is more significantly reduced in respect with the relative control cells (Mean ± SEM: $SPLICS_S$ (CTRL) 300 ± 7, n = 14 cells; shRNA SCR 274 ± 10, n = 5 cells; shRNA STIM1 192 ± 4, n = 36 cells; shRNA ORAI1 192 ± 3, n = 55 cells; Figure 28D-E). These results are in agreement with the data present in literature, because it is well established that the distance between these two membranes during SOCE process is below 10 nm and the short sensor detect the ER-PM interactions below 10 nm.

We performed the same experiment using the $SPLICS_L$ probes to detect the ER-PM long interactions. Under basal condition, when STIM1 or ORAI1 protein are downregulated the ER-PM long interactions significantly decrease in the number compared to control (Mean ± SEM: untreated $SPLICS_L$ (CTRL) 277 ± 9, n = 11 cells; shRNA SCR 259 ± 14, n = 9 cells; shRNA STIM1 169 ± 4, n = 38 cells; shRNA ORAI1 174 ± 4, n = 42 cells) (Figure 29A-B). Under conditions of ER Ca^{2+} depletion (Figure 29C-D**)**, we observed that the downregulation of STIM1 or ORAI1 proteins is still effective in reducing the number of $SPLICS_L$ dots (Mean ± SEM: treated $SPLICS_L$ (CTRL) 331 ± 13, n = 13 cells; shRNA SCR 303 ± 19, n = 8 cells shRNA STIM1 193 ± 4, n = 33 cells; shRNA ORAI1 196 ± 4, n = 31 cells).

All together these data are interesting not only because revealed the participation of STIM1 and ORAI1 proteins in the formation of contacts between ER and PM in a distance range between 10 nm and 40 nm under basal condition, but also because indicate that our $SPLICS_{S/L}$ probe is suitable to monitor the heterogeneity of the contact sites in term of different lengths.

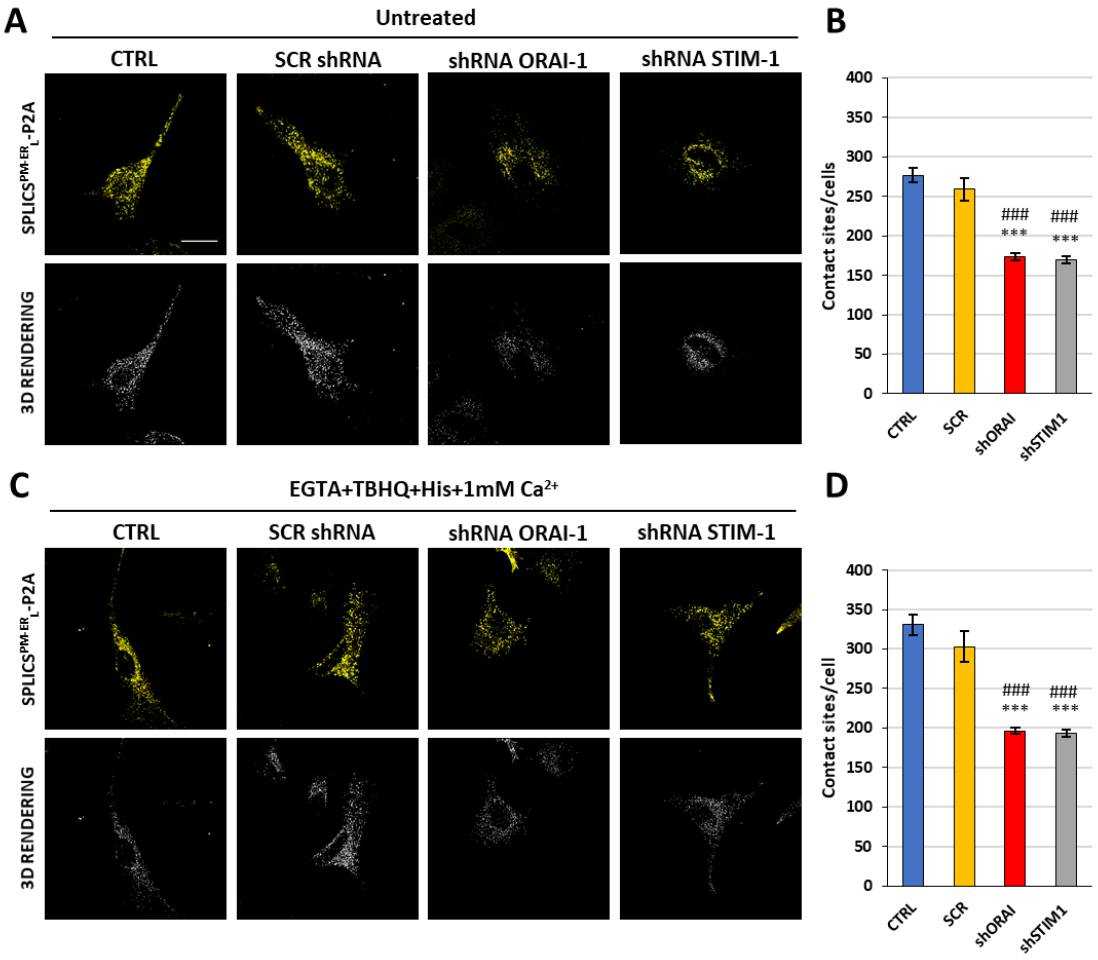

Figure 29. *Effect of STIM1/ORAI1 silencing and ER Ca^{2+} depletion on long range between ER and PM.* **A**) Representative confocal pictures of untreated HeLa cells expressing the $SPLICS_L$ probe (514 nm excitation wavelength). **B**) Quantification of $SPLICS_L$ contacts by 3D rendering of complete z-stacks. Mean ± SEM: $SPLICS_L$ (CTRL) 277 ± 9, n = 11 cells; shRNA STIM1 169 ± 4, n = 38 cells; shRNA ORAI1 174 ± 4, n = 42 cells. **C**) Representative confocal pictures of treated HeLa cells expressing the $SPLICS_L$ probe (514 nm excitation wavelength). **D**) Quantification of $SPLICS_L$ contacts by 3D rendering of complete z-stacks. Mean ± SEM: $SPLICS_L$ (CTRL) 331 ± 13, n = 13 cells; shRNA STIM1 193 ± 4, n = 33 cells; shRNA ORAI1 196 ± 4, n = 31 cells. Data shown are the result of three independent experiments. *** $p \leq 0.001$ vs control. ### $p \leq 0.001$ vs scramble**.**

Discussion and Conclusions

Neurodegenerative diseases are a heterogenous group of disabling disorders of the central nervous system (CNS), characterized by the progressive and selective degeneration of neuronal subtypes. They share critical processes such as the presence of misfolded and/or aggregated proteins, neuroinflammation, impairment of autophagy, oxidative stress and mitochondrial anomalies.

Mitochondria play a pivotal role in essential cell processes from bioenergetics to cell death, and mitochondrial dysfunction, especially in the case of neurons due to their high energy requirements, make cells more to injury and degeneration (Filosto et al., 2011). In particular, alterations in mitochondrial Ca^{2+} handling seem to be a common features among a wide spectrum of neuropathological conditions (Calì et al., 2012b).

The molecular understanding of the involvement of mitochondrial dysfunction in pathogenesis of neurodegenerative disease, including Alzheimer's disease (AD), Parkinson's disease (PD), Huntington's disease (HD), and amyotrophic lateral sclerosis (ALS), is important to find potential novel therapeutic targets for their treatments (Lin and Beal, 2006). In particular, alterations in mitochondrial Ca^{2+} handling seems to be a common features among a wide spectrum of neuropathological conditions (Calì et al., 2012b).

An important aspect, particularly relevant for my PhD project, was that in recent years PINK1 and PKA have been jointed for their neuroprotective role in preventing dopaminergic neuronal degeneration. Several different pathways have been proposed to be involved in the interplay between PINK1 and PKA, ranging from the regulation of dendrites remodelling through the modulation of mitochondria trafficking by Miro1 (Das Banerjee et al. 2017), to the prevention of mitochondrial fission through the regulation of Drp1 activity (Dagda et al. 2011) and also to the modulation of mitochondrial Ca^{2+} by the activation of the mitochondrial Na^{+}/Ca^{2+} exchanger, NCLX (Kostic et al. 2015).

The question whether PKA must be recruited to mitochondria to exert this action is still open, even if evidence for the existence of a pool of cAMP in the mitochondrial matrix generated by resident soluble adenylate cyclases has been proven (Di Benedetto et al., 2013).

During these three years of my PhD program, my research activity was mainly focused on investigating the possible localization of PKA protein in the mitochondrial compartments. To this end, we decided to develop a new experimental approach based on splitGFP protein and BiFC (Bimolecular Fluorescent Complementation) tool. Our results revealed that, in HeLa cells, upon PKA catalytic overexpression, at least a fraction of CATα subunit not only

can distribute at the OMM, as amply documented in the literature, but can also reach the IMS and the mitochondrial matrix. Interestingly, the localization in the mitochondrial matrix was revealed only for the CATα subunit while the regulatory subunits, RIα and RIIβ, were exclusively visualized at the OMM (Figures 13A-C and 14A-C). These data indicate that in the absence of specific condition or stimuli CATα subunit can enter in the mitochondrial matrix, but regulatory subunits are prevented to reach the IMS and the mitochondrial matrix. This result was interesting considering that the CATα activity is regulated by the regulatory subunits that detach from it upon cAMP concentration increases and promote kinase activity. The fact that we did not detect RIα and RIIβ regulatory subunits in the mitochondrial matrix or in the IMS could suggest that CATα can enter the mitochondria in an activated form once released from the regulatory subunits, but this open the question on how it can be inactivated once in the mitochondria.

Considering the fact that our data suggest the existence of an isoform specific mechanism for the mitochondrial import of PKA and that additional PKA regulatory subunits have been described, i.e., RIIα and RIβ, it will be very interesting to investigate them in terms of mitochondrial distribution and CATα interaction.

We have also to consider the possibility that specific conditions may locally increase cAMP concentration in mitochondria proximity that may eventually favour the release of OMM anchored CATα from the regulatory subunits and its translocation inside the mitochondria. This aspect will be further investigated.

According this observation we could argue that the binding of the regulatory subunits to CATα could prevent its entry in the matrix and that PKA kinase activity inside the mitochondria does not require the increase in the intramitochondrial cAMP levels but rather the detachment of CATα from regulatory subunits in the cytosol.

Thus, we focused on the possibility that by co-expressing the regulatory subunits together with the CATα subunits in the presence of our splitGFP sensor we could detect a possible interference of the co-expressed regulatory subunits in the localization of the CATα subunit at the mitochondrial level. Interestingly, we have found that the co-expression of RIIβ subunit abolished the complementation of β11-CATα with mt-GFP_{1-10}, since no GFP fluorescence upon excitation at 488nm wavelength was detected, suggesting that the entry of CATα subunit in the mitochondrial matrix was prevented by RIIβ binding. Even more interesting, when we performed the same experiment in the presence of co-expressed RIα

subunit we appreciated a green fluorescent signal in the mitochondrial matrix, indicating that this isoform of regulatory subunit is not able to prevent the localization of CATα subunit in the mitochondrial matrix (Figure 15).

These results unequivocally indicate that CATα subunit can enter in the mitochondrial matrix and thus we decided whether the overexpression of CATα subunit could have an effect on mitochondrial Ca^{2+} handling, and if any, whether we could specifically attribute it to the pool of the CATα subunit localized in the matrix rather than to a general activation of the cAMP-PKA pathway.

This aspect was of particular relevance since in PINK1 deficient neurons PKA protein activation has been shown to exert a neuroprotective role by recovering impairment in mitochondrial Ca^{2+} efflux (Kostic et al., 2015).

First, we monitored the effect of CATα overexpression on mitochondrial and cytosolic Ca^{2+} transients induced upon cell stimulation with agonist which induces the release of Ca2+ from the intracellular stores and its consequent entry from the extracellular ambient. A strong reduction in both mitochondrial and cytosolic Ca^{2+} transients was detected (Figure 17A-B). Then, we co-expressed CATα and RIIβ subunits and we have found that, in this case, the reduction of the Ca2+ transients induced by cell stimulation was almost completely abolished (Figure 19A-B). Mitochondrial and cytosolic Ca^{2+} measurements were performed also in cells co-expressing CATα together with the RIα subunit: in this case the CATα-induced reduction of the mitochondrial Ca^{2+} transients was not abolished by the presence of the RIα subunit, suggesting that the modulation of the effects of CATα on Ca^{2+} transients is dependent on the regulatory subunit in an isoform specific manner (Figure 20). These data also suggest the possibility that the modulation of mitochondrial Ca2+ transients by CATα could be dependent by the pool of CATα subunit located inside the mitochondrial matrix and are in agreement with the fact that we have observed that when we prevent the localization of CATα subunit in the matrix we also block its effect on mitochondrial Ca2+ handling.

At this point, our hypothesis was that CATα could exert its action on the mitochondrial Ca^{2+} handling acting inside the matrix and that it is able to get in only when it is not engaged with the RIIβ subunit. To support this specific role of CATα we decided to selectively express it inside the matrix by using a construct where the CATα moiety was fused at its N-terminal with a mitochondrial targeting sequence (mtCATα). We have found that the selective

expression of mtCATα specifically reduced histamine induced mitochondrial Ca^{2+} transients (Figure 18B) but it was completely ineffective on cytosolic Ca^{2+} transients (Figure 18C). This result is very encouraging since it underlies the existence of a specific role for mitochondrial PKA on mitochondrial Ca^{2+} homeostasis and supports the existence of mitochondrial targets for PKA action inside the mitochondria. Unexpectedly, the effects of mtCATα on mitochondrial Ca^{2+} were completely abolished when RIIβ subunit was co-expressed (Figure 21A), and in these conditions we also failed to detect any mitochondrial localization of CATα subunit, that instead remained totally confined in the cytoplasm of the cells co-expressing mtCATα and RIIβ (Figure 21B). The mechanism through which RIIβ could prevent mtCATα import in the mitochondrial matrix is presently unknown and deserves further analysis. We can exclude that it could be related to different stability of the protein or increased turnover since by a Western blotting analysis we detected that in the case of co-transfection of CATα subunit together with the regulatory subunits RIα and RIIβ the amount of CATα is even higher than in the case of single transfection.

To evaluate possible molecular targets of PKA activity in the modulation of mitochondrial Ca^{2+} handling, we decided to interfere with the Ca^{2+} efflux or influx mitochondrial pathways. As mentioned above, when PKA is activated by forskolin it is able to rescue defects in PINK1 deficient dopaminergic neurons by phosphorylating the exchanger NCLX. To evaluate whether the reduction of mitochondrial Ca2+ transients in the presence of overexpressed mtCATα could be related to the activation of NCLX, we monitored the effect of PKA activity in cells where the NCLX exchanger was inhibited by the incubation with a specific inhibitor, the CGP37157 compound. The finding that mtCATα was still able to reduce mitochondrial Ca^{2+} transients when NCLX is inhibited could suggest that, unless it is able to overcome pharmacological inhibition of NCLX, it could have another mitochondrial target different from NCLX exchanger. For this reason, we augmented mitochondrial Ca2+ entry by manipulating MCU pore channel subunit which overexpression is well known to enhance mitochondrial Ca2+ transients. The co-expression of mtCATα completely abolished the enhancement of mitochondrial Ca^{2+} enhancement due to overexpressed MCU, suggesting that PKA may control excessive Ca^{2+} entry and prevent mitochondrial Ca^{2+} overload under condition that may promote it. In this direction, we have obtained preliminary encouraging results: we have indeed found that in PINK1 KO MEF cells, which display both higher basal mitochondrial Ca^{2+} level and enhanced mitochondrial Ca2+ transients upon cell stimulation, the percentage of cells showing CATα in the

mitochondrial matrix is higher than that in control wt MEF cells. Further experiments are necessary to better understand these results, as well as, to identify physiological or pathological conditions that may eventually favor PKA translocation to the mitochondrial matrix.

In addition to the work on PKA, during my PhD program, I carried out another project based on a different application of the split-GFP system and BiFC methodology. Specifically, this methodology was used to evaluate organelles interaction, in particular the ER-plasma membrane (PM) contact sites.

The major effort of my project was the validation of a new tool to monitor ER-PM contact sites, based on that we had previously developed in the laboratory to monitor ER-mitochondria contact sites (SPLICS, Cieri *et al.*, 2018). The splitGFP methodology turns out to be very versatile not only to monitor protein-protein interaction or the distribution of a specific protein in a specific cellular compartment, but also to detect membrane proximity between different organelles. A big advantage of this technique is represented by the fact that the fluorescent signal that originates from the complementation of the two splitGFP moieties is detected in the absence of any background signal that could be confounding and furthermore that, by introducing linkers of different length in the construction of the ER membrane targeted fragment it is virtually to modulate the sensitivity, in term of the distance between the membrane involved in the formation of the contact sites, of the probe. Taking advantage from this potentiality we generated two different tools which are sensitive to monitor the interactions between ER and PM occurring at two different distance: in a short- (8-10 nm) and in long-range (40-50 nm). By applying this tool, we were able to monitor changes in contact sites induced by pharmacological and genetic manipulations.

First of all, we have proved the existence of short and long contact sites under basal condition and found that on average there are about 350 contacts per cell in the long range and about 200 per cell in the short range. Considering that ER-PM contacts occurring upon intracellular Ca^{2+} stores depletion have been widely investigated and the proteins involved in their formation have been identified we challenged our $SPLICS_{S/L}$ probes by genetic and pharmacological manipulation of the SOCE (Store-Operated Ca^{2+} Entry). As mentioned in the introduction, this process is induced as a consequence of the ER Ca^{2+} depletion and it is dependent on the dynamic interaction between the ER resident protein stromal interaction molecule 1 (STIM1), that acts as Ca^{2+} sensor, and Orai1, the protein forming the channel in the PM that permits Ca^{2+} entry from the extracellular space (Nwokonko and Gill, 2012).

Interestingly we have found that our probes were able to reveal changes in the number of contact sites upon silencing of STIM1 and upon silencing of ORAI1, thus suggesting the existence of ER-PM contact sites that are both STIM1 and ORAI1 dependent also under basal condition, i.e., when massive ER Ca^{2+} depletion is not occurring. Our probes also have revealed that that STIM1 and Orai1 are important to maintain contacts between ER and PM in a distance range between 10 nm and 40 nm.

We have also found that our probe was responsive to pharmacological treatments that are well known to induce STIM1 clustering on the ER membrane and puncta formation by approaching Orai1 at the PM and getting in close contact with it.

Indeed, the ER Ca^{2+} depletion induced by SERCA pump inhibition increased both the short and the long ER-PM interactions, since the $SPLICS_S$ and the $SPLICS_L$ signals significantly increased. STIM1 or ORAI1 downregulation upon ER Ca^{2+} depletion strongly decreased the number of $SPLICS_S$ and the $SPLICS_L$ dots. The finding that both the short and the long ER PM contacts appeared to be regulated with the same extent is interesting, since it suggests that two kinds of contacts are involved in the SOCE process. However, this finding could be also explained by the observation that the contacts monitored by the $SPLICS_L$ probably are both short and long (but in any case, shorter than 40nm) and that the changes observed with the long-range probe are probably relative to the changes in the short contact sites.

It will be now interesting to modulate the expression of proteins such as α-synuclein and tau, well known for interacting with cell membranes and follow whether and how they are able to modify ER-PM contact sites and their signalling related processes. Indeed, both of them have been proposed to play a role in the modulation of Ca2+ entry from the extracellular ambient.

All together, these data reveal that the SPLICS methodology is a useful and sensitive tool adapted to monitor short and long ranges ER-PM interactions and their changes upon pharmacological and genetic manipulations. In the future, we will apply this molecular tool to investigate the ER-PM cross talk in model cells for PD, i.e., upon the overexpression of wildtype and PD-related mutants α-synuclein or in PINK1-KO cells.

Materials and Methods

5.1. Plasmid Vectors

The full length CATα, RIα and RIIβ -β11 constructs have been generated by PCR using the following primers:

CATα-β11 (BamHI) For. 5'GAAGTTCGGATCCATGGGCAACGCCGCCGCCGCCAA-3'

(XhoI) Rev. 5'-ACTTCTCACTCGAGTTATGTGATGCCGGCGGCGTTC-3';

RIα-β11 (BamHI) For5'GAAGTTCGGATCCATGGAGTCTGGCAGTACCGCCGC-3';

(XhoI) Rev. 5'-ACTTCTCACTCGAGTTATGTGATGCCGGCGGCGTTC-3';

RIIβ-β11 (EcoRI) For. 5'-GTAGTTCGAATTCATGAGCATCGAGATCCCCGCGGGGCT-3';

(XhoI) Rev. 5'-ACTTCTCACTCGAGTTATGTGATGCCGGCGGCGTTC-3'.

These constructs were inserted into the vector pcDNA3 between the indicated restriction sites. The DNA constructs encoding for the CATα, RIα and RIIβ PKA subunits used as a template are a kind gift of Prof. Giulietta Di Benedetto (National Research Council, CNR Padova). Other cDNA for the expression of the proteins of interest were already present in the laboratory (cytAEQ, mtAEQ, MCU, MICU1).

The mitochondrial matrix- and OMM- targeted humanized GFP_{1-10} expressing vectors have been previously generated by PCR amplification from the GPI-GFP_{1-10} template kindly provided by Dr F. Pinaud (University of Southern California, USA) using forward primers containing the mitochondrial matrix pre-sequence of the subunit VIII of cytochrome c oxidase and the N-terminal 33 amino acids sequence of TOM20 protein. The $GFP_{1–10}$ targeted to the IMS has been created by genetic fusion to the leader sequence of the IMS protein LACTB 45 and created by DNA synthesis (Thermo Scientific). The S11 b strand has been added to the C-terminal domain of PKA protein by PCR amplification.

To generate **SPLICS$_S^{ER-PM}$** and **SPLICS$_L^{ER-PM}$** probes $ER_{S/L}$-β11 and YFP_{1-10} were PCR amplified using the following primers:

SPLICS$_{S/L}^{ER-PM}$ (BamHI) For5'GAAGTTCGGATCCATGCGGGACCACATGGTGC-3';

(XhoI) Rev. 5'-ACTTCTCACTCGAGTTATGTTCCTTTTTCATTTGG-3'.

These constructs were inserted into the vector pcDNA3 between BamHI and XhoI restriction sites. The chimeric sequences composed by the minimal Sac1 ER targeting sequence and the Sac1 ER targeting sequence containing additional 267 bp of the helix-FRB fragment (derived from the pEGFP-C3/CFP-HA-FRB-helix-ER plasmid) (ER_L- β11) were fused with the β11 tag to generate the ERs-β11 and the ER_L-β11 constructs, respectively. The PCR

products were purified using the GenElute Gel Extraction Kit (Sigma), digested with BamHI and XhoI and then ligated into the pSYC-187 vector (Addgene) digested with the same restriction enzymes. All constructs were verified by Sanger sequencing.

The described plasmids were then used employing the following *in vitro* approaches. First, One shot TOP 10 E. coli (Invitrogen) were chemically competent cells (calcium chloride homemade protocol) that allow stable replication of high-copy number plasmids. Plasmids used for the cloning and manipulation of DNA have been engineered to harbour the genes for antibiotic resistance. Thus, the bacterial transformation is plated onto media containing, for example, ampicillin, and only bacteria which possess the plasmid DNA have the ability to metabolize ampicillin and form colonies. In this way, bacterial cells containing plasmid DNA are selected. Transformant colonies were used to perform plasmid purification, i.e. Pure LinkTM HiPure plasmid Maxi prep kit (Cat. K210006, Invitrogen). The purified plasmid was quantified byNanoDrop. Positive colonies were stocked in liquid LB supplemented with glycerol 20% (v/v) at -80° C.

5.2. Cell Culture and Transfection Procedures

HeLa cells and PINK1 wildtype (wt) or knockdown (KO) MEF cells were grown in DMEM high glucose (Euroclone) containing 10% fetal bovine serum (FBS, Gibco), supplemented with 100 U/ml penicillin (Euroclone) and 100 µg/ml streptomycin (Euroclone), in a humidified atmosphere containing 5% CO2. Cells were seeded onto 13 diameter glass coverslips or on six multiwell plates and transfection was performed at 60-80% confluence using the Ca^{2+}-phosphate procedure for HeLa cells or Lipofectamine TM 3000 Transfection Reagent (Life Technologies) for MEF cells.

5.2.1. Ca^{2+}-phosphate transfection

HeLa cells were transfected with a standard Ca^{2+}-phosphate procedure. For Ca^{2+}-phosphate transfection procedure the following stock solution need to be prepared and conserved at -20°C until used: $CaCl_2$ 2.5 M; HEPES Buffered Solution 2X (HBS2X: 280 mM NaCl, 50 mM Hepes, 1.5 mM Na_2HPO_4, pH 7.12). All solutions were sterilized by filtration using 0.22 µm filters. Just before the transfection procedure, cells are washed with fresh medium. For one 13 mm coverslip, 5 µl of 2.5 M $CaCl_2$ were added to the DNA dissolved in 45 µl of H_2O. Routinely, 4 µg of DNA or 25 nM shRNA were used to transfect 1 coverslip and in the case of co-transfection a 1:2 ratio in favour to PKA subunits expressing plasmids was adopted. The solution was then mixed under vortex with 50 µl of HBS and incubated to 30 minutes at room temperature. For Ca^{2+} measurement cells were co-transfected with aequorin

construct targeted to the mitochondrial matrix and to the cytosol. For one of six multiwell plate the amount of solution and DNA was 15 µl of 2.5M CaCl2, 12 µg of DNA in 135 µl of H_2O and 150 µl of HBS. The transfection mix was then added directly to the cell monolayer drop by drop. Sixteen hours after addition of the transfection mix, cells were washed with phosphate-buffered saline (PBS: 140mM NaCl, 2mM KCl, 1.5mM KH2PO4, 8mM Na2HPO4 pH 7.4).

The cells were generally analysed 36 h after transfection. Where indicated, the cells were treated with 2,5-tertbutylhydroquinone (THBQ) 20 µM and Histamine 100 µM 24 hours after transfection for 5' at 37°C in a 5% CO_2 atmosphere.

5.2.2. Lipofectamine™ 3000

MEF cells were transfected with Lipofectamine™ 3000 and using Lipofectamine™ 3000 Protocol (Invitrogen). For a 24 well plate, 1 µg of DNA per well was added to 50 µL of Opti-MEM™ Medium and 2 µL of P3000™ Reagent, and 50 µL of Opti-MEM™ Medium and 1 µL of Lipofectamine™ 3000 Reagent were prepared. Following this, the two tubes containing DNA-Opti-MEM and Lipofectamine-Opti-MEM were mixed well by flicking for 30 s and left at room temperature for 10 min. During this incubation time, media from the 24 well plate was removed. To each well, 400 µL of Opti-MEM were added. After incubation, 100 µL of the mixture was added to each well drop by drop, dispersing evenly. The plate was placed back into the incubator at 37 °C and 5% CO2 until the day of experiment.

5.3. Western blotting Analysis

To monitor endogenous and overexpressed protein regulation, cells were lysate in Chaps-buffer [(HBS1X pH 6.8 (0.5 M Hepes, 2 M NaCl), CHAPS 1X, 200 mM PMSF(phenyl methane sulfonyl fluoride), 20 mM NEM (N-etil maleimide), 1 M PIC (protease inhibitor cocktail)] and after 30 minutes of incubation once, 20 µg of total proteins were loaded, according to Bradford quantification. Proteins were separated by SDS-PAGE electrophoresis, in commercial 10% acrylamide gels (Life Technologies) and transferred into nitrocellulose membranes (Life Technologies) by wet electrophoretic transfer (Trans-Blot® Turbo™). Blots were blocked 1 hour at RT with 5% non-fat dry milk (BioRad) in TBS-Tween 1X (TBS 10X: 200 mM Tris-Sigma, 1.5 M NaCl, pH 7.6; 0.01% Tween) solution and incubated over night at 4°C with specific primary antibodies. Secondary

antibodies were incubated 1 hour at RT. Washes after antibody incubations were done on an orbital shaker, three times for 10'each, with TBS-Tween 1X.

We used the following antibodies: anti-CATα (1:1000, Cell Signaling), anti-RIα (1:500, Santa Cruz), anti-RIIβ (1:500, Santa Cruz), anti-STIM1 (1:1000, BD Transduction Laboratories^{TM}), anti-Orai1 (1:1000, Proscience), anti-GAPDH (1:1000, Millipore), anti-β-actin (1:1000, Santa Cruz). Detection was carried out by incubation with secondary horseradish peroxidase-conjugated anti-rabbit or anti-mouse IgG antibody (1:2000, Santa Cruz Biotechnology) for 1.5 h at room temperature.

5.4. Immunocytochemistry

Thirty-six hours after transfection, cells plated on 13 mm glass coverslips were washed twice with PBS and fixed for 20 minutes with 4 % formaldehyde. Cells permeabilization was performed by 20 minutes incubation with 0.1% Triton X-100 in PBS, followed by 30 minutes wash with 1% gelatine (type IV, from calf skin, Sigma) in PBS. The coverslips were then incubated for 90 minutes at 37°C in a wet chamber with the specific primary antibody diluted in PBS. Staining was revealed by the incubation with specific Alexa Fluor secondary antibody (Life technologies) for 45 minutes at room temperature. Confocal images were acquired on a Leica SP5-TCS-II-RS. For all images, pinhole was set to 1 airy unit, pixel size was about 100 nm and a Z-stack was acquired for the whole depth of the cell by sampling at 130 nm in the Z plane. Quantification of the number was performed from ImageJ program.

We used the following antibodies: anti-CATα (1:50, Cell Signaling), anti-RIα (1:50, Santa Cruz), anti-RIIβ (1:50, Santa Cruz), anti-KDEL (1:150, Invitrogen), anti-TOM20 (1:50, Santa Cruz). Detection was carried out by incubation with Alexa Fluor secondary fluorophore-conjugated goat anti-rabbit or anti-mouse antibody (Alexa Fluor 405, 488, 594, 633, 1:2000, Santa Cruz Biotechnology) for 40 minutes at room temperature.

Fluorescence was analyzed with a Leica Confocal SP5 microscope. Images were acquired by using Leica AS software (Leica Microsystems, Wetzlar, Germany).

5.5. Confocal Analysis

Cells were generally imaged 36 hours after transfection with a Leica TSC SP5 inverted confocal microscope, using either a HCX PL APO 63X/numerical aperture 1.40–0.60 or a HCX PL APO ×100/numerical aperture 1.4 oil-immersion objective. Images were acquired by using the Leica AS software. To count ER–PM contacts, a complete z-stack of the cell was acquired every 0.29 μm. Z-stacks were processed using Fiji: images were first

convolved, and then filtered using the Gaussian Blur filter. A 3D reconstruction of the resulting image was obtained using the Volume J plugin (http://bij.isi.uu.nl/vr.htm). A selected face of the 3D rendering was then thresholded and used to count ER–PM contact sites.

5.6. Aequorin as a Ca^{2+} indicator

Aequorin is a 21 kDa photoprotein isolated from jellyfish Aequorea Victoria which emits blue light in the presence of Ca^{2+}. The aequorin originally purified from the jellyfish is a mixture of different isoforms called "heterogeneous aequorin" (Shimomura, 1986). In its active form the photoprotein includes an apoprotein and a covalently bound prosthetic group, called coelenterazine. The apoprotein contains four helix-loop-helix "EF-hand" domains, three of which are Ca^{2+}-binding sites. These domains confer to the protein a particular globular structure forming the hydrophobic core cavity that accommodates the ligand coelenterazine. When Ca^{2+} ions bind to the three high affinity EF-hand sites, coelenterazine is oxidized to coelenteramide, with a concomitant release of CO_2 and emission of light (Head et al. 2000). Although this reaction is irreversible, an active aequorin can be obtained in vitro by incubating the apoprotein with coelenterazine in the presence of oxygen and 2-mercaptoethanol. Reconstitution of an active aequorin (expressed recombinantly) can be obtained also in living cells by simple addition of coelenterazine into the medium. Coelenterazine is highly hydrophobic and has been shown to permeate cell membranes of various cell types. Different coelenterazine analogues have been synthetized and are now commercially available.

The possibility of using aequorin as Ca^{2+} indicator is based on the existence of a well-characterized relationship between the rate of photon emission and the free $[Ca^{2+}]$. The first method used to correlate the number of photons emitted to the free $[Ca^{2+}]$ was that described by Allen and Blinks (Blinks, 1978). In the following years, this system was improved to achieve a simple algorithm that converts luminescence into $[Ca^{2+}]$ values. Under physiological conditions of pH, temperature and ionic strength, this relationship is more than quadratic in the range of $[Ca^{2+}]$ 10-5-10-7 M. The presence of 3 Ca^{2+} binding sites in aequorin is responsible for the steep relationship between photon emission rate and free $[Ca^{2+}]$. The $[Ca^{2+}]$ can be calculated from the formula L/Lmax where L is the rate of photon emission at any instant during the experiment and Lmax is the maximal rate of photon emission at saturating $[Ca^{2+}]$. The rate of aequorin luminescence is independent of $[Ca^{2+}]$ at very high (>10-4 M) and very low $[Ca^{2+}]$ (< 10-7 M). However, as described below in more details, it is possible to expand the range of $[Ca^{2+}]$ that can be monitored with aequorin.

Although aequorin luminescence is not influenced either by K^+ or Mg^{2+} (which are the most abundant cations in the intracellular environment and thus the most likely source of interference under physiological settings) both ions are competitive inhibitors of Ca^{2+} activated luminescence. pH was also shown to affect aequorin luminescence but at values below 7. Due to the characteristics described above, experiments with aequorin need to be done in well-controlled conditions of pH and ionic concentrations, notably of Mg^{2+}.

5.7. Recombinant aequorins

Aequorin began to be widely used when the cDNA encoding the photoprotein was cloned, thus avoiding the purification of the native polypeptide and its microinjection. Moreover, the cloning of aequorin gene opened the way to recombinant expression and thus has largely expanded the applications of this tool for investigating Ca^{2+} handling in living cells. In particular, recombinant aequorin can be expressed not only in the cytoplasm, but also in specific intracellular compartments by including specific targeting sequences in the engineered cDNAs. Extensive manipulations of the N-terminal of aequorin have been shown not to alter the chemiluminescence properties of the photoprotein and its Ca^{2+} affinity. On the other hand, even marginal alterations of the C-terminal either abolish luminescence or drastically increase Ca^{2+} independent photon emission. For these reasons, all targeted aequorins synthesized in our laboratory include modifications of the photoprotein N-terminal. Three targeting strategies have been adopted:

1. Inclusion of a minimal targeting signal sequence to the photoprotein cDNA. This strategy was initially used to design the mitochondrial aequorin and was followed also to synthesize an aequorin localized in the nucleus and in the lumen of the Golgi apparatus.

2. Fusion of the cDNA encoding aequorin to that of a resident protein of the compartments of interest. This approach has been used to engineer aequorins localized in the sarcoplasmic reticulum (SR), in the nucleoplasm and cytoplasm (shuttling between the two compartments depending on the concentration of steroid hormones), on the cytoplasmic surface of the endoplasmic reticulum (ER) and Golgi and in the sub-plasmalemma cytoplasmic rim.

3. Addition to the aequorin cDNA of sequences that code for polypeptides that bind to endogenous proteins. This strategy was adopted to localize aequorin in the ER lumen.

The construct used in our experiments is the mutated isoform of mitochondrial targeted aequorin (Brini, 2008): mtAEQmut. It was generated to measure the $[Ca^{2+}]$ of the mitochondrial matrix of various cell types. This construct includes the targeting pre-

sequence of subunit VIII of human cytochrome c oxidase fused to the aequorin cDNA. To expand the range of Ca^{2+} sensitivity that can be monitored the photoprotein was also mutated (Asp119>Ala). This point mutation affects specifically the second EF hand motive of wild type aequorin. The affinity for Ca^{2+} of this mutated aequorin (mtAEQmut) is about 20-fold lower than that of the wild type.

5.8. Luminescence detection

The aequorin detection system is derived from that described by Cobbold and Lee (Cobbold and Bourne, 1984) and is based on the use of a low noise photomultiplier placed in close proximity (2-3 mm) with aequorin expressing cells. Cells are seeded on 13-mm coverslips and put into a perfusion chamber. The volume of the chamber is kept to a minimum (about 200 µl). Cells are continuously perfused via peristaltic pump with KRB saline solution, thermostated via a water bath at 37°C.

The photomultiplier (Hamamatsu H7301) is kept into a dark box. The output of the amplifier- discriminator is captured by C8855-01-photoncounting board in an IBM compatible microcomputer and stored for further analysis.

5.9. Ca^{2+} measurements

Thirty-six hours after transfection mitochondrial low affinity aequorin (mtAEQ) was reconstituted by incubating cells for 1.5 h with 5 µM wt coelenterazine (Santacruz) in Krebs-Ringer modified buffer (KRB,125 mM NaCl, 5 mM KCl, 1 mM Na_3PO_4, 1 mM $MgSO_4$, 5.5 mM glucose, 20 mM HEPES, pH 7.4, 37 °C) at 37 °C in a 5% CO_2 atmosphere. After reconstitution, cells were transferred to the chamber of a purpose-built luminometer, and Ca^{2+} measurements were started in KRB supplemented with 1 mM $CaCl_2$ by stimulating HeLa cells with 100 µM histamine. The experiments were terminated by cell permeabilization with 100 µM digitonin in a hypotonic Ca^{2+}-rich solution (10 mM $CaCl_2$ in H_2O) to discharge the remaining unused aequorin pool. The light signal was collected and calibrated off-line into Ca^{2+} concentration values using a computer algorithm based on the Ca^{2+} response curve of mitochondrial aequorin as previously described 59.

5.10. Statistical Analysis

All of the data are representative of at least three independent experiments. Values are expressed as mean ± SEM. Significance was calculated by Student's t-test.

References

Abramov, A.Y., Berezhnov, A. V., Fedotova, E.I., Zinchenko, V.P., and Dolgacheva, L.P. (2017). Interaction of misfolded proteins and mitochondria in neurodegenerative disorders. Biochem. Soc. Trans.

Acin-Perez, R., Salazar, E., Kamenetsky, M., Buck, J., Levin, L.R., and Manfredi, G. (2009). Cyclic AMP Produced inside Mitochondria Regulates Oxidative Phosphorylation. Cell Metab. *9*, 265–276.

Acin-Perez, R., Russwurm, M., Günnewig, K., Gertz, M., Zoidl, G., Ramos, L., Buck, J., Levin, L.R., Rassow, J., Manfredi, G., et al. (2011a). A phosphodiesterase 2A isoform localized to mitochondria regulates respiration. J. Biol. Chem.

Acin-Perez, R., Gatti, D.L., Bai, Y., and Manfredi, G. (2011b). Protein phosphorylation and prevention of cytochrome oxidase inhibition by ATP: Coupled mechanisms of energy metabolism regulation. Cell Metab.

Aerts, L., Craessaerts, K., De Strooper, B., and Morais, V.A. (2015). PINK1 kinase catalytic activity is regulated by phosphorylation on serines 228 and 402. J. Biol. Chem.

Affaitati, A., Cardone, L., De Cristofaro, T., Carlucci, A., Ginsberg, M.D., Varrone, S., Gottesman, M.E., Avvedimento, E. V., and Feliciello, A. (2003). Essential role of A-Kinase anchor protein 121 for cAMP signaling to mitochondria. J. Biol. Chem.

Akabane, S., Uno, M., Tani, N., Shimazaki, S., Ebara, N., Kato, H., Kosako, H., and Oka, T. (2016). PKA Regulates PINK1 Stability and Parkin Recruitment to Damaged Mitochondria through Phosphorylation of MIC60. Mol. Cell *62*, 371–384.

Amadoro, G., Corsetti, V., Florenzano, F., Atlante, A., Ciotti, M.T., Mongiardi, M.P., Bussani, R., Nicolin, V., Nori, S.L., Campanella, M., et al. (2014). AD-linked, toxic NH2 human tau affects the quality control of mitochondria in neurons. Neurobiol. Dis.

Andreazza, A.C., Shoo, L., Wang, J.F., and Trevor Young, L. (2010). Mitochondrial Complex i Activity and Oxidative Damage to Mitochondrial Proteins in the Prefrontal Cortex of Patients with Bipolar Disorder. Arch. Gen. Psychiatry.

Arena, G., Gelmetti, V., Torosantucci, L., Vignone, D., Lamorte, G., De Rosa, P., Cilia, E., Jonas, E.A., and Valente, E.M. (2013). PINK1 protects against cell death induced by mitochondrial depolarization, by phosphorylating Bcl-xL and impairing its pro-apoptotic cleavage. Cell Death Differ.

Arokium, H., Ouerfelli, H., Velours, G., Camougrand, N., Vallette, F.M., and Manon, S. (2007). Substitutions of potentially phosphorylatable serine residues of bax reveal how they may regulate its interaction with mitochondria. J. Biol. Chem.

Das Banerjee, T., Dagda, R.Y., Dagda, M., Chu, C.T., Rice, M., Vazquez-Mayorga, E., and

Dagda, R.K. (2017). PINK1 regulates mitochondrial trafficking in dendrites of cortical neurons through mitochondrial PKA. J. Neurochem. *142*, 545–559.

Barsukova, A.G., Bourdette, D., and Forte, M. (2011). Mitochondrial calcium and its regulation in neurodegeneration induced by oxidative stress. Eur. J. Neurosci.

Baughman, J.M., Perocchi, F., Girgis, H.S., Plovanich, M., Belcher-Timme, C.A., Sancak, Y., Bao, X.R., Strittmatter, L., Goldberger, O., Bogorad, R.L., et al. (2011). Integrative genomics identifies MCU as an essential component of the mitochondrial calcium uniporter. Nature *476*, 341–345.

Bayne, A.N., and Trempe, J.F. (2019). Mechanisms of PINK1, ubiquitin and Parkin interactions in mitochondrial quality control and beyond. Cell. Mol. Life Sci.

Beal, M.F. (2005). Mitochondria take center stage in aging and neurodegeneration. Ann. Neurol.

Di Benedetto, G., Scalzotto, E., Mongillo, M., and Pozzan, T. (2013). Mitochondrial Ca2+ uptake induces cyclic AMP generation in the matrix and modulates organelle ATP levels. Cell Metab. *17*, 965–975.

Di Benedetto, G., Pendin, D., Greotti, E., Pizzo, P., and Pozzan, T. (2014). Ca2+ and cAMP cross-talk in mitochondria. J. Physiol. *592*, 305–312.

Bernardi, P. (2017). Mitochondrial Transport of Cations: Channels, Exchangers, and Permeability Transition. Physiol. Rev. *79*, 1127–1155.

Berridge, M.J. (2009). Inositol trisphosphate and calcium signalling mechanisms. Biochim. Biophys. Acta - Mol. Cell Res.

Betarbet, R., Sherer, T.B., MacKenzie, G., Garcia-Osuna, M., Panov, A. V., and Greenamyre, J.T. (2000). Chronic systemic pesticide exposure reproduces features of Parkinson's disease. Nat. Neurosci.

Birsa, N., Norkett, R., Higgs, N., Lopez-Domenech, G., and Kittler, J.T. (2013). Mitochondrial trafficking in neurons and the role of the Miro family of GTPase proteins. In Biochemical Society Transactions, p.

van der Bliek, A.M., Shen, Q., and Kawajiri, S. (2013). Mechanisms of mitochondrial fission and fusion. Cold Spring Harb. Perspect. Biol.

Bogaerts, V., Theuns, J., and Van Broeckhoven, C. (2008). Genetic findings in Parkinson's disease and translation into treatment: A leading role for mitochondria? Genes, Brain Behav.

Bonifati, V. (2014). Genetics of Parkinson's disease - state of the art, 2013. Park. Relat. Disord.

Bravo-Sagua, R., Parra, V., Ortiz-Sandoval, C., Navarro-Marquez, M., Rodríguez, A.E.,

Diaz-Valdivia, N., Sanhueza, C., Lopez-Crisosto, C., Tahbaz, N., Rothermel, B.A., et al. (2018). Caveolin-1 impairs PKA-DRP1-mediated remodelling of ER–mitochondria communication during the early phase of ER stress. Cell Death Differ. *1*.

Brini, M. (2008). Calcium-sensitive photoproteins. Methods.

Burré, J., Sharma, M., Tsetsenis, T., Buchman, V., Etherton, M.R., and Südhof, T.C. (2010). α-Synuclein promotes SNARE-complex assembly in vivo and in vitro. Science (80-.).

Calì, T., Ottolini, D., Negro, A., and Brini, M. (2012a). α-synuclein controls mitochondrial calcium homeostasis by enhancing endoplasmic reticulum-mitochondria interactions. J. Biol. Chem.

Calì, T., Ottolini, D., and Brini, M. (2012b). Mitochondrial Ca2+ and neurodegeneration. Cell Calcium *52*, 73–85.

Calì, T., Ottolini, D., Negro, A., and Brini, M. (2013). Enhanced parkin levels favor ER-mitochondria crosstalk and guarantee Ca2+ transfer to sustain cell bioenergetics. Biochim. Biophys. Acta - Mol. Basis Dis. *1832*, 495–508.

Calì, T., Ottolini, D., and Brini, M. (2014). Calcium signaling in Parkinson's disease. Cell Tissue Res. *357*, 439–454.

Calì, T., Ottolini, D., Soriano, M.E., and Brini, M. (2015). A new split-GFP-based probe reveals DJ-1 translocation into the mitochondrial matrix to sustain ATP synthesis upon nutrient deprivation. Hum. Mol. Genet. *24*, 1045–1060.

Calì, T., Ottolini, D., Vicario, M., Catoni, C., Vallese, F., Cieri, D., Barazzuol, L., and Brini, M. (2019). splitGFP Technology Reveals Dose-Dependent ER-Mitochondria Interface Modulation by α-Synuclein A53T and A30P Mutants. Cells.

Chan, C.S., Guzman, J.N., Ilijic, E., Mercer, J.N., Rick, C., Tkatch, T., Meredith, G.E., and Surmeier, D.J. (2007). "Rejuvenation" protects neurons in mouse models of Parkinson's disease. Nature.

Chang, C.L., Hsieh, T.S., Yang, T.T., Rothberg, K.G., Azizoglu, D.B., Volk, E., Liao, J.C., and Liou, J. (2013a). Feedback regulation of receptor-induced ca2+ signaling mediated by e-syt1 and nir2 at endoplasmic reticulum-plasma membrane junctions. Cell Rep. *5*, 813–825.

Chang, C.L., Hsieh, T.S., Yang, T.T., Rothberg, K.G., Azizoglu, D.B., Volk, E., Liao, J.C., and Liou, J. (2013b). Feedback regulation of receptor-induced ca2+ signaling mediated by e-syt1 and nir2 at endoplasmic reticulum-plasma membrane junctions. Cell Rep.

Chen, Q., Lin, R.Y., and Rubin, C.S. (1997). Organelle-specific targeting of protein kinase AII (PKAII): Molecular and in situ characterization of murine A kinase anchor proteins that recruit regulatory subunits of PKAII to the cytoplasmic surface of mitochondria. J. Biol.

Chem.

Chen, Y., Cann, M.J., Litvin, T.N., Iourgenko, V., Sinclair, M.L., Levin, L.R., and Buck, J. (2000). Soluble adenylyl cyclase as an evolutionarily conserved bicarbonate sensor. Science (80-.).

Cieri, D., Vicario, M., Giacomello, M., Vallese, F., Filadi, R., Wagner, T., Pozzan, T., Pizzo, P., Scorrano, L., Brini, M., et al. (2018). SPLICS: A split green fluorescent protein-based contact site sensor for narrow and wide heterotypic organelle juxtaposition. Cell Death Differ. *25*, 1131–1145.

Clark, I.E., Dodson, M.W., Jiang, C., Cao, J.H., Huh, J.R., Seol, J.H., Yoo, S.J., Hay, B.A., and Guo, M. (2006). Drosophila pink1 is required for mitochondrial function and interacts genetically with parkin. Nature *441*, 1162–1166.

Csordás, G., Thomas, A.P., and Hajnóczky, G. (2001). Calcium signal transmission between ryanodine receptors and mitochondria in cardiac muscle. Trends Cardiovasc. Med.

Csordás, G., Renken, C., Várnai, P., Walter, L., Weaver, D., Buttle, K.F., Balla, T., Mannella, C.A., and Hajnóczky, G. (2006). Structural and functional features and significance of the physical linkage between ER and mitochondria. J. Cell Biol. *174*, 915–921.

Csordás, G., Golenár, T., Seifert, E.L., Kamer, K.J., Sancak, Y., Perocchi, F., Moffat, C., Weaver, D., De la Fuente, S., Bogorad, R., et al. (2013). MICU1 controls both the threshold and cooperative activation of the mitochondrial Ca2+ uniporter. Cell Metab.

d'Amora, M., Angelini, C., Marcoli, M., Cervetto, C., Kitada, T., and Vallarino, M. (2011). Expression of PINK1 in the brain, eye and ear of mouse during embryonic development. J. Chem. Neuroanat.

Dagda, R.K., Gusdon, A.M., Pien, I., Strack, S., Green, S., Li, C., Van Houten, B., Cherra, S.J., and Chu, C.T. (2011). Mitochondrially localized PKA reverses mitochondrial pathology and dysfunction in a cellular model of Parkinson's disease. Cell Death Differ. *18*, 1914–1923.

Dagda, R.K., Pien, I., Wang, R., Zhu, J., Wang, K.Z.Q., Callio, J., Banerjee, T. Das, Dagda, R.Y., and Chu, C.T. (2014). Beyond the mitochondrion: Cytosolic PINK1 remodels dendrites through Protein Kinase A. J. Neurochem.

Damier, P., Hirsch, E.C., Agid, Y., and Graybiel, A.M. (1999). The substantia nigra of the human brain: I. Nigrosomes and the nigral matrix, a compartmental organization based on calbindin D(28K) immunohistochemistry. Brain.

Dash, R.K., and Beard, D.A. (2008). Analysis of cardiac mitochondrial Na2+-Ca2+

exchanger kinetics with a biophysical model of mitochondrial Ca2+ handing suggests a 3: 1 stoichiometry. J. Physiol. *586*, 3267–3285.

Deng, H., Dodson, M.W., Huang, H., and Guo, M. (2008). The Parkinson's disease genes pink1 and parkin promote mitochondrial fission and/or inhibit fusion in Drosophila. Proc. Natl. Acad. Sci. U. S. A.

Devi, L., Raghavendran, V., Prabhu, B.M., Avadhani, N.G., and Anandatheerthavarada, H.K. (2008). Mitochondrial import and accumulation of α-synuclein impair complex I in human dopaminergic neuronal cultures and Parkinson disease brain. J. Biol. Chem.

Dingsdale, H., Okeke, E., Awais, M., Haynes, L., Criddle, D.N., Sutton, R., and Tepikin, A. V. (2013). Saltatory formation, sliding and dissolution of ER-PM junctions in migrating cancer cells. Biochem. J.

Domingo, A., and Klein, C. (2018). Genetics of Parkinson disease. In Handbook of Clinical Neurology, p.

Donnelly, M.L.L., Luke, G., Mehrotra, A., Li, X., Hughes, L.E., Gani, D., and Ryan, M.D. (2001). Analysis of the aphthovirus 2A/2B polyprotein "cleavage" mechanism indicates not a proteolytic reaction, but a novel translational effect: A putative ribosomal "skip." J. Gen. Virol. *82*, 1013–1025.

Duda, J., Pötschke, C., and Liss, B. (2016). Converging roles of ion channels, calcium, metabolic stress, and activity pattern of Substantia nigra dopaminergic neurons in health and Parkinson's disease. J. Neurochem.

Eisenberg-Bord, M., Shai, N., Schuldiner, M., and Bohnert, M. (2016). A Tether Is a Tether Is a Tether: Tethering at Membrane Contact Sites. Dev. Cell *39*, 395–409.

Elmore, S. (2007). Apoptosis: A Review of Programmed Cell Death. Toxicol. Pathol.

Elrod, J.W., Wong, R., Mishra, S., Vagnozzi, R.J., Sakthievel, B., Goonasekera, S.A., Karch, J., Gabel, S., Farber, J., Force, T., et al. (2010). Cyclophilin D controls mitochondrial pore - Dependent Ca2+ exchange, metabolic flexibility, and propensity for heart failure in mice. J. Clin. Invest.

Emmanouilidou, E., Melachroinou, K., Roumeliotis, T., Garbis, S.D., Ntzouni, M., Margaritis, L.H., Stefanis, L., and Vekrellis, K. (2010). Cell-Produced -Synuclein Is Secreted in a Calcium-Dependent Manner by Exosomes and Impacts Neuronal Survival. J. Neurosci.

Farrer, M.J. (2006). Genetics of Parkinson disease: Paradigm shifts and future prospects. Nat. Rev. Genet.

Fernández-Busnadiego, R., Saheki, Y., and De Camilli, P. (2015). Three-dimensional

architecture of extended synaptotagmin-mediated endoplasmic reticulum–plasma membrane contact sites. Proc. Natl. Acad. Sci. *112*, E2004–E2013.

Fernandez-Marcos, P.J., and Auwerx, J. (2011). Regulation of PGC-1α, a nodal regulator of mitochondrial biogenesis. In American Journal of Clinical Nutrition, p.

Filadi, R., Greotti, E., and Pizzo, P. (2018). Highlighting the endoplasmic reticulum-mitochondria connection: Focus on Mitofusin 2. Pharmacol. Res.

Filosto, M., Scarpelli, M., Cotelli, M.S., Vielmi, V., Todeschini, A., Gregorelli, V., Tonin, P., Tomelleri, G., and Padovani, A. (2011). The role of mitochondria in neurodegenerative diseases. J. Neurol.

Frederick, R.L., and Shaw, J.M. (2007). Moving mitochondria: Establishing distribution of an essential organelle. Traffic.

Friedman, J.R., and Voeltz, G.K. (2011). The ER in 3D: A multifunctional dynamic membrane network. Trends Cell Biol.

Friedman, J.R., Lackner, L.L., West, M., DiBenedetto, J.R., Nunnari, J., and Voeltz, G.K. (2011). ER tubules mark sites of mitochondrial division. Science (80-.).

Furukawa, K., Matsuzaki-Kobayashi, M., Hasegawa, T., Kikuchi, A., Sugeno, N., Itoyama, Y., Wang, Y., Yao, P.J., Bushlin, I., and Takeda, A. (2006). Plasma membrane ion permeability induced by mutant α-synuclein contributes to the degeneration of neural cells. J. Neurochem.

Gandhi, S., Muqit, M.M.K., Stanyer, L., Healy, D.G., Abou-Sleiman, P.M., Hargreaves, I., Heales, S., Ganguly, M., Parsons, L., Lees, A.J., et al. (2006). PINK1 protein in normal human brain and Parkinson's disease. Brain *129*, 1720–1731.

Gandhi, S., Wood-Kaczmar, A., Yao, Z., Plun-Favreau, H., Deas, E., Klupsch, K., Downward, J., Latchman, D.S., Tabrizi, S.J., Wood, N.W., et al. (2009a). PINK1-Associated Parkinson's Disease Is Caused by Neuronal Vulnerability to Calcium-Induced Cell Death. Mol. Cell *33*, 627–638.

Gandhi, S., Wood-Kaczmar, A., Yao, Z., Plun-Favreau, H., Deas, E., Klupsch, K., Downward, J., Latchman, D.S., Tabrizi, S.J., Wood, N.W., et al. (2009b). PINK1-Associated Parkinson's Disease Is Caused by Neuronal Vulnerability to Calcium-Induced Cell Death. Mol. Cell.

García-Bermúdez, J., Sánchez-Aragó, M., Soldevilla, B., del Arco, A., Nuevo-Tapioles, C., and Cuezva, J.M. (2015). PKA Phosphorylates the ATPase Inhibitory Factor 1 and Inactivates Its Capacity to Bind and Inhibit the Mitochondrial H+-ATP Synthase. Cell Rep.

Gehrke, S., Wu, Z., Klinkenberg, M., Sun, Y., Auburger, G., Guo, S., and Lu, B. (2015).

PINK1 and parkin control localized translation of respiratory chain component mRNAs on mitochondria outer membrane. Cell Metab.

Gelmetti, V., De Rosa, P., Torosantucci, L., Marini, E.S., Romagnoli, A., Di Rienzo, M., Arena, G., Vignone, D., Fimia, G.M., and Valente, E.M. (2017). PINK1 and BECN1 relocalize at mitochondria-associated membranes during mitophagy and promote ER-mitochondria tethering and autophagosome formation. Autophagy *13*, 654–669.

Gerbeth, C., Schmidt, O., Rao, S., Harbauer, A.B., Mikropoulou, D., Opalinska, M., Guiard, B., Pfanner, N., and Meisinger, C. (2013). Glucose-induced regulation of protein import receptor tom22 by cytosolic and mitochondria-bound kinases. Cell Metab.

Giorgi, C., Baldassari, F., Bononi, A., Bonora, M., De Marchi, E., Marchi, S., Missiroli, S., Patergnani, S., Rimessi, A., Suski, J.M., et al. (2012). Mitochondrial Ca2+ and apoptosis. Cell Calcium.

Giorgi, C., Missiroli, S., Patergnani, S., Duszynski, J., Wieckowski, M.R., and Pinton, P. (2015). Mitochondria-Associated Membranes: Composition, Molecular Mechanisms, and Physiopathological Implications. Antioxidants Redox Signal.

Glitsch, M.D., Bakowski, D., and Parekh, A.B. (2002). Store-operated Ca2+ entry depends on mitochondrial Ca2+ uptake. EMBO J.

Greene, A.W., Grenier, K., Aguileta, M.A., Muise, S., Farazifard, R., Haque, M.E., McBride, H.M., Park, D.S., and Fon, E.A. (2012). Mitochondrial processing peptidase regulates PINK1 processing, import and Parkin recruitment. EMBO Rep.

Guardia-Laguarta, C., Area-Gomez, E., Rub, C., Liu, Y., Magrane, J., Becker, D., Voos, W., Schon, E.A., and Przedborski, S. (2014). -Synuclein Is Localized to Mitochondria-Associated ER Membranes. J. Neurosci.

Gunter, K.K., Zuscik, M.J., and Gunter, T.E. (1991). The Na+-independent Ca2+efflux mechanism of liver mitochondria is not a passive Ca2+/2H+exchanger. J. Biol. Chem. *266*, 21640–21648.

Hao, X., Tang, J., Rietdorf, K., Teboul, L., Chuang, K., Parrington, J., Ma, J., Evans, A.M., Galione, A., and Zhu, M.X. (2009). NAADP mobilizes calcium from acidic organelles through two-pore channels. Nature *459*, 596–600.

Hayakawa, K., Esposito, E., Wang, X., Terasaki, Y., Liu, Y., Xing, C., Ji, X., and Lo, E.H. (2016). Transfer of mitochondria from astrocytes to neurons after stroke. Nature.

Heeman, B., Van den Haute, C., Aelvoet, S.-A., Valsecchi, F., Rodenburg, R.J., Reumers, V., Debyser, Z., Callewaert, G., Koopman, W.J.H., Willems, P.H.G.M., et al. (2011). Depletion of PINK1 affects mitochondrial metabolism, calcium homeostasis and energy

maintenance. J. Cell Sci. *124*, 1115–1125.

Hodge, T., and Colombini, M. (1997). Regulation of metabolite flux through voltage-gating of VDAC channels. J. Membr. Biol.

Hoeflich, K.P., and Ikura, M. (2002). Calmodulin in action: Diversity in target recognition and activation mechanisms. Cell.

Huang, E., Qu, D., Huang, T., Rizzi, N., Boonying, W., Krolak, D., Ciana, P., Woulfe, J., Klein, C., Slack, R.S., et al. (2017). PINK1-mediated phosphorylation of LETM1 regulates mitochondrial calcium transport and protects neurons against mitochondrial stress. Nat. Commun.

Hurley, M.J., Brandon, B., Gentleman, S.M., and Dexter, D.T. (2013). Parkinson's disease is associated with altered expression of Ca <inf>V</inf>1 channels and calcium-binding proteins. Brain.

James Surmeier, D., Guzman, J.N., Sanchez, J., and Schumacker, P.T. (2012). Physiological phenotype and vulnerability in Parkinson's disease. Cold Spring Harb. Perspect. Med.

Jiang, D., Zhao, L., and Clapham, D.E. (2009). Genome-wide RNAi screen identifies Letm1 as a mitochondrial Ca 2+ /H + antiporter. Science (80-.). *326*, 144–147.

Jin, S.M., and Youle, R.J. (2013). The accumulation of misfolded proteins in the mitochondrial matrix is sensed by PINK1 to induce PARK2/Parkin-mediated mitophagy of polarized mitochondria. Autophagy.

Jin, S.M., Lazarou, M., Wang, C., Kane, L.A., Narendra, D.P., and Youle, R.J. (2010). Mitochondrial membrane potential regulates PINK1 import and proteolytic destabilization by PARL. J. Cell Biol. *191*, 933–942.

Junn, E., Jang, W.H., Zhao, X., Jeong, B.S., and Mouradian, M.M. (2009). Mitochondrial localization of DJ-1 leads to enhanced neuroprotection. J. Neurosci. Res.

Kanaji, S., Iwahashi, J., Kida, Y., Sakaguchi, M., and Mihara, K. (2000). Characterization of the signal that directs Tom20 to the mitochondrial outer membrane. J. Cell Biol.

Kaupp, U.B., and Seifert, R. (2002). Cyclic nucleotide-gated ion channels. Physiol. Rev.

Kawasaki, H., Springett, G.M., Mochizuki, N., Toki, S., Nakaya, M., Matsuda, M., Housman, D.E., and Graybiel, A.M. (1998). A family of cAMP-binding proteins that directly activate Rap1. Science (80-.).

Kitada, T., Asakawa, S., Hattori, N., Matsumine, H., Yamamura, Y., Minoshima, S., Yokochi, M., Mizuno, Y., and Shimizu, N. (1998). Mutations in the parkin gene cause autosomal recessive juvenile parkinsonism. Nature.

Kostic, M., H.R., L.M., Hilmar, B., Michal, H., Erin, S., T, C.C., Y, A.A., and Sekler1, I.

(2015). PKA Phosphorylation of NCLX Reverses Mitochondrial Calcium Overload and Depolarization, Promoting Survival of PINK1- Deficient Dopaminergic Neurons. Cell Rep. *13*, 376–386.

Kozjak-Pavlovic, V. (2017). The MICOS complex of human mitochondria. Cell Tissue Res.

Kumar, S., Kostin, S., Flacke, J.P., Reusch, H.P., and Ladilov, Y. (2009). Soluble adenylyl cyclase controls mitochondria-dependent apoptosis in coronary endothelial cells. J. Biol. Chem.

Van Laar, V.S., Roy, N., Liu, A., Rajprohat, S., Arnold, B., Dukes, A.A., Holbein, C.D., and Berman, S.B. (2015). Glutamate excitotoxicity in neurons triggers mitochondrial and endoplasmic reticulum accumulation of Parkin, and, in the presence of N-acetyl cysteine, mitophagy. Neurobiol. Dis.

Langston, J., Ballard, P., Tetrud, J., and Irwin, I. (1983). Chronic Parkinsonism in humans due to a product of meperidine-analog synthesis. Science (80-.).

Lashuel, H.A., Petre, B.M., Wall, J., Simon, M., Nowak, R.J., Walz, T., and Lansbury, P.T. (2002). α-synuclein, especially the parkinson's disease-associated mutants, forms pore-like annular and tubular protofibrils. J. Mol. Biol.

Lazarou, M., Jin, S.M., Kane, L.A., and Youle, R.J. (2012). Role of PINK1 Binding to the TOM Complex and Alternate Intracellular Membranes in Recruitment and Activation of the E3 Ligase Parkin. Dev. Cell.

Lazarou, M., Sliter, D.A., Kane, L.A., Sarraf, S.A., Wang, C., Burman, J.L., Sideris, D.P., Fogel, A.I., and Youle, R.J. (2015). The ubiquitin kinase PINK1 recruits autophagy receptors to induce mitophagy. Nature.

Lee, J., Kim, C.H., Simon, D.K., Aminova, L.R., Andreyev, A.Y., Kushnareva, Y.E., Murphy, A.N., Lonze, B.E., Kim, K.S., Ginty, D.D., et al. (2005). Mitochondrial cyclic AMP response element-binding protein (CREB) mediates mitochondrial gene expression and neuronal survival. J. Biol. Chem.

Lefkimmiatis, K., and Zaccolo, M. (2014). CAMP signaling in subcellular compartments. Pharmacol. Ther.

Lefkimmiatis, K., Leronni, D., and Hofer, A.M. (2013). The inner and outer compartments of mitochondria are sites of distinct cAMP/PKA signaling dynamics. J. Cell Biol. *202*, 453–462.

Lin, M.T., and Beal, M.F. (2006). Mitochondrial dysfunction and oxidative stress in neurodegenerative diseases. Nature.

Litvin, T.N., Kamenetsky, M., Zarifyan, A., Buck, J., and Levin, L.R. (2003). Kinetic

properties of “soluble” adenylyl cyclase: Synergism between calcium and bicarbonate. J. Biol. Chem.

Livigni, A., Scorziello, A., Agnese, S., Adornetto, A., Carlucci, A., Garbi, C., Castaldo, I., Annunziato, L., Avvedimento, E. V., and Feliciello, A. (2006). Mitochondrial AKAP121 links cAMP and src signaling to oxidative metabolism. Mol. Biol. Cell.

Lucero, M., Suarez, A.E., and Chambers, J.W. (2019). Phosphoregulation on mitochondria: Integration of cell and organelle responses. CNS Neurosci. Ther.

Luongo, T.S., Lambert, J.P., Gross, P., Nwokedi, M., Lombardi, A.A., Shanmughapriya, S., Carpenter, A.C., Kolmetzky, D., Gao, E., Van Berlo, J.H., et al. (2017). The mitochondrial Na + /Ca 2+ exchanger is essential for Ca 2+ homeostasis and viability HHS Public Access. *545*, 93–97.

Lur, G., Haynes, L.P., Prior, I.A., Gerasimenko, O. V., Feske, S., Petersen, O.H., Burgoyne, R.D., and Tepikin, A. V. (2009). Ribosome-free Terminals of Rough ER Allow Formation of STIM1 Puncta and Segregation of STIM1 from IP3 Receptors. Curr. Biol.

Lustbader, J.W., Cirilli, M., Lin, C., Xu, H.W., Takuma, K., Wang, N., Caspersen, C., Chen, X., Pollak, S., Chaney, M., et al. (2004). ABAD Directly Links Aβ to Mitochondrial Toxicity in Alzheimer’s Disease. Science (80-.).

Luth, E.S., Stavrovskaya, I.G., Bartels, T., Kristal, B.S., and Selkoe, D.J. (2014). Soluble, prefibrillar α-synuclein oligomers promote complex I-dependent, Ca2+-induced mitochondrial dysfunction. J. Biol. Chem.

Di Maio, R., Barrett, P.J., Hoffman, E.K., Barrett, C.W., Zharikov, A., Borah, A., Hu, X., McCoy, J., Chu, C.T., Burton, E.A., et al. (2016). α-synuclein binds to TOM20 and inhibits mitochondrial protein import in Parkinson’s disease. Sci. Transl. Med.

Mammucari, C., Raffaello, A., Vecellio Reane, D., and Rizzuto, R. (2016). Molecular structure and pathophysiological roles of the Mitochondrial Calcium Uniporter. Biochim. Biophys. Acta - Mol. Cell Res.

Mannella, C.A., Buttle, K., Rath, B.K., and Marko, M. (1998). Electron microscopic tomography of rat-liver mitochondria and their interactions with the endoplasmic reticulum. BioFactors.

Marongiu, R., Spencer, B., Crews, L., Adame, A., Patrick, C., Trejo, M., Dallapiccola, B., Valente, E.M., and Masliah, E. (2009). Mutant Pink1 induces mitochondrial dysfunction in a neuronal cell model of Parkinson’s disease by disturbing calcium flux. J. Neurochem.

Matenia, D., and Mandelkow, E.M. (2014). Emerging modes of PINK1 signaling: Another task for MARK2. Front. Mol. Neurosci.

Matteucci, A., Patron, M., Reane, D.V., Gastaldello, S., Amoroso, S., Rizzuto, R., Brini, M., Raffaello, A., and Calì, T. (2018). Parkin-dependent regulation of the MCU complex component MICU1. Sci. Rep.

McCormack, J.G., Halestrap, A.P., and Denton, R.M. (2017). Role of calcium ions in regulation of mammalian intramitochondrial metabolism. Physiol. Rev.

Means, C.K., Lygren, B., Langeberg, L.K., Jain, A., Dixon, R.E., Vega, A.L., Gold, M.G., Petrosyan, S., Taylor, S.S., Murphy, A.N., et al. (2011). An entirely specific type I A-kinase anchoring protein that can sequester two molecules of protein kinase A at mitochondria. Proc. Natl. Acad. Sci. U. S. A.

Meier, P.J., Spycher, M.A., and Meyer, U.A. (1981). Isolation and characterization of rough endoplasmic reticulum associated with mitochondria from normal rat liver. BBA - Biomembr.

Merrill, R.A., Dagda, R.K., Dickey, A.S., Cribbs, J.T., Green, S.H., Usachev, Y.M., and Strack, S. (2011). Mechanism of neuroprotective mitochondrial remodeling by pka/akap1. PLoS Biol.

van der Merwe, C., Jalali Sefid Dashti, Z., Christoffels, A., Loos, B., and Bardien, S. (2015). Evidence for a common biological pathway linking three Parkinson's disease-causing genes: Parkin, PINK1 and DJ-1. Eur. J. Neurosci.

Metuzals, J., Chang, D., Hammar, K., and Reese, T.S. (1997). Organization of the cortical endoplasmic reticulum in the squid giant axon. J. Neurocytol.

Moisoi, N., Klupsch, K., Fedele, V., East, P., Sharma, S., Renton, A., Plun-Favreau, H., Edwards, R.E., Teismann, P., Esposti, M.D., et al. (2009). Mitochondrial dysfunction triggered by loss of HtrA2 results in the activation of a brain-specific transcriptional stress response. Cell Death Differ.

Morais, V.A., Verstreken, P., Roethig, A., Smet, J., Snellinx, A., Vanbrabant, M., Haddad, D., Frezza, C., Mandemakers, W., Vogt-Weisenhorn, D., et al. (2009). Parkinson's disease mutations in PINK1 result in decreased Complex I activity and deficient synaptic function. EMBO Mol. Med.

Morais, V.A., Haddad, D., Craessaerts, K., De Bock, P.J., Swerts, J., Vilain, S., Aerts, L., Overbergh, L., Gruñewald, A., Seibler, P., et al. (2014). PINK1 loss-of-function mutations affect mitochondrial complex I activity via NdufA10 ubiquinone uncoupling. Science (80-.).

Moujalled, D., Weston, R., Anderton, H., Ninnis, R., Goel, P., Coley, A., Huang, D.C., Wu, L., Strasser, A., and Puthalakath, H. (2011). Cyclic-AMP-dependent protein kinase A

regulates apoptosis by stabilizing the BH3-only protein Bim. EMBO Rep.

Murata, H., Sakaguchi, M., Jin, Y., Sakaguchi, Y., Futami, J.I., Yamada, H., Kataoka, K., and Huh, N.H. (2011). A new cytosolic pathway from a Parkinson disease-associated kinase, BRPK/PINK1: Activation of AKT via MTORC2. J. Biol. Chem.

Narendra, D.P., Kane, L.A., Hauser, D.N., Fearnley, I.M., and Youle, R.J. (2010a). p62/SQSTM1 is required for Parkin-induced mitochondrial clustering but not mitophagy; VDAC1 is dispensable for both. Autophagy.

Narendra, D.P., Jin, S.M., Tanaka, A., Suen, D.F., Gautier, C.A., Shen, J., Cookson, M.R., and Youle, R.J. (2010b). PINK1 is selectively stabilized on impaired mitochondria to activate Parkin. PLoS Biol. *8*.

Nwokonko, R.M., and Gill, D.L. (2012). Store-operated Ca2+ entry (SOCE) pathways. Store-Operated Ca2+ Entry Pathways 83–98.

Okatsu, K., Oka, T., Iguchi, M., Imamura, K., Kosako, H., Tani, N., Kimura, M., Go, E., Koyano, F., Funayama, M., et al. (2012). PINK1 autophosphorylation upon membrane potential dissipation is essential for Parkin recruitment to damaged mitochondria. Nat. Commun. *3*, 1010–1016.

Okatsu, K., Uno, M., Koyano, F., Go, E., Kimura, M., Oka, T., Tanaka, K., and Matsuda, N. (2013). A dimeric pink1-containing complex on depolarized mitochondria stimulates parkin recruitment. J. Biol. Chem.

Ottolini, D., Calì, T., Negro, A., and Brini, M. (2013). The Parkinson disease-related protein DJ-1 counteracts mitochondrial impairment induced by the tumour suppressor protein p53 by enhancing endoplasmic reticulum-mitochondria tethering. Hum. Mol. Genet. *22*, 2152–2168.

Ottolini, D., Calì, T., and Brini, M. (2014). Methods to measure intracellular Ca2+ fluxes with organelle-targeted aequorin-based probes. Methods Enzymol. *543*, 21–45.

Paillusson, S., Gomez-Suaga, P., Stoica, R., Little, D., Gissen, P., Devine, M.J., Noble, W., Hanger, D.P., and Miller, C.C.J. (2017). α-Synuclein binds to the ER–mitochondria tethering protein VAPB to disrupt Ca2+ homeostasis and mitochondrial ATP production. Acta Neuropathol.

Palty, R., Silverman, W.F., Hershfinkel, M., Caporale, T., Sensi, S.L., Parnis, J., Nolte, C., Fishman, D., Shoshan-Barmatz, V., Herrmann, S., et al. (2010). NCLX is an essential component of mitochondrial Na+/Ca2+ exchange. Proc. Natl. Acad. Sci. *107*, 436–441.

Parihar, M.S., Parihar, A., Fujita, M., Hashimoto, M., and Ghafourifar, P. (2008). Mitochondrial association of alpha-synuclein causes oxidative stress. Cell. Mol. Life Sci.

Patron, M., Checchetto, V., Raffaello, A., Teardo, E., VecellioReane, D., Mantoan, M., Granatiero, V., Szabò, I., DeStefani, D., and Rizzuto, R. (2014). MICU1 and MICU2 finely tune the mitochondrial Ca2+ uniporter by exerting opposite effects on MCU activity. Mol. Cell *53*, 726–737.

Pchitskaya, E., Popugaeva, E., and Bezprozvanny, I. (2018). Calcium signaling and molecular mechanisms underlying neurodegenerative diseases. Cell Calcium.

Pérez-Sancho, J., Tilsner, J., Samuels, A.L., Botella, M.A., Bayer, E.M., and Rosado, A. (2016). Stitching Organelles: Organization and Function of Specialized Membrane Contact Sites in Plants. Trends Cell Biol.

Perocchi, F., Gohil, V.M., Girgis, H.S., Bao, X.R., McCombs, J.E., Palmer, A.E., and Mootha, V.K. (2010). MICU1 encodes a mitochondrial EF hand protein required for Ca2+ uptake. Nature.

Pickrell, A.M., and Youle, R.J. (2015). The roles of PINK1, Parkin, and mitochondrial fidelity in parkinson's disease. Neuron.

Pidoux, G., Witczak, O., Jarnss, E., Myrvold, L., Urlaub, H., Stokka, A.J., Küntziger, T., and Taskén, K. (2011). Optic atrophy 1 is an A-kinase anchoring protein on lipid droplets that mediates adrenergic control of lipolysis. EMBO J.

Pivovarova, N.B., and Andrews, S.B. (2010). Calcium-dependent mitochondrial function and dysfunction in neurons: Minireview. FEBS J.

Plovanich, M., Bogorad, R.L., Sancak, Y., Kamer, K.J., Strittmatter, L., Li, A.A., Girgis, H.S., Kuchimanchi, S., De Groot, J., Speciner, L., et al. (2013). MICU2, a Paralog of MICU1, Resides within the Mitochondrial Uniporter Complex to Regulate Calcium Handling. PLoS One.

Polianskyte, Z., Peitsaro, N., Dapkunas, A., Liobikas, J., Soliymani, R., Lalowski, M., Speer, O., Seitsonen, J., Butcher, S., Cereghetti, G.M., et al. (2009). LACTB is a filament-forming protein localized in mitochondria. Proc. Natl. Acad. Sci. *106*, 18960–18965.

PORTER, K.R., and PALADE, G.E. (1957). Studies on the endoplasmic reticulum. III. Its form and distribution in striated muscle cells. J. Biophys. Biochem. Cytol.

Prabu, S.K., Anandatheerthavarada, H.K., Raza, H., Srinivasan, S., Spear, J.F., and Avadhani, N.G. (2006). Protein kinase A-mediated phosphorylation modulates cytochrome c oxidase function and augments hypoxia and myocardial ischemia-related injury. J. Biol. Chem.

Pridgeon, J.W., Olzmann, J.A., Chin, L.S., and Li, L. (2007). PINK1 protects against oxidative stress by phosphorylating mitochondrial chaperone TRAP1. PLoS Biol.

Pryde, K.R., Smith, H.L., Chau, K.Y., and Schapira, A.H.V. (2016). PINK1 disables the anti-fission machinery to segregate damaged mitochondria for mitophagy. J. Cell Biol. *213*, 163–171.

QIN, S., GAO, J., WANG, X., and SU, B. (2018). Mitochondrial dynamics in neurodegenerative diseases. Sci. Sin. Vitae.

Raffaello, A., Stefani, D. De, Sabbadin, D., Teardo, E., Merli, G., Picard, A., Checchetto, V., and Moro, S. (2013). The mitochondrial calcium uniporter is a multimer that can include a dominant-negative. *32*, 2362–2376.

Rao, S., Schmidt, O., Harbauer, A.B., Schönfisch, B., Guiard, B., Pfanner, N., and Meisinger, C. (2012). Biogenesis of the preprotein translocase of the outer mitochondrial membrane: Protein kinase A phosphorylates the precursor of Tom40 and impairs its import. Mol. Biol. Cell.

Rasmo, D. De, Palmisano, G., Scacco, S., Technikova-Dobrova, Z., Panelli, D., Cocco, T., Sardanelli, A.M., Gnoni, A., Micelli, L., Trani, A., et al. (2010). Phosphorylation pattern of the NDUFS4 subunit of complex I of the mammalian respiratory chain. Mitochondrion.

De Rasmo, D., Panelli, D., Sardanelli, A.M., and Papa, S. (2008). cAMP-dependent protein kinase regulates the mitochondrial import of the nuclear encoded NDUFS4 subunit of complex I. Cell. Signal.

De Rasmo, D., Signorile, A., Roca, E., and Papa, S. (2009). CAMP response element-binding protein (CREB) is imported into mitochondria and promotes protein synthesis. FEBS J.

De Rasmo, D., Signorile, A., Santeramo, A., Larizza, M., Lattanzio, P., Capitanio, G., and Papa, S. (2015). Intramitochondrial adenylyl cyclase controls the turnover of nuclear-encoded subunits and activity of mammalian complex I of the respiratory chain. Biochim. Biophys. Acta - Mol. Cell Res.

De Rasmo, D., Micelli, L., Santeramo, A., Signorile, A., Lattanzio, P., and Papa, S. (2016). CAMP regulates the functional activity, coupling efficiency and structural organization of mammalian FOF1 ATP synthase. Biochim. Biophys. Acta - Bioenerg.

Rasola, A., and Bernardi, P. (2011). Mitochondrial permeability transition in Ca2+-dependent apoptosis and necrosis. Cell Calcium.

Rego, A.C., and Oliveira, C.R. (2003). Mitochondrial dysfunction and reactive oxygen species in excitotoxicity and apoptosis: Implications for the pathogenesis of neurodegenerative diseases. Neurochem. Res.

Rizzuto, R., Nakase, H., Darras, B., Francke, U., Fabrizi, G.M., Mengel, T., Walsh, F.,

Kadenbach, B., DiMauro, S., and Schon, E.A. (1989). A gene specifying subunit VIII of human cytochrome c oxidase is localized to chromosome 11 and is expressed in both muscle and non-muscle tissues. J. Biol. Chem.

Rizzuto, R., Simpson, A.W.M., Brini, M., and Pozzan, T. (1992). Rapid changes of mitochondrial Ca2+ revealed by specifically targeted recombinant aequorin. Nature.

Rizzuto, R., Brini, M., Murgia, M., and Pozzan, T. (1993). Microdomains with high Ca2+close to IP3-sensitive channels that are sensed by neighboring mitochondria. Science (80-.).

Rizzuto, R., Pinton, P., Carrington, W., Fay, F.S., Fogarty, K.E., Lifshitz, L.M., Tuft, R.A., and Pozzan, T. (1998). Close contacts with the endoplasmic reticulum as determinants of mitochondrial Ca2+ responses. Science (80-.).

Ronzitti, G., Bucci, G., Emanuele, M., Leo, D., Sotnikova, T.D., Mus, L. V., Soubrane, C.H., Dallas, M.L., Thalhammer, A., Cingolani, L.A., et al. (2014). Exogenous -Synuclein Decreases Raft Partitioning of Cav2.2 Channels Inducing Dopamine Release. J. Neurosci.

ROSENBLUTH, J. (1962). Subsurface cisterns and their relationship to the neuronal plasma membrane. J. Cell Biol.

Ryu, H., Lee, J., Impey, S., Ratan, R.R., and Ferrante, R.J. (2005). Antioxidants modulate mitochondrial PKA and increase CREB binding to D-loop DNA of the mitochondrial genome in neurons. Proc. Natl. Acad. Sci. U. S. A.

Schmidt, F., Levin, J., Kamp, F., Kretzschmar, H., Giese, A., and Bötzel, K. (2012). Single-channel electrophysiology reveals a distinct and uniform pore complex formed by α-synuclein oligomers in lipid membranes. PLoS One.

Schmidt, O., Harbauer, A.B., Rao, S., Eyrich, B., Zahedi, R.P., Stojanovski, D., Schönfisch, B., Guiard, B., Sickmann, A., Pfanner, N., et al. (2011). Regulation of mitochondrial protein import by cytosolic kinases. Cell.

Schreiner, B., Hedskog, L., Wiehager, B., and Ankarcrona, M. (2015). Amyloid-β peptides are generated in mitochondria-associated endoplasmic reticulum membranes. J. Alzheimer's Dis.

Schrepfer, E., and Scorrano, L. (2016). Mitofusins, from Mitochondria to Metabolism. Mol. Cell.

Schwoch, G., Trinczek, B., and Bode, C. (1990). Localization of catalytic and regulatory subunits of cyclic AMP-dependent protein kinases in mitochondria from various rat tissues. Biochem. J.

Scorrano, L., De Matteis, M.A., Emr, S., Giordano, F., Hajnóczky, G., Kornmann, B.,

Lackner, L.L., Levine, T.P., Pellegrini, L., Reinisch, K., et al. (2019). Coming together to define membrane contact sites. Nat. Commun.

Shiba-Fukushima, K., Imai, Y., Yoshida, S., Ishihama, Y., Kanao, T., Sato, S., and Hattori, N. (2012). PINK1-mediated phosphorylation of the Parkin ubiquitin-like domain primes mitochondrial translocation of Parkin and regulates mitophagy. Sci. Rep.

Shore, G.C., and Tata, J.R. (1977). Two fractions of rough endoplasmic reticulum from rat liver. I. Recovery of rapidly sedimenting endoplasmic reticulum in association with mitochondria. J. Cell Biol.

Soman, S., Keatinge, M., Moein, M., Da Costa, M., Mortiboys, H., Skupin, A., Sugunan, S., Bazala, M., Kuznicki, J., and Bandmann, O. (2017). Inhibition of the mitochondrial calcium uniporter rescues dopaminergic neurons in pink1−/− zebrafish. Eur. J. Neurosci.

Spacek, J., and Harris, K.M. (1997). Three-dimensional organization of smooth endoplasmic reticulum in hippocampal CA1 dendrites and dendritic spines of the immature and mature rat. J. Neurosci.

Spillantini, M.G., Schmidt, M.L., Lee, V.M.Y., Trojanowski, J.Q., Jakes, R., and Goedert, M. (1997). α-synuclein in Lewy bodies [8]. Nature.

De Stefani, D., Raffaello, A., Teardo, E., Szabó, I., and Rizzuto, R. (2011). A forty-kilodalton protein of the inner membrane is the mitochondrial calcium uniporter. Nature.

De Stefani, D., Bononi, A., Romagnoli, A., Messina, A., De Pinto, V., Pinton, P., and Rizzuto, R. (2012). VDAC1 selectively transfers apoptotic Ca 2 signals to mitochondria. Cell Death Differ.

De Stefani, D., Rizzuto, R., and Pozzan, T. (2016). Enjoy the Trip: Calcium in Mitochondria Back and Forth. Annu. Rev. Biochem. *85*, 161–192.

Surmeier, D.J. (2018). Determinants of dopaminergic neuron loss in Parkinson's disease. FEBS J. *285*, 3657–3668.

Surmeier, D.J., and Schumacker, P.T. (2013). Calcium, bioenergetics, and neuronal vulnerability in Parkinson's disease. J. Biol. Chem.

Surmeier, D.J., Schumacker, P.T., Guzman, J.D., Ilijic, E., Yang, B., and Zampese, E. (2017). Calcium and Parkinson's disease. Biochem. Biophys. Res. Commun. *483*, 1013–1019.

Tanaka, A., Cleland, M.M., Xu, S., Narendra, D.P., Suen, D.F., Karbowski, M., and Youle, R.J. (2010). Proteasome and p97 mediate mitophagy and degradation of mitofusins induced by Parkin. J. Cell Biol.

Taylor, S.S., Lev-Ram, V., Ellisman, M.H., Goldberg, J.L., Ilouz, R., Stiles, T.L., Bushong,

E.A., Douglas, C., and Friedmann-Morvinski, D. (2017). Isoform-specific subcellular localization and function of protein kinase A identified by mosaic imaging of mouse brain. Elife *6*, 1–23.

Twig, G., Hyde, B., and Shirihai, O.S. (2008). Mitochondrial fusion, fission and autophagy as a quality control axis: The bioenergetic view. Biochim. Biophys. Acta - Bioenerg.

Vais, H., Mallilankaraman, K., Mak, D.O.D., Hoff, H., Payne, R., Tanis, J.E., and Foskett, J.K. (2016). EMRE Is a Matrix Ca2+ Sensor that Governs Gatekeeping of the Mitochondrial Ca2+ Uniporter. Cell Rep.

Valente, E.M., Caputo, V., Salvi, S., Dallapiccola, B., Abou-Sleiman, P.M., Muqit, M.M.K., Healy, D.G., Gilks, W.P., Wood, N.W., Latchman, D.S., et al. (2004). Hereditary early-onset Parkinson's disease caused by mutations in PINK1. Science (80-.). *304*, 1158–1160.

Várnai, P., Tóth, B., Tóth, D.J., Hunyady, L., and Balla, T. (2007). Visualization and manipulation of plasma membrane-endoplasmic reticulum contact sites indicates the presence of additional molecular components within the STIM1-Orai1 complex. J. Biol. Chem. *282*, 29678–29690.

Vicario, M., and Calì, T. (2019). Measuring Ca2+ levels in subcellular compartments with genetically encoded GFP-based indicators. In Methods in Molecular Biology, p.

Voigt, A., Berlemann, L.A., and Winklhofer, K.F. (2016). The mitochondrial kinase PINK1: functions beyond mitophagy. J. Neurochem. *139*, 232–239.

Wang, X., Yan, M.H., Fujioka, H., Liu, J., Wilson-delfosse, A., Chen, S.G., Perry, G., Casadesus, G., and Zhu, X. (2012). LRRK2 regulates mitochondrial dynamics and function through direct interaction with DLP1. Hum. Mol. Genet.

Xia, Q. (2008). Proteomic identification of novel proteins associated with Lewy bodies. Front. Biosci.

Xiong, H., Wang, D., Chen, L., Yeun, S.C., Ma, H., Tang, C., Xia, K., Jiang, W., Ronai, Z., Zhuang, X., et al. (2009). Parkin, PINK1, and DJ-1 form a ubiquitin E3 ligase complex promoting unfolded protein degradation. J. Clin. Invest.

Yamano, K., and Youle, R.J. (2013). PINK1 is degraded through the N-end rule pathway. Autophagy *9*, 1758–1769.

Yamano, K., Matsuda, N., and Tanaka, K. (2016). The ubiquitin signal and autophagy: an orchestrated dance leading to mitochondrial degradation. EMBO Rep.

Yang, Y., Ouyang, Y., Yang, L., Beal, M.F., McQuibban, A., Vogel, H., and Lu, B. (2008). Pink1 regulates mitochondrial dynamics through interaction with the fission/fusion machinery. Proc. Natl. Acad. Sci. *105*, 7070–7075.

Zallo, F., Gardenal, E., Verkhratsky, A., and Rodríguez, J.J. (2018). Loss of calretinin and parvalbumin positive interneurones in the hippocampal CA1 of aged Alzheimer's disease mice. Neurosci. Lett.

Zhao, X., León, I.R., Bak, S., Mogensen, M., Wrzesinski, K., Højlund, K., and Jensen, O.N. (2011). Phosphoproteome analysis of functional mitochondria isolated from resting human muscle reveals extensive phosphorylation of inner membrane protein complexes and enzymes. Mol. Cell. Proteomics.

Zhao, X., Bak, S., Pedersen, A.J.T., Jensen, O.N., and Højlund, K. (2014). Insulin increases phosphorylation of mitochondrial proteins in human skeletal muscle in vivo. J. Proteome Res.

Zhou, W., Chen, K.H., Cao, W., Zeng, J., Liao, H., Zhao, L., and Guo, X. (2010). Mutation of the protein kinase A phosphorylation site influences the anti-proliferative activity of mitofusin 2. Atherosclerosis.

BBA - Molecular Basis of Disease 1864 (2018) 3247–3256

Contents lists available at ScienceDirect

BBA - Molecular Basis of Disease

journal homepage: www.elsevier.com/locate/bbadis

Tau localises within mitochondrial sub-compartments and its caspase cleavage affects ER-mitochondria interactions and cellular Ca^{2+} handling

Domenico Cieri[a,1], Mattia Vicario[a,1], Francesca Vallese[a], Beatrice D'Orsi[a], Paola Berto[a], Alessandro Grinzato[a], Cristina Catoni[b], Diego De Stefani[a], Rosario Rizzuto[a], Marisa Brini[b], Tito Calì[a,c,*]

[a] Department of Biomedical Sciences, University of Padova, Padova, Italy
[b] Department of Biology, University of Padova, Padova, Italy
[c] Padova Neuroscience Center (PNC), University of Padova, Padova, Italy

ARTICLE INFO

Keywords:
Tau
Mitochondria
ER-mitochondria contact sites
SPLICS
Mitochondrial sub-compartments

ABSTRACT

Intracellular neurofibrillary tangles (NFT) composed by tau and extracellular amyloid beta (Aβ) plaques accumulate in Alzheimer's disease (AD) and contribute to neuronal dysfunction. Mitochondrial dysfunction and neurodegeneration are increasingly considered two faces of the same coin and an early pathological event in AD. Compelling evidence indicates that tau and mitochondria are closely linked and suggests that tau-dependent modulation of mitochondrial functions might be a trigger for the neurodegeneration process; however, whether this occurs either directly or indirectly is not clear. Furthermore, whether tau influences cellular Ca^{2+} handling and ER-mitochondria cross-talk is yet to be explored. Here, by focusing on wt tau, either full-length (2N4R) or the caspase 3-cleaved form truncated at the C-terminus (2N4RΔC_{20}), we examined the above-mentioned aspects. Using new genetically encoded split-GFP-based tools and organelle-targeted aequorin probes, we assessed: i) tau distribution within the mitochondrial sub-compartments; ii) the effect of tau on the short- (8–10 nm) and the long- (40–50 nm) range ER-mitochondria interactions; and iii) the effect of tau on cytosolic, ER and mitochondrial Ca^{2+} homeostasis. Our results indicate that a fraction of tau is found at the outer mitochondrial membrane (OMM) and within the inner mitochondrial space (IMS), suggesting a potential tau-dependent regulation of mitochondrial functions. The ER Ca^{2+} content and the short-range ER-mitochondria interactions were selectively affected by the expression of the caspase 3-cleaved 2N4RΔC_{20} tau, indicating that Ca^{2+} mis-handling and defects in the ER-mitochondria communications might be an important pathological event in tau-related dysfunction and thereby contributing to neurodegeneration. Finally, our data provide new insights into the molecular mechanisms underlying tauopathies.

1. Introduction

Intracellular tau neurofibrillary tangles (NFTs) and extracellular formation of Aβ-plaques represent key pathologic hallmarks of Alzheimer's disease (AD) [1,2]. NFTs have been found in neurons of the entorhinal cortex and the hippocampus. The increase in NTFs levels within the brain clinically correlates with dementia [3,4]. Tau, a highly soluble microtubule-associated protein (MAP) that promotes their assembly and stabilisation, is the main constituent of NTFs [5]. Post-translational modifications, including truncation, hyper-phosphorylation and conformational changes, are at the basis of tau-mediated pathology [6]. In the fibrillar pathologies of AD, caspase 3 cleavage of tau at Asp421 occurs before the nuclear events of apoptosis [7] and generates a truncated protein that aggregates more rapidly due to a conformational change induced by the lack of its basic C-terminal 20 amino acids. Under physiological conditions, this C-terminal domain inhibits tau filament assembly [8], possibly by self-association with the acidic N-terminal projection domain, which is also involved in the interaction with other cytoskeletal elements, including mitochondria or neuronal plasma membrane [9–11]. Truncated tau associates with both early and late NFTs markers and its presence correlates with cognitive decline [1,12,13]. Additionally, truncated tau is aberrantly phosphorylated and its caspase-mediated cleavage is an early event that may precede hyper-phosphorylation [7]. Tau hyper-phosphorylation is indeed a common

* Corresponding author at: Department of Biomedical Sciences, University of Padova, Padova, Italy.
E-mail address: tito.cali@unipd.it (T. Calì).
[1] Equal contribution.

https://doi.org/10.1016/j.bbadis.2018.07.011
Received 28 March 2018; Received in revised form 16 June 2018; Accepted 6 July 2018
Available online 11 July 2018
0925-4439/

feature of the neurofibrillary changes that occur in all tauopathies [14]. There are six different isoforms of tau in the adult human brain, 0 N, 1 N or 2 N with 3R or 4R [15]. They differ on the number of the 29-residue near-N-terminal insert (N) encoded by exons 2 and 3, and depending on whether they contain three or four C-terminal repeat domains (R; the second of which is encoded by exon 10). The tau sequence contains several phosphorylation sites that, in AD patients' brain, undergo hyperphosphorylation and aggregation in paired helical filaments (PHF) [16]. The phosphorylation state of tau has an impact on the functional state of the protein, affecting both its binding to microtubules and its aggregation properties. Tau accumulation triggers a cascade of events that eventually leads to its propagation from cell to cell in a prion-like mode, spreading tauopathy to other areas of the brain [17]. Despite the importance of tau modifications in the aetiology of AD has been well described, how it affects cellular function and leads to neurodegeneration is still unclear. Mitochondrial alterations were demonstrated in transgenic mice overexpressing tau protein and mice injected with tau oligomers [18,19]. The expression of wt (2N4R) or caspase 3-cleaved tau (2N4RΔC_{20}; able to induce fibrillation and seeding of wt tau as well [20,21]) has been reported to cause perinuclear clustering of mitochondria [22–25] and changes in mitochondrial shaping proteins expression levels [22,23] in fibroblasts from sporadic AD patients, rat hippocampal neurons as well as several mammalian cell lines, suggesting an intimate relationship between mitochondria and tau.

Tau overexpression increases retrograde mitochondrial transport, whereas it decreases complex I activity and ATP levels [23]. Mitophagy deficits and changes in mitochondrial membrane potential were reported both in *in vitro* and *in vivo* models for tau accumulation [27], and alterations of mitochondrial trafficking were detected in the axon of sensory neurons of zebrafish embryos expressing mutant tau and in cells expressing different forms of tau [28,29]. Thus, mitochondria might be an important route through which tau leads to the degeneration and death of specific subsets of neuronal cells. Nevertheless, whether these events occur as a consequence of tau-induced dysfunctions that fall back on mitochondria or can be directly triggered by tau at mitochondrial level is still unclear. Some evidence supporting the localisation of tau (wt, phosphorylated form or caspase cleaved N-terminal fragment) within mitochondria or its association with the OMM has recently emerged [18,27,30,31] and suggested the intriguing possibility that “mitochondrial” tau may also play a role in the cellular dysfunctions found in tauopathies. In the present study, we investigated the localisation of tau at mitochondria and within sub-mitochondrial compartments by employing a novel and improved split-GFP based bimolecular fluorescence complementation (BiFC) methodology [32,33]. This tool was originally developed by us to selectively monitor DJ-1 sub-mitochondrial distribution [34]. In addition to the previously described OMM- and matrix-targeted $GFP_{1–10}$ [34], a new IMS targeted non-fluorescent $GFP_{1–10}$ moiety has been generated to selectively track protein translocation within the IMS. Two different tau constructs were C-terminally tagged with the GFP beta strand 11 (β_{11}): one encoding the wt full-length tau (2N4R) and the other one encoding the C-terminally deleted tau at position 421 (2N4RΔC_{20}). 2N4RΔC_{20} expression has been shown to induce mitochondrial fragmentation, increase of reactive oxygen species, reduction in mitochondrial motility and decrease of Ca^{2+} buffering capacity upon thapsigargin treatment [26,35–37]. The GFP-moieties-fused proteins were employed to specifically monitor and quantify tau distribution at the OMM, IMS and mitochondrial matrix. We also evaluated whether tau expression could result in Ca^{2+} signalling alterations. To this end, we assessed the consequences of tau 2N4R and 2N4RΔC_{20} overexpression on cytosolic, ER and mitochondrial Ca^{2+} homeostasis using organelle targeted aequorin-luminescent probes [38]. Lastly, we estimated the tau-dependent effect on ER-mitochondria interactions by the quantification of the number of short- (8–10 nm) and long- (40–50 nm) range contacts, [39], using a novel probe that we have recently developed. Hence, we detected constitutive presence of tau at the OMM and in the IMS, but not in the mitochondrial matrix. Moreover, we observed that caspase 3-cleaved tau, typically found in the brain of patients with mild cognitive impairment stage of AD [7,20] and associated with the formation of tau aggregates, affects ER Ca^{2+} levels and short-, but not long-, range ER-mitochondria interactions. These data suggest that tau may directly participate in the pathophysiology of mitochondria-related activities by interfering with ER-mitochondria communication, reinforcing the concept that an early involvement of mitochondrial dysfunctions, Ca^{2+} dyshomeostasis and ER-mitochondria Ca^{2+} cross-talk impairment might have a role in the pathogenesis of AD.

2. Materials and methods

2.1. DNA constructs

The full length hTau WT-β_{11} construct (2N4R) has been generated by PCR using the following primers: FL-hTau WT-S11 (*Bam*HI) For 5′-ATAAGTTCGGATCCATGGCTGAGCCCCGCCAGGAGTTCG-3′; FL-hTau WT-S11(*Xho*I) Rev. 5′-ACTTCTCACTCGAGTCATGTGATGCCGGC GGCGTTCACGTACTCGTGCAGCACCATGTGGTCCCGGCTGCCGCCGCC GCTGCCGCCGTCGCCCAAACCCTGCTTCGCGAGGGAGGCAG-3′. The ΔC_{20} hTau-β_{11} construct (2N4RΔC_{20}) has been amplified by PCR using the FL-hTau WT-S11 (*Bam*HI) For primer and the ΔC_{20}-S11 (*Xho*I) Rev. 5′-ACTTCTCACTCGAGTCATGTGATGCCGGCGGCGTTCACGTACTCGTG CAGCACCATGTGGTCCCGGCTGCCGCCGCCGCTGCCGCCGTCGCCGTC TACCATGTCGATGCTGCCGGTGG-3′. The DNA construct encoding for the human tau in pcDNA3, used as a template, was a kind gift of Dr. Paolo Paganetti (Laboratory for Biomedical Neurosciences, Neurocenter of Southern Switzerland). The β_{11} tagged Cytochrome-*c* at the C-terminus was produced by DNA synthesis (Thermo Scientific). The $GFP_{1–10}$ targeted to the intermembrane space (IMS) has been created by genetic fusion to the leader sequence of the IMS protein LACTB [40,41] and created by DNA synthesis (Thermo Scientific). To specifically monitor ER-mitochondria interactions with the newly generated split-GFP based sensor (SPLICS), the untagged versions of each tau constructs were generated introducing a stop codon before the β_{11} tag by site-direct mutagenesis. All constructs were confirmed by sequencing.

2.2. Cell culture and transfection

HeLa cells were grown in DMEM high glucose medium (Euroclone) supplemented with 10% Fetal bovine serum (FBS, GIBCO), 100 U/ml penicillin (Euroclone) and 100 μg/ml streptomycin (Euroclone).

For immunocytochemistry and contacts quantification, cells were seeded onto 13 mm glass coverslips, whereas for western blotting and Ca^{2+} measurements onto 6-multiwell plates, and allowed to grow to 60–80% confluence. Transfection was carried out 12 h after seeding with the Ca^{2+} phosphate procedure using 5 μg of total DNA for each 13 mm glass coverslip and 12 μg for each well of the 6-multiwell plate. For Ca^{2+} measurements, cells were co-transfected with Aequorin constructs targeted to different cell compartments (mtAEQ, cytAEQ and erAEQ) and pcDNA3 empty vector (control) or tau FL-hTau WT and ΔC_{20} with a 1:2 ratio in favour of tau. For ER-mitochondria contact sites quantification, HeLa cells were co-transfected with $SPLICS_S$ (short range contacts) or $SPLICS_L$ (long range contacts) in combination with void vector or FL-hTau WT or ΔC_{20} in a 1,5:1,5:2 ratio in favour of the overexpressed protein.

2.3. Preparation of post-natal mouse neocortical neurons

Primary cultures of cortical neurons were prepared from post-natal days 0–2. To isolate the cortical neurons, mouse pups were euthanized by cutting their heads off with large scissors. The cerebral cortices were isolated from each pup and pooled in a dissection medium on ice (PBS with 0.25% glucose, 0.3% bovine serum albumin [BSA]). The tissue was incubated with 0.25% trypsin-EDTA at 37 °C for 15 min. After the

incubation, the trypsinisation was stopped by the addition of fresh plating medium (minimal essential medium [MEM] containing 5% fetal bovine serum, 5% horse serum, 100 U/ml penicillin/streptomycin [Pen/Strep], 0.5 mM L-glutamine, 0.6% D-glucose). The neurons were then dissociated by gentle pipetting and after centrifugation (1500 rpm, 3 min), the medium containing trypsin was aspirated. Neocortical neurons were resuspended in plating medium, plated at 2×10^5 cells per cm^2 on poly-D-lysine-coated plates (final concentration of 5 μg/ml), and then incubated at 37 °C and 5% CO_2. The plating medium was exchanged with 50% feeding medium (NBM-embryonic containing 100 U/ml of Pen/Strep, 2% B27 and 0.5 mM L-glutamine), 50% plating medium with additional mitotic inhibitor cytosine arabinofuranoside (600 nM). Two days later the medium was again exchanged for complete feeding medium. Neocortical neurons (days in vitro, DIV 5) were transfected using Lipofectamine 2000 (Invitrogen) and stainings were performed on DIV 7.

2.4. Calcium measurements

Ca^{2+} concentration measurements were carried out in a Perkin-Elmer Envision plate reader equipped with a two-injector unit. Twenty-four hours after transfection, cells were plated onto a 96-well plate. The day after, recombinant wt cytAEQ or mutant mtAEQ were reconstituted by incubating HeLa cells for 1,5 h with 5 μM wt coelenterazine (Santa Cruz Biotechnology) in modified Krebs Ringer Buffer (KRB: 125 mM NaCl, 5 mM KCl, 400 mM KH2PO4, 1 mM $MgSO_4$, 20 mM Hepes, pH 7.4) supplemented with 5 mM glucose at 37 °C. To functionally reconstitute low affinity ER targeted aequorin, the ER Ca^{2+} content was drastically reduced by incubating cells for 1,5 h at 4 °C with KBR supplemented with 5 μM of the Ca^{2+} ionophore ionomycin (Sigma), 600 μM EGTA and 5 μM coelenterazine n (Biotium). Cells were then washed with KRB supplemented with 2% bovine serum albumin (Sigma) and 1 mM EGTA. After reconstitution, cells were placed in 70 μl of KRB supplemented as indicated in the figures and luminescence from each well was measured for the indicated period of time. According to the experiment, Ca^{2+} transients were generated by the addition of 100 μM histamine (Sigma) or 2 mM $CaCl_2$ at the final concentration. The experiments were terminated by lysing the cells with 100 μM digitonin (Sigma) in a hypotonic Ca^{2+}-rich solution (10 mM $CaCl_2$ in H_2O) to discharge the remaining reconstituted aequorin pool. Output data were analysed and calibrated with a custom made macro-enabled Excel workbook.

2.5. Western blot analysis

36 h after transfection, HeLa cells were processed for western blot analysis. Cells were washed with ice-cold PBS and solubilised in ice-cold lysis buffer (150 mM NaCl, 50 mM Tris-HCl, pH 7.4, 10 mM EGTA/Tris, pH 7.4, 1% Triton X-100) containing 1 mM protease inhibitors cocktail (Sigma). Postnuclear supernatants were collected after 10 min of centrifugation at 10,000 *g* at 4 °C. The total protein content was determined by the Bradford assay (Bio-Rad). Samples were loaded on a 15% SDS-PAGE Tris/HCl gel, transferred onto PVDF membranes (Merck Millipore), blocked for 1 h with 5% milk in TBS-T (Tris Buffered Saline-Tween, 20 mM Tris, 0.137 M NaCl, pH 7.6, 0.1% Tween 20) at 4 °C and incubated overnight with a mouse monoclonal antibody recognizing all tau isoforms (Anti-tau 4-repeat isoform RD4, clone 1E1/A6, Merck Millipore), and mouse monoclonal anti β-Actin (Sigma), mouse polyclonal anti Tom20 (Santa Cruz) or tubulin (Santa Cruz) as endogenous control (dilutions are 1:1000). Detection was carried out by incubation with secondary horseradish peroxidase-conjugated anti-mouse IgG antibody (Santa Cruz) for 1 h at room temperature and proteins were visualized by the chemiluminescent reagent Luminata Western HRP substrate (Merck Millipore).

2.6. Cellular fractionation

Cells were plated on a Petri dish and transfected with 30 μg of total DNA. 36 h after transfection cells were washed with PBS and harvested using a scraper. Cells were then collected in a tube, centrifuged at 1400 rpm for 4 min at 4 °C, washed with 10 mM Hepes supplemented with 0.25 M sucrose and resuspended in 500 μl of the same solution. Cells were then lysate using a potter and centrifuged 10 min at 1000 *g* to pellet nuclei. 50 μl of the supernatant were collected and used as total lysate (PNS: post-nuclear supernatant). The remaining supernatant was centrifuged at 10,000 *g* for 6 min to pellet mitochondria. The resulting supernatant (cytosol) was collected and lysed by adding 1% Triton X-100. Both mitochondria and cytosol were washed and centrifuged 5–6 times with Hepes supplemented with sucrose (dealing with the cytosol, each time 20 μl of lysate were left in the tube to dilute contamination with other cellular fractions). Mitochondria were resuspended in 300 mM NaCl, 10 mM $CaCl_2$, 100 mM Tris HCl pH 8.5 and 0.5% NP40 for 30 min at 4 °C.

2.7. Immunocytochemistry analysis

36 h after transfection, HeLa cells were stained for immunofluorescence. The cells were washed twice with PBS (140 mM NaCl, 2 mM KCl, 1.5 mM KH_2PO_4, 8 mM Na_2HPO_4, pH 7.4), fixed for 20 min in 3.7% formaldehyde (Sigma) and washed three times with PBS. The cells were then permeabilised in 0.1% Triton X-100 in PBS, followed by a 1 h wash with 1% gelatin (type IV, from calf skin) (Sigma) in PBS. Cells were then incubated for 1 h at 37 °C in a wet chamber with a mouse monoclonal antibody recognizing all tau isoforms (Anti-tau 4-repeat isoform RD4, clone 1E1/A6, Merck Millipore) or with a rabbit polyclonal anti-Tom20 antibody (Santa Cruz Biotechnology) at a 1:20 dilution in PBS. Staining was performed with Alexa Fluor 488 or 633-labeled anti-mouse or Alexa Fluor 594 anti-rabbit secondary antibody (Molecular Probes, Carlsbad, CA) at a 1:50 dilution in PBS.

36 h post transfection, cortical neurons grown on 13-mm coverslips and transfected with the different constructs were loaded with the MitoTracker Mitochondrion-selective probe Red (Invitrogen, 200 nM) for 30 min. Following incubation time, neurons were washed once in PBS and fixed with 4% paraformaldehyde for 15 min, permeabilised in PBS containing 0.1% Triton X-100 and washed three times with PBS. For nuclear staining, Hoechst 33258 (Sigma; 1 μg/ml) was then added into the wells for 30 min, after which coverslips were then transferred to glass slides with a mounting medium and sealed around the edges with clear varnish. Images were acquired with a Leica SP5 inverted confocal microscope and analysed by ImageJ software.

2.8. Quantification of biFC at the IMS

To quantify biFC at the IMS, a complete z-stack of cells showing a clear fluorescence signal was acquired using a Leica SP5 confocal microscope. The total corrected cell fluorescence (TCCF) was calculated as previously described [42]. Briefly, the selected cell was outlined using the freehand selection of Fiji and the remaining signal coming from outside the cell was removed. Area, integrated density and mean grey value were then measured within the cells and three selected non-fluorescent area in the image were chosen as background. The TCCF was calculated as follow: integrated density – (area of selected cell × mean fluorescence of background readings). The calculated TCCF was then normalised against the TCCF values of wt tau-expressing cells. The results are shown as fold change increase/decrease over 2N4R-tau expressing cells TCCF levels.

2.9. Mitochondrial distribution analysis

To quantify mitochondrial distribution within the cell, we used the Radial Profile Plot plugin available on Fiji (https://imagej.nih.gov/ij/

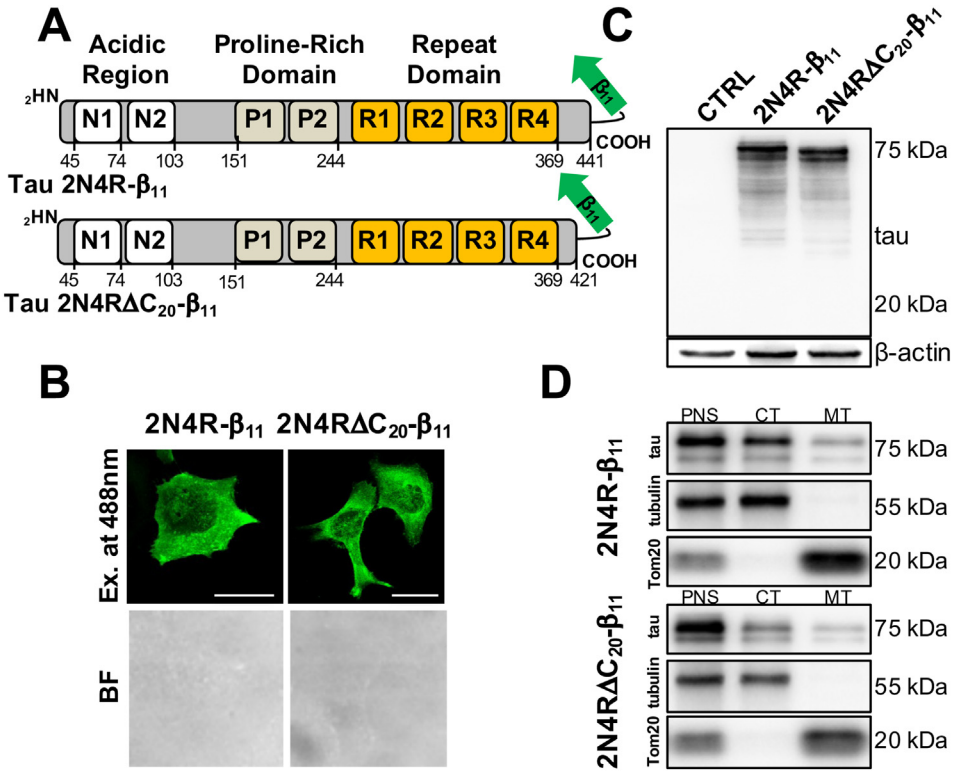

Fig. 1. Tau-β_{11} expression in HeLa cells. (A) Schematic representation of the different tau forms expressed in HeLa cells. The C-terminally-fused β_{11} fragment is depicted in green. (B) Representative confocal images of tau-β_{11} transfected HeLa cells immunostained with an anti-tau antibody. Scale bar = 25 μm. (C) Western blot from total cell lysates showing tau-β_{11} expression levels in HeLa cells. The membrane was incubated with a tau antibody and β-actin was used as loading control. (D) Western blot from cellular fractionation of tau transfected cells and empty vector control showing tau in the different cellular compartments. Tubulin and Tom20 were employed as markers of the cytosolic and mitochondrial fraction, respectively. PNS: Post-nuclear supernatant, CT: cytosol; MT: mitochondria. (For interpretation of the references to color in this figure legend, the reader is referred to the web version of this article.)

plugins/radial-profile.html). The plugin analyses the distribution of normalised integrated intensities around concentric circles starting from a specific point: in our case, the nucleus of the cell, set manually by drawing a circle. The distribution of fluorescence intensities was analysed on a radius of 200–300 pixels, sufficient to cover, on most cases, the overall area occupied by the cell. Spatial calibration was used to measure the maximal distance occupied by mitochondria in microns: for each cell, the first value of "Normalised Integrated Intensity" above 0.1 was considered as the most distant point in which mitochondria could be detected (Max. Radius in the graph in Fig. 2C).

2.10. ER-mitochondria contact sites quantification

48 h after transfection, HeLa cells were excited at 488nm and analysed by using a Leica TSC SP5 inverted microscope equipped with a HCX PL APO 100×/numerical aperture 1.4 oil immersion objective. A complete z-stack of each cell was captured every 0.29 μm with the Leica AS software. To quantify inter-organelle contact sites, images were processed using Fiji software. Images were convolved, filtered with Gaussian Blur and reconstructed in three dimensions using the Volume J plugin. A selected face of the 3D rendering was then thresholded and used to count ER-mitochondria contacts.

2.11. Statistical analysis

Results shown are mean values ± SEM. Student's unpaired two-tailed *t*-test was used for comparisons involving two groups when sample followed a Gaussian distribution. Differences between groups were considered significant when $p \leq 0.05$. All statistical analyses were performed using GraphPad Prism version 6.00 for Mac OS X, GraphPad Software (La Jolla, California, USA). The exact values of n and their means are indicated in the text. $^{*}p \leq 0.01$, $^{**}p \leq 0.0005$, $^{***}p \leq 0.0001$.

3. Results

3.1. Tau localises to mitochondria

In order to verify tau mitochondrial localisation, we employed split GFP-based tools and generated two constructs encoding two variants of human wt tau tagged with the GFP-β_{11} at their C-terminus (Fig. 1A): the full-length tau containing 4 repeats (2N4R-β_{11}) and a truncated tau form at position 421 (2N4RΔC_{20}-β_{11}). The tau-encoding constructs were transfected in HeLa cells and their expression and subcellular localisation were assessed by immunocytochemistry and western blot analysis. Anti-tau antibody staining showed a diffused distribution of the protein within the cell (Fig. 1B). Western blots on total lysates from HeLa cells transfected with the different constructs confirmed their correct expression at the expected molecular weights (Fig. 1C). Similar results were obtained with the untagged human tau constructs (Fig. S1), demonstrating that the expression and subcellular localisation of the protein were not altered by the addition of the β_{11} fragment at their C-terminus. We next performed subcellular fractionation experiments on HeLa cells transfected with the human tau-β_{11} constructs and observed their localisation within mitochondria. As shown in Fig. 1D, the 2N4R-β_{11} protein, corresponding to the wt full-length tau, was found in the post nuclear supernatant fraction (PNS) and in the cytosolic fraction (CT), as expected. Interestingly, the crude mitochondrial fraction (MT) also contained the protein, as previously observed [23,27,31,43]. Analogously, the 2N4RΔC_{20}-β_{11} tau was detected in PNS and CT fractions and, surprisingly, in the mitochondrial fraction as well. The purity of the fractionation experiment was verified by probing the blotting membrane with specific antibodies against proteins of the cytosol (tubulin) and mitochondria (Tom20). Altogether, these data suggest that under basal conditions a fraction of the cellular tau is associated to mitochondria. Whether the tau fraction at mitochondrial level has a physiological meaning or represents a product of degradation of this "fibrillogenic" protein is still unknown.

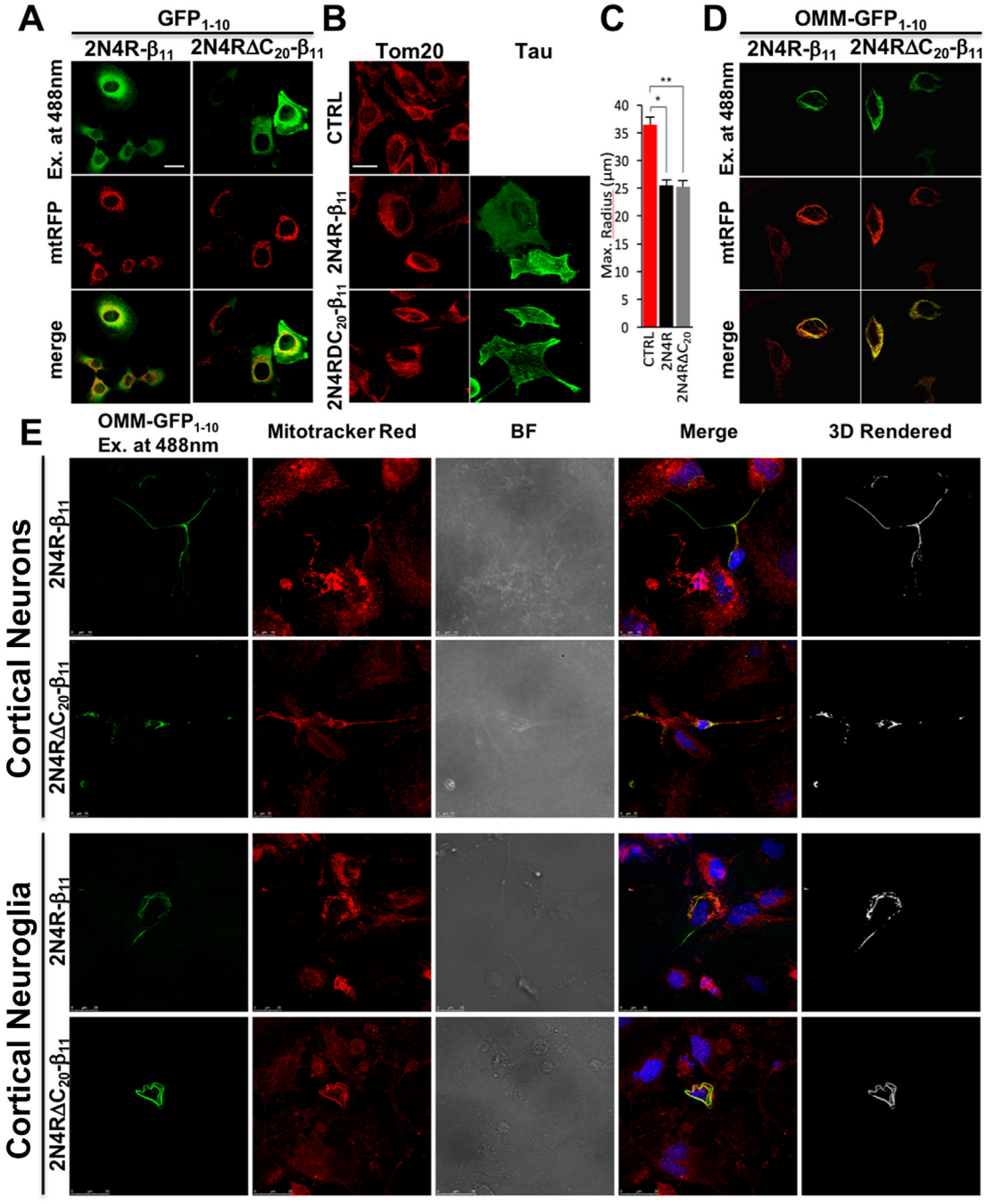

Fig. 2. Cytosolic and outer mitochondrial membrane distribution of tau revealed by GFP biFC and tau-induced mitochondrial alterations. The interaction between tau-β_{11} and the different $GFP_{1–10}$ fragments results in biFC that is detected as a fluorescent signal. (A) Confocal pictures showing HeLa cells co-transfected with tau-β_{11}, cytosolic $GFP_{1–10}$ and mitochondrial RFP (mtRFP). (B) Confocal images showing mitochondrial distribution in control and tau-transfected HeLa cells. Mitochondria and tau were immunostained with an anti-Tom20 (red) and anti-tau (green) antibody, respectively. (C) Histogram representing mitochondrial distribution in HeLa cells upon the conditions shown in B. (D) GFP biFC was used to analyse tau localisation at the outer mitochondrial membrane. Co-transfection of HeLa cells with 2N4R-β_{11}, the 2N4RΔC_{20}-β_{11} tau and OMM-$GFP_{1–10}$ resulted in GFP biFC at the OMM that co-localised with the mitochondria-targeted pTagRFP-mito plasmid. The merge of the GFP biFC and the mitochondrial signal are shown on the right. (E) Confocal imaging showing the OMM localisation of tau in mouse primary cortical neurons (top) and non-neuronal cells, mainly neuroglia (bottom). Scale bar = 25 μm. (For interpretation of the references to color in this figure legend, the reader is referred to the web version of this article.)

3.2. A split-GFP based approach to reveal tau distribution within the mitochondria

To better identify tau function at the mitochondrial level, it was necessary to define its presence in the different sub-mitochondrial compartments. Despite cellular fractionation clearly showed tau association with mitochondria, this technique does not allow to discriminate in which specific compartment it is distributed. To address this aspect, we exploited the split-GFP based approach, developed and successfully employed by our group, to selectively assess the sub-mitochondrial localisation of the PD-related protein DJ-1 [34]. This technique is based on the ability of the super folder GFP variants, namely the $GFP_{1–10}$ (GFP without an essential β-strand) and the β_{11} (the lacking β-strand required for the reconstitution of the chromophore), to

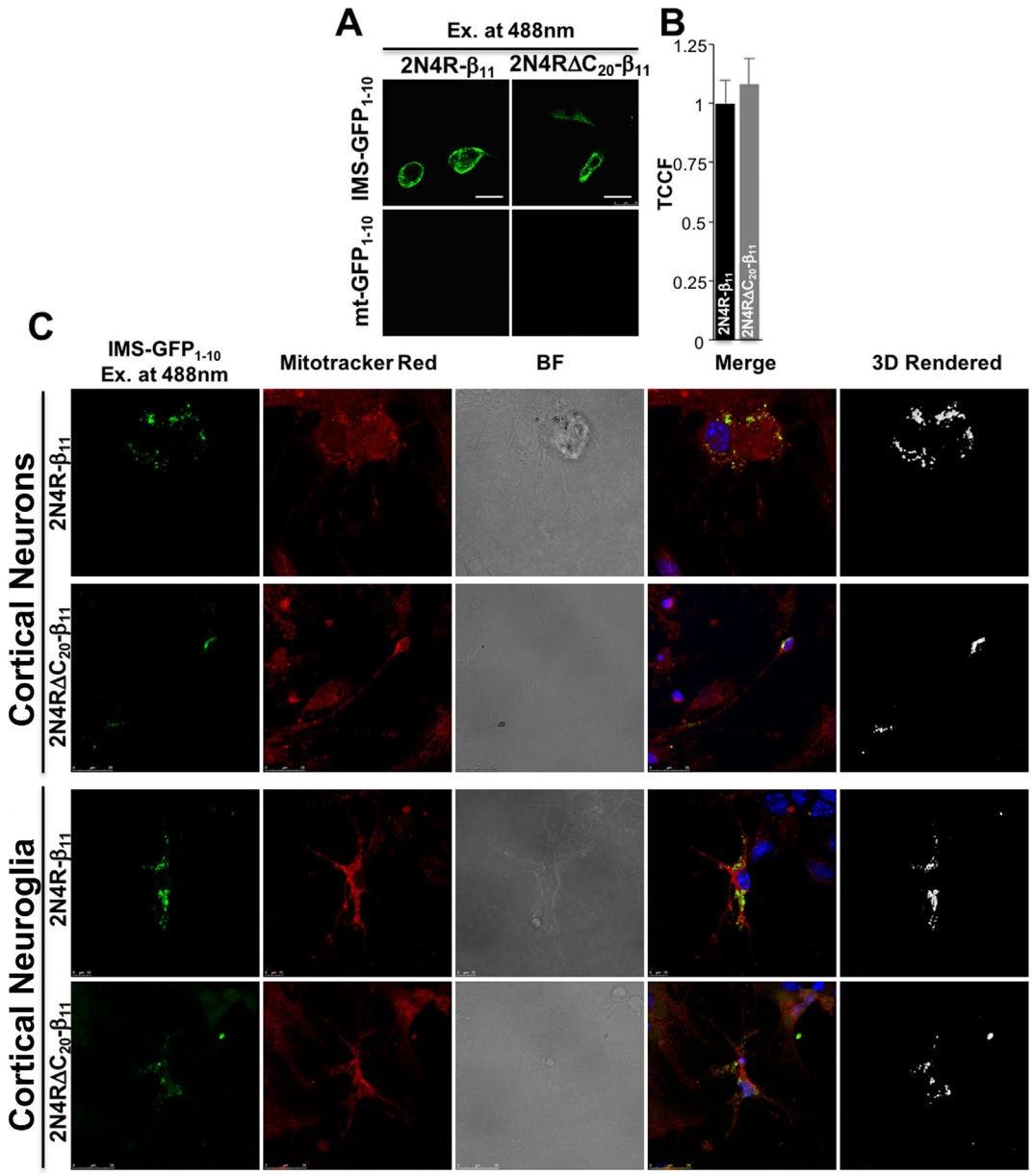

Fig. 3. Sub-mitochondrial distribution of tau revealed by GFP biFC. (A) GFP biFC was used to analyse tau localisation at the inter membrane space (top) and (bottom) mitochondrial matrix. (B) Histogram showing the quantification of the GFP biFC signal detected with the IMS-GFP$_{1–10}$ fragment. (D) Confocal images showing the IMS localisation of tau in mouse primary cortical neurons (top) and non-neuronal cells, mainly neuroglia (bottom). Scale bar = 25 μm.

self-assemble and, thus, reconstitute the GFP fluorescence [32,33]. In addition to the previously described GFP$_{1–10}$ constructs targeted to either the outer mitochondrial membrane (OMM-GFP$_{1–10}$) or the mitochondrial matrix (mt-GFP$_{1–10}$) [44], we have now expanded and completed the palette of constructs available to detect protein localisation/translocation within all the mitochondrial sub-compartments by developing a novel GFP$_{1–10}$ construct targeted to the intermembrane space (IMS-GFP$_{1–10}$). First, we verified whether the proper self-assembly of the newly generated GFP fragments efficiently occurred also in the IMS by co-transfecting HeLa cells with IMS-GFP$_{1–10}$ and a β_{11}-tagged cytochrome-*c* constructs. Fig. S2 clearly documented the appearance of a mitochondrial signal that perfectly co-localises with a mitochondrialtargeted RFP. To assess whether and where the β_{11} tau constructs were able to assemble and reconstitute GFP fluorescence, we initially co-transfected them in HeLa cells together with an untargeted cytosolic GFP$_{1–10}$. The resulting diffused fluorescence pattern (Fig. 2A) confirmed that GFP reconstitution mainly occurred in the cytosol, where the β_{11} tau proteins were detected by immunocytochemistry analysis (Fig. 1B). Interestingly, we noticed that, upon the expression of either 2N4R-β_{11} and 2N4RΔC$_{20}$-β_{11} tau, mitochondria appeared fused and mostly distributed at the perinuclear region (see mtRFP signal in Fig. 2A). To explore in more detail this aspect, we labeled mitochondria with an anti-Tom20 antibody to evaluate their distribution both in controls and in cells expressing 2N4R or 2N4RΔC$_{20}$ tau. In control cells, mitochondria occupied most of the cell area, spreading from the perinuclear region to cell periphery (Fig. 2B, top panel, CTRL). On the contrary, 2N4R and 2N4RΔC$_{20}$ tau expression conferred a peculiar cell phenotype: mitochondria were largely concentrated at the perinuclear region and excluded from cell periphery, as previously reported [23,24] (Fig. 2B, middle and bottom panels). Quantification of the radial distribution of mitochondria from the center of the cell confirmed this observation (Fig. 2C, max. radius values (μm): 36,51 ± 2,4 n = 15 for control cells; 25,49 ± 1,17 n = 16 for 2N4R-β_{11}; 25,22 ± 1,73 n = 18 for 2N4RΔC$_{20}$-β_{11}). These results also suggested that the C-terminal 20

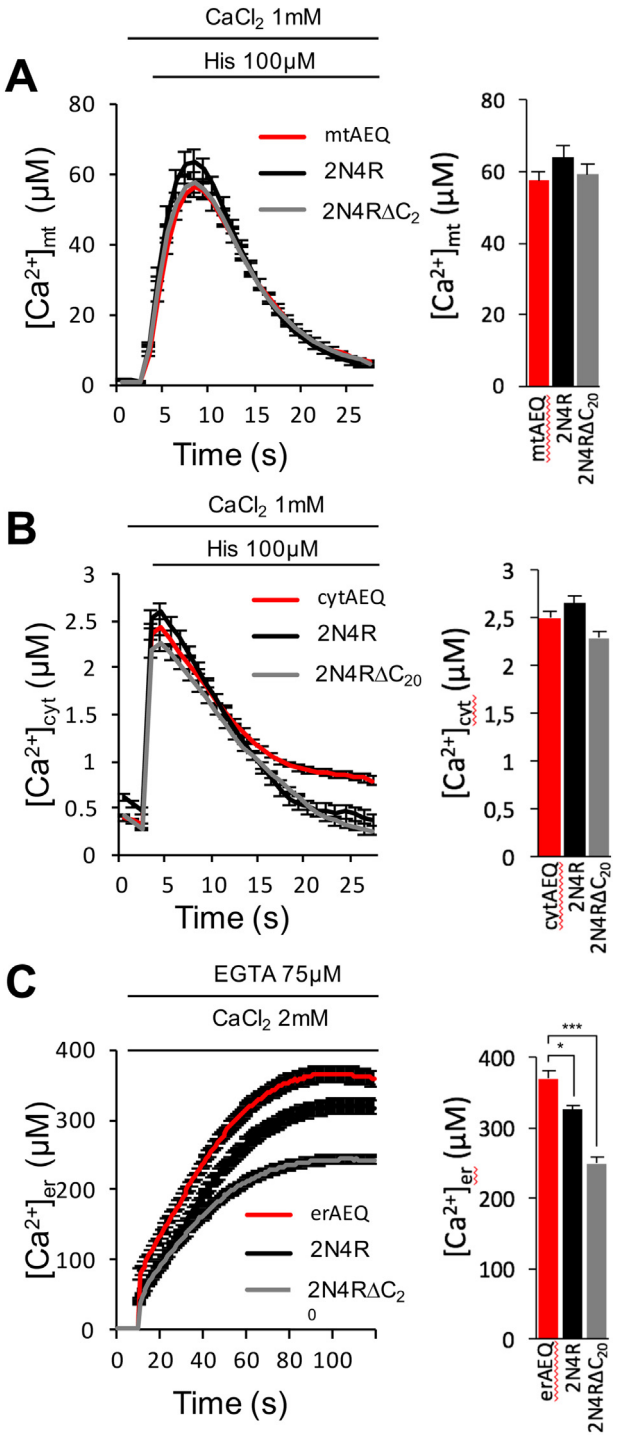

Fig. 4. Ca^{2+} handling in HeLa cells overexpressing the tau constructs. Ca^{2+} was measured in the different compartments by using mitochondrial (A), cytosolic (B) or ER-targeted (C) Aequorin. Ca^{2+} transients are shown on the left, whereas average Ca^{2+} peaks on the right.

amino acids of tau are dispensable for the observed effect on mitochondrial distribution.

To investigate in which specific sub-mitochondrial compartment tau localises and/or translocates, 2N4R-β_{11} and 2N4RΔC_{20}-β_{11} tau constructs were separately co-transfected in HeLa cells along with different $GFP_{1–10}$ plasmids targeted to either the OMM, IMS or the mitochondrial matrix. Fluorescence reconstitution at mitochondrial level is expected to take place only in the compartments where tau is effectively present. As shown in Fig. 2D, co-expression of either the 2N4R-β_{11} and 2N4RΔC_{20}-β_{11} constructs with the OMM-$GFP_{1–10}$ fragment led to a green fluorescence signal, which is fully overlapping with that of the mitochondrial marker, mtRFP. Of note, the GFP-reconstituted signal revealed strong mitochondrial fusion and, although we could not exclude that the GFP reconstitution might drive part of cytosolic tau to concentrate at the mitochondrial surface and/or affect its dissociation from the OMM, suggests that tau accumulation at the OMM might be important for the regulation of the mitochondrial fission/fusion. Tau localisation at the OMM and the above-mentioned effects on mitochondrial morphology were also confirmed in a more complex cellular system, i.e., in mouse primary cortical neurons (Fig. 2E, top panels) as well as in non-neuronal cells, mainly neuroglia, present, in small percentage, in the post-natal neuronal culture (Fig. 2E, bottom panels).

Analogously, to verify whether tau localises in the IMS and/or the mitochondrial matrix, the β_{11}-tagged tau constructs were co-transfected in HeLa cells with the IMS-$GFP_{1–10}$ or the mt-$GFP_{1–10}$ fragments (Fig. 3A). 2N4R-β_{11} and 2N4RΔC_{20}-β_{11} tau constructs were able to reconstitute the GFP fluorescence within the IMS (upper panel), indicating that a fraction of the two tau forms was present there. We have also quantified the total corrected cell fluorescence (for details, see materials and methods section) and found that the abundance of the two tau constructs within the cell was similar (Fig. 3B; TCCF values: 1 ± 0,09 n = 26 for 2N4R-β_{11}; 1,08 ± 0,1 n = 29 for 2N4RΔC_{20}-β_{11}). When the tau constructs were co-expressed with the mt-$GFP_{1–10}$ probe targeted to the mitochondrial matrix, we could not detect any specific mitochondria-localised signal, suggesting that none of the tested tau forms localised to this sub-compartment (bottom panel). We have also verified the presence of tau at the IMS in mouse cortical neurons (Fig. 3C, top panels) as well as in non-neuronal cells (Fig. 3C, bottom panels). As shown in the figure, a strong fluorescence was detected upon co-expression of the β_{11}-tagged tau constructs along with the IMS targeted $GFP_{1–10}$, suggesting that a fraction of tau was present at the level of the IMS also in these cells.

Altogether, these data showed that, under physiological conditions, a fraction of tau localises both at the OMM and in the IMS, and that tau affects mitochondrial morphology independently from its C-terminal 20 amino acids.

3.3. Effect of tau expression on cell Ca^{2+} handling and ER-mitochondrial interactions

The detection of tau at the OMM and the IMS prompted us to examine mitochondrial parameters that may be affected by tau expression. Thus, we monitored Ca^{2+} homeostasis and ER-mitochondria interactions in the short- (8–10 nm) and long- (40–50 nm) range using the newly generated split-GFP based sensors (SPLICS) [39]. Because the β_{11}-tagged tau constructs interfere with SPLICS reconstitution, we used their untagged versions for the evaluation of ER-mitochondria contact sites.

Firstly, we employed organelle-targeted aequorin probes to analyse Ca^{2+}-handling in specific cellular compartments, i.e., mtAEQmut for the mitochondrial matrix, cytAEQ for the cytoplasm and erAEQ for the ER lumen [38]. Considering the effects of tau expression on mitochondrial morphology, we initially assessed the ability of mitochondria to take up Ca^{2+} upon cell stimulation with the $InsP_3$-linked agonist histamine. The expression of both 2N4R and 2N4RΔC_{20} tau did not result in an altered mitochondrial Ca^{2+} handling (Fig. 4A. peak values: 57.58 ± 2.3 n = 30 for control cells; 63.87 ± 3.23 n = 32 for 2N4R-β_{11}; 59.24 ± 2.7 n = 31 for 2N4RΔC_{20}-β_{11}). Similarly, no differences were observed in cytosolic Ca^{2+} transients generated by histamine stimulation (Fig. 4B. peak values: 2.49 ± 0.07 n = 32 for control cells; 2.65 ± 0.07 n = 32 for 2N4R-β_{11}; 2.28 ± 0.07 n = 32 for 2N4RΔC_{20}-β_{11}), suggesting that the expression of wt and truncated tau did not affect bulk cellular Ca^{2+} handling.

However, both 2N4R and 2N4RΔC_{20} tau overexpression decreased

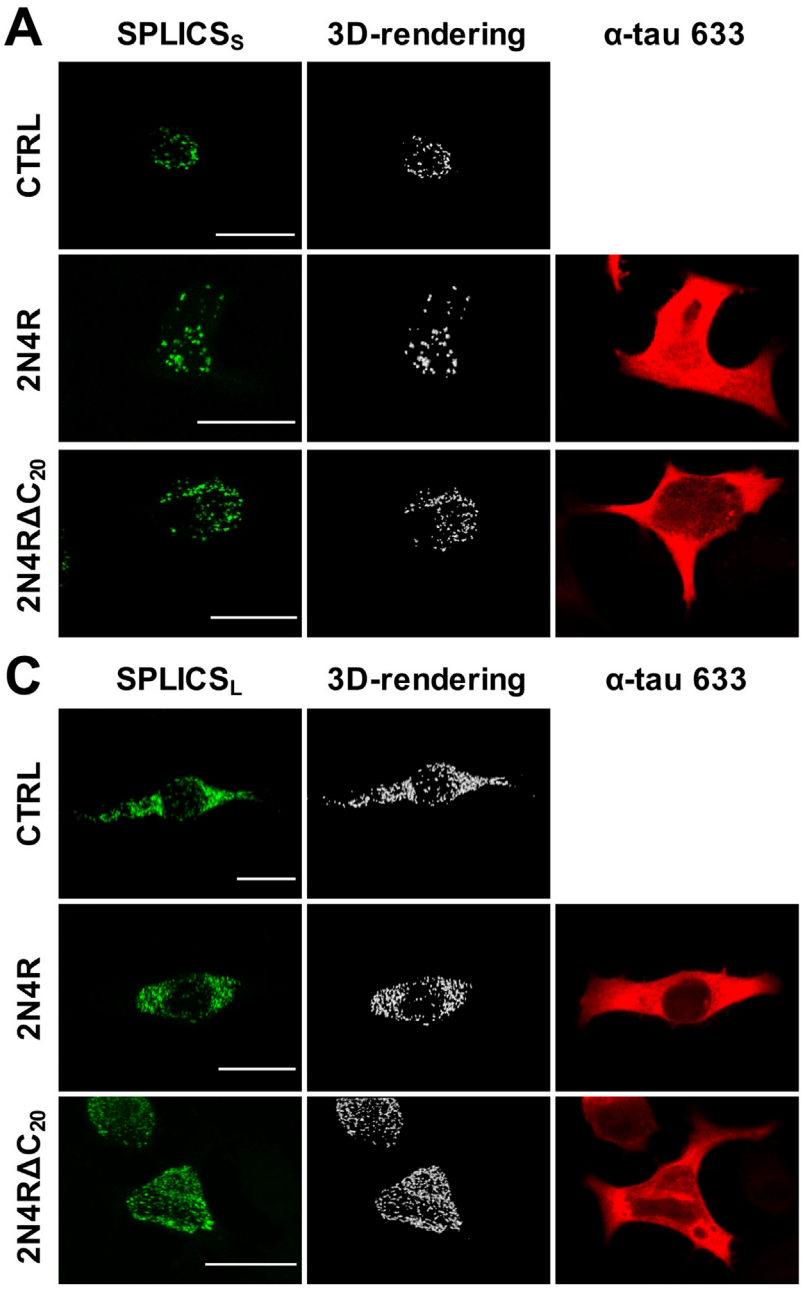

Fig. 5. Effects of tau expression on ER-mitochondria contact sites. Immunofluorescence against tau (red) is shown on the right, whereas ER-mitochondria contact sites detected with the SPLICS on the left (green). (A) Representative confocal images of HeLa cells expressing the SPLICS$_S$ probe. (B) Quantification of the SPLICS$_S$ contact sites number by 3D rendering of complete z-stacks. (C) Representative confocal images of HeLa cells expressing the SPLICS$_L$ probe. (D) Quantification of the SPLICS$_L$ contact sites number by 3D rendering of complete z-stacks. Scale bar = 25 μm. (For interpretation of the references to color in this figure legend, the reader is referred to the web version of this article.)

the steady-state ER Ca^{2+} content, as the caspase-cleaved tau form is more effective than the wt level (Fig. 4C. plateau values: 370.62 ± 11.64 $n = 20$ for control cells; 326.29 ± 6.44 $n = 22$ for 2N4R-β_{11}; 249.31 ± 9.29 $n = 24$ for 2N4RΔC_{20}-β_{11}).

Because the observed reduction in ER Ca^{2+} content did not result in a diminished mitochondrial Ca^{2+} transients, we hypothesised that the ER-mitochondria connection may be affected by tau expression and, in particular, by the 2N4RΔC_{20} mutant. The coupling between ER and mitochondria is indeed fundamental for ER-mitochondria Ca^{2+} transfer; in fact, this transfer and the correct proximity between the two organelles is regulated by several proteins, some of which have been involved in familial forms of neurodegenerative diseases [45]. To date, only one study reported a possible relationship between tau protein and ER-mitochondria tethering, showing that the number of contacts between mitochondria and RER membranes is increased in motor neurons derived from JNPL3 mice overexpressing P301L mutant tau compared to their controls [46]. Interestingly, this study also confirmed the presence of tau at mitochondria by EM analysis. We therefore quantified the number of ER-mitochondria contact sites in our cell models and discriminated their nature using SPLICS approach recently developed in our laboratory [39]. Indeed, the development of the two versions of SPLICS (SPLICS$_S$ or SPLICS$_L$) not only highlighted the heterogeneity in the ER-mitochondria contact sites, but also unravelled their differential modulation upon different cellular conditions [39]. Both short (8–10 nm) and long- (40–50 nm) range ER-mitochondria interactions were measured in HeLa cells transfected with SPLICS$_S$ or SPLICS$_L$ in the absence and in the presence of 2N4R and 2N4RΔC_{20} tau. As shown in Fig. 5A (and quantified in Fig. 5B), the expression of 2N4RΔC_{20}, but not of the full-length 2N4R tau, significantly increased the number of the tight ER-mitochondria interactions (number of ER-mitochondria contacts/cell: 67.83 ± 5.03 $n = 31$ for control cells; 71.55 ± 6.11 $n = 27$ for 2N4R-β_{11}; 120.42 ± 11.12 $n = 28$ for 2N4RΔC_{20}-β_{11}). On the other hand, long range ER-mitochondria contacts sites were not affected in both cases (Fig. 5C and quantification in 5D; number of ER-mitochondria contacts/cell: 198.07 ± 8.24 $n = 26$ for control cells; 174.7 ± 9.85 n = 27 for 2N4R-β_{11}; 190.64 ± 11.52 $n = 25$ for

2N4RΔC$_{20}$-β$_{11}$). The increased juxtaposition between the two organelles observed in the presence of 2N4RΔC$_{20}$ tau may serve to mitigate the reduction in the [Ca^{2+}]$_{er}$ (Fig. 4C), possibly to keep unaltered mitochondrial Ca^{2+}-transients (Fig. 4A) and, thus, to guarantee a proper ER-mitochondrial Ca^{2+} transfer to efficiently cope with the bioenergetic demand of the cell.

4. Discussion

Increasing evidence links tau to impaired mitochondrial functions [47]. Full-length tau, as well as the caspase-3 cleaved form 2N4RΔC$_{20}$, were detected at the mitochondrial level, suggesting the intriguing possibility that several mitochondria-related functions may be directly influenced by tau at this site [18,27,30,31]. Nevertheless, due to the lack of tools to unequivocally establish its distribution in the sub-mitochondrial compartments, the role of tau at the mitochondrial level is still not clear and essentially unexplored. Furthermore, whether and how tau may affect the formation/stabilisation of the contact sites between the ER and mitochondria, in turn impacting on the ER and mitochondrial Ca^{2+} uptake, is largely unknown. Using a split-GFP based approach, we here showed that GFP fluorescence reconstitution occurs upon co-expression of either the 2N4R-β$_{11}$ or 2N4RΔC$_{20}$-β$_{11}$ constructs with the OMM-GFP$_{1–10}$ and the IMS-GFP$_{1–10}$ fragments, but not with the mtGFP$_{1–10}$, demonstrating the presence of a tau faction both at the OMM and the mitochondrial IMS, and its absence in the mitochondrial matrix. Under basal conditions, the tau presence in these sub-compartments suggests that the protein might exert important functions locally, by acting on targets at the OMM (e.g., OPA1 and mitofusins, including Mfn1, Mfn2) [23]) and/or in the IMS. Indeed, we have found that, also in our conditions, tau expression affects mitochondrial distribution. Additional experiments are required to better understand how and why tau localises at these sub-mitochondrial compartments, nevertheless it is tempting to consider the possibility that it is related to the cytosolic proteostasis maintenance mechanism through the import of misfolded/aggregation prone proteins into mitochondria [48]. Although under basal conditions we did not detect tau in the mitochondrial matrix, we cannot exclude its translocation there under specific conditions, as previously demonstrated for the PD-related protein DJ-1 [34].

A strong reduction of the ER Ca^{2+} content was observed in cells expressing the 2N4RΔC$_{20}$ truncation form of tau. This decrease is accompanied by a strong enhancement in the short-range ER-mitochondria contact sites, suggesting potential compensatory mechanisms able to maintain the correct ER-mitochondria Ca^{2+} transfer. Indeed, mitochondrial Ca^{2+} transients were similar to control cells. Regarding wt tau, the modest, but statistically significant, reduction in the ER Ca^{2+} content was probably not enough to be compensated by an increase in the short-range ER-mitochondria associations, suggesting that only the caspase-3 cleaved form of tau selectively impacts on the ER-mitochondria axis possibly through a ER Ca^{2+} mishandling mechanism. This might be due to a direct effect on the ER Ca^{2+} handling machinery, such as the SERCA pump, the IP_3R or indirectly via an ER stress response triggered by the 2N4RΔC$_{20}$ mutant tau. However, further experiments would be required to better understand and clarify this hypothesis. At present, we cannot establish whether the reduction of ER Ca^{2+} level or the increase in ER-mitochondrial tethering occurs first; however, we can conclude that tau accumulation interferes with this key signalling, a feature shared with other proteins linked to neurodegenerative diseases such as Presenilin2, α-synuclein or VAPB/PTPIP51 [49–51].

Supplementary data to this article can be found online at https://doi.org/10.1016/j.bbadis.2018.07.011.

Transparency document

The Transparency document associated this article can be found, in online version.

Acknowledgements

We would like to thank Prof. Paola Pizzo and Dr. Riccardo Filadi (Department of Biomedical Sciences, University of Padova) for critically reading the manuscript and for helpful suggestions. We also thank Dr. Paolo Paganetti (Laboratory for Biomedical Neurosciences, Neurocenter of Southern Switzerland, Switzerland) for kindly providing the tau expression vector. The work is supported by grants from the Ministry of University and Research (Bando SIR 2014 n° RBSI14C65Z to T.C.) and from the Università degli Studi di Padova (Progetto Giovani 2012 n° GRIC128SP0 to T.C., Progetto di Ateneo 2016 n° CALI_SID16_01 to T.C. and Progetto di Ateneo 2015 n° CPDA153402 to M.B.).

Conflict of interest

The authors declare that they have no conflicts of interest with the contents of this article.

References

[1] I. Grundke-Iqbal, K. Iqbal, Y.C. Tung, M. Quinlan, H.M. Wisniewski, L.I. Binder, Abnormal phosphorylation of the microtubule-associated protein tau (tau) in Alzheimer cytoskeletal pathology, Proc. Natl. Acad. Sci. U. S. A. 83 (1986) 4913–4917.
[2] I. Grundke-Iqbal, K. Iqbal, L. George, Y.C. Tung, K.S. Kim, H.M. Wisniewski, Amyloid protein and neurofibrillary tangles coexist in the same neuron in Alzheimer disease, Proc. Natl. Acad. Sci. U. S. A. 86 (1989) 2853–2857.
[3] A.C. McKee, K.S. Kosik, N.W. Kowall, Neuritic pathology and dementia in Alzheimer's disease, Ann. Neurol. 30 (1991) 156–165.
[4] P.V. Arriagada, J.H. Growdon, E.T. Hedley-Whyte, B.T. Hyman, Neurofibrillary tangles but not senile plaques parallel duration and severity of Alzheimer's disease, Neurology 42 (1992) 631–639.
[5] M.D. Weingarten, A.H. Lockwood, S.Y. Hwo, M.W. Kirschner, A protein factor essential for microtubule assembly, Proc. Natl. Acad. Sci. U. S. A. 72 (1975) 1858–1862.
[6] Y. Wang, E. Mandelkow, Tau in physiology and pathology, Nat. Rev. Neurosci. 17 (2016) 5–21.
[7] T.C. Gamblin, F. Chen, A. Zambrano, A. Abraha, S. Lagalwar, A.L. Guillozet, M. Lu, Y. Fu, F. Garcia-Sierra, N. Lapointe, R. Miller, R.W. Berry, L.I. Binder, V.L. Cryns, Caspase cleavage of tau: linking amyloid and neurofibrillary tangles in Alzheimer's disease, Proc. Natl. Acad. Sci. U. S. A. 100 (2003) 10032–10037.
[8] A. Abraha, N. Ghoshal, T.C. Gamblin, V. Cryns, R.W. Berry, J. Kuret, L.I. Binder, C-terminal inhibition of tau assembly in vitro and in Alzheimer's disease, J. Cell Sci. 113 (Pt 21) (2000) 3737–3745.
[9] D. Jung, D. Filliol, M. Miehe, A. Rendon, Interaction of brain mitochondria with microtubules reconstituted from brain tubulin and MAP2 or TAU, Cell Motil. Cytoskeleton 24 (1993) 245–255.
[10] R. Brandt, J. Leger, G. Lee, Interaction of tau with the neural plasma membrane mediated by tau's amino-terminal projection domain, J. Cell Biol. 131 (1995) 1327–1340.
[11] J. Al-Bassam, R.S. Ozer, D. Safer, S. Halpain, R.A. Milligan, MAP2 and tau bind longitudinally along the outer ridges of microtubule protofilaments, J. Cell Biol. 157 (2002) 1187–1196.
[12] M. Novak, J. Kabat, C.M. Wischik, Molecular characterization of the minimal protease resistant tau unit of the Alzheimer's disease paired helical filament, EMBO J. 12 (1993) 365–370.
[13] Y. Kim, H. Choi, W. Lee, H. Park, T.I. Kam, S.H. Hong, J. Nah, S. Jung, B. Shin, H. Lee, T.Y. Choi, H. Choo, K.K. Kim, S.Y. Choi, R. Kayed, Y.K. Jung, Caspase-cleaved tau exhibits rapid memory impairment associated with tau oligomers in a transgenic mouse model, Neurobiol. Dis. 87 (2016) 19–28.
[14] M.L. Billingsley, R.L. Kincaid, Regulated phosphorylation and dephosphorylation of tau protein: effects on microtubule interaction, intracellular trafficking and neurodegeneration, Biochem. J. 323 (Pt 3) (1997) 577–591.
[15] G. Lee, N. Cowan, M. Kirschner, The primary structure and heterogeneity of tau protein from mouse brain, Science 239 (1988) 285–288.
[16] M. Goedert, M.G. Spillantini, N.J. Cairns, R.A. Crowther, Tau proteins of Alzheimer paired helical filaments: abnormal phosphorylation of all six brain isoforms, Neuron 8 (1992) 159–168.
[17] M. Goedert, M. Masuda-Suzukake, B. Falcon, Like prions: the propagation of aggregated tau and alpha-synuclein in neurodegeneration, Brain 140 (2017) 266–278.
[18] C.A. Lasagna-Reeves, D.L. Castillo-Carranza, U. Sengupta, A.L. Clos, G.R. Jackson, R. Kayed, Tau oligomers impair memory and induce synaptic and mitochondrial dysfunction in wild-type mice, Mol. Neurodegener. 6 (2011) 39.
[19] D.C. David, S. Hauptmann, I. Scherping, K. Schuessel, U. Keil, P. Rizzu, R. Ravid, S. Drose, U. Brandt, W.E. Muller, A. Eckert, J. Gotz, Proteomic and functional analyses reveal a mitochondrial dysfunction in P301L tau transgenic mice, J. Biol. Chem. 280 (2005) 23802–23814.

[20] R.A. Rissman, W.W. Poon, M. Blurton-Jones, S. Oddo, R. Torp, M.P. Vitek, F.M. Laferla, T.T. Rohn, C.W. Cotman, Caspase-cleavage of tau is an early event in Alzheimer disease tangle pathology, J. Clin. Invest. 114 (2004) 121–130.
[21] J.J. Jarero-Basulto, J. Luna-Munoz, R. Mena, Z. Kristofikova, D. Ripova, G. Perry, L.I. Binder, F. Garcia-Sierra, Proteolytic cleavage of polymeric tau protein by caspase-3: implications for Alzheimer disease, J. Neuropathol. Exp. Neurol. 72 (2013) 1145–1161.
[22] X. Wang, B. Su, H. Fujioka, X. Zhu, Dynamin-like protein 1 reduction underlies mitochondrial morphology and distribution abnormalities in fibroblasts from sporadic Alzheimer's disease patients, Am. J. Pathol. 173 (2008) 470–482.
[23] X.C. Li, Y. Hu, Z.H. Wang, Y. Luo, Y. Zhang, X.P. Liu, Q. Feng, Q. Wang, K. Ye, G.P. Liu, J.Z. Wang, Human wild-type full-length tau accumulation disrupts mitochondrial dynamics and the functions via increasing mitofusins, Sci. Rep. 6 (2016) 24756.
[24] W. Stoothoff, P.B. Jones, T.L. Spires-Jones, D. Joyner, E. Chhabra, K. Bercury, Z. Fan, H. Xie, B. Bacskai, J. Edd, D. Irimia, B.T. Hyman, Differential effect of three-repeat and four-repeat tau on mitochondrial axonal transport, J. Neurochem. 111 (2009) 417–427.
[25] K.J. Kopeikina, G.A. Carlson, R. Pitstick, A.E. Ludvigson, A. Peters, J.I. Luebke, R.M. Koffie, M.P. Frosch, B.T. Hyman, T.L. Spires-Jones, Tau accumulation causes mitochondrial distribution deficits in neurons in a mouse model of tauopathy and in human Alzheimer's disease brain, Am. J. Pathol. 179 (2011) 2071–2082.
[26] M.J. Perez, K. Vergara-Pulgar, C. Jara, F. Cabezas-Opazo, R.A. Quintanilla, Caspase-cleaved tau impairs mitochondrial dynamics in Alzheimer's disease, Mol. Neurobiol. 55 (2) (2018) 1004–1018.
[27] Y. Hu, X.C. Li, Z.H. Wang, Y. Luo, X. Zhang, X.P. Liu, Q. Feng, Q. Wang, Z. Yue, Z. Chen, K. Ye, J.Z. Wang, G.P. Liu, Tau accumulation impairs mitophagy via increasing mitochondrial membrane potential and reducing mitochondrial Parkin, Oncotarget 7 (2016) 17356–17368.
[28] G. Plucinska, D. Paquet, A. Hruscha, L. Godinho, C. Haass, B. Schmid, T. Misgeld, In vivo imaging of disease-related mitochondrial dynamics in a vertebrate model system, J. Neurosci. 32 (2012) 16203–16212.
[29] K. Shahpasand, I. Uemura, T. Saito, T. Asano, K. Hata, K. Shibata, Y. Toyoshima, M. Hasegawa, S. Hisanaga, Regulation of mitochondrial transport and inter-microtubule spacing by tau phosphorylation at the sites hyperphosphorylated in Alzheimer's disease, J. Neurosci. 32 (2012) 2430–2441.
[30] Z. Tang, E. Ioja, E. Bereczki, K. Hultenby, C. Li, Z. Guan, B. Winblad, J.J. Pei, mTor mediates tau localization and secretion: implication for Alzheimer's disease, Biochim. Biophys. Acta 1853 (2015) 1646–1657.
[31] G. Amadoro, V. Corsetti, A. Stringaro, M. Colone, S. D'Aguanno, G. Meli, M. Ciotti, G. Sancesario, A. Cattaneo, R. Bussani, D. Mercanti, P. Calissano, A NH_2 tau fragment targets neuronal mitochondria at AD synapses: possible implications for neurodegeneration, J. Alzheimers Dis. 21 (2010) 445–470.
[32] S. Cabantous, T.C. Terwilliger, G.S. Waldo, Protein tagging and detection with engineered self-assembling fragments of green fluorescent protein, Nat. Biotechnol. 23 (2005) 102–107.
[33] J.D. Pedelacq, S. Cabantous, T. Tran, T.C. Terwilliger, G.S. Waldo, Engineering and characterization of a superfolder green fluorescent protein, Nat. Biotechnol. 24 (2006) 79–88.
[34] T. Cali, D. Ottolini, M.E. Soriano, M. Brini, A new split-GFP-based probe reveals DJ-1 translocation into the mitochondrial matrix to sustain ATP synthesis upon nutrient deprivation, Hum. Mol. Genet. 24 (4) (2015) 1045–1060.
[35] R.A. Quintanilla, T.A. Matthews-Roberson, P.J. Dolan, G.V. Johnson, Caspase-cleaved tau expression induces mitochondrial dysfunction in immortalized cortical neurons: implications for the pathogenesis of Alzheimer disease, J. Biol. Chem. 284 (2009) 18754–18766.
[36] R.A. Quintanilla, R. von Bernhardi, J.A. Godoy, N.C. Inestrosa, G.V. Johnson, Phosphorylated tau potentiates Aβ-induced mitochondrial damage in mature neurons, Neurobiol. Dis. 71 (2014) 260–269.
[37] R.A. Quintanilla, P.J. Dolan, Y.N. Jin, G.V. Johnson, Truncated tau and Abeta cooperatively impair mitochondria in primary neurons, Neurobiol. Aging 33 (619) (2012) e625–e635.
[38] D. Ottolini, T. Cali, M. Brini, Methods to measure intracellular ca(2+) fluxes with organelle-targeted aequorin-based probes, Methods Enzymol. 543 (2014) 21–45.
[39] D. Cieri, M. Vicario, M. Giacomello, F. Vallese, R. Filadi, T. Wagner, T. Pozzan, P. Pizzo, L. Scorrano, M. Brini, T. Cali, SPLICS: a split green fluorescent protein-based contact site sensor for narrow and wide heterotypic organelle juxtaposition, Cell Death Differ. 25 (6) (2018) 1131–1145.
[40] Z. Polianskyte, N. Peitsaro, A. Dapkunas, J. Liobikas, R. Soliymani, M. Lalowski, O. Speer, J. Seitsonen, S. Butcher, G.M. Cereghetti, M.D. Linder, M. Merckel, J. Thompson, O. Eriksson, LACTB is a filament-forming protein localized in mitochondria, Proc. Natl. Acad. Sci. U. S. A. 106 (2009) 18960–18965.
[41] V. Hung, P. Zou, H.W. Rhee, N.D. Udeshi, V. Cracan, T. Svinkina, S.A. Carr, V.K. Mootha, A.Y. Ting, Proteomic mapping of the human mitochondrial intermembrane space in live cells via ratiometric APEX tagging, Mol. Cell 55 (2014) 332–341.
[42] R.A. McCloy, S. Rogers, C.E. Caldon, T. Lorca, A. Castro, A. Burgess, Partial inhibition of Cdk1 in G 2 phase overrides the SAC and decouples mitotic events, Cell Cycle 13 (2014) 1400–1412.
[43] G. Amadoro, V. Corsetti, F. Florenzano, A. Atlante, M.T. Ciotti, M.P. Mongiardi, R. Bussani, V. Nicolin, S.L. Nori, M. Campanella, P. Calissano, AD-linked, toxic NH_2 human tau affects the quality control of mitochondria in neurons, Neurobiol. Dis. 62 (2014) 489–507.
[44] T. Cali, D. Ottolini, M.E. Soriano, M. Brini, A new split-GFP-based probe reveals DJ-1 translocation into the mitochondrial matrix to sustain ATP synthesis upon nutrient deprivation, Hum. Mol. Genet. 24 (2015) 1045–1060.
[45] S. Paillusson, R. Stoica, P. Gomez-Suaga, D.H. Lau, S. Mueller, T. Miller, C.C. Miller, There's something wrong with my MAM; the ER-mitochondria axis and neurodegenerative diseases, Trends Neurosci. 39 (2016) 146–157.
[46] S. Perreault, O. Bousquet, M. Lauzon, J. Paiement, N. Leclerc, Increased association between rough endoplasmic reticulum membranes and mitochondria in transgenic mice that express P301L tau, J. Neuropathol. Exp. Neurol. 68 (2009) 503–514.
[47] A.Y. Abramov, A.V. Berezhnov, E.I. Fedotova, V.P. Zinchenko, L.P. Dolgacheva, Interaction of misfolded proteins and mitochondria in neurodegenerative disorders, Biochem. Soc. Trans. (2017), https://doi.org/10.1042/BST20170024.
[48] L. Ruan, C. Zhou, E. Jin, A. Kucharavy, Y. Zhang, Z. Wen, L. Florens, R. Li, Cytosolic proteostasis through importing of misfolded proteins into mitochondria, Nature 543 (2017) 443–446.
[49] R. Filadi, E. Greotti, G. Turacchio, A. Luini, T. Pozzan, P. Pizzo, Mitofusin 2 ablation increases endoplasmic reticulum-mitochondria coupling, Proc. Natl. Acad. Sci. U. S. A. 112 (2015) E2174–E2181.
[50] T. Calì, D. Ottolini, A. Negro, M. Brini, alpha-Synuclein controls mitochondrial calcium homeostasis by enhancing endoplasmic reticulum-mitochondria interactions, J. Biol. Chem. 287 (2012) 17914–17929.
[51] K.J. De Vos, G.M. Morotz, R. Stoica, E.L. Tudor, K.F. Lau, S. Ackerley, A. Warley, C.E. Shaw, C.C. Miller, VAPB interacts with the mitochondrial protein PTPIP51 to regulate calcium homeostasis, Hum. Mol. Genet. 21 (2012) 1299–1311.

frontiers in Molecular Neuroscience

MINI REVIEW
published: 22 March 2019
doi: 10.3389/fnmol.2019.00055

Calcium, Dopamine and Neuronal Calcium Sensor 1: Their Contribution to Parkinson's Disease

*Cristina Catoni[1], Tito Calì[2] and Marisa Brini[1]**

[1] Department of Biology, University of Padova, Padua, Italy, [2] Department of Biomedical Sciences, University of Padova, Padua, Italy

Parkinson's disease (PD) is a debilitating neurodegenerative disorder characterized by loss of dopaminergic neurons in the substantia nigra pars compacta. The causes of PD in humans are still unknown, although metabolic characteristics of the neurons affected by the disease have been implicated in their selective susceptibility. Mitochondrial dysfunction and proteostatic stress are recognized to be important in the pathogenesis of both familial and sporadic PD, and they both culminate in bioenergetic deficits. Exposure to calcium overload has recently emerged as a key determinant, and pharmacological treatment that inhibits Ca^{2+} entry diminishes neuronal damage in chemical models of PD. In this review, we first introduce general concepts on neuronal Ca^{2+} signaling and then summarize the current knowledge on fundamental properties of substantia nigra pars compacta dopaminergic neurons, on the role of the interplay between Ca^{2+} and dopamine signaling in neuronal activity and susceptibility to cell death. We also discuss the possible involvement of a "neglected" player, the Neuronal Calcium Sensor-1 (NCS-1), which has been shown to participate to dopaminergic signaling by regulating dopamine dependent receptor desensitization in normal brain but, data supporting a direct role in PD pathogenesis are still missing. However, it is intriguing to speculate that the Ca^{2+}-dependent modulation of NCS-1 activity could eventually counteract dopaminergic neurons degeneration.

Keywords: calcium signaling, Cav1.3 calcium channel, ncs-1, dopamine, Parkinson's disease

OPEN ACCESS

Edited by:
Daniele Dell'Orco, University of Verona, Italy

Reviewed by:
Rosanna Parlato, University of Ulm, Germany
Teresa Duda, Salus University, United States

****Correspondence:***
Marisa Brini
marisa.brini@unipd.it

Received: *25 October 2018*
Accepted: *14 February 2019*
Published: *22 March 2019*

Citation:
Catoni C, Calì T and Brini M (2019) Calcium, Dopamine and Neuronal Calcium Sensor 1: Their Contribution to Parkinson's Disease. Front. Mol. Neurosci. 12:55. doi: 10.3389/fnmol.2019.00055

NEURONAL CALCIUM SIGNALING

Calcium (Ca^{2+}) homeostasis is essential for neuronal function and survival. Intracellular Ca^{2+} signaling in neurons is extremely fine-tuned, because it controls gene transcription, membrane excitability, neurotransmitters secretion and many other cellular processes, including synaptic plasticity (Berridge, 1998; Brini et al., 2014). Like other cells, neurons use both extracellular and intracellular sources of Ca^{2+} and, as a consequence of their excitability, they are exposed to large Ca^{2+} fluctuations and thus to a major risk of Ca^{2+} overload.

The coordinated action of the different systems that handle Ca^{2+} fluxes guarantees the generation of high Ca^{2+} concentration microdomains with precise spatiotemporal features that are crucial to specifically activate different cellular processes (La Rovere et al., 2016; Filadi et al., 2017a; Samanta and Parekh, 2017). For instance, those generated upon the opening of the endoplasmic reticulum Ca^{2+} channels are sensed by mitochondria that use them to drive

bioenergetic metabolism for the production of ATP and mitochondrial substrates for anabolic process (Tarasov et al., 2012).

However, exaggerated mitochondrial Ca^{2+} accumulation may be dangerous, since can lead to mitochondrial permeability transition pore (mPTP) opening, cytochrome *c* release and can activate apoptotic cell death (Bernardi et al., 2015). Thus, once Ca^{2+}-regulated processes have been engaged, Ca^{2+} ions must be rapidly extruded (and/or buffered) to avoid that their excessive accumulation could trigger mitochondrial dysfunction (Calì et al., 2012a; Muller et al., 2018). The "Ca^{2+} machinery" that is in place to tune Ca^{2+} concentration includes transport proteins such as channels, exchangers and pumps that move the ion across the membranes (i.e., the plasma membrane and the membranes of organelles), and Ca^{2+} binding proteins that act as Ca^{2+} buffer and/or transducer (**Figure 1**).

Increasing evidence suggests that defective Ca^{2+} handling plays an important role in aging and neurodegeneration (Berridge, 1998; Calì et al., 2014; Pchitskaya et al., 2018). Despite of neurodegenerative diseases are a large group of heterogeneous disorders characterized by relative selectivity in the death of neuronal subtypes, they share some common tracts that include disturbance in cellular quality mechanisms (i.e., ER stress, autophagy, accumulation of aggregated proteins), oxidative stress, neuroinflammation and defective Ca^{2+} signaling (Brini et al., 2014; Hetz and Saxena, 2017; Kurtishi et al., 2018; Muller et al., 2018). Furthermore, recent studies have indicated that defective ER-mitochondria communication, by impinging on energetic metabolism, lipid synthesis, autophagy, could have detrimental consequences for cell function and survival (Filadi et al., 2017b). Many regulators of ER-mitochondria interface are proteins whose mutations are linked to familial forms of Alzheimer's disease (AD) and PD, suggesting that defects at the ER-mitochondria contact sites could have a role in the onset and/or the progression of these neurodegenerative diseases (Calì et al., 2013a; Filadi et al., 2016; Area-Gomez and Schon, 2017).

As mentioned above, in addition to the Ca^{2+} transport across the membranes, another important mechanism that contributes to the regulation of Ca^{2+} homeostasis is the processes of Ca^{2+} buffering that is managed by mitochondrial Ca^{2+} uptake but largely relies on the existence of several cytosolic Ca^{2+} binding proteins. Among them, the ubiquitous EF-hand Ca^{2+} protein calmodulin (CaM) is mainly responsible for translating the increases of the cytosolic Ca^{2+} concentration into a biochemical signal through conformational changes of its targets (Sharma and Parameswaran, 2018). It is present at high concentration in the brain, where it plays a key role in the regulation of ions channels activity and synaptic plasticity (Xia and Storm, 2005). Other Ca^{2+}-binding proteins such as Calbindin D-28K (CB-28K), calretinin (CR), and parvalbumin (PV) are also present in the nervous system. By buffering Ca^{2+} levels with different capacity, affinity and kinetics (Schwaller, 2012; Paillusson et al., 2017) and thanks to their cell-specific abundance, they guarantee the selective activation of different biological processes. Cell-type-specific distribution of Ca^{2+} binding proteins could also account for the selective susceptibility to cell death of the specific neuronal populations affected in different neurodegenerative diseases. Indeed, it has been observed that CB-28K containing cells are spared from cell death in pharmacological-induced parkinsonism in mice and that CB-28K immunoreactivity in cholinergic neurons of the basal forebrain (the same neurons that are preferentially loss in AD) was reduced in an age-related manner in humans, suggesting a role for CB-28K also in the selective neuronal vulnerability in AD (Yamada et al., 1990; German et al., 1992; Mouatt-Prigent et al., 1994; Damier et al., 1999; Geula et al., 2003; Zallo et al., 2018).

PARKINSON'S DISEASE, CALCIUM AND SELECTIVE VULNERABILITY OF SUBSTANTIA NIGRA PAR COMPACTA

PD is the second most common neurodegenerative disorder in humans after AD. PD patients present motor symptoms such as resting tremor, bradykinesia and postural rigidity. However, the appearance of other disturbances such as constipation, sleep disorders, olfactory deficit, apathy, pain, sexual difficulties, and in some case cognitive decline is currently observed to anticipate motor deficits in many patients (de Lau and Breteler, 2006) and indicates that regions of the brain that are not involved in motor symptoms are also compromised. At histological levels, the hallmarks for PD are the selective loss of the dopamine (DA)-containing neurons of the substantia nigra pars compacta (SNc) and the presence of proteinaceous cytosolic inclusions known as Lewy bodies, mainly constituted by alpha-synuclein (Goedert et al., 2013). The progressive SNc DA cells death leads to decreased DA levels and the worsening of the symptoms. SNc DA cells release DA from their axonal terminals and from their cell bodies and dendrites within both the dorsal striatum and the midbrain, respectively. DA release is crucial for voluntary movement and it is strictly Ca^{2+}- and electrical activity-dependent. Indeed, the continuous supply of DA to the connected brain areas is guaranteed by autonomous pacemaking, which occurs in the absence of conventional synaptic input and thank to the orchestrated action of different ion channels. In particular, the presence of voltage-dependent L-type Ca^{2+} channels containing a distinctive Cav1.3 pore forming subunit, which opens at relatively hyperpolarized potentials, allows Ca^{2+} entry with an oscillatory pathway that contributes to the membrane potential threshold, underlying autonomous pacemaking (Chan et al., 2007; Puopolo et al., 2007; Guzman et al., 2010). Continuous Ca^{2+} influx is necessary to modulate physiological DA release by SNc DA neurons, but, its long-lasting presence may synergize with the exposure to risk factors (i.e., aging, mitochondrial toxins, mutations) and generate metabolic stress and mitochondrial damage (Surmeier et al., 2011; Guzman et al., 2018).

It is widely recognized that in PD, the major risk of Ca^{2+}-induced toxicity is represented by Ca^{2+} entry through the voltage gated Ca^{2+} channels during the normal activity of the dopaminergic neurons (Ilijic et al., 2011; Liss and Striessnig, 2019), that, in this way, become more vulnerable to death than other neuronal populations. Cell damage could be further exacerbated by environmental factors such as exposure to

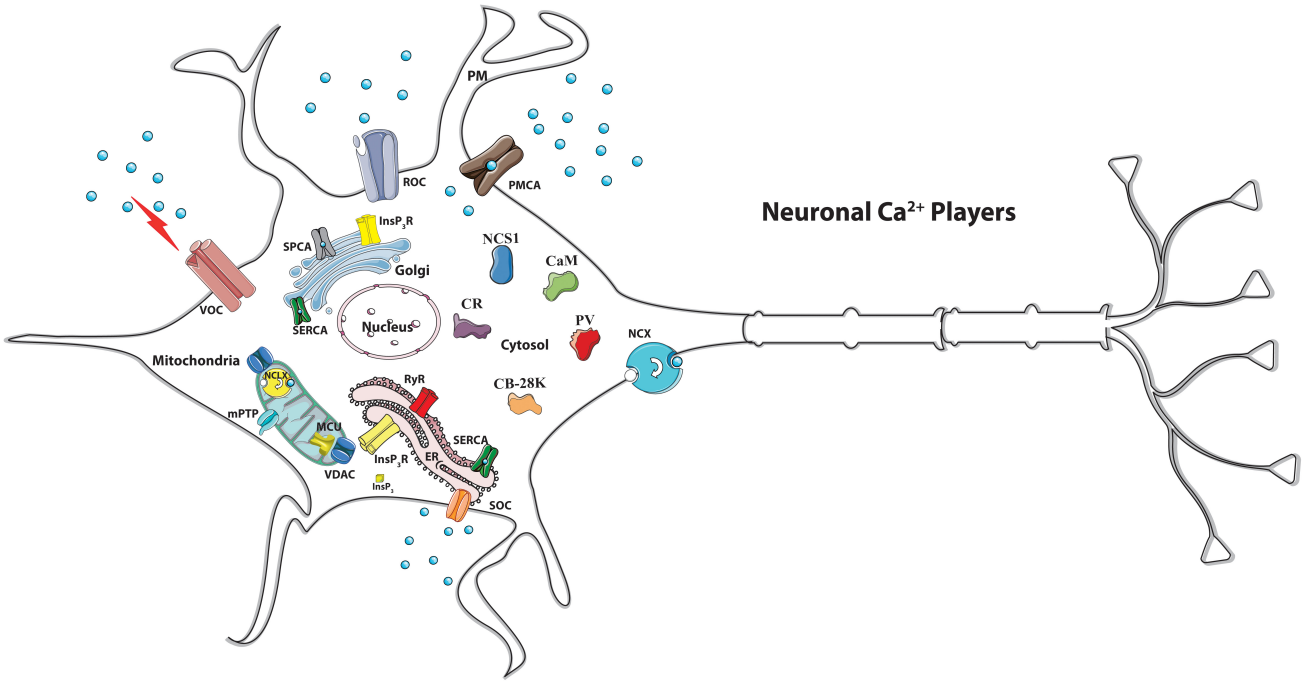

FIGURE 1 | Schematic view of the main neuronal Ca^{2+} players. Many Ca^{2+} transport proteins contribute to Ca^{2+} handling: the inositol 1,4,5-trisphosphate receptor (*InsP$_3$R*), the ryanodine receptor (*RyR*) at the sarco/endoplasmic reticulum (*SR/ER*) membranes, and the voltage (*VOC*), the receptor (*ROC*)-activated and the store-operated (SOC) Ca^{2+} channels of the plasma membrane. Ca^{2+} extrusion depends on the activity of the plasma membrane Ca^{2+} ATPase (*PMCA*) and the plasma membrane Na^+/Ca^{2+} exchanger (*NCX*). Ca^{2+} reuptake in the intracellular stores is operated by the ER/SR Ca^{2+} ATPase (*SERCA*) and the secretory pathway Ca^{2+} ATPase (*SPCA*) of the Golgi apparatus. The mitochondrial Ca^{2+} handling systems and the cytosolic Ca^{2+}-binding/buffering proteins are indicated. *MCU*, mitochondrial Ca^{2+} uniporter. *NCLX*, mitochondrial Na^+/Ca^{2+} exchanger. *VDAC*, voltage-dependent anion channels. *MPTP*, mitochondrial permeability transition pore. CaM, calmodulin. CR, calretinin. CB-28K, calbindin D-28K. NCS-1, Neuronal Calcium Sensor 1.

mitochondrial toxins [i.e., MPTP (1-methyl-4-phenyl-1,2,3,6-tetrahydropyridine), rotenone, 6-hydroxy dopamine (6-OHDA), paraquat (1,1′-dimethyl-4,4′-bipyridine)] or upon loss of function of specific proteins such as alpha-synuclein, Parkin, PINK1 and DJ-1, whose mutations are linked to genetic forms of PD. Interestingly, all these proteins, despite their different intracellular localization and function, are able to interfere with Ca^{2+} signaling (Calì et al., 2014). Indeed extracellular and intracellular deposition of alpha-synuclein aggregates has been proposed to enhance Ca^{2+} influx through the plasma membrane by forming pore-like structures (Danzer et al., 2007; Surguchev and Surguchov, 2015; Angelova et al., 2016) or by interfering with Ca^{2+} channels (Liu et al., 2013; Ronzitti et al., 2014), as well as PINK1 has been proposed to participate to the regulation of both influx or efflux of Ca^{2+} ions from mitochondria (Gandhi et al., 2009; Marongiu et al., 2009). We have found that the overexpression of PD-linked alpha-synuclein, parkin and DJ-1 proteins enhanced ER-mitochondria Ca^{2+} transfer by favoring ER-mitochondria juxtaposition, and provided evidence that through this action, physiological amounts of these proteins are able to tune ATP production (Calì et al., 2012b, 2013b; Ottolini et al., 2013). The loss of this function is likely to be particularly damaging to neurons that are heavily dependent on proper Ca^{2+}signaling and ATP production. Accordingly, Paillusson et al. (2017) have documented loss of ER-mitochondria association in induced pluripotent stem cells derived neurons from PD patients harboring alpha-synuclein gene triplication.

In summary, if by one side Ca^{2+} entry through Cav1.3 pore subunit is essential to sustain pacemaking activity of SNc DA neurons, by the other it exposes these neurons to metabolic burden and mitochondrial stress. Differently, DA neurons from the ventral tegumental area (VTA), which are also autonomous pacemakers, are significantly less vulnerable than SNc DA neurons from which they differ in respect with two main features: they have smaller Ca^{2+} currents (Khaliq and Bean, 2010) and strong intrinsic Ca^{2+} buffering capacity due to higher calbindin levels (Dopeso-Reyes et al., 2014).

The most convincing argument in favor of the "Ca^{2+} hypothesis" in PD onset is that epidemiologic studies on patients under clinical trial with L-type channel antagonists for the treatment of hypertension have shown a reduced risk of developing PD (Becker et al., 2008; Ritz et al., 2010; Pasternak et al., 2012). The voltage gated L-type Ca^{2+} plasma membrane channels inhibitor isradipine has been demonstrated to be neuroprotective in a mouse model of PD (Ilijic et al., 2011) and phase III of clinical trial is currently under evaluation to establish whether treatment with isradipine is able to slow the progression of PD in humans (Liss and Striessnig, 2019).

Despite general consensus agrees with the fact that the anatomical, physiological, and biochemical phenotype of the SNc

DA neurons predisposes them to mitochondrial dysfunction, the molecular bases of the subtype-selective neuronal vulnerability are still obscure and of big interest.

Interestingly, computer imaging and immunohistochemical staining techniques have revealed a strict correlation between the distribution of the Ca^{2+}-binding proteins CB-28K and CR and cell survival in midbrain dopaminergic regions: cells that are spared from death in animals treated with the DA neurotoxin MPTP (German et al., 1992; Mouatt-Prigent et al., 1994) are those that display higher expression levels of CB-28K and CR in control untreated animals. Interestingly, this observation has been reinforced by a comparative study performed on post-mortem brain from neurologically normal individuals and PD patients in which the distribution of calbindin, calmodulin and calretinin did not associate with the regions prone to neurodegeneration. It has also been observed that the expression of Cav1.3 subtypes increased in the brain of patients at early stage of the disease, even before the appearance of recognized pathological signs (Hurley et al., 2013), suggesting that Ca^{2+} dysregulation could be an early event in PD pathogenesis.

Low expression levels of Ca^{2+}-binding proteins in the brain area more susceptible to cell death in PD suggest that those neuronal populations are characterized by low Ca^{2+} buffering capacity. This parameter has been directly evaluated in neurons from the ventral and medial SNc by applying a protocol originally developed by E. Neher (Neher and Augustine, 1992; Zhou and Neher, 1993; Neher, 1998). Foehring and colleagues (Foehring et al., 2009) have loaded the cells with an exogenous Ca^{2+}-indicator/buffer and calculated the Ca^{2+} binding ratio (K_S) by measuring changes in Ca^{2+}-bound buffer and dividing by the free Ca^{2+} increase. Interestingly, despite the intrinsic Ca^{2+} buffering in DA cells increases with postnatal age ($K_S \simeq 110$ at postnatal day 13–18 and $\simeq$179 at postnatal day 25–32), it remains low at both age ranges. Other neuronal populations (e.g., neocortical pyramidal cells or cortical GABAergic interneurons), that are not endowed with pacemaking activity, display similar or higher values and Purkinje cells have the highest K_S values ($\sim$2,000) (Fierro and Llano, 1996).

Considering that, in addition to Ca^{2+} binding proteins, also mitochondria play a role in buffering cytosolic Ca^{2+}, a reduction of mitochondria amount or/and the presence of dysfunctional mitochondria could account for differences in Ca^{2+} buffering capacity among different neuronal midbrain populations. In line with these considerations, a study has found that the mitochondrial mass in SNc DA neurons is reduced in respect with that of other neurons from the midbrain (Liang et al., 2007). Thus, also this peculiarity may account for selective vulnerability of DA SNc neurons.

At the end of this discussion, it is worth to mention that other observations suggest that additional sources of Ca^{2+} (other than Ca^{2+} entry from the extracellular ambient) could contribute to SNc DA neurons vulnerability. In this respect, defects in intracellular Ca^{2+} stores handling and ER stress have been frequently documented in PD cellular models (Wang and Takahashi, 2007; Mercado et al., 2013).

All together it is clear that the equilibrium between Ca^{2+} signaling and SNc DA neurons activity is extremely critical: upon conditions of increased metabolic demand, i.e., when continuous dopamine release into the dorsal striatum is required for movement, elevated metabolic burden could originate a vicious cycle that further impairs mitochondrial function, resulting in increased metabolic stress. Interestingly, it has been proposed that Ca^{2+} load may further contribute to exacerbate neurodegeneration by promoting an increase of the neurotoxic catecholamine intracellular levels (Mosharov et al., 2009).

DOPAMINE RELEASE AND NEURONAL CALCIUM SENSOR 1: POSSIBLE IMPLICATIONS IN PARKINSON DISEASE?

Among the Ca^{2+}-binding proteins, the components of the subfamily of Neuronal Ca^{2+} Sensors (NCS) are particularly abundant in neurons and photoreceptors and deserve special attention since their properties distinguish them from CaM or CB-28K, CR and PV and allow them to play non-reduntant roles. Differences in Ca^{2+} affinities, in cellular expression and distribution and in target proteins are at the basis of the specialization of NCS function (McCue et al., 2010). Neuronal Ca^{2+} Sensor-1 (NCS-1) is the most ancient member of the family (Pongs et al., 1993), and it is implicated in the regulation of cell-surface receptors and ion channels, and in neurotransmitter release, gene transcription, cell growth and survival (Burgoyne, 2007).

NCS-1 has been linked to a large spectrum of diseases possibly because its differential interaction with partners. Changes in the abundance of NCS-1 result in altered relationship with target proteins and determine cell dysfunction. An up-regulation of NCS-1 mRNA was found in a variety of non-neurological and neurological diseases. NCS-1 has been proposed to be a biomarker in aggressive breast cancer (Moore et al., 2017). In the heart, altered Ca^{2+} signaling mediated by NCS-1 and inositol 1,4,5 trisphosphate receptor interaction was linked to cardiac arrhythmias (Zhang et al., 2010). Schizophrenia, bipolar disorder (BD) (Koh et al., 2003) and autism (Piton et al., 2008; Handley et al., 2010) have been associated with upregulation or mutations in NCS-1 protein.

Increased levels of NCS-1 mRNA were measured in neurons from SNc of PD patients (Dragicevic et al., 2014) and NCS-1 was shown to co-localize with the D2 type-dopamine receptors in dendrites, spines, and occasionally in axonal buttons of rat and monkey striatal neurons (Kabbani et al., 2002), thus supporting the involvement of NCS-1 in the process of dopaminergic signaling, but also suggesting its possible link with PD.

As mentioned above, numerous convincing biophysical and pharmacological findings support the hypothesis that Cav1.3 channels by sustaining pacemaker-activity exposes SNc DA neurons to continuous Ca^{2+} load and mitochondrial stress (Surmeier et al., 2011). However, other studies investigating dopamine receptor mediated autoinhibition of neuronal activity have shown that Ca^{2+} entry through Cav1.3 channels, in addition to sustain pacemaker activity, regulates dopamine autoreceptors (Dragicevic et al., 2014). Considering that current

therapies to alleviate PD symptoms and progression are based on the administration of dopamine precursor L-Dopa and/or dopamine D2 receptor agonists (Oertel and Schulz, 2016), the understanding of Cav1.3 physiology becomes crucial to better define the pathways involved in PD onset and develop therapeutic strategies.

Dopaminergic transmission is dependent on two main families of DA receptors, namely D1- and D2-type (Beaulieu and Gainetdinov, 2011) that are both members of the G protein-coupled receptor (GPCR) superfamily. The D1-like receptors activate $G\alpha_{s/olf}$ and stimulate cAMP production, whereas the D2-like receptors activate $G\alpha_{i/o}$ and inhibit adenylate cyclase activity and cAMP production. The two DA receptor types differ in their localization: the D1-like receptors are predominately localized post-synaptically (Levey et al., 1993), whereas the D2-like receptors are present post-synaptically on dopaminergic target neurons (Levey et al., 1993; Sesack et al., 1994), but pre-synaptically and as autoreceptors (D2-AR) on DA neurons (Mercuri et al., 1997; L'hirondel et al., 1998). The response of SNc neurons to DA is highly regulated and chronic loss of dopamine leads to receptor sensitization (Schultz and Ungerstedt, 1978). In particular, DA binding to the D2-AR leads to activation of G-protein-coupled, inwardly rectifying potassium channels (GIRK2) (Luscher and Slesinger, 2010; Beaulieu and Gainetdinov, 2011) that promotes K^+ efflux and hyperpolarization, and consequently reduces SNc DA activity (Beckstead et al., 2004). At the same time, however, D2-AR internalization occurring in response to DA stimulation reduces the DA-induced inhibitory effect on SNc DA neurons firing and tonic Ca^{2+} entry through L-type voltage channels promotes desensitization of D2 receptor-dependent activation of GIRK channels (Gantz et al., 2015).

In other words, DA itself, upon release, acts in a negative feedback loop: by binding to D2-subtype receptors, it inhibits SNc DA neurons electrical activity and further DA release, but both Ca^{2+} influx and receptor desensitization limit this action.

Dragicevic et al. (2014) have observed that, in contrast to juvenile SNc neurons, mature neurons have lost D2-autoreceptors desensitization, and, accordingly, upon *in vivo* exposure to high DA level also juvenile neurons present the same D2-autoreceptors desensitizing response. According to their results, Cav 1.3 mediated Ca^{2+} influx is essential for age-dependent modulation of somatodendritic D2-autoreceptors responses and D2 autoreceptor sensitization requires both Cav1.3 and NCS-1 activation.

NCS-1 and D2 receptors co-localize both in primate and rodent brain (Kabbani et al., 2002) and NCS-1 attenuates agonist-induced receptor internalization via a mechanism that involves a reduction in D2 receptor phosphorylation. Interestingly, amino acid substitutions that affect NCS-1 Ca^{2+} binding ability abolished its modulation on D2 receptor signaling (Kabbani et al., 2012) and NCS-1 deletion in mouse has been reported to decrease DA secretion (Ng et al., 2016), thus implying important contribution of NCS-1 impairment in defective dopaminergic signaling.

The finding that, in juvenile mice, Cav1.3 can adapt SNc DA neurons activity in response to high extracellular DA-levels by providing the Ca^{2+} source for neuronal Ca^{2+} sensor NCS-1 (Dragicevic et al., 2014) strongly indicates the existence of an adaptive signaling network (Cav1.3/NCS-1/D2/GIRK2)

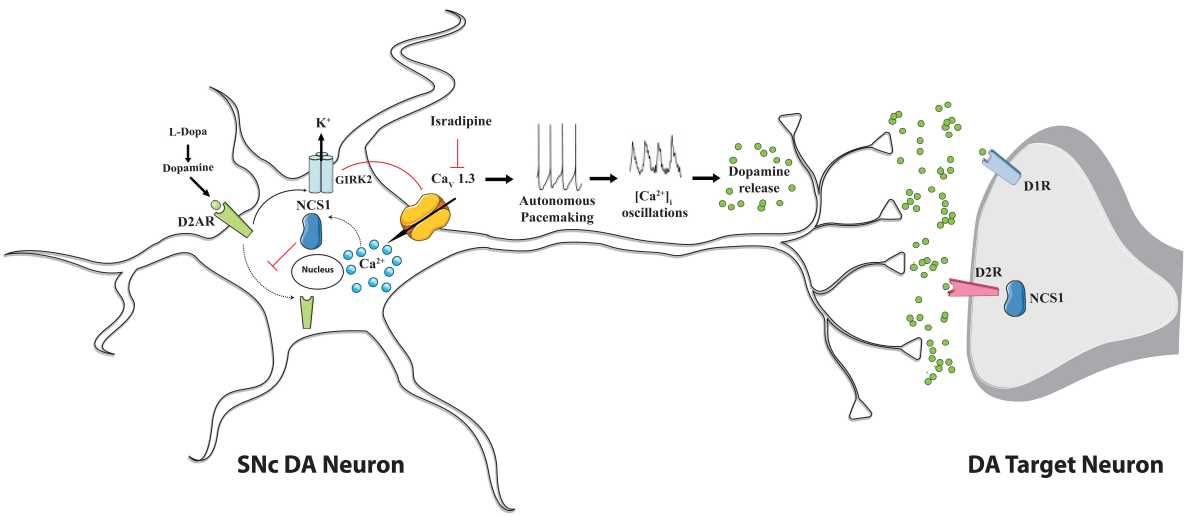

FIGURE 2 | Proposed mechanism for Cav1.3 L-type Ca^{2+} channel action and NCS-1 contribute during autonomous firing of substantia nigra pars compacta dopaminergic neurons. Cav 1.3 channels activity sustains dopamine release. Dopamine binding to D1 and D2 receptors on dopaminergic target neurons promotes motor function. Dopamine binding to D2-autoreceptors (D2-AR) on SNc DA neurons controls their firing rate by promoting the inhibitory effect of GIRK2 K^+ channels and, at the same time, the D2-AR internalization thus contributing to desensitization process. NCS-1 participates in the regulation of dopaminergic signaling since upon Cav 1.3 channels-mediated Ca^{2+} influx it becomes active and, by blocking D2-AR internalization, prevents receptors desensitization. Upon pharmacological treatment with L-DOPA and/or Cav.1.3 antagonist isradipine a vicious loop may be activated: D2-AR desensitization could be facilitated, since reduced Ca^{2+} influx may affect NCS-1 inhibition of receptor internalization and the ability of dopamine to inhibit neuronal activity may be compromised, altogether leading to excitotoxicity. This possibility deserves further investigation, even if no evidence in this direction has been provided so far.

that may have protective role by preventing D2 autoreceptors desensitization. A simplified model that summarizes this concept is shown in **Figure 2**. According to it, increases in the intracellular Ca^{2+} concentration activate NCS-1 that opposes somatodendritic D2-autoreceptors internalization and blocks their desensitization counteracting in this way the inhibitory effect mediated by GIRK2 channels on Cav1.3 and finally promotes dopamine release also through this mechanism. Apparently, this could result in a sort of vicious circle that exacerbate Ca^{2+} entry. However, no desensitization was found during development in KO mice for Cav1.3 and no evidence for exacerbated excitotoxicity upon treatment with the dihydropyridine L-type Ca^{2+} channel blocker isradipine has been reported so far, thus suggesting that other compensatory mechanisms intervene.

In line with this suggestion, loss of Cav1.3 (or its pharmacological inhibition) does not severely compromise pacemaking activity both in juvenile and adult SNc DA neurons, but rather altered its precision and regular occurrence (Poetschke et al., 2015). The appearance of compensatory response due both to NCS-1 upregulation and to the existence of alternative Ca^{2+} source in SNc DA cells that are able to mediate NCS-1/D2-AR interactions could explain the findings. Indeed, an upregulation of both T-type Ca^{2+} Cav 1.2 channels and NCS-1 protein has been found in Cav1.3 KO mice (Poetschke et al., 2015).

All together these observations strongly support the idea that Ca^{2+} and DA are critical components in the disease and underline the complexity of their interplay in the modulation of dopaminergic response.

CONCLUSION

The distinctive physiology of the DA midbrain neurons within the SNc has attracted attention as possible reason for their selective vulnerability. Slow rhythmic activity (accompanied by oscillations in intracellular Ca^{2+} concentration) and high dendritic arborization distinguishes these neurons from the other neurons in the brain. Cav1.3 mediated Ca^{2+} influx is essential to sustain DA release, to guarantee high energy demands that are required for this function and to provide necessary amount of ATP at axonal and dendrites sites. But if continuous Ca^{2+} entry sustains DA secretion and mitochondrial metabolism, at the same time it exposes cells to "Ca^{2+} stress," that may synergize with intrinsic low Ca^{2+} buffering capacity, aging, mutations or mitochondria damage and culminate in cell degeneration. *In vitro* and *in vivo* studies strongly implicated Cav1.3 activity in the high vulnerability of SNc DA neurons, however the complexity of DA metabolism that includes an autoregulatory nature of DA secretion underlines that selective vulnerability of SNc neurons is still an obscure issue. The characterization of the Cav1.3 Ca^{2+} channels physiology and of the alternative pathways that are engaged to compensate pharmacological inhibition of Cav.1.3 channels upon isradipine treatment certainly deserves more investigations. The outcome of isradipine phase III clinical trial will shed light on these aspects.

At this point we can conclude that the deciphering of the molecular mechanisms involved in dopaminergic signaling is the best we can do to develop therapeutic strategy, but we have to be aware that the complexity of the system is increased by interactive pathways that are engaged in compensatory mechanisms and this makes the investigations very challenging.

DATA AVAILABILITY

All datasets generated for this study are included in the manuscript and/or the supplementary files.

AUTHOR CONTRIBUTIONS

All authors listed have made a substantial, direct and intellectual contribution to the work, and approved it for publication.

FUNDING

This work was supported by grants from the Università degli Studi di Padova (Progetto di Ateneo 2015 n. CPDA 153402 to MB, Progetto Giovani 2012 n.GRIC128SP0 to TC and Progetto di Ateneo 2016 n. CALI_SID16_01 to TC) and from the Ministry of University and Research (Bando SIR 2014 n. RBSI14C65Z to TC).

REFERENCES

Angelova, P. R., Ludtmann, M. H., Horrocks, M. H., Negoda, A., Cremades, N., Klenerman, D., et al. (2016). Ca2+ is a key factor in alpha-synuclein-induced neurotoxicity. *J. Cell Sci.* 129, 1792–1801. doi: 10.1242/jcs.180737

Area-Gomez, E., and Schon, E. A. (2017). On the pathogenesis of alzheimer's disease: the mam hypothesis. *FASEB J.* 31, 864–867. doi: 10.1096/fj.201601309

Beaulieu, J. M., and Gainetdinov, R. R. (2011). The physiology, signaling, and pharmacology of dopamine receptors. *Pharmacol. Rev.* 63, 182–217. doi: 10.1124/pr.110.002642

Becker, C., Jick, S. S., and Meier, C. R. (2008). Use of antihypertensives and the risk of parkinson disease. *Neurology* 70, 1438–1444. doi: 10.1212/01.wnl.0000303818.38960.44

Beckstead, M. J., Grandy, D. K., Wickman, K., and Williams, J. T. (2004). Vesicular dopamine release elicits an inhibitory postsynaptic current in midbrain dopamine neurons. *Neuron* 42, 939–946. doi: 10.1016/j.neuron.2004.05.019

Bernardi, P., Rasola, A., Forte, M., and Lippe, G. (2015). The mitochondrial permeability transition pore: channel formation by f-atp synthase, integration in signal transduction, and role in pathophysiology. *Physiol. Rev.* 95, 1111–1155. doi: 10.1152/physrev.00001.2015

Berridge, M. J. (1998). Neuronal calcium signaling. *Neuron* 21, 13–26. doi: 10.1016/S0896-6273(00)80510-3

Brini, M., Calì, T., Ottolini, D., and Carafoli, E. (2014). Neuronal calcium signaling: function and dysfunction. *Cell Mol. Life Sci.* 71, 2787–2814. doi: 10.1007/s00018-013-1550-7

Burgoyne, R. D. (2007). Neuronal calcium sensor proteins: generating diversity in neuronal Ca^{2+} signalling. *Nat. Rev. Neurosci.* 8, 182–193. doi: 10.1038/nrn2093

Calì, T., Ottolini, D., and Brini, M. (2012a). Mitochondrial Ca(2+) and neurodegeneration. *Cell Calcium* 52, 73–85. doi: 10.1016/j.ceca.2012.04.015

Calì, T., Ottolini, D., Negro, A., and Brini, M. (2012b). alpha-Synuclein controls mitochondrial calcium homeostasis by enhancing endoplasmic reticulum-mitochondria interactions. *J. Biol. Chem.* 287, 17914–17929. doi: 10.1074/jbc.M111.302794

Calì, T., Ottolini, D., and Brini, M. (2013a). Calcium and endoplasmic reticulum-mitochondria tethering in neurodegeneration. *DNA Cell. Biol.* 32, 140–146. doi: 10.1089/dna.2013.2011

Calì, T., Ottolini, D., Negro, A., and Brini, M. (2013b). Enhanced parkin levels favor ER-mitochondria crosstalk and guarantee Ca(2+) transfer to sustain cell bioenergetics. *Biochim. Biophys. Acta* 1832, 495–508. doi: 10.1016/j.bbadis.2013.01.004

Calì, T., Ottolini, D., and Brini, M. (2014). Calcium signaling in parkinson's disease. *Cell Tissue Res.* 357, 439–454. doi: 10.1007/s00441-014-1866-0

Chan, C. S., Guzman, J. N., Ilijic, E., Mercer, J. N., Rick, C., Tkatch, T., et al. (2007). 'Rejuvenation' protects neurons in mouse models of parkinson's disease. *Nature* 447, 1081–1086. doi: 10.1038/nature05865

Damier, P., Hirsch, E. C., Agid, Y., and Graybiel, A. M. (1999). The substantia nigra of the human brain. I. Nigrosomes and the nigral matrix, a compartmental organization based on calbindin D(28K) immunohistochemistry. *Brain* 122(Pt 8), 1421–1436. doi: 10.1093/brain/122.8.1421

Danzer, K. M., Haasen, D., Karow, A. R., Moussaud, S., Habeck, M., Giese, A., et al. (2007). Different species of alpha-synuclein oligomers induce calcium influx and seeding. *J. Neurosci.* 27, 9220–9232. doi: 10.1523/JNEUROSCI.2617-07.2007

de Lau, L. M., and Breteler, M. M. (2006). Epidemiology of Parkinson's disease. *Lancet Neurol.* 5, 525–535. doi: 10.1016/S1474-4422(06)70471-9

Dopeso-Reyes, I. G., Rico, A. J., Roda, E., Sierra, S., Pignataro, D., Lanz, M., et al. (2014). Calbindin content and differential vulnerability of midbrain efferent dopaminergic neurons in macaques. *Front. Neuroanat.* 8:146. doi: 10.3389/fnana.2014.00146

Dragicevic, E., Poetschke, C., Duda, J., Schlaudraff, F., Lammel, S., Schiemann, J., et al. (2014). Cav1.3 channels control D2-autoreceptor responses via NCS-1 in substantia nigra dopamine neurons. *Brain* 137, 2287–2302. doi: 10.1093/brain/awu131

Fierro, L., and Llano, I. (1996). High endogenous calcium buffering in purkinje cells from rat cerebellar slices. *J. Physiol.* 496(Pt 3), 617–625. doi: 10.1113/jphysiol.1996.sp021713

Filadi, R., Basso, E., Lefkimmiatis, K., and Pozzan, T. (2017a). Beyond intracellular signaling: the ins and outs of second messengers microdomains. *Adv. Exp. Med. Biol.* 981, 279–322. doi: 10.1007/978-3-319-55858-5_12

Filadi, R., Theurey, P., and Pizzo, P. (2017b). The endoplasmic reticulum-mitochondria coupling in health and disease: molecules, functions and significance. *Cell Calcium* 62, 1–15. doi: 10.1016/j.ceca.2017.01.003

Filadi, R., Greotti, E., Turacchio, G., Luini, A., Pozzan, T., and Pizzo, P. (2016). Presenilin 2 modulates endoplasmic reticulum-mitochondria coupling by tuning the antagonistic effect of mitofusin 2. *Cell Rep.* 15, 2226–2238. doi: 10.1016/j.celrep.2016.05.013

Foehring, R. C., Zhang, X. F., Lee, J. C., and Callaway, J. C. (2009). Endogenous calcium buffering capacity of substantia nigral dopamine neurons. *J. Neurophysiol.* 102, 2326–2333. doi: 10.1152/jn.00038.2009

Gandhi, S., Wood-Kaczmar, A., Yao, Z., Plun-Favreau, H., Deas, E., Klupsch, K., et al. (2009). PINK1-associated Parkinson's disease is caused by neuronal vulnerability to calcium-induced cell death. *Mol. Cell* 33, 627–638. doi: 10.1016/j.molcel.2009.02.013

Gantz, S. C., Robinson, B. G., Buck, D. C., Bunzow, J. R., Neve, R. L., Williams, J. T., et al. (2015). Distinct regulation of dopamine D2S and D2L autoreceptor signaling by calcium. *eLife* 4:e09358. doi: 10.7554/eLife.09358

German, D. C., Manaye, K. F., Sonsalla, P. K., and Brooks, B. A. (1992). Midbrain dopaminergic cell loss in Parkinson's disease and MPTP-induced parkinsonism: sparing of calbindin-D28k-containing cells. *Ann. N. Y. Acad. Sci.* 648, 42–62. doi: 10.1111/j.1749-6632.1992.tb24523.x

Geula, C., Bu, J., Nagykery, N., Scinto, L. F., Chan, J., Joseph, J., et al. (2003). Loss of calbindin-D28k from aging human cholinergic basal forebrain: relation to neuronal loss. *J. Comp. Neurol.* 455, 249–259. doi: 10.1002/cne.10475

Goedert, M., Spillantini, M. G., Del Tredici, K., and Braak, H. (2013). 100 years of lewy pathology. *Nat. Rev. Neurol.* 9, 13–24. doi: 10.1038/nrneurol.2012.242

Guzman, J. N., Ilijic, E., Yang, B., Sanchez-Padilla, J., Wokosin, D., Galtieri, D., et al. (2018). Systemic isradipine treatment diminishes calcium-dependent mitochondrial oxidant stress. *J. Clin. Invest.* 128, 2266–2280. doi: 10.1172/JCI95898

Guzman, J. N., Sanchez-Padilla, J., Wokosin, D., Kondapalli, J., Ilijic, E., Schumacker, P. T., et al. (2010). Oxidant stress evoked by pacemaking in dopaminergic neurons is attenuated by DJ-1. *Nature* 468, 696–700. doi: 10.1038/nature09536

Handley, M. T., Lian, L. Y., Haynes, L. P., and Burgoyne, R. D. (2010). Structural and functional deficits in a neuronal calcium sensor-1 mutant identified in a case of autistic spectrum disorder. *PLoS One* 5:e10534. doi: 10.1371/journal.pone.0010534

Hetz, C., and Saxena, S. (2017). ER stress and the unfolded protein response in neurodegeneration. *Nat. Rev. Neurol.* 13, 477–491. doi: 10.1038/nrneurol.2017.99

Hurley, M. J., Brandon, B., Gentleman, S. M., and Dexter, D. T. (2013). Parkinson's disease is associated with altered expression of CaV1 channels and calcium-binding proteins. *Brain* 136, 2077–2097. doi: 10.1093/brain/awt134

Ilijic, E., Guzman, J. N., and Surmeier, D. J. (2011). The L-type channel antagonist isradipine is neuroprotective in a mouse model of Parkinson's disease. *Neurobiol. Dis.* 43, 364–371. doi: 10.1016/j.nbd.2011.04.007

Kabbani, N., Negyessy, L., Lin, R., Goldman-Rakic, P., and Levenson, R. (2002). Interaction with neuronal calcium sensor NCS-1 mediates desensitization of the D2 dopamine receptor. *J. Neurosci.* 22, 8476–8486. doi: 10.1523/JNEUROSCI.22-19-08476.2002

Kabbani, N., Woll, M. P., Nordman, J. C., and Levenson, R. (2012). Dopamine receptor interacting proteins: targeting neuronal calcium sensor-1/D2 dopamine receptor interaction for antipsychotic drug development. *Curr. Drug Targets* 13, 72–79. doi: 10.2174/138945012798868515

Khaliq, Z. M., and Bean, B. P. (2010). Pacemaking in dopaminergic ventral tegmental area neurons: depolarizing drive from background and voltage-dependent sodium conductances. *J. Neurosci.* 30, 7401–7413. doi: 10.1523/JNEUROSCI.0143-10.2010

Koh, P. O., Undie, A. S., Kabbani, N., Levenson, R., Goldman-Rakic, P. S., and Lidow, M. S. (2003). Up-regulation of neuronal calcium sensor-1 (NCS-1) in the prefrontal cortex of schizophrenic and bipolar patients. *Proc. Natl. Acad. Sci. U.S. A.* 100, 313–317. doi: 10.1073/pnas.232693499

Kurtishi, A., Rosen, B., Patil, K. S., Alves, G. W., and Moller, S. G. (2018). Cellular proteostasis in neurodegeneration. *Mol. Neurobiol.* doi: 10.1007/s12035-018-1334-z [Epub ahead of print].

L'hirondel, M., Cheramy, A., Godeheu, G., Artaud, F., Saiardi, A., Borrelli, E., et al. (1998). Lack of autoreceptor-mediated inhibitory control of dopamine release in striatal synaptosomes of D2 receptor-deficient mice. *Brain Res.* 792, 253–262. doi: 10.1016/S0006-8993(98)00146-2

La Rovere, R. M., Roest, G., Bultynck, G., and Parys, J. B. (2016). Intracellular Ca(2+) signaling and Ca(2+) microdomains in the control of cell survival, apoptosis and autophagy. *Cell Calcium* 60, 74–87. doi: 10.1016/j.ceca.2016.04.005

Levey, A. I., Hersch, S. M., Rye, D. B., Sunahara, R. K., Niznik, H. B., Kitt, C. A., et al. (1993). Localization of D1 and D2 dopamine receptors in brain with subtype-specific antibodies. *Proc. Natl. Acad. Sci. U.S.A.* 90, 8861–8865. doi: 10.1073/pnas.90.19.8861

Liang, C. L., Wang, T. T., Luby-Phelps, K., and German, D. C. (2007). Mitochondria mass is low in mouse substantia nigra dopamine neurons: implications for Parkinson's disease. *Exp. Neurol.* 203, 370–380. doi: 10.1016/j.expneurol.2006.08.015

Liss, B., and Striessnig, J. (2019). The potential of l-type calcium channels as a drug target for neuroprotective therapy in Parkinson's disease. *Annu. Rev. Pharmacol. Toxicol.* 59, 263–289. doi: 10.1146/annurev-pharmtox-010818-021214

Liu, Q., Emadi, S., Shen, J. X., Sierks, M. R., and Wu, J. (2013). Human alpha4beta2 nicotinic acetylcholine receptor as a novel target of oligomeric alpha-synuclein. *PLoS One* 8:e55886. doi: 10.1371/journal.pone.0055886

Luscher, C., and Slesinger, P. A. (2010). Emerging roles for G protein-gated inwardly rectifying potassium (GIRK) channels in health and disease. *Nat. Rev. Neurosci.* 11, 301–315. doi: 10.1038/nrn2834

Marongiu, R., Spencer, B., Crews, L., Adame, A., Patrick, C., Trejo, M., et al. (2009). Mutant pink1 induces mitochondrial dysfunction in a neuronal cell model of Parkinson's disease by disturbing calcium flux. *J. Neurochem.* 108, 1561–1574. doi: 10.1111/j.1471-4159.2009.05932.x

McCue, H. V., Haynes, L. P., and Burgoyne, R. D. (2010). The diversity of calcium sensor proteins in the regulation of neuronal function. *Cold Spring Harb. Perspect. Biol.* 2:a004085. doi: 10.1101/cshperspect.a004085

Mercado, G., Valdes, P., and Hetz, C. (2013). An ERcentric view of Parkinson's disease. *Trends Mol. Med.* 19, 165–175. doi: 10.1016/j.molmed.2012.12.005

Mercuri, N. B., Saiardi, A., Bonci, A., Picetti, R., Calabresi, P., Bernardi, G., et al. (1997). Loss of autoreceptor function in dopaminergic neurons from dopamine D2 receptor deficient mice. *Neuroscience* 79, 323–327.

Moore, L. M., England, A., Ehrlich, B. E., and Rimm, D. L. (2017). Calcium sensor, ncs-1, promotes tumor aggressiveness and predicts patient survival. *Mol. Cancer Res.* 15, 942–952. doi: 10.1158/1541-7786.MCR-16-0408

Mosharov, E. V., Larsen, K. E., Kanter, E., Phillips, K. A., Wilson, K., Schmitz, Y., et al. (2009). Interplay between cytosolic dopamine, calcium, and alpha-synuclein causes selective death of substantia nigra neurons. *Neuron* 62, 218–229. doi: 10.1016/j.neuron.2009.01.033

Mouatt-Prigent, A., Agid, Y., and Hirsch, E. C. (1994). Does the calcium binding protein calretinin protect dopaminergic neurons against degeneration in Parkinson's disease? *Brain Res.* 668, 62–70. doi: 10.1016/0006-8993(94)90511-8

Muller, M., Ahumada-Castro, U., Sanhueza, M., Gonzalez-Billault, C., Court, F. A., and Cardenas, C. (2018). Mitochondria and calcium regulation as basis of neurodegeneration associated with aging. *Front. Neurosci.* 12:470. doi: 10.3389/fnins.2018.00470

Neher, E. (1998). Usefulness and limitations of linear approximations to the understanding of Ca++ signals. *Cell Calcium* 24, 345–357. doi: 10.1016/S0143-4160(98)90058-6

Neher, E., and Augustine, G. J. (1992). Calcium gradients and buffers in bovine chromaffin cells. *J. Physiol.* 450, 273–301. doi: 10.1113/jphysiol.1992.sp019127

Ng, E., Varaschin, R. K., Su, P., Browne, C. J., Hermainski, J., Le Foll, B., et al. (2016). Neuronal calcium sensor-1 deletion in the mouse decreases motivation and dopamine release in the nucleus accumbens. *Behav. Brain Res.* 301, 213–225. doi: 10.1016/j.bbr.2015.12.037

Oertel, W., and Schulz, J. B. (2016). Current and experimental treatments of parkinson disease: a guide for neuroscientists. *J. Neurochem.* 139(Suppl. 1), 325–337. doi: 10.1111/jnc.13750

Ottolini, D., Calì, T., Negro, A., and Brini, M. (2013). The Parkinson disease-related protein DJ-1 counteracts mitochondrial impairment induced by the tumour suppressor protein p53 by enhancing endoplasmic reticulum-mitochondria tethering. *Hum. Mol. Genet.* 22, 2152–2168. doi: 10.1093/hmg/ddt068

Paillusson, S., Gomez-Suaga, P., Stoica, R., Little, D., Gissen, P., Devine, M. J., et al. (2017). alpha-Synuclein binds to the ER-mitochondria tethering protein VAPB to disrupt Ca(2+) homeostasis and mitochondrial ATP production. *Acta Neuropathol.* 134, 129–149. doi: 10.1007/s00401-017-1704-z

Pasternak, B., Svanstrom, H., Nielsen, N. M., Fugger, L., Melbye, M., and Hviid, A. (2012). Use of calcium channel blockers and Parkinson's disease. *Am. J. Epidemiol.* 175, 627–635. doi: 10.1093/aje/kwr362

Pchitskaya, E., Popugaeva, E., and Bezprozvanny, I. (2018). Calcium signaling and molecular mechanisms underlying neurodegenerative diseases. *Cell Calcium* 70, 87–94. doi: 10.1016/j.ceca.2017.06.008

Piton, A., Michaud, J. L., Peng, H., Aradhya, S., Gauthier, J., Mottron, L., et al. (2008). Mutations in the calcium-related gene IL1RAPL1 are associated with autism. *Hum. Mol. Genet.* 17, 3965–3974. doi: 10.1093/hmg/ddn300

Poetschke, C., Dragicevic, E., Duda, J., Benkert, J., Dougalis, A., Dezio, R., et al. (2015). Compensatory T-type Ca2+ channel activity alters D2-autoreceptor responses of Substantia nigra dopamine neurons from Cav1.3 L-type Ca2+ channel KO mice. *Sci. Rep.* 5:13688. doi: 10.1038/srep13688

Pongs, O., Lindemeier, J., Zhu, X. R., Theil, T., Engelkamp, D., Krah-Jentgens, I., et al. (1993). Frequenin–a novel calcium-binding protein that modulates synaptic efficacy in the Drosophila nervous system. *Neuron* 11, 15–28. doi: 10.1016/0896-6273(93)90267-U

Puopolo, M., Raviola, E., and Bean, B. P. (2007). Roles of subthreshold calcium current and sodium current in spontaneous firing of mouse midbrain dopamine neurons. *J. Neurosci.* 27, 645–656. doi: 10.1523/JNEUROSCI.4341-06.2007

Ritz, B., Rhodes, S. L., Qian, L., Schernhammer, E., Olsen, J. H., and Friis, S. (2010). L-type calcium channel blockers and Parkinson disease in Denmark. *Ann. Neurol.* 67, 600–606.

Ronzitti, G., Bucci, G., Emanuele, M., Leo, D., Sotnikova, T. D., Mus, L. V., et al. (2014). Exogenous alpha-synuclein decreases raft partitioning of Cav2.2 channels inducing dopamine release. *J. Neurosci.* 34, 10603–10615. doi: 10.1523/JNEUROSCI.0608-14.2014

Samanta, K., and Parekh, A. B. (2017). Spatial Ca(2+) profiling: decrypting the universal cytosolic Ca(2+) oscillation. *J. Physiol.* 595, 3053–3062. doi: 10.1113/JP272860

Schultz, W., and Ungerstedt, U. (1978). Striatal cell supersensitivity to apomorphine in dopamine-lesioned rats correlated to behaviour. *Neuropharmacology* 17, 349–353. doi: 10.1016/0028-3908(78)90005-9

Schwaller, B. (2012). The use of transgenic mouse models to reveal the functions of Ca2+ buffer proteins in excitable cells. *Biochim. Biophys. Acta* 1820, 1294–1303. doi: 10.1016/j.bbagen.2011.11.008

Sesack, S. R., Aoki, C., and Pickel, V. M. (1994). Ultrastructural localization of D2 receptor-like immunoreactivity in midbrain dopamine neurons and their striatal targets. *J. Neurosci.* 14, 88–106. doi: 10.1523/JNEUROSCI.14-01-00088.1994

Sharma, R. K., and Parameswaran, S. (2018). Calmodulin-binding proteins: a journey of 40 years. *Cell Calcium* 75, 89–100. doi: 10.1016/j.ceca.2018.09.002

Surguchev, A., and Surguchov, A. (2015). Effect of alpha-synuclein on membrane permeability and synaptic transmission: a clue to neurodegeneration? *J. Neurochem.* 132, 619–621. doi: 10.1111/jnc.13045

Surmeier, D. J., Guzman, J. N., Sanchez-Padilla, J., and Schumacker, P. T. (2011). The role of calcium and mitochondrial oxidant stress in the loss of substantia nigra pars compacta dopaminergic neurons in Parkinson's disease. *Neuroscience* 198, 221–231. doi: 10.1016/j.neuroscience.2011.08.045

Tarasov, A. I., Griffiths, E. J., and Rutter, G. A. (2012). Regulation of ATP production by mitochondrial Ca(2+). *Cell Calcium* 52, 28–35. doi: 10.1016/j.ceca.2012.03.003

Wang, H. Q., and Takahashi, R. (2007). Expanding insights on the involvement of endoplasmic reticulum stress in Parkinson's disease. *Antioxid. Redox Signal.* 9, 553–561. doi: 10.1089/ars.2006.1524

Xia, Z., and Storm, D. R. (2005). The role of calmodulin as a signal integrator for synaptic plasticity. *Nat. Rev. Neurosci.* 6, 267–276. doi: 10.1038/nrn1647

Yamada, T., Mcgeer, P. L., Baimbridge, K. G., and Mcgeer, E. G. (1990). Relative sparing in Parkinson's disease of substantia nigra dopamine neurons containing calbindin-D28K. *Brain Res.* 526, 303–307. doi: 10.1016/0006-8993(90)91236-A

Zallo, F., Gardenal, E., Verkhratsky, A., and Rodriguez, J. J. (2018). Loss of calretinin and parvalbumin positive interneurones in the hippocampal CA1 of aged Alzheimer's disease mice. *Neurosci. Lett.* 681, 19–25. doi: 10.1016/j.neulet.2018.05.027

Zhang, K., Heidrich, F. M., Degray, B., Boehmerle, W., and Ehrlich, B. E. (2010). Paclitaxel accelerates spontaneous calcium oscillations in cardiomyocytes by interacting with NCS-1 and the InsP3R. *J. Mol. Cell. Cardiol.* 49, 829–835. doi: 10.1016/j.yjmcc.2010.08.018

Zhou, Z., and Neher, E. (1993). Mobile and immobile calcium buffers in bovine adrenal chromaffin cells. *J. Physiol.* 469, 245–273. doi: 10.1113/jphysiol.1993.sp019813

Conflict of Interest Statement: The authors declare that the research was conducted in the absence of any commercial or financial relationships that could be construed as a potential conflict of interest.

cells

MDPI

Article

splitGFP Technology Reveals Dose-Dependent ER-Mitochondria Interface Modulation by α-Synuclein A53T and A30P Mutants

Tito Calì [1,2,*], Denis Ottolini [3], Mattia Vicario [1], Cristina Catoni [3], Francesca Vallese [1], Domenico Cieri [1], Lucia Barazzuol [1] and Marisa Brini [3,*]

1 Department of Biomedical Sciences, University of Padova, Padova 35131, Italy; mattiavicario@hotmail.it (M.V.); francesca.vallese84@gmail.com (F.V.); domenico.cieri87@gmail.com (D.C.); luciabarazzuol@gmail.com (L.B.)
2 Padova Neuroscience Center (PNC), University of Padova, Padova 35131, Italy
3 Department of Biology, University of Padova, Padova 35131, Italy; ottolinidenis@gmail.com (D.O.); cristina.catoni@phd.unipd.it (C.C.)
* Correspondence: tito.cali@unipd.it (T.C.); marisa.brini@unipd.it (M.B.); Tel.: +39-049-8276144 (T.C.); +39-049-8276135 (M.B.)

Received: 4 August 2019; Accepted: 11 September 2019; Published: 12 September 2019

Abstract: Familial Parkinson's disease (PD) is associated with duplication or mutations of α-synuclein gene, whose product is a presynaptic cytosolic protein also found in mitochondria and in mitochondrial-associated ER membranes. We have originally shown the role of α-syn as a modulator of the ER-mitochondria interface and mitochondrial Ca^{2+} transients, suggesting that, at mild levels of expression, α-syn sustains cell metabolism. Here, we investigated the possibility that α-syn action on ER-mitochondria tethering could be compromised by the presence of PD-related mutations. The clarification of this aspect could contribute to elucidate key mechanisms underlying PD. The findings reported so far are not consistent, possibly because of the different methods used to evaluate ER-mitochondria connectivity. Here, the effects of the PD-related α-syn mutations A53T and A30P on ER-mitochondria relationship were investigated in respect to Ca^{2+} handling and mitochondrial function using a newly generated SPLICS sensor and aequorin-based Ca^{2+}measurements. We provided evidence that A53T and A30P amino acid substitution does not affect the ability of α-syn to enhance ER/mitochondria tethering and mitochondrial Ca^{2+} transients, but that this action was lost as soon as a high amount of TAT-delivered A53T and A30P α-syn mutants caused the redistribution of α-syn from cytoplasm to foci. Our results suggest a loss of function mechanism and highlight a possible connection between α-syn and ER-mitochondria Ca^{2+} cross-talk impairment to the pathogenesis of PD.

Keywords: Parkinson's disease; alpha-synuclein; calcium; mitochondria; ER-mitochondria contact sites

1. Introduction

Structural alterations and toxic misfolding of susceptible proteins are common hallmarks of many neurodegenerative diseases, including amyotrophic lateral sclerosis, Alzheimer's, Parkinson's, and Huntington's disease, and are linked to the degeneration and death of specific neuronal populations in the human brain [1,2]. Parkinson's disease (PD) is characterized by loss of dopaminergic neurons of the substantia nigra pars compacta in ventral mid-brain [3] and accumulation of intra-cytoplasmic fibrillary aggregates, termed as Lewy bodies, mainly constituted by α-synuclein (α-syn) [4]. α-syn is a 140-amino acid unfolded protein highly expressed in the nervous system with a preferential distribution at the

presynaptic terminals [5]. PD familial studies have identified a number of α-syn mutations, leading to either an early (A53T, A30P, E46K, G51D) or a late (H50Q) onset of the disease [6]. Besides its role in neuronal synaptic transmission [7–9] the function of α-syn within the cells is not yet fully understood. Under pathological conditions, monomeric cytosolic α-syn undergoes structural changes that cause its aggregation and insolubility [10–15] typically observed in many forms of neurodegeneration [16,17]. Several studies have shown that α-syn interacts with membrane phospholipids and that it can selectively bind to mitochondrial sub-compartments [18–23]. Mitochondrial dysfunctions are a common element in the pathogenesis of many neurodegenerative diseases, including PD [24], being pivotal mitochondrial processes directly influenced by α-syn [25]. Alterations in mitochondrial phenotypes have been consistently reported in mutant α-syn transgenic [26,27] and null mice [28], as well as in model cells overexpressing wt and mutant α-syn [29]. α-syn has also been shown to participate in the maintenance of mitochondrial integrity by regulating the fission/fusion machinery and the autophagic process [30–33]. Interestingly, we have previously demonstrated that α-syn positively enhanced mitochondrial Ca^{2+} transients generated upon Ca^{2+} release from the endoplasmic reticulum (ER) by increasing the ER-mitochondria contact sites in a dose-dependent manner [34]. A dose-dependent effect has been confirmed also for α-syn modulation of other mitochondria-related activities [22,35,36]. Although prevalently cytosolic, α-syn is present in the nucleus [37–39], in the mitochondria [19,20,40,41] and in the mitochondria-associated ER membranes (MAMs) fraction [30,42]. Despite its ability to affect ER-mitochondria tethering, a general consensus on the precise action of α-syn at this interface is still lacking and it is unclear whether it interferes directly or indirectly with the tethering machinery. The possibility that a loss of function mechanism could be in place, thus explaining the different findings [30,34,42], is therefore interesting. In the present study, in order to provide further insights into the role of α-syn in key mechanisms underlying PD, we investigated the effects of A53T and A30P α-syn PD-related mutants on ER-mitochondria associations and mitochondrial Ca^{2+} handling. We have found that the aggregation-prone A53T and A30P mutants recapitulate the previously observed effect of WT α-syn [34]. Interestingly, the A53T and A30P α-syn mutants (reported to be more susceptible to aggregation) were able to increase the number of ER-mitochondria contact sites (as clearly documented by our newly generated split-GFP based ER-mitochondria contact sensor (SPLICS)) [43] and enhance mitochondria Ca^{2+} transients in our cell model under conditions in which their distribution is cytosolic. However, their ability to positively modulate mitochondrial Ca^{2+} transients was lost when their redistribution occurred. These results indicate that the increased aggregation propensity of the α-syn mutants is a key element in the pathogenesis of PD since it might lead to premature sequestration of α-syn into non-functional aggregates and through a loss-of-function mechanism affect the ER-mitochondria interface and, in turn, essential mitochondrial functions.

2. Materials and Methods

2.1. DNA Constructs

Plasmids encoding wt and mutant α-syn and TAT-fusion wt and mutant α-syn recombinant proteins were previously described [34,44]. Briefly, the SPLICS-P2A construct has been generated by cloning the ER_{short}-β_{11} and the OMM-$GFP_{1–10}$ coding sequences described in [43], respectively, upstream and downstream of a viral 2A peptide sequence contained in the pSYC-181 plasmid (Addgene, Watertown, MA, USA), previously reported to be cleaved within the cell to generate an equimolar amount of the two genes [45]. From this construct, named pSYC-$SPLICS_S$-P2A [43], the sequence encoding SPLICS-P2A was excised using BamHI and XbaI restriction enzymes and subcloned in mammalian expression vector pCDNA3.1. All the constructs were verified by sequencing. Mitochondria-targeted GFP (mtGFP) expression vector was kindly provided by Prof. R. Rizzuto, University of Padova [46]. Plasmids encoding recombinant targeted aequorin probes were previously described, cytAEQ in [47], mtAEQ in [48] and erAEQ in [49]. For a comprehensive view of the tools and the methodology please refer to [50–53].

2.2. Cell lines and Transfection

HeLa cells were maintained in DMEM (Euroclone, Milan, Italy) supplemented with 10% FBS (Euroclone, Milan), 100 units/mL penicillin, and 100 µg/mL streptomycin, and kept at 37 °C in a humidified atmosphere of 5% CO_2. Cells were seeded onto 13-mm (for aequorin measurements) or 24-mm (for ER-mitochondria contact sites analysis) glass coverslips for 12 h before transfection. For [Ca^{2+}] measurements, HeLa cells were co-transfected by calcium-phosphate procedure with aequorin encoding plasmids and pcDNA3 empty plasmid (mock) or α-syn expressing vectors in a 1:2 ratio as previously described [34]. Ca^{2+} measurements were performed 36 h later.

Cells plated for Western blotting were collected 24–36 h after transfection. For TAT-mediated delivery, recombinant TAT fusion proteins were added directly onto the seeded aequorin-transfected cells and incubated for 2.5–5 h in DMEM, 10% FBS, and antibiotics at 37 °C in a 5% CO_2 atmosphere. After incubation with TAT fusion proteins, the cells were extensively washed with PBS before starting Ca^{2+} measurements [34].

2.3. Western Blotting

HeLa cells were flooded on ice with 20 mM ice-cold *N*-ethylmaleimide in PBS to prevent post-lysis oxidation of free cysteines. Cell extracts were prepared by solubilizing cells in ice-cold 2% CHAPS in Hepes-buffered saline (50 mM HEPES, 0.2 M NaCl, pH 6.8) containing *N*-ethylmaleimide, 1 mM PMSF, and mixture protease inhibitors (Sigma, St. Louis, MO, USA). Postnuclear supernatants were collected after centrifugation 10 min at 10,000× *g* at 4 °C. The total protein content was determined by the Bradford assay (Bio-Rad, Hercules, CA, USA). Samples were loaded on a 15% SDS-PAGE Tris/HCl gel, transferred onto PVDF membranes (Bio-Rad, Hercules, CA, USA), and incubated overnight with the specific primary antibody at 4 °C. Detection was carried out by incubation with secondary horseradish peroxidase-conjugated anti-rabbit or anti-mouse IgG antibody (Santa Cruz Biotechnology, Dallas, TX, USA) for 1.5 h at room temperature. The proteins were visualized by the chemiluminescent reagent Immobilon Western (Merck KGaA, Darmstadt, Germany). Mouse monoclonal anti-α-syn antibody (sc-12767, Santa Cruz Biotechnology, Inc.) was used at a 1:30 dilution in immunocytochemistry analysis and at a 1:500 dilution in Western blotting analysis. Mouse monoclonal anti-β-actin (AC-15, Merck KGaA, Darmstadt, Germany) was used at a 1:90.000 dilution in Western blotting.

2.4. Immunocytochemistry Analysis

Transfected or TAT α-syn loaded HeLa cells plated on coverslips were fixed with 3.7% formaldehyde in phosphate-buffered saline (PBS; 140 mM NaCl, 2 mM KCl, 1.5 mM KH_2PO_4, 8 m MNa_2HPO_4, pH 7.4) for 20 min and washed three times with PBS. Cell permeabilization was performed by 20 min of incubation in 0.1% Triton X-100 PBS followed by 30 min wash in 1% gelatin (type IV, from bovine skin, Merck KGaA, Darmstadt, Germany) in PBS at room temperature. The coverslips were then incubated for 90 min at 37 °C in a wet chamber with the specific antibody diluted in PBS. Staining was revealed by the incubation with specific AlexaFluor 488 or 594 secondary antibodies for 45 min at room temperature (1:100 dilution in PBS; Thermo Fisher Scientific, Waltham, MA, USA). Fluorescence was analyzed with a Zeiss Axiovert microscope equipped with a 12-bit digital cooled camera (Micromax-1300Y; Princeton Instruments Inc., Trenton, NJ, USA) or Leica Confocal SP5 microscope. Images were acquired by using Axiovision 3.1 or Leica AS software (Leica Microsystems, Wetzlar, Germany).

2.5. Aequorin Measurements

Mitochondrial low-affinity aequorin (mtAEQ) and cytosolic wt aequorin (cytAEQ) were reconstituted by incubating cells for 3 h (cytAEQ) or 1.5 h (mtAEQ) with 5 µM wt coelenterazine (Invitrogen) in DMEM supplemented with 1% fetal bovine serum at 37 °C in a 5% CO_2 atmosphere. To functionally reconstitute low-affinity ER-targeted aequorin (erAEQ), the ER Ca^{2+} content had to

be drastically reduced. To this end, cells were incubated for 1.5 h at 4 °C in Krebs–Ringer modified buffer (KRB, 125 mM NaCl, 5 mM KCl, 1 mM Na_3PO_4, 1 mM $MgSO_4$, 5.5 mM glucose, 20 mM HEPES, pH 7.4, 37 °C) supplemented with the Ca^{2+} ionophore ionomycin (5 µM), 600 µM EGTA, and 5 µM coelenterazine (Thermo Fisher Scientific, Waltham, MA, USA). Cells were then extensively washed with KRB supplemented with 2% bovine serum albumin and 1 mM EGTA [53]. After reconstitution, cells were transferred to the chamber of a purpose-built luminometer, and Ca^{2+} measurements were started in KRB medium added with 1 mM$CaCl_2$ or 100 µM EGTA or 1 mM EGTA according to the different protocols and aequorin probes. 100 µM histamine was added, as specified in the figure legends. All the experiments were terminated by cell lysis with 100 µM digitonin in a hypotonic Ca^{2+}-rich solution (10 mM $CaCl_2$ in H_2O) to discharge the remaining reconstituted active aequorin pool. The light signal was collected and calibrated off-line into Ca^{2+}concentration values, as previously described [47,54].

2.6. ER-Mitochondria Contact Site Analysis

Cells plated on 13-mm-diameter coverslips were transfected with SPLICS [43] together with empty or WT or mutants α-syn expressing vectors or incubated with TAT α-syn upon the transfection with SPLICS. Fluorescence was analyzed 48–72 h after transfection with a Leica TSC SP5 inverted confocal microscope, using HCX PL APO 63X/numerical aperture 1.40–0.60 upon excitation at 488 nm. Images were acquired by using the Leica AS software. To count ER–mitochondria contacts, a complete z-stack of the cell was acquired every 0.29 µm. Z-stacks were processed using Fiji [55]. Images were first convolved, and then filtered using the Gaussian blur filter. A 3D reconstruction of the resulting image was obtained using the Volume J plugin (http://bij.isi.uu.nl/vr.htm). A selected face of the 3D rendering was then thresholded and used to count ER–mitochondria contact sites as already described [43,56].

2.7. Statistical Analysis

Data are given as means ± SD (standard deviation). Where multiple groups were compared, statistical significance was calculated by one-way ANOVA with a post hoc Dunett correction. Normally distributed data were analyzed using ANOVA and unpaired Student's two-tailed *t*-test for two-group comparison with no correction assuming the same SD. All statistical significance was calculated at $p = 0.05$, using GraphPad Prism 6 (Graphpad, San Diego, CA, USA). For all the analysis, the samples were collected and processed simultaneously and, therefore, no randomization was appropriate. n = number of independent experiments or cells from at least three different transfection/treatments. When significant, *p*-values were stated in the figure legends. (GraphPad Prism, *** $p < 0.0005$, ** $p < 0.001$, and * $p < 0.05$).

3. Results

3.1. α-syn A53T and A30P Mutants Physically Modulate ER-Mitochondria Contact Sites

We had previously demonstrated that mild α-syn overexpression promotes ER-mitochondria contact sites formation/stabilization and favors Ca^{2+} transfer from the ER to mitochondria, while its silencing causes mitochondrial impairments by loosening the ER-mitochondria interface [34]. Later on, other reports established that α-syn is also present at the MAMs and that PD-related mutations might contribute to the onset of the pathogenic phenotype by differentially interfering with MAMs functions [31,42]. Since we have hypothesized that exaggerated α-syn expression leads to loss of function at the ER-mitochondria interface, we decided to explore whether the familial PD-related A30P and A53T α-syn mutants could have an impact on the ER-mitochondria contact sites. We took advantage from the use of a novel splitGFP-based sensor for organelles proximity, the SPLICS, recently developed by our group [43] and based on the ability of two organelle targeted split-GFP fragments to reconstitute the GFP fluorescence when the membranes come in close proximity. As a result, a dotty pattern of fluorescence where organelle tethering occurs will be detected and quantified on 3D

reconstructions of complete Z-stacks analysis. We have decided to test it in cells overexpressing A30P and A53T α-syn mutants, but at the same time, we have also repeated the experiments in HeLa cells overexpressing WT α-syn to confirm our previous data obtained by calculating Manders' coefficient of mitochondrial-targeted RFP and ER targeted GFP [34]. First, the expression level and the sub-cellular localization of the overexpressed A53T and A30P α-syn mutants were analysed in HeLa cells at 36 h after transfection and compared to those detected in empty-vector- and in WT α-syn-transfected cells. As shown and quantified in Figure 1A, the endogenous expression level of α-syn in empty vector-transfected cells (ctrl) was barely detectable compared to that of WT, A53T, and A30P in α-syn-overexpressing HeLa cells. It is also appreciable that, in our experimental conditions, WT, A53T, and A30P α-syn mutants-overexpressing HeLa cells displayed either comparable protein expression levels (Figure 1A and quantification, values are: 0.0051 ± 0.0025 for control cells, 0.9021 ± 0.1797 for WT α-syn; 1.009 ± 0.3979 for A53T α-syn and 0.9390 ± 0.2006 for A53T α-syn, n = 3) and prevalent cytosolic distribution (Figure 1B), as determined by Western blotting and immunocytochemistry analysis, respectively. Equal loading of proteins was verified by probing the membrane with an anti-β-actin antibody.

These findings allowed us to exclude that differences observed in the following experiments could be dependent on α-syn expression levels. Then, we monitored ER-mitochondria interactions occurring at a short-range distance (8–10 nm), i.e., those that are involved in ER-mitochondria Ca^{2+} transfer [57,58] in the presence of either WT, A30P, and A53T α-syn. As shown in Figure 1B (and quantified in Figure 1C), the expression of WT, A30P, and A53T α-syn, significantly increased the number of the tight ER-mitochondria interactions (number of ER-mitochondria contacts/cell: 70.6 ± 23.73 n = 26 for control cells; 88.4 ± 23.39 n = 25 for WT α-syn, $p < 0.01$; 88.3 ± 28.89 n = 22 for A53T α-syn $p < 0.05$; 89 ± 30.40 n = 23 for A30P α-syn $p < 0.05$). These results confirm our previous report on the positive effect of WT α-syn on the ER-mitochondria interface and demonstrate that the PD-related A30P and A53T amino acids substitutions do not affect the ability of α-syn to increase ER-mitochondria associations.

3.2. Overexpression of A53T and A30P α-Synuclein Mutants Enhances Mitochondrial Ca^{2+} Transients with the Same Extent than wt α-Synuclein

As previously documented by our group, the increase in ER-mitochondria tethering induced by WT α-syn overexpression was paralleled by increased mitochondria Ca^{2+} uptake upon cell stimulation with an $InsP_3$-linked agonist [34]. We thus analyzed mitochondrial Ca^{2+} transients generated upon stimulation with 100 μM histamine, as well as the general Ca^{2+} handling of the cell in the presence of A53T and A30P α-syn. We performed Ca^{2+} measurements using organelle-targeted aequorin probes specific for the mitochondrial matrix (mtAEQ) (A), the cytoplasm (cytAEQ) (B) or the ER lumen (erAEQ) (C) [53].

The overexpression of either A53T or A30P α-syn mutants resulted in significantly increased mitochondrial Ca^{2+} transients compared to the control transfected HeLa cells when exposed to the $InsP_3$-linked agonist histamine (100 μM; Figure 2A top). However, quantification of individual mitochondrial Ca^{2+} responses revealed equal amplitude between A53T and A30P α-syn mutants (Figure 2A, bottom) ($[Ca^{2+}]_{mt}$ μM: 114.49 ± 19.37 n = 13 for control cells; 144 ± 12.31 n = 11 for WT α-syn, $p < 0.001$ vs. control; 147.88 ± 20.75 n = 12 for A53T α-syn, $p < 0.001$ vs. control; 147.85 ± 18.76 n = 16 for A30P α-syn, $p < 0.001$ vs. control). For comparison, similar Ca^{2+} measurements were performed on HeLa cells overexpressing WT α-syn, and also in this case, we observed an increase in mitochondrial Ca^{2+} transients upon cells stimulation. No differences were instead detected among control untransfected cells, WT α-syn and A53T or A30P α-syn mutants, respectively, in cytosolic Ca^{2+} transients generated upon histamine stimulation (Figure 2B) or ER Ca^{2+} content (Figure 2C) ($[Ca^{2+}]_c$ μM: 3.33 ± 0.13 n = 14 for control cells; 3.24 ± 0.14 n = 13 for WT α-syn; 3.29 ± 0.22 n = 12 for A53T α-syn; 3.20 ± 0.22 n = 12 for A30P α-syn; $[Ca^{2+}]_{ER}$ μM: 424 ± 71.15 n = 15 for control cells; 415.9 ± 86.61 n = 13 for WT α-syn; 419.9 ± 79.84 n = 17 for A53T α-syn; 416.7 ± 78.30 n = 16 for A30P

α-syn), reinforcing the hypothesis that, as previously shown for WT α-syn [34], also in the case of the PD-related A53T or A30P α-syn mutants the modulation of the ER-mitochondria interface exclusively enhances mitochondrial Ca^{2+} transients, leaving cytosolic and ER Ca^{2+} levels unaffected.

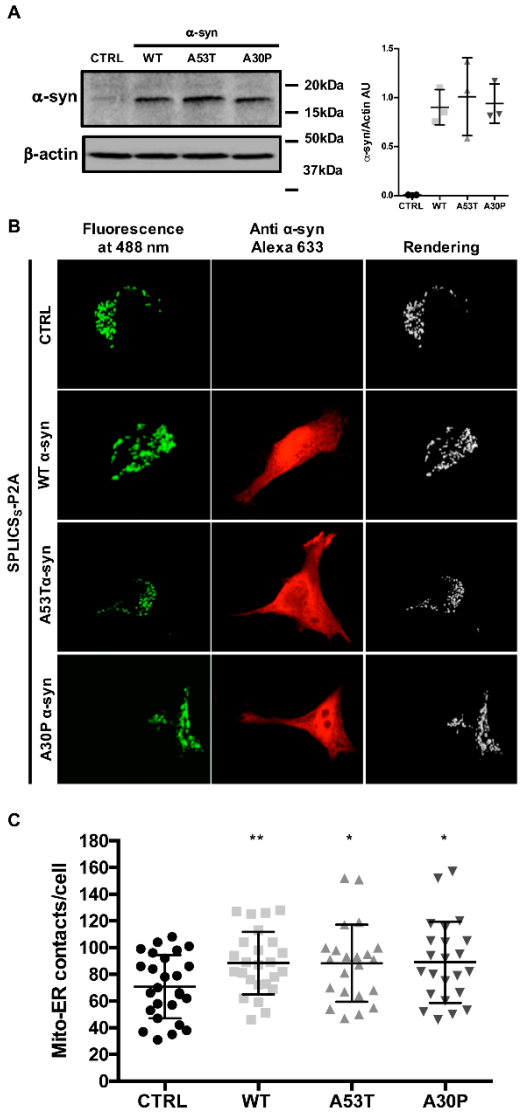

Figure 1. α-syn A53T and A30P mutants physically modulate ER-mitochondria contact sites. (**A**) HeLa cells were transfected with wt, A53T, and A30P α-syn expression plasmids and analyzed by Western blotting with an anti α-syn antibody. Equal loading was verified by probing the membrane with an anti β-actin antibody. Quantification of three independent experiments (**B**) HeLa cells were co-transfected with wt, A53T and A30P α-syn expression vectors and the SPLICS$_S$ sensor to assess short-range ER-mitochondria associations. Reconstitution of the fluorescent signal was observed upon 488 nm wavelength excitation in α-syn positive cells probed with an anti α-syn primary antibody and revealed by an Alexa 633 secondary antibody. The 3D rendering of the Z-stacks acquired for the SPLICS$_S$ probe is shown on the right. (**C**) Quantification of the ER-mitochondria contact sites/cell in the different conditions is shown as mean ± SD. *, $p < 0.05$, **, $p < 0.01$. One-way ANOVA test retrieved a p-value of 0.04. Unpaired Student's two-tailed t-test was used for two-group comparison. No correction was applied since the same SD was assumed. Dunnet's post-test was also applied to compare wt and α-syn mutants each other but no significance was detected. The asterisks refer to Student's two-tailed t-test where the comparison was for each independent sample vs. mock cells.

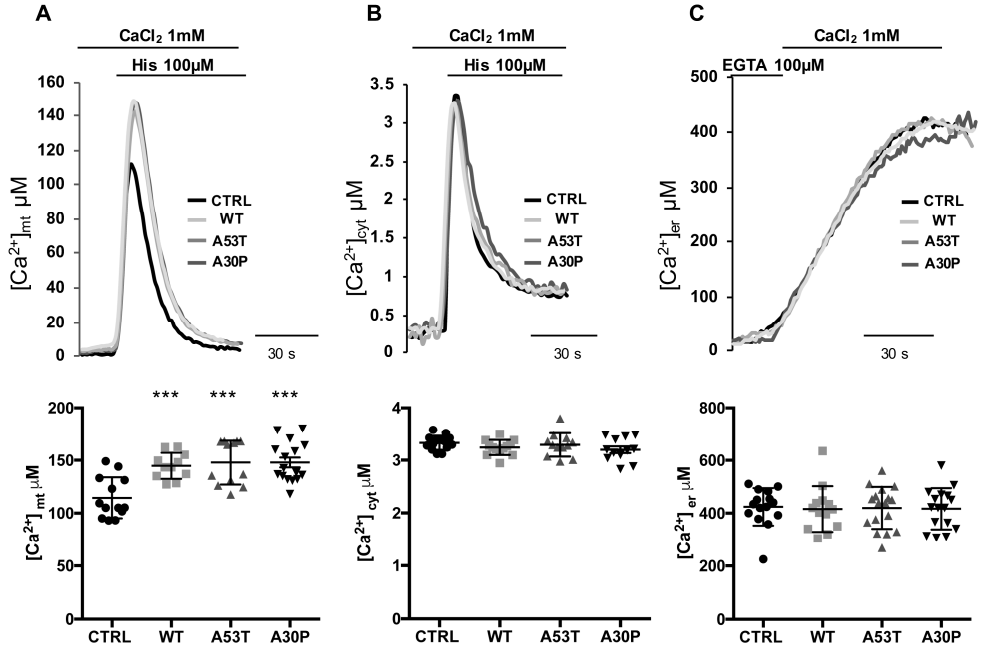

Figure 2. Overexpression of A53T and A30P α-synuclein mutants enhances mitochondrial Ca^{2+} transients. (**A**) Mitochondrial $[Ca^{2+}]_{mt}$, (**B**) cytosolic $[Ca^{2+}]_c$ Ca^{2+} transients, and (**C**) the kinetics of ER refilling upon re-addition of $CaCl_2$ 1 mM to Ca^{2+}-depleted cells (see Materials and Methods) in HeLa cells either mock-transfected or overexpressing A53T or A30P α-syn are shown. Cells were transfected with AEQ (either mitochondrial, cytosolic or targeted to the ER) (controls, mtAEQ, cytAEQ or erAEQ, respectively) or co-transfected with AEQ and WT or A53T or A30P α-syn. Traces refer to representative experiments selected from at least three independent experiments. Quantification of $[Ca^{2+}]_{mt}$, $[Ca^{2+}]_c$ and $[Ca^{2+}]_{er}$ in HeLa cells mock-transfected or overexpressing WT or A53T or A30P α-syn is shown at the bottom. Scatter plots represent the mean $[Ca^{2+}]$ peaks upon stimulation or after ER-refilling ± SD ***, $p < 0.0005$. One-way ANOVA test retrieved a p-value of 0.0001, for multiparametric analysis a Dunnet's post-test was applied.

3.3. α-syn A53T and A30P Mutants Enhance ER-Mitochondria Ca^{2+} Transfer but Impair Mitochondrial Ca^{2+} Uptake from the Extracellular Milieu

The experiments shown above suggest that the mitochondrial Ca^{2+} uptake is indeed modulated by the overexpression of α-syn independently of PD-related A53T and A30P mutations. Nevertheless, the mitochondrial Ca^{2+} transients are shaped by the Ca^{2+} released from the ER and the Ca^{2+} entering from the extracellular milieu. To gain further insights into the specificity of the observed phenotype, these two contributions were analyzed separately. To this aim, HeLa cells overexpressing mitochondrial aequorin and either empty vector, WT α-syn or A53T or A30P mutants were perfused in KRB buffer containing 100 μM EGTA and stimulated with 100 μM histamine to generate a peak transient exclusively reflecting the mobilization of the ER Ca^{2+}. Then the perfusion medium was switched to KRB supplemented with 2 mM $CaCl_2$ (in the continuous presence of histamine), thus causing Ca^{2+} entry from the extracellular milieu that was primarily sensed by mitochondria located beneath the plasma membrane. Figure 3A–C for the representative traces of the experiments and D for the statistical analysis. The mitochondrial Ca^{2+} peaks in response to ER Ca^{2+} mobilization (first peak) was significantly higher in cells overexpressing in WT or A53T or A30P α-syn as compared with control cells, thus reinforcing the fact that α-syn-mediated mitochondrial Ca^{2+} modulation is dependent on its action in favoring the ER-mitochondria interface, ($[Ca^{2+}]_{mt}$ μM 1st Peak: 25.46 ± 7.4 n = 23 for control cells; 35.47 ± 9.66 n = 18 for WT α-syn, $p < 0.0006$ vs. control; 31.7 ± 7.8 n = 9 for A53T α-syn, $p < 0.05$ vs. control; 38.39 ± 8.8 n = 9 for A30P α-syn, $p < 0.001$ vs. control (the significance was indicated with *)). The mitochondrial Ca^{2+} transients obtained in response to Ca^{2+} influx (second peak) were

instead reduced in cells overexpressing WT or A53T or A30P α-syn (Figure 3A–C for representative traces of the experiments and D for the statistical analysis) $[Ca^{2+}]_{mt}$ μM 2nd Peak: 6.99 ± 1.95 n = 19 for control cells; 5.19 ± 0.87 n = 11 for WT α-syn, $p < 0.01$ vs. control; 4.77 ± 0.48 n = 6 for A53T α-syn, $p < 0.05$ vs. control; 3.85 ± 0.86 n = 7 for A30T α-syn, $p < 0.001$ vs. control (the significance was indicated with #). The reduction in the peak generated by the re-addition of 2 mM $CaCl_2$ is probably due to the α-syn-induced reduction of the influx pathways triggered by store depletion, as previously documented [59], and here, sensed mainly by mitochondria beneath the plasma membrane.

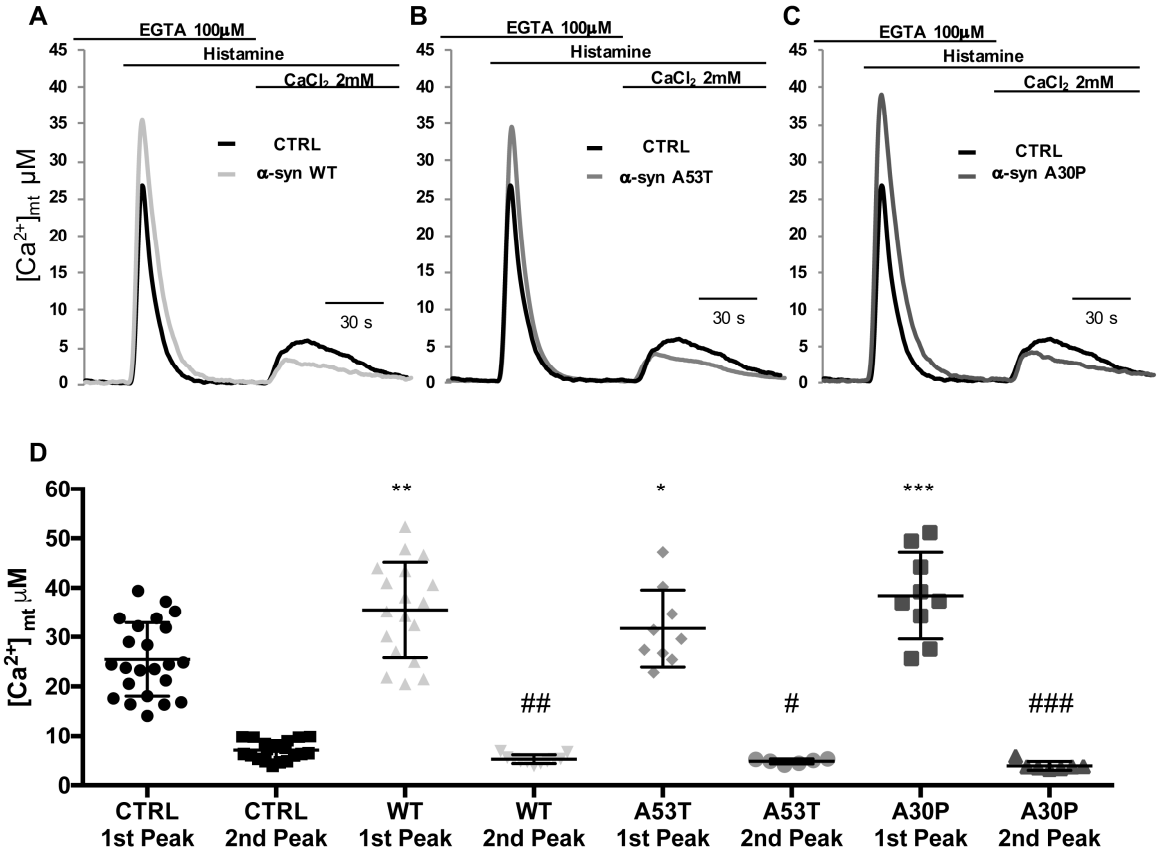

Figure 3. α-syn A53T and A30P mutants differently impinge on Ca^{2+} transients generated by ER Ca^{2+} release and Ca^{2+} influx from the extracellular milieu. HeLa cells were co-transfected with mtAEQ and WT α-syn (**A**) or A53T (**B**) or A30P (**C**) α-syn constructs or transfected with mtAEQ only (control). To discriminate the contribution of Ca^{2+} release from the ER and of Ca^{2+} influx from the extracellular ambient to the generation of $[Ca^{2+}]_{mt}$ transients, HeLa cells were perfused in KRB/EGTA 100 μM buffer and stimulated with histamine to release Ca^{2+} from the intracellular stores (first peak). Then, the perfusion medium was switched to KRB/$CaCl_2$ 2 mM (in the continuous presence of histamine) to stimulate Ca^{2+} entry from the extracellular ambient (second peak). (**D**), Scatter plots represent mean $[Ca^{2+}]$ peak values upon stimulation ± SD. * and # $p < 0.05$, ** $p < 0.01$, ## $p < 0.005$ *** $p < 0.0005$, ###$p < 0.001$. The results are the mean of at least three independent experiments. One-way ANOVA test retrieved a *p*-value of 0.0001. Unpaired Student's two-tailed *t*-test was used for two-group comparison. No correction was applied since the same SD was assumed. Dunnet's post-test was also applied to compare wt and α-syn mutants each other but no significance was detected. 1st and 2nd peak mean values were analyzed separately. The asterisks refer to Student's two-tailed *t*-test where the comparison was for each independent sample vs. mock cells.

3.4. TAT-Mediated Delivery of A53T and A30P α-Synuclein Mutants Affects α-Syn Intracellular Distribution and Its Modulation of Mitochondrial Ca^{2+} Transients in a Dose-Dependent Manner

Exogenous exposure of TAT WT α-syn fusion protein in HeLa cells was previously used to modulate intracellular α-syn content and shown to dose-dependently affect mitochondrial Ca^{2+} handling [34]. By following the same approach, we decided to use a TAT-mediated delivery system to fine-tune the intracellular levels of A53T and A30P α-syn mutants and to monitor mitochondrial Ca^{2+} transients in the same conditions. To this end, Hela cells were in parallel transfected with mtGFP or mtAEQ probes to specifically follow mitochondrial morphology and mitochondrial Ca^{2+} transients, respectively, and then incubated with TAT A53T or A30P at different doses (Figure 4). We selected ranges of TAT A53T (0.05 – 2 μM) and A30P (0.025 – 0.1 μM) concentrations at which we observed intracellular re-distribution of α-syn and monitored mitochondrial morphology by co-transfected mitochondrially targeted GFP (mtGFP in Figure 4A,B).

None of the concentrations tested macroscopically affected mitochondrial morphology as shown by the mtGFP signal, suggesting that the α-syn levels were not strong enough to induce mitochondrial fission [32]. Immunocytochemistry analysis performed by incubating the cells with a primary antibody against α-syn revealed a dose-dependent increase of the diffuse cytosolic α-syn signal up to 0.75 μM TAT A53T (Figure 4A) and 0.075 μM TAT A30P (Figure 4B). Over these concentrations α-syn intracellular redistribution to localized cytoplasmic foci occurred (at 2 μM TAT A53T and 0.1 μM TAT A30P, respectively). Mitochondrial Ca^{2+} measurements in HeLa cells subjected to increasing doses of TAT A53T or A30P exhibited a significant rise in mitochondrial Ca^{2+} uptake at 0.1-0.75 μM TAT A53T (Figure 4A right) and 0.05 μM TAT A30P (Figure 4B right), i.e., when the α-syn distribution is still cytosolic, but as soon as cytoplasmic foci appears, mitochondrial Ca^{2+} transients amplitude decreases, suggesting that α-syn is not available anymore to support ER-mitochondria Ca^{2+} transfer. Notably, in the case of A30P mutant the reduction occurs already at 0.075 μM when cytosolic foci are not yet evident, possibly suggesting that the transition is occurring precisely at this point. ($[Ca^{2+}]_{mt}$ μM: 104.82 ± 17.13 n = 46 for control cells; 113.08 ± 14.77 n = 13 for 0.05 μM A53T α-syn; 118.89 ± 21.16 n = 14 for 0.1 μM A53T α-syn, $p = 0.01$; 130.04 ± 21.83 n = 10 for 0.75 μM A53T α-syn, $p = 0.001$; 112.81 ± 20.05 n = 13 for 2 μM A53T α-syn and 103.76 ± 12.49 n = 29 for control cells; 113.09 ± 13.79 n = 10 for 0.025μM A30P α-syn; 119.74 ± 15.02 n = 16 for 0.05 μM A30P α-syn, $p < 0.005$; 110.41 ± 12.80 n = 10 for 0.075 μM A30P α-syn; 103.6 ± 22.55 n = 10 for 0.1 μM A30P α-syn and 112.7 ± 11.15 n = 9 for control cells; 114.4 ± 10.64 n = 5 for 0.1 μM WT α-syn; 128.3 ± 12.16 n = 4 for 2 μM WT α-syn; 140.3 ± 17.01 n = 8 for 4 μM WT α-syn, $p < 0.0005$; 89.73 ± 12.72 n = 6 for 8 μM WT α-syn, $p < 0.005$). Similar results were found when titration of intracellular α-syn was obtained with TAT WT α-syn. For comparison, these data are shown in Figure 4C and their quantification on the right, in this case the appearance of cytoplasmic foci occurred upon incubation with 8 μM TAT WT.

As a proof of concept experiment, we decided to link the number of the ER-mitochondria contact sites with the α-syn aggregation state by exogenous exposure of TAT WT α-syn at the concentrations at which intracellular re-distribution of α-syn from cytosolic to intracellular foci was observed. As reported in Figure 5A and quantified in Figure 5B, the number of ER-mitochondria contact sites significantly increased upon expression of α-syn at concentrations in which a diffuse cytosolic signal was observed (i.e., at 4 μM TAT WT α-syn), in line with experiments of mitochondrial Ca^{2+} uptake shown in Figures 2A and 4, thus enforcing the idea that increased levels of the protein can positively affect the number of ER-mitochondria contact sites. Interestingly enough, a drop was instead observed when redistribution to localized cytoplasmic foci occurred (i.e., at 8 μM TAT WT α-syn), suggesting that sequestration of functional α-syn into foci negatively affected the ER-mitochondria interface with a loss of function mechanism (number of ER-mitochondria contacts/cell: 60.86 ± 14.47 n = 22 for control cells; 79.14 ± 15.29 n = 29 for 4 μM TAT WT α-syn, $p < 0.0001$; 30.5 ± 11.82 n = 28 for 8 μM TAT WT α-syn $p < 0.0001$). Notably, redistribution of α-syn into foci induced a significant reduction of the ER-mitochondria contact sites as compared to control cells suggesting the intriguing possibility that

also endogenous α-syn (or other important tethering factors as already suggested [60]) could indeed be redistributed into intracellular foci, thus affecting their physiological function.

Altogether, these experiments indicate that the aggregation propensity of α-syn protein, through a loss of function mechanism impinging on the ER-mitochondria interface, may have a role in inducing mitochondrial Ca^{2+} signaling impairment that, in turn, could affect bioenergetic metabolism.

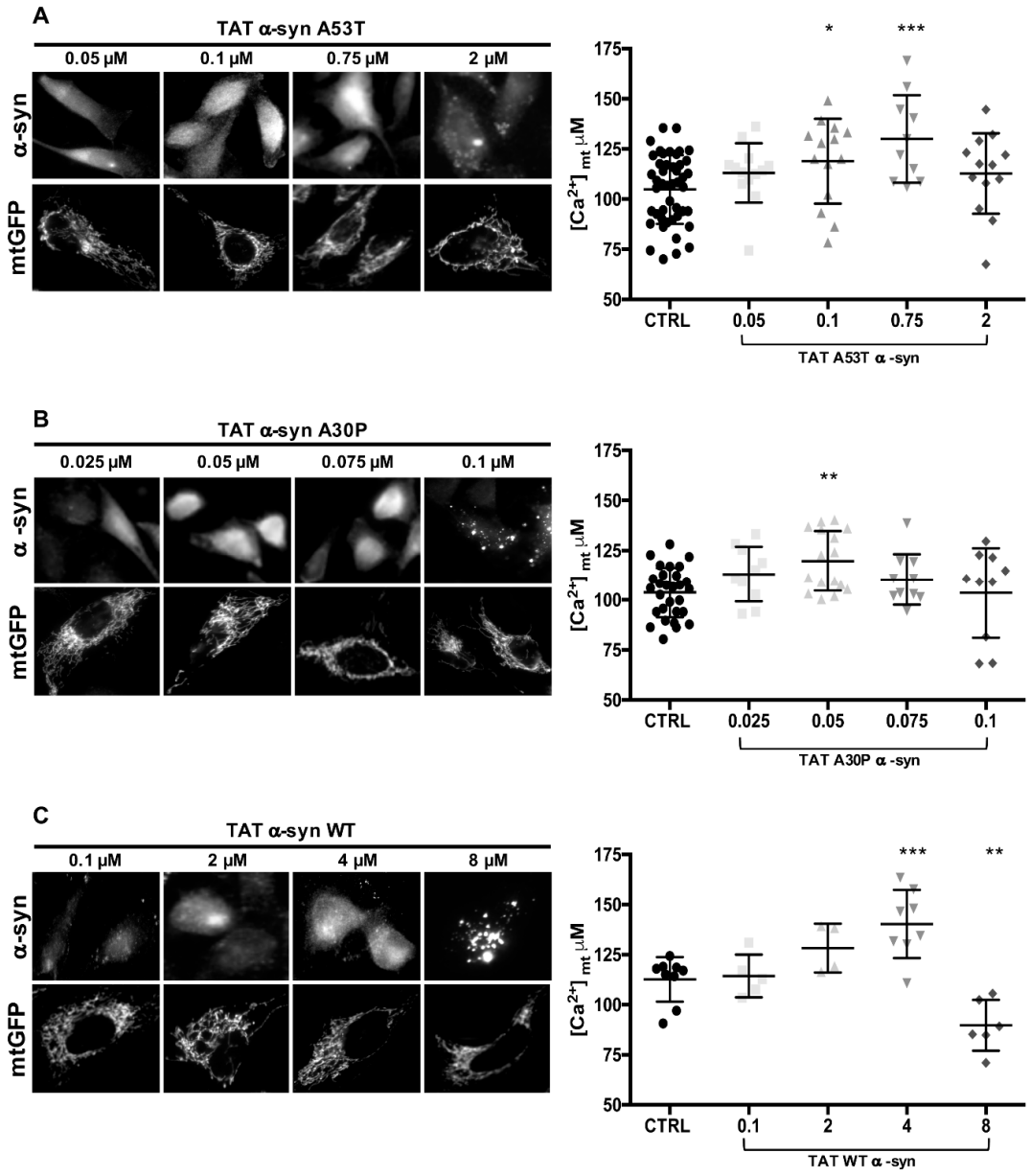

Figure 4. TAT-mediated delivery of A53T and A30P α-synuclein mutants induces dose-dependent α-syn redistribution and different effect on mitochondrial Ca^{2+} transients. HeLa cells were transfected with mtGFP or mtAEQ and then incubated with the indicated doses of TAT A53T (**A**) or TAT A30P (**B**) or TAT WT (**C**) α-syn. Immunolocalization of TAT mutant α-syn (**top**) and mitochondrial network (**bottom**) are revealed by α-syn primary antibodies and mtGFP fluorescence, respectively. The images revealing mitochondrial morphology were randomly acquired from TAT α-syn treated cells. Mitochondrial Ca^{2+} measurements were performed in HeLa cells upon treatment with TAT A53T or A30P or WT α-syn at the indicated doses. Panels on the right show the scatter plots representing the mean $[Ca^{2+}]_{mt}$ peak values upon cell stimulation with histamine. Results are the mean ± SD obtained from at least three independent experiments. *, $p < 0.01$; **, $p < 0.005$; ***, $p < 0.0005$. One-way ANOVA test retrieved a p-value of 0.0001, for multiparametric analysis a Dunnet's post-test was applied.

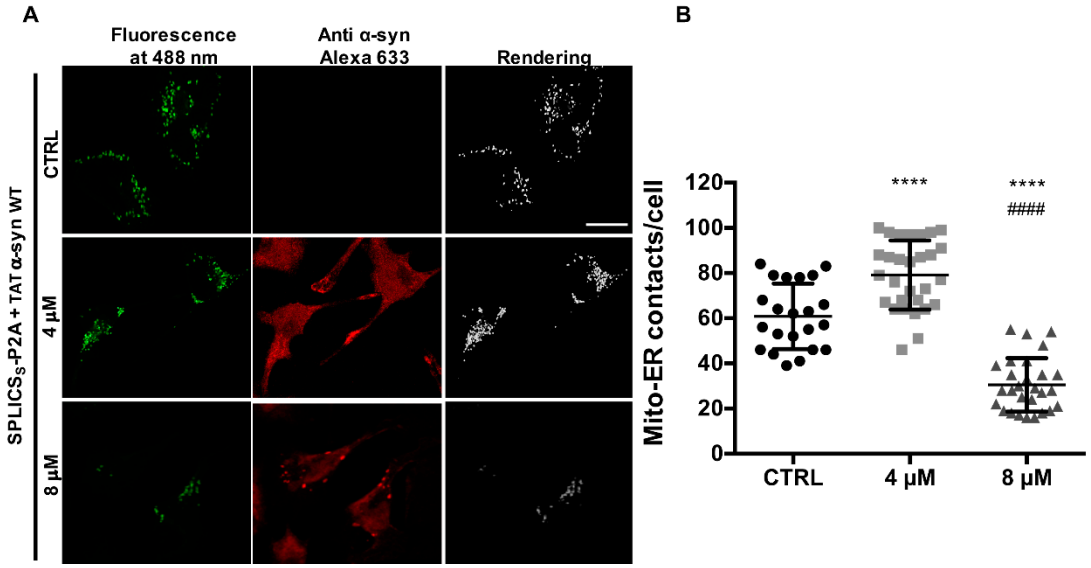

Figure 5. TAT-mediated delivery of α-syn affects ER-mitochondria contact sites in a dose-dependent manner. (**A**) HeLa cells were transfected with SPLICSs sensor to assess short-range ER-mitochondria associations and then incubated with the indicated doses of TAT WT α-syn. SPLICS$_S$. Reconstitution of the fluorescent signal was observed upon 488 nm wavelength excitation in α-syn positive cells probed with an anti α-syn primary antibody and revealed by an Alexa 633 secondary antibody. The 3D rendering of the Z-stacks acquired for the SPLICS$_S$ probe is shown on the right. (**B**) Quantification of the ER-mitochondria contact sites/cell in the different conditions is shown as mean ± SD. **** vs. CTRL or #### vs. 4 μM, $p < 0.0001$. One-way ANOVA test retrieved a p-value of 0.0001. Results are the mean ± SD obtained from at least two independent transfections, for multiparametric analysis a Dunnet's post-test was applied.

4. Discussion

Parkinson's disease (PD) affects six million individuals worldwide. The formation of intracellular inclusions of α-syn [61], whose autosomal dominant mutations [62] are found in familial forms of the disease, and the neuronal loss in the substantia nigra pars compacta [3] are the main hallmarks. Although prevalently cytosolic, α-syn is also present in different cellular locations such as the nucleus [37–39,63], the mitochondria [18–20,40,41,64] and the mitochondria-associated ER membranes (MAMs) fraction [30,42]. Its close relationship with mitochondria is also well established [25]. We have shown for the first time the involvement of α-syn in the modulation of mitochondrial Ca^{2+} handling and the ER-mitochondria communication [34]: It positively enhanced mitochondrial Ca^{2+} transients generated upon Ca^{2+} release from the endoplasmic reticulum (ER) by increasing the ER-mitochondria contact sites. Interestingly, we have proposed a dose-dependent mechanism of action that, more recently, has been confirmed to be in place for α-syn modulation of other mitochondrial functions [22,35,36]. To date, two additional studies have investigated the effect of α-syn on ER-mitochondria tethering directly [30,42], and they have reached different conclusions. The first study clearly showed that α-syn is indeed present in the MAM fraction and that its distribution in this location is altered by the PD-related mutations. Furthermore, by using confocal microscopy, they found that in M17 cells stably expressing the α-syn pathogenic mutants (A53T and A30P) the degree of ER-mitochondrial apposition was lower than in the cells transfected with the WT α-syn and the empty-vector control, suggesting that α-syn PD-related mutants may impinge on ER-mitochondria tethering by a gain of toxic function mechanism. Interestingly, when measured in HeLa cells, the ER-mitochondrial apposition was reduced also in the WT α-syn expressing cells compared to empty-vector control and to the same extent of the PD-related mutants [30], suggesting, on the other hand, that a loss of function mechanism could be involved instead (possibly related to the amount of overexpressed

α-syn). The second study, by using EM, proximity ligation assays, and super resolution SIM methods, revealed that expression of WT and mutants (either A53T or A30P) α-syn decreased ER-mitochondria contacts to the same extent [42], again suggesting the occurrence of a loss of function mechanism. Although different appropriate methods have been used for quantifying contacts over the years, none of those mentioned above, nor among the existing ones, is still able to fulfill the essential requirements ensuring the best conditions to properly quantify the ER-mitochondria interactions: A good resolution coupled with the possibility to detect them in the most physiological condition, i.e., in living cells. This could certainly account for the discrepancies observed within the same or between different studies. Nevertheless, additional fundamental factors could be the key to understand the mechanism/s by which α-syn affect the ER-mitochondria interface, i.e., the aggregation tendency of α-syn itself and how the PD-related mutations affect this behavior. Indeed, none of the above-mentioned studies addresses the question following ER-mitochondria interaction both in the presence of different amounts of α-syn protein and monitoring its intracellular distribution to correlate its effects with changes in its aggregation propensity or with its soluble state [65–67]. In our previous study [34], we were able to fine-tune the intracellular levels of α-syn either by mild transient transfection conditions, i.e., the calcium phosphate procedure, or by artificially or pharmacologically increasing them. Under those conditions, we found a correlation between aggregation propensity of WT α-syn and its effects on mitochondrial Ca^{2+} uptake. Although indirectly, we hypothesized that this effect was dependent on the modulation of ER-mitochondria contact sites, evaluated by calculating Menders' coefficient upon overexpression of two organelle targeted fluorescent proteins [34]. Here, we extended our previous analysis to the α-syn PD-related pathogenic mutations. To this aim, we employed the SPLICS probe that we have recently developed [43] and widely used in other studies by us and others to quantify the ER-mitochondria interactions under physiological conditions [43,56,68–72]. Our results confirmed the ability of WT α-syn to increase the ER-mitochondria contact sites and revealed that the introduction of A53T and A30P PD-related mutations does not abolish this action. In α-syn A53T and A30P expressing cells, the increase in ER-mitochondria interactions was also paralleled by a concomitant increase in mitochondria Ca^{2+} uptake upon cell stimulation with an $InsP_3$ generating agonist which mobilized Ca^{2+} from the ER, suggesting that the PD-related mutants, when expressed at low levels, retain the ability to exert their effect at the MAMs. Noteworthy, this was also the main difference with the above-mentioned studies which employed Lipofectamine-based methods to induce high α-syn expression or selected highly expressing stable clones. To enforce our original idea that impairment in this ability could be due to a loss of function mechanism dependent on the sequestration of functional α-syn in aggregates rather than to the presence of mutations that could affect the ER-mitochondria tethering machinery, we induced α-syn intracellular re-distribution by exogenously applying an increasing amount of recombinant TAT WT, TAT A53T, and TAT A30P α-syn. Mitochondrial Ca^{2+} uptake upon cells stimulation was measured in these conditions. We had previously identified the TAT WT α-syn is able to positively modulate ER-mitochondria contact sites and mitochondrial Ca^{2+} uptake when applied at doses in the range of 4 μM. We had also previously shown that when TAT WT α-syn was applied at high doses, i.e., 8 μM, the diffuse cytosolic α-syn cellular distribution was compromised and the modulatory effect was lost, suggesting a loss of function mechanism [34]. Now, by applying an increasing amount of TAT A53T, and A30P α-syn we found the appearance of intracellular foci and/or aggregates of α-syn at lower concentrations, i.e., in the range of 0.1–2 μM, being the concentration even lower for the A30P in respect with the A53T mutant. These data indicate that these α-syn mutants are indeed characterized by an intrinsically higher aggregation/oligomerization propensity than WT α-syn, as already reported [65,66,73]. However, although many studies showed that A53T [66,74,75] aggregate more rapidly than WT α-synuclein in vitro using recombinant proteins and that more fibrils could be detected in cells [76,77], A30P [66,75] was found to aggregate to the same or a lesser extent than WT α-synuclein in vitro and form the same number of fibrils in cells. Thus, the question of their aggregation propensity in respect to the disease relevance needs to be further dissected. A recent study showed that the types of oligomers formed by A30P and A53T are different [78] and, interestingly,

it has been also reported that the A30P, E46K, H50Q, G51D, and A53T mutants exhibited identical propensities to oligomerize in living cells, but had distinct abilities to form inclusions. While the A30P mutant reduced the percentage of cells with inclusions, the E46K mutant had the opposite effect [76], thus offering different experimental models to study oligomers/aggregates-induced cell toxicity. Noteworthy, in a proof-of-concept experiment, the number of ER-mitochondria contact sites was measured in conditions in which the amount of WT α-syn was fine-tuned to either increase its intracellular level without any apparent change in its cytosolic distribution or to promote strong subcellular re-localization into foci/aggregates. Under those conditions, we could observe a statistically significant increase (in the former) or a decrease (in the latter), respectively. These findings argue in favor of the hypothesis that α-syn could play a direct role in the modulation of the ER-mitochondria interface and suggest that protein aggregation could be responsible for clustering overexpressed, as well as endogenous α-syn (or important factors or tethering factors [60]), and compromising its action according to a loss of function mechanism. Interestingly, it should be noticed that an intracellular threshold of α-syn should also be reached in order to recapitulate the observed phenotypes. Indeed, despite the differences observed between the WT and the mutant forms of α-syn in the concentrations applied for the TAT-mediated delivery, upon transient transfection the cytosolic distribution of the protein (no matter whether WT or mutant) was sufficient to sustain increased ER-mitochondria contacts and mitochondrial Ca^{2+} transients. This suggests the intriguing possibility that the intracellular level of α-syn must indeed be tightly regulated and, although it is difficult to directly link the intracellular concentration of the protein with the phenotype, it could be argued that by transient transfection we are below the threshold required to induce the foci formation but α-syn levels are sufficient to positively modulate ER-mitochondria contacts and mitochondrial Ca^{2+}. In this context it will be interesting to investigate whether the modulation of ER/mitochondria contact sites and mitochondrial Ca^{2+} handling could be differentially affected not only dose-dependently, as shown in the present paper, but also by the different α-syn species, i.e., oligomers rather than fibrils or amorphous aggregates. At the moment, these kinds of studies in a cell context are very difficult, however, the possibility that the α-syn-induced aggregates are not toxic per se and that impairments in the ER-mitochondria interface are early events preceding aggregation is fascinating and certainly deserves further investigations.

5. Conclusions

These results suggest that the ability of α-syn to act as a positive regulator of the ER-mitochondria interface is not affected by the PD-related mutations A53T and A30P, rather, their increased aggregation propensity prevents α-syn from exerting its activity at the MAM, thus hampering the possibility to sustain ER-mitochondria interactions and their related function, through a loss of function mechanism.

Author Contributions: Conceptualization, M.B. and T.C.; data curation, T.C., D.O., M.V., F.V., D.C., M.B., methodology, T.C., D.O., M.V., F.V., D.C.; investigation, T.C., D.O., M.V., C.C., F.V., D.C, L.B.; writing—original draft preparation, T.C. and M.B.; writing—review and editing, M.B. and T.C.; project administration, M.B. and T.C.; funding acquisition, M.B. and T.C.

Funding: This research was funded by grants from the Ministry of University and Research (Bando SIR 2014 n° RBSI14C65Z and PRIN2017 to T.C.) and from the Università degli Studi di Padova (Progetto Giovani 2012 n° GRIC128SP0 to T.C., Progetto di Ateneo 2016 n° CALI_SID16_01 to T.C. and Progetto di Ateneo 2015 n° CPDA153402 to M.B.).

Acknowledgments: We thank Alessandro Negro (University of Padova) for proving TAT-WT, A53T and A30P α-syn.

Conflicts of Interest: The authors declare no conflict of interest.

References

1. Bayer, T.A. Proteinopathies, a core concept for understanding and ultimately treating degenerative disorders? *Eur. Neuropsychopharmacol.* **2015**, *25*, 713–724. [CrossRef] [PubMed]
2. Spillantini, M.G.; Crowther, R.A.; Jakes, R.; Cairns, N.J.; Lantos, P.L.; Goedert, M. Filamentous alpha-synuclein inclusions link multiple system atrophy with parkinson's disease and dementia with lewy bodies. *Neurosci. Lett.* **1998**, *251*, 205–208. [CrossRef]
3. Hirsch, E.C.; Hunot, S.; Faucheux, B.; Agid, Y.; Mizuno, Y.; Mochizuki, H.; Tatton, W.G.; Tatton, N.; Olanow, W.C. Dopaminergic neurons degenerate by apoptosis in parkinson's disease. *Mov. Disord.* **1999**, *14*, 383–385. [CrossRef]
4. Spillantini, M.G.; Crowther, R.A.; Jakes, R.; Hasegawa, M.; Goedert, M. Alpha-synuclein in filamentous inclusions of lewy bodies from parkinson's disease and dementia with lewy bodies. *Proc. Natl. Acad. Sci. USA* **1998**, *95*, 6469–6473. [CrossRef] [PubMed]
5. Kahle, P.J.; Neumann, M.; Ozmen, L.; Muller, V.; Jacobsen, H.; Schindzielorz, A.; Okochi, M.; Leimer, U.; van Der Putten, H.; Probst, A.; et al. Subcellular localization of wild-type and parkinson's disease-associated mutant alpha -synuclein in human and transgenic mouse brain. *J. Neurosci.* **2000**, *20*, 6365–6373. [CrossRef]
6. Fujioka, S.; Ogaki, K.; Tacik, P.M.; Uitti, R.J.; Ross, O.A.; Wszolek, Z.K. Update on novel familial forms of parkinson's disease and multiple system atrophy. *Parkinsonism Relat. Disord.* **2014**, *20* (Suppl. 1), S29–34. [CrossRef]
7. Burre, J.; Sharma, M.; Tsetsenis, T.; Buchman, V.; Etherton, M.R.; Sudhof, T.C. Alpha-synuclein promotes snare-complex assembly in vivo and in vitro. *Science* **2010**, *329*, 1663–1667. [CrossRef]
8. Sun, J.; Wang, L.; Bao, H.; Premi, S.; Das, U.; Chapman, E.R.; Roy, S. Functional cooperation of alpha-synuclein and vamp2 in synaptic vesicle recycling. *Proc. Natl. Acad. Sci. USA* **2019**, *116*, 11113–11115. [CrossRef]
9. Atias, M.; Tevet, Y.; Sun, J.; Stavsky, A.; Tal, S.; Kahn, J.; Roy, S.; Gitler, D. Synapsins regulate alpha-synuclein functions. *Proc. Natl. Acad. Sci. USA* **2019**, *116*, 11116–11118. [CrossRef]
10. Jao, C.C.; Hegde, B.G.; Chen, J.; Haworth, I.S.; Langen, R. Structure of membrane-bound alpha-synuclein from site-directed spin labeling and computational refinement. *Proc. Natl. Acad. Sci. USA* **2008**, *105*, 19666–19671. [CrossRef]
11. Eliezer, D.; Kutluay, E.; Bussell, R., Jr.; Browne, G. Conformational properties of alpha-synuclein in its free and lipid-associated states. *J. Mol. Biol.* **2001**, *307*, 1061–1073. [CrossRef] [PubMed]
12. Mor, D.E.; Tsika, E.; Mazzulli, J.R.; Gould, N.S.; Kim, H.; Daniels, M.J.; Doshi, S.; Gupta, P.; Grossman, J.L.; Tan, V.X.; et al. Dopamine induces soluble alpha-synuclein oligomers and nigrostriatal degeneration. *Nat. Neurosci.* **2017**, *20*, 1560–1568. [CrossRef] [PubMed]
13. Winner, B.; Jappelli, R.; Maji, S.K.; Desplats, P.A.; Boyer, L.; Aigner, S.; Hetzer, C.; Loher, T.; Vilar, M.; Campioni, S.; et al. In vivo demonstration that alpha-synuclein oligomers are toxic. *Proc. Natl. Acad. Sci. USA* **2011**, *108*, 4194–4199. [CrossRef] [PubMed]
14. Luth, E.S.; Stavrovskaya, I.G.; Bartels, T.; Kristal, B.S.; Selkoe, D.J. Soluble, prefibrillar alpha-synuclein oligomers promote complex i-dependent, ca2+-induced mitochondrial dysfunction. *J. Biol. Chem.* **2014**, *289*, 21490–21507. [CrossRef] [PubMed]
15. Luk, K.C.; Song, C.; O'Brien, P.; Stieber, A.; Branch, J.R.; Brunden, K.R.; Trojanowski, J.Q.; Lee, V.M. Exogenous alpha-synuclein fibrils seed the formation of lewy body-like intracellular inclusions in cultured cells. *Proc. Natl. Acad. Sci. USA* **2009**, *106*, 20051–20056. [CrossRef] [PubMed]
16. Spillantini, M.G.; Goedert, M. The alpha-synucleinopathies: Parkinson's disease, dementia with lewy bodies, and multiple system atrophy. *Ann. N. Y. Acad. Sci.* **2000**, *920*, 16–27. [CrossRef] [PubMed]
17. Jellinger, K.A. Interaction between alpha-synuclein and tau in parkinson's disease comment on wills et al.: Elevated tauopathy and alpha-synuclein pathology in postmortem parkinson's disease brains with and without dementia. *Exp. Neurol.* **2011**, *227*, 13–18. [CrossRef] [PubMed]
18. Cole, N.B.; Dieuliis, D.; Leo, P.; Mitchell, D.C.; Nussbaum, R.L. Mitochondrial translocation of alpha-synuclein is promoted by intracellular acidification. *Exp. Cell Res.* **2008**, *314*, 2076–2089. [CrossRef] [PubMed]
19. Shavali, S.; Brown-Borg, H.M.; Ebadi, M.; Porter, J. Mitochondrial localization of alpha-synuclein protein in alpha-synuclein overexpressing cells. *Neurosci. Lett.* **2008**, *439*, 125–128. [CrossRef]

20. Devi, L.; Raghavendran, V.; Prabhu, B.M.; Avadhani, N.G.; Anandatheerthavarada, H.K. Mitochondrial import and accumulation of alpha-synuclein impair complex i in human dopaminergic neuronal cultures and parkinson disease brain. *J. Biol. Chem.* **2008**, *283*, 9089–9100. [CrossRef]
21. Wang, X.; Becker, K.; Levine, N.; Zhang, M.; Lieberman, A.P.; Moore, D.J.; Ma, J. Pathogenic alpha-synuclein aggregates preferentially bind to mitochondria and affect cellular respiration. *Acta Neuropathol. Commun.* **2019**, *7*, 41. [CrossRef] [PubMed]
22. Grassi, D.; Diaz-Perez, N.; Volpicelli-Daley, L.A.; Lasmezas, C.I. Palpha-syn* mitotoxicity is linked to mapk activation and involves tau phosphorylation and aggregation at the mitochondria. *Neurobiol. Dis.* **2018**, *124*, 248–262. [CrossRef] [PubMed]
23. Ludtmann, M.H.R.; Angelova, P.R.; Horrocks, M.H.; Choi, M.L.; Rodrigues, M.; Baev, A.Y.; Berezhnov, A.V.; Yao, Z.; Little, D.; Banushi, B.; et al. Alpha-synuclein oligomers interact with atp synthase and open the permeability transition pore in parkinson's disease. *Nat. Commun.* **2018**, *9*, 2293. [CrossRef] [PubMed]
24. Cieri, D.; Brini, M.; Cali, T. Emerging (and converging) pathways in parkinson's disease: Keeping mitochondrial wellness. *Biochem. Biophys. Res. Commun.* **2017**, *483*, 1020–1030. [CrossRef] [PubMed]
25. Vicario, M.; Cieri, D.; Brini, M.; Calì, T. The close encounter between alpha-synuclein and mitochondria. *Front. Neurosci.* **2018**, *12*, 388. [CrossRef] [PubMed]
26. Martin, L.J.; Pan, Y.; Price, A.C.; Sterling, W.; Copeland, N.G.; Jenkins, N.A.; Price, D.L.; Lee, M.K. Parkinson's disease alpha-synuclein transgenic mice develop neuronal mitochondrial degeneration and cell death. *J. Neurosci.* **2006**, *26*, 41–50. [CrossRef] [PubMed]
27. Subramaniam, S.R.; Vergnes, L.; Franich, N.R.; Reue, K.; Chesselet, M.F. Region specific mitochondrial impairment in mice with widespread overexpression of alpha-synuclein. *Neurobiol. Dis.* **2014**, *70*, 204–213. [CrossRef]
28. Ellis, C.E.; Murphy, E.J.; Mitchell, D.C.; Golovko, M.Y.; Scaglia, F.; Barcelo-Coblijn, G.C.; Nussbaum, R.L. Mitochondrial lipid abnormality and electron transport chain impairment in mice lacking alpha-synuclein. *Mol. Cell. Biol.* **2005**, *25*, 10190–10201. [CrossRef]
29. Hsu, L.J.; Sagara, Y.; Arroyo, A.; Rockenstein, E.; Sisk, A.; Mallory, M.; Wong, J.; Takenouchi, T.; Hashimoto, M.; Masliah, E. Alpha-synuclein promotes mitochondrial deficit and oxidative stress. *Am. J. Pathol.* **2000**, *157*, 401–410. [CrossRef]
30. Guardia-Laguarta, C.; Area-Gomez, E.; Rub, C.; Liu, Y.; Magrane, J.; Becker, D.; Voos, W.; Schon, E.A.; Przedborski, S. Alpha-synuclein is localized to mitochondria-associated er membranes. *J. Neurosci.* **2014**, *34*, 249–259. [CrossRef]
31. Guardia-Laguarta, C.; Area-Gomez, E.; Schon, E.A.; Przedborski, S. A new role for alpha-synuclein in parkinson's disease: Alteration of er-mitochondrial communication. *Mov. Disord.* **2015**, *30*, 1026–1033. [CrossRef]
32. Nakamura, K.; Nemani, V.M.; Azarbal, F.; Skibinski, G.; Levy, J.M.; Egami, K.; Munishkina, L.; Zhang, J.; Gardner, B.; Wakabayashi, J.; et al. Direct membrane association drives mitochondrial fission by the parkinson disease-associated protein alpha-synuclein. *J. Biol. Chem.* **2011**, *286*, 20710–20726. [CrossRef]
33. Winslow, A.R.; Chen, C.W.; Corrochano, S.; Acevedo-Arozena, A.; Gordon, D.E.; Peden, A.A.; Lichtenberg, M.; Menzies, F.M.; Ravikumar, B.; Imarisio, S.; et al. Alpha-synuclein impairs macroautophagy: Implications for parkinson's disease. *J. Cell Biol.* **2010**, *190*, 1023–1037. [CrossRef]
34. Calì, T.; Ottolini, D.; Negro, A.; Brini, M. Alpha-synuclein controls mitochondrial calcium homeostasis by enhancing endoplasmic reticulum-mitochondria interactions. *J. Biol. Chem.* **2012**, *287*, 17914–17929. [CrossRef] [PubMed]
35. Martinez, J.H.; Fuentes, F.; Vanasco, V.; Alvarez, S.; Alaimo, A.; Cassina, A.; Coluccio Leskow, F.; Velazquez, F. Alpha-synuclein mitochondrial interaction leads to irreversible translocation and complex i impairment. *Arch. Biochem. Biophys.* **2018**, *651*, 1–12. [CrossRef]
36. Ding, H.; Xiong, Y.; Sun, J.; Chen, C.; Gao, J.; Xu, H. Asiatic acid prevents oxidative stress and apoptosis by inhibiting the translocation of alpha-synuclein into mitochondria. *Front. Neurosci.* **2018**, *12*, 431. [CrossRef]
37. Ma, K.L.; Song, L.K.; Yuan, Y.H.; Zhang, Y.; Han, N.; Gao, K.; Chen, N.H. The nuclear accumulation of alpha-synuclein is mediated by importin alpha and promotes neurotoxicity by accelerating the cell cycle. *Neuropharmacology* **2014**, *82*, 132–142. [CrossRef]

38. Kontopoulos, E.; Parvin, J.D.; Feany, M.B. Alpha-synuclein acts in the nucleus to inhibit histone acetylation and promote neurotoxicity. *Hum. Mol. Genet.* **2006**, *15*, 3012–3023. [CrossRef]
39. Goers, J.; Manning-Bog, A.B.; McCormack, A.L.; Millett, I.S.; Doniach, S.; Di Monte, D.A.; Uversky, V.N.; Fink, A.L. Nuclear localization of alpha-synuclein and its interaction with histones. *Biochemistry* **2003**, *42*, 8465–8471. [CrossRef]
40. Parihar, M.S.; Parihar, A.; Fujita, M.; Hashimoto, M.; Ghafourifar, P. Mitochondrial association of alpha-synuclein causes oxidative stress. *Cell. Mol. Life Sci.* **2008**, *65*, 1272–1284. [CrossRef]
41. Devi, L.; Anandatheerthavarada, H.K. Mitochondrial trafficking of app and alpha synuclein: Relevance to mitochondrial dysfunction in alzheimer's and parkinson's diseases. *Biochim. Biophys. Acta* **2010**, *1802*, 11–19. [CrossRef]
42. Paillusson, S.; Gomez-Suaga, P.; Stoica, R.; Little, D.; Gissen, P.; Devine, M.J.; Noble, W.; Hanger, D.P.; Miller, C.C.J. Alpha-synuclein binds to the er-mitochondria tethering protein vapb to disrupt ca2+ homeostasis and mitochondrial atp production. *Acta Neuropathol.* **2017**, *134*, 129–149. [CrossRef]
43. Cieri, D.; Vicario, M.; Giacomello, M.; Vallese, F.; Filadi, R.; Wagner, T.; Pozzan, T.; Pizzo, P.; Scorrano, L.; Brini, M.; et al. Splics: A split green fluorescent protein-based contact site sensor for narrow and wide heterotypic organelle juxtaposition. *Cell Death Differ.* **2018**, *25*, 1131–1145. [CrossRef]
44. Albani, D.; Peverelli, E.; Rametta, R.; Batelli, S.; Veschini, L.; Negro, A.; Forloni, G. Protective effect of tat-delivered alpha-synuclein: Relevance of the c-terminal domain and involvement of hsp70. *FASEB J.* **2004**, *18*, 1713–1715. [CrossRef]
45. Kim, J.H.; Lee, S.R.; Li, L.H.; Park, H.J.; Park, J.H.; Lee, K.Y.; Kim, M.K.; Shin, B.A.; Choi, S.Y. High cleavage efficiency of a 2a peptide derived from porcine teschovirus-1 in human cell lines, zebrafish and mice. *PLoS ONE* **2011**, *6*, e18556. [CrossRef]
46. Rizzuto, R.; Brini, M.; Pizzo, P.; Murgia, M.; Pozzan, T. Chimeric green fluorescent protein as a tool for visualizing subcellular organelles in living cells. *Curr. Biol.* **1995**, *5*, 635–642. [CrossRef]
47. Brini, M.; Marsault, R.; Bastianutto, C.; Alvarez, J.; Pozzan, T.; Rizzuto, R. Transfected aequorin in the measurement of cytosolic ca2+ concentration ([ca2+]c). A critical evaluation. *J. Biol. Chem.* **1995**, *270*, 9896–9903. [CrossRef]
48. Rizzuto, R.; Simpson, A.W.; Brini, M.; Pozzan, T. Rapid changes of mitochondrial ca2+ revealed by specifically targeted recombinant aequorin. *Nature* **1992**, *358*, 325–327. [CrossRef]
49. Montero, M.; Brini, M.; Marsault, R.; Alvarez, J.; Sitia, R.; Pozzan, T.; Rizzuto, R. Monitoring dynamic changes in free ca2+ concentration in the endoplasmic reticulum of intact cells. *EMBO J.* **1995**, *14*, 5467–5475. [CrossRef]
50. Rizzuto, R.; Brini, M.; Bastianutto, C.; Marsault, R.; Pozzan, T. Photoprotein-mediated measurement of calcium ion concentration in mitochondria of living cells. *Methods Enzymol.* **1995**, *260*, 417–428.
51. Brini, M. Calcium-sensitive photoproteins. *Methods* **2008**, *46*, 160–166. [CrossRef]
52. Rizzuto, R.; Brini, M.; Pozzan, T. Targeting recombinant aequorin to specific intracellular organelles. *Methods Cell Biol.* **1994**, *40*, 339–358.
53. Ottolini, D.; Cali, T.; Brini, M. Methods to measure intracellular ca(2+) fluxes with organelle-targeted aequorin-based probes. *Methods Enzymol.* **2014**, *543*, 21–45.
54. Barrero, M.J.; Montero, M.; Alvarez, J. Dynamics of [ca2+] in the endoplasmic reticulum and cytoplasm of intact hela cells. A comparative study. *J. Biol. Chem.* **1997**, *272*, 27694–27699. [CrossRef]
55. Schindelin, J.; Arganda-Carreras, I.; Frise, E.; Kaynig, V.; Longair, M.; Pietzsch, T.; Preibisch, S.; Rueden, C.; Saalfeld, S.; Schmid, B.; et al. Fiji: An open-source platform for biological-image analysis. *Nat. Methods* **2012**, *9*, 676–682. [CrossRef]
56. Cieri, D.; Vicario, M.; Vallese, F.; D'Orsi, B.; Berto, P.; Grinzato, A.; Catoni, C.; De Stefani, D.; Rizzuto, R.; Brini, M.; et al. Tau localises within mitochondrial sub-compartments and its caspase cleavage affects er-mitochondria interactions and cellular ca(2+) handling. *Biochim. Biophys. Acta Mol. Basis Dis.* **2018**, *1864*, 3247–3256. [CrossRef]
57. Giacomello, M.; Drago, I.; Bortolozzi, M.; Scorzeto, M.; Gianelle, A.; Pizzo, P.; Pozzan, T. Ca2+ hot spots on the mitochondrial surface are generated by ca2+ mobilization from stores, but not by activation of store-operated ca2+ channels. *Mol. Cell* **2010**, *38*, 280–290. [CrossRef]

58. Csordas, G.; Varnai, P.; Golenar, T.; Roy, S.; Purkins, G.; Schneider, T.G.; Balla, T.; Hajnoczky, G. Imaging interorganelle contacts and local calcium dynamics at the er-mitochondrial interface. *Mol. Cell* **2010**, *39*, 121–132. [CrossRef]
59. Hettiarachchi, N.T.; Parker, A.; Dallas, M.L.; Pennington, K.; Hung, C.C.; Pearson, H.A.; Boyle, J.P.; Robinson, P.; Peers, C. Alpha-synuclein modulation of ca2+ signaling in human neuroblastoma (sh-sy5y) cells. *J. Neurochem.* **2009**, *111*, 1192–1201. [CrossRef]
60. Olzscha, H.; Schermann, S.M.; Woerner, A.C.; Pinkert, S.; Hecht, M.H.; Tartaglia, G.G.; Vendruscolo, M.; Hayer-Hartl, M.; Hartl, F.U.; Vabulas, R.M. Amyloid-like aggregates sequester numerous metastable proteins with essential cellular functions. *Cell* **2011**, *144*, 67–78. [CrossRef]
61. Spillantini, M.G.; Schmidt, M.L.; Lee, V.M.; Trojanowski, J.Q.; Jakes, R.; Goedert, M. Alpha-synuclein in lewy bodies. *Nature* **1997**, *388*, 839–840. [CrossRef] [PubMed]
62. Hardy, J.; Lewis, P.; Revesz, T.; Lees, A.; Paisan-Ruiz, C. The genetics of parkinson's syndromes: A critical review. *Curr. Opin. Genet. Dev.* **2009**, *19*, 254–265. [CrossRef] [PubMed]
63. Schell, H.; Hasegawa, T.; Neumann, M.; Kahle, P.J. Nuclear and neuritic distribution of serine-129 phosphorylated alpha-synuclein in transgenic mice. *Neuroscience* **2009**, *160*, 796–804. [CrossRef] [PubMed]
64. Li, W.W.; Yang, R.; Guo, J.C.; Ren, H.M.; Zha, X.L.; Cheng, J.S.; Cai, D.F. Localization of alpha-synuclein to mitochondria within midbrain of mice. *Neuroreport* **2007**, *18*, 1543–1546. [CrossRef] [PubMed]
65. Narhi, L.; Wood, S.J.; Steavenson, S.; Jiang, Y.; Wu, G.M.; Anafi, D.; Kaufman, S.A.; Martin, F.; Sitney, K.; Denis, P.; et al. Both familial parkinson's disease mutations accelerate alpha-synuclein aggregation. *J. Biol. Chem.* **1999**, *274*, 9843–9846. [CrossRef] [PubMed]
66. Conway, K.A.; Lee, S.J.; Rochet, J.C.; Ding, T.T.; Williamson, R.E.; Lansbury, P.T., Jr. Acceleration of oligomerization, not fibrillization, is a shared property of both alpha-synuclein mutations linked to early-onset parkinson's disease: Implications for pathogenesis and therapy. *Proc. Natl. Acad. Sci. USA* **2000**, *97*, 571–576. [CrossRef] [PubMed]
67. Goldberg, M.S.; Lansbury, P.T., Jr. Is there a cause-and-effect relationship between alpha-synuclein fibrillization and parkinson's disease? *Nat. Cell Biol.* **2000**, *2*, E115–E119. [CrossRef]
68. Gómez-Suaga, P.; Pérez-Nievas, B.G.; Glennon, E.B.; Lau, D.H.W.; Paillusson, S.; Mórotz, G.M.; Calì, T.; Pizzo, P.; Noble, W.; Miller, C.C.J. The vapb-ptpip51 endoplasmic reticulum-mitochondria tethering proteins are present in neuronal synapses and regulate synaptic activity. *Acta Neuropathol. Commun.* **2019**, *7*, 35. [CrossRef]
69. Yeshaw, W.M.; van der Zwaag, M.; Pinto, F.; Lahaye, L.L.; Faber, A.I.; Gomez-Sanchez, R.; Dolga, A.M.; Poland, C.; Monaco, A.P.; van IJzendoorn, S.C.; et al. Human vps13a is associated with multiple organelles and influences mitochondrial morphology and lipid droplet motility. *eLife* **2019**, *8*, e43561. [CrossRef]
70. Filadi, R.; Leal, N.S.; Schreiner, B.; Rossi, A.; Dentoni, G.; Pinho, C.M.; Wiehager, B.; Cieri, D.; Calì, T.; Pizzo, P.; et al. Tom70 sustains cell bioenergetics by promoting ip3r3-mediated er to mitochondria ca 2+ transfer. *Curr. Biol.* **2018**, *28*, 369–382. [CrossRef]
71. Granatiero, V.; Giorgio, V.; Cali, T.; Patron, M.; Brini, M.; Bernardi, P.; Tiranti, V.; Zeviani, M.; Pallafacchina, G.; De Stefani, D.; et al. Reduced mitochondrial ca transients stimulate autophagy in human fibroblasts carrying the 13514a>g mutation of the nd5 subunit of nadh dehydrogenase. *Cell Death Differ.* **2016**, *23*, 231. [CrossRef] [PubMed]
72. Doghman-Bouguerra, M.; Granatiero, V.; Sbiera, S.; Sbiera, I.; Lacas-Gervais, S.; Brau, F.; Fassnacht, M.; Rizzuto, R.; Lalli, E. Fate1 antagonizes calcium- and drug-induced apoptosis by uncoupling er and mitochondria. *EMBO Rep.* **2016**, *17*, 1264–1280. [CrossRef] [PubMed]
73. Serpell, L.C.; Berriman, J.; Jakes, R.; Goedert, M.; Crowther, R.A. Fiber diffraction of synthetic alpha-synuclein filaments shows amyloid-like cross-beta conformation. *Proc. Natl. Acad. Sci. USA* **2000**, *97*, 4897–4902. [CrossRef]
74. Li, J.; Uversky, V.N.; Fink, A.L. Effect of familial parkinson's disease point mutations a30p and a53t on the structural properties, aggregation, and fibrillation of human alpha-synuclein. *Biochemistry* **2001**, *40*, 11604–11613. [CrossRef]
75. Conway, K.A.; Harper, J.D.; Lansbury, P.T. Accelerated in vitro fibril formation by a mutant alpha-synuclein linked to early-onset parkinson disease. *Nat. Med.* **1998**, *4*, 1318–1320. [CrossRef]

76. Lazaro, D.F.; Rodrigues, E.F.; Langohr, R.; Shahpasandzadeh, H.; Ribeiro, T.; Guerreiro, P.; Gerhardt, E.; Krohnert, K.; Klucken, J.; Pereira, M.D.; et al. Systematic comparison of the effects of alpha-synuclein mutations on its oligomerization and aggregation. *PLoS Genet.* **2014**, *10*, e1004741. [CrossRef] [PubMed]
77. Pandey, N.; Schmidt, R.E.; Galvin, J.E. The alpha-synuclein mutation e46k promotes aggregation in cultured cells. *Exp. Neurol.* **2006**, *197*, 515–520. [CrossRef]
78. Tosatto, L.; Horrocks, M.H.; Dear, A.J.; Knowles, T.P.; Dalla Serra, M.; Cremades, N.; Dobson, C.M.; Klenerman, D. Single-molecule fret studies on alpha-synuclein oligomerization of parkinson's disease genetically related mutants. *Sci. Rep.* **2015**, *5*, 16696. [CrossRef]

Vicario et al. *Cell Death and Disease* (2019)10:857
https://doi.org/10.1038/s41419-019-2092-1

Cell Death & Disease

ARTICLE Open Access

A split-GFP tool reveals differences in the sub-mitochondrial distribution of wt and mutant alpha-synuclein

Mattia Vicario[1], Domenico Cieri[1], Francesca Vallese[1], Cristina Catoni[2], Lucia Barazzuol[1], Paola Berto[1], Alessandro Grinzato[1], Laura Barbieri[1], Marisa Brini[2] and Tito Calì[1,3]

Abstract

Parkinson's disease (PD), the second most common neurodegenerative disorder, is characterized by dopaminergic neuronal loss that initiates in the substantia nigra pars compacta and by the formation of intracellular inclusions mainly constituted by aberrant α-synuclein (α-syn) deposits known as Lewy bodies. Most cases of PD are sporadic, but about 10% are familial, among them those caused by mutations in *SNCA* gene have an autosomal dominant transmission. *SNCA* encodes α-syn, a small 140-amino acids protein that, under physiological conditions, is mainly localized at the presynaptic terminals. It is prevalently cytosolic, but its presence has been reported in the nucleus, in the mitochondria and, more recently, in the mitochondria-associated ER membranes (MAMs). Whether different cellular localizations may reflect specific α-syn activities is presently unclear and its action at mitochondrial level is still a matter of debate. Mounting evidence supports a role for α-syn in several mitochondria-derived activities, among which maintenance of mitochondrial morphology and modulation of complex I and ATP synthase activity. α-syn has been proposed to localize at the outer membrane (OMM), in the intermembrane space (IMS), at the inner membrane (IMM) and in the mitochondrial matrix, but a clear and comparative analysis of the sub-mitochondrial localization of WT and mutant α-syn is missing. Furthermore, the reasons for this spread sub-mitochondrial localization under physiological and pathological circumstances remain elusive. In this context, we decided to selectively monitor the sub-mitochondrial distribution of the WT and PD-related α-syn mutants A53T and A30P by taking advantage from a bimolecular fluorescence complementation (BiFC) approach. We also investigated whether cell stress could trigger α-syn translocation within the different mitochondrial sub-compartments and whether PD-related mutations could impinge on it. Interestingly, the artificial targeting of α-syn WT (but not of the mutants) to the mitochondrial matrix impacts on ATP production, suggesting a potential role within this compartment.

Introduction

Parkinson's disease (PD) affects 6 million individuals worldwide. The neuronal loss in the substantia nigra pars compacta[1] and the formation of intracellular inclusions of aberrant α-synuclein (α-syn)[2], whose autosomal dominant mutations[3] are found in familial forms of the disease, are the main hallmarks. Mounting evidence indicates that α-syn regulates vesicles release at the synaptic level and stabilizes the assembly of *SNARE* complex[4–7]. Although prevalently cytosolic, α-syn can also be found in the nucleus[8–11], in the mitochondria[12–17] and in the mitochondria-associated ER membranes (MAMs) fraction[18,19]. Its close relationship with mitochondria has been extensively supported by convincing works showing altered mitochondrial functions and dynamics in different

Correspondence: Marisa Brini (marisa.brini@unipd.it) or Tito Calì (tito.cali@unipd.it)
[1]Department of Biomedical Sciences, University of Padova, Padova, Italy
[2]Department of Biology, University of Padova, Padova, Italy
Full list of author information is available at the end of the article.
These authors contributed equally: Mattia Vicario, Domenico Cieri, Francesca Vallese
Edited by P.G. Mastroberardino

SPRINGER NATURE CDDpress

cellular and animal models where the expression level of α-syn was manipulated by overexpression and/or silencing and where α-syn mutants were introduced. Accumulation of WT α-syn causes a reduction in mitochondrial complex I activity[14,20–22] while α-syn null mice display striking resistance to the neurotoxin 1-methyl-4-phenyl-1,2,3,6-tetrahydropyridine (MPTP)-induced degeneration of dopaminergic neurons and reduced dopamine release[23,24]. Alterations including increased oxidative stress, lipid abnormalities, complex I deficiency, increased mitochondrial fragmentation, loss of membrane potential and cytochrome c release were reported in mutant α-syn transgenic[25,26] and null mice[27], as well as in cells overexpressing wt α-syn[28]. Moreover, α-syn has been shown to participate in the maintenance of mitochondrial integrity by regulating the fission/fusion machinery and the autophagic process[18,29–31]. Finally, we have previously demonstrated that α-syn positively enhanced mitochondrial Ca^{2+} transients generated upon Ca^{2+} release from the endoplasmic reticulum (ER) by increasing the ER-mitochondria contact sites[32]. A dose-dependent mechanism of this action has been proposed by us[32] and, more recently, confirmed to be important also for α-syn modulation of other mitochondria related activities[33–35].

Interestingly, α-syn was found to localize both in vitro and in vivo at the outer membrane (OMM), the intermembrane space (IMS), the inner membrane or in the mitochondrial matrix depending on cell lines, species and culture conditions[12,13,15,19,36–39]. Whether the presence of α-syn at specific sub-mitochondrial localization could be related to precise physiological and pathological circumstances remains elusive. Thus, we decided to investigate the sub-mitochondrial distribution of the WT and the PD-associated mutants of α-syn. We also evaluated conditions that may favour α-syn translocation into mitochondria in order to identify possible peculiar function for the specific sub-organelle targeted α-syn.

We have applied a bimolecular fluorescence complementation (BiFC) approach[40–42], previously developed[43] and recently improved[44] by our group, to selectively monitor the sub-mitochondrial distribution of WT and PD-related α-syn mutants A53T and A30P and test whether selected cellular stimuli could change their distribution.

This approach led us to identify WT and mutants α-syn pools that under basal conditions constitutively reside at the OMM and in the IMS. No α-syn molecules were instead detected in the mitochondrial matrix. Interestingly, a quantitative evaluation of the reconstituted fluorescent signal has permitted to establish that the presence of PD-related mutations A30P and A53T significantly enhanced the fraction of α-syn found at the IMS. Moreover, we have found that oxidative stress induction, complex I inhibition and impairment of the endosome-lysosome acidification system selectively promoted the accumulation of WT but not of A30P and A53T mutant α-syn within the IMS. Finally, we took advantage from the possibility to artificially targeting α-syn to the mitochondrial matrix and to monitor whether its presence inside this sub-mitochondrial compartment could affect bioenergetic metabolism. Intriguingly, we have found that the presence of WT α-syn in the mitochondrial matrix, but not that of the PD-related A30P and A53T mutants, was able to sustain mitochondrial ATP synthesis, underling a new possible physiological role for WT α-syn and a new pathological mechanism for PD-associated mutations.

Results

A split-GFP based tool to monitor sub-mitochondrial localization

In order to follow the exact sub-mitochondrial localisation of α-syn we applied the split-GFP based tool we had previously developed and described for other proteins of interest[43,44]. The GFP_{1-10} moiety lacking the S11 β-strand fused to the first 33 amino acids of the TOM20 N-terminal tail (OMM GFP_{1-10}) or to the leader sequence of the inter membrane space protein LACTB (IMS GFP_{1-10}) were employed to reveal the distribution of α-syn at the cytosolic surface of the outer mitochondrial membrane and at the inter membrane space, respectively[45,46]. To reveal the presence of α-syn in the mitochondrial matrix the GFP_{1-10} moiety was delivered to this sub-mitochondrial compartment by the fusion with the presequence of the subunit VIII of human cytochrome c oxidase (mt GFP_{1-10}) as previously described[43]. As shown in Fig. 1a, these targeted GFP_{1-10} chimerae will properly reconstitute their fluorescence only when a protein tagged with the lacking S11 β-strand is located at the same compartment[43,44]. Control experiments confirmed the proper targeting and the absence of fluorescent signal of the mtGFP_{1-10} moiety, Fig. S1, as well as their ability to undergo self-complementation, Fig. S2[43,44].

WT and mutant α-syn reside at the OMM and IMS but not in the mitochondrial matrix and their overexpression modulates mitochondrial ATP production

To investigate the sub-mitochondrial localization of WT α-syn and its pathologic mutants, we co-transfected HeLa (Fig. 1b) and SHSY5Y neuroblastoma (Fig. 1c) cells with the above described GFP_{1-10} constructs and the untargeted WT, A53T and A30P α-syn fused at their C-terminal with the S11 β-strand. The expression of α-syn was verified using an anti α-syn antibody, that has revealed a diffuse cytosolic pattern (Fig. 1b, c, in red). GFP complementation in cells overexpressing the OMM GFP_{1-10} and the IMS GFP_{1-10} with the untargeted WT, A53T

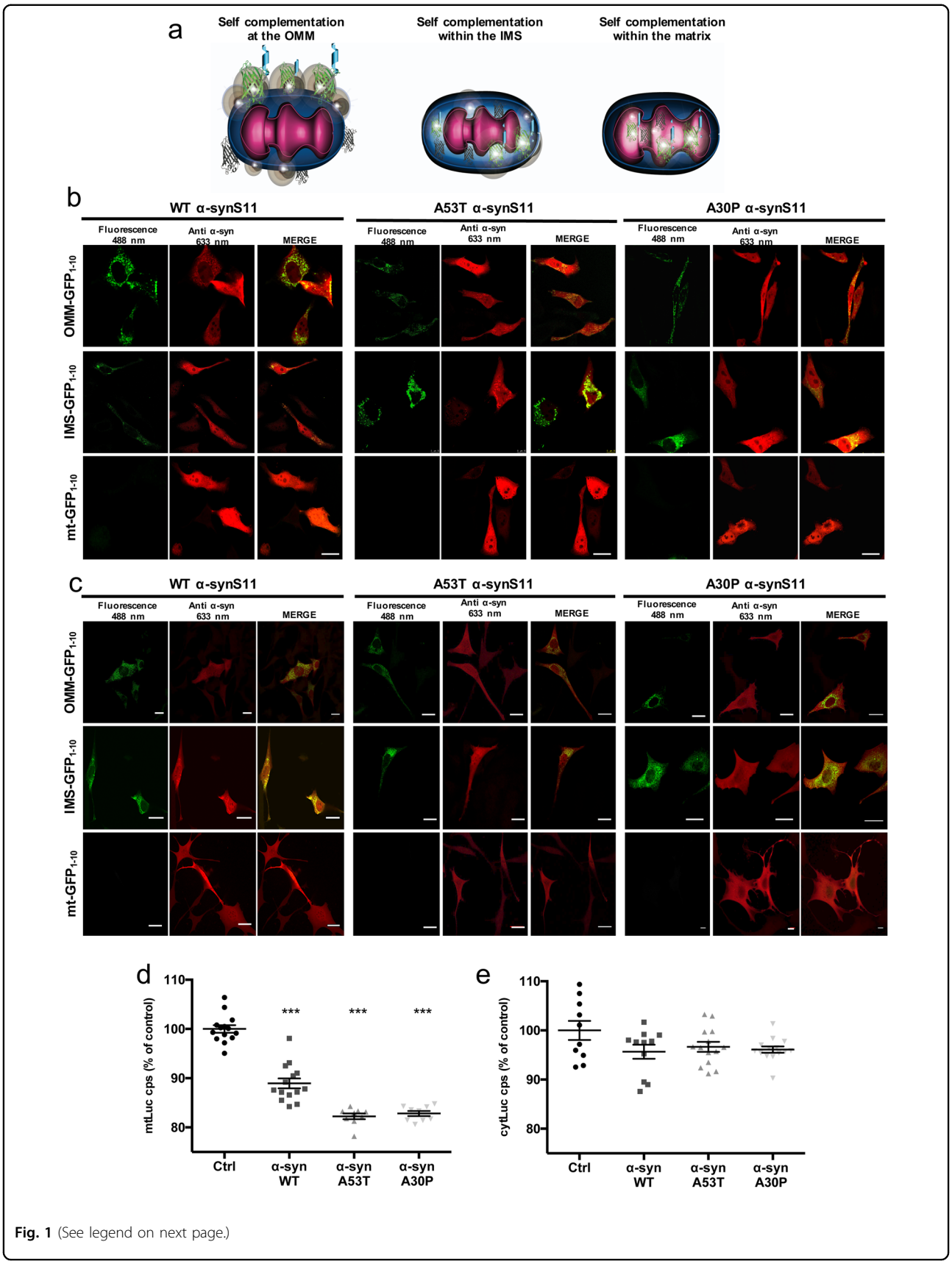

Fig. 1 (See legend on next page.)

(see figure on previous page)
Fig. 1 a Cartoon of targeted split-GFP chimeras are able to complement at the OMM, within the IMS and in the mitochondrial matrix. Sub-mitochondrial localization of wild type and mutant α-syn was analyzed in HeLa **b** and SHSY5Y **c** cells by the co-expression of the OMM, IMS and mitochondrial matrix targeted GFP_{1-10} non-fluorescent moiety and of the WT, A53T and A30P α-synS11. Confocal images were acquired at 488 and 594 nm excitation wavelength. Transfected cells were incubated with an anti α-syn primary antibody and stained with an Alexa 633 conjugated secondary antibody. Complementation of the GFP probes was revealed by fluorescent acquisition at 488 nm excitation wavelength. **d** Mitochondrial (****$p < 0.0001$ vs. control cells) and **e** cytosolic ATP production upon histamine stimulation measured by mtLuc probe in HeLa cells overexpressing α-syn wt and mutants. At least 9 independent measurements for three independent transfections have been done for each construct. One-way ANOVA retrieved a p value of 0.0001. Dunnett's multiple comparison test retrieved a statistically significant difference between Ctrl and WT, A53T, and A30P $p < 0.0001$ **d** while no statistically significant differences were found for panel **e** with one-way ANOVA. Average values shown as mean % calculated from the counts per second (cps) with respect to control cells. Scale bar is 20 μm

and A30P α-synS11 revealed that a pool of overexpressed α-syn is localized both at the cytosolic surface of the outer mitochondrial membrane and in the intermembrane space (Fig. 1b, c, upper and middle panels). Interestingly, no fluorescence signal following excitation at 488 nm wavelength was detected in the mitochondrial matrix upon co-expression of the $mtGFP_{1-10}$ and WT and mutant α-synS11, indicating that the overexpression of α-syn does not induce the accumulation of α-syn in the mitochondrial matrix (Fig. 1b, c lower panels). To confirm the above mentioned results in a different dopaminergic-like cell model, we also performed the experiments in undifferentiated and differentiated BE(2)-M17 cell lines (Fig. 2 left and right, respectively and Fig. S3) and, as in the case of HeLa and SHSY5Y cells, we detected α-syn at the OMM and the IMS but not in the mitochondrial matrix. The anti TOM20 immunostaining confirmed the mitochondrial specificity of GFP emission signals (Fig. 3a–c).

To support our findings obtained with splitGFP method and to assess whether α-syn variants differentially associate with the mitochondria, α-syn abundance in cytosolic and mitochondrial fractions were obtained from HeLa cells transfected with WT, A30P, or A53T α-syn expressing vectors was verified by Western Blot analysis (Fig. S4).

Quantification of mitochondrial α-syn amount in respect to mitochondrial content, calculated as the normalized mitochondrial α-syn/TOM20 ratio, showed no differences among the three different batches of transfected cells. Taken together, these results confirmed the presence of WT, A30P, or A53T α-syn in mitochondrial fraction but did not revealed any differences in their quantitative distribution.

To assess whether α-syn overexpression could affect mitochondrial bioenergetics, we analyzed mitochondrial and cytosolic ATP production upon cell stimulation with histamine, an inositol 1,4,5 tris-phosphate (InsP3)-producing agonist that mobilize Ca^{2+} from the endoplasmic reticulum. Mitochondrial (mtLUC) or cytosolic (cytLUC) recombinant luciferase probes and WT and mutant α-syn were co-expressed in HeLa cells and ATP levels were monitored upon addition of luciferin, as previously described[47]. Figure 1d shows the increment in light emission relative to the ATP production upon histamine stimulation, i.e., upon enhancement of energy requirement. Indeed, histamine stimulation by inducing transient mitochondrial Ca^{2+} concentration increases, stimulates Krebs cycle enzymes and enhances ATP production[47]. Mitochondrial ATP synthesis in cells overexpressing both the WT α-syn as well as the pathologic α-syn mutants is reduced of about 20% compared to control cells (whose levels are reported as 100%), suggesting that α-syn overexpression impaired ATP production independently from its PD-related mutations (mtLuc 100 ± 0.77 $n = 14$; WT α-syn 88.94 ± 1.02 $n = 14$; A53T α-syn 82.25 ± 0.59 $n = 9$; A30P α-syn $82{,}82 \pm 0.51$ $n = 9$). Cytosolic ATP levels were instead essentially unaffected by the presence of overexpressed α-syn (cytLuc 100 ± 1.95 $n = 10$; WT α-syn 95.66 ± 1.43 $n = 11$; A53T α-syn 96.65 ± 1.02 $n = 14$; A30P α-syn 96.10 ± 0.64 $n = 14$) (Fig. 1e).

α-syn mitochondrial distribution is altered by the occurrence of pathogenic mutations and cellular stress conditions

In order to investigate whether WT and mutant α-syn possess different propensity to localize at the mitochondria compartment, we quantified GFP fluorescence in HeLa cells co-transfected with OMM and IMS GFP_{1-10} along with WT, A53T and A30P α-synS11. From the images shown in Fig. 4a, it is evident that GFP fluorescent signal reconstituted by WT α-synS11 at the OMM is much more intense with respect to that reconstituted upon the overexpression of the pathogenic mutants. The quantification of the corrected total cell fluorescence (CTCF) revealed that WT α-synS11 has major propensity to localize at the OMM compared to mutant α-synS11 (CTCF: WT α-syn 1 ± 0.08 $n = 32$; A53T α-syn 0.59 ± 0.05 $n = 34$; A30P α-syn 0.71 ± 0.06 $n = 29$) (Fig. 4b), whereas, on the opposite, a greater fluorescence signal is detectable at the IMS for the mutant constructs (Fig. 4c), indicating that the occurrence of pathogenic mutations is able to favor the translocation of the protein across the OMM in the IMS (CTCF: WT α-syn 1 ± 0.06 $n = 50$; A53T α-syn

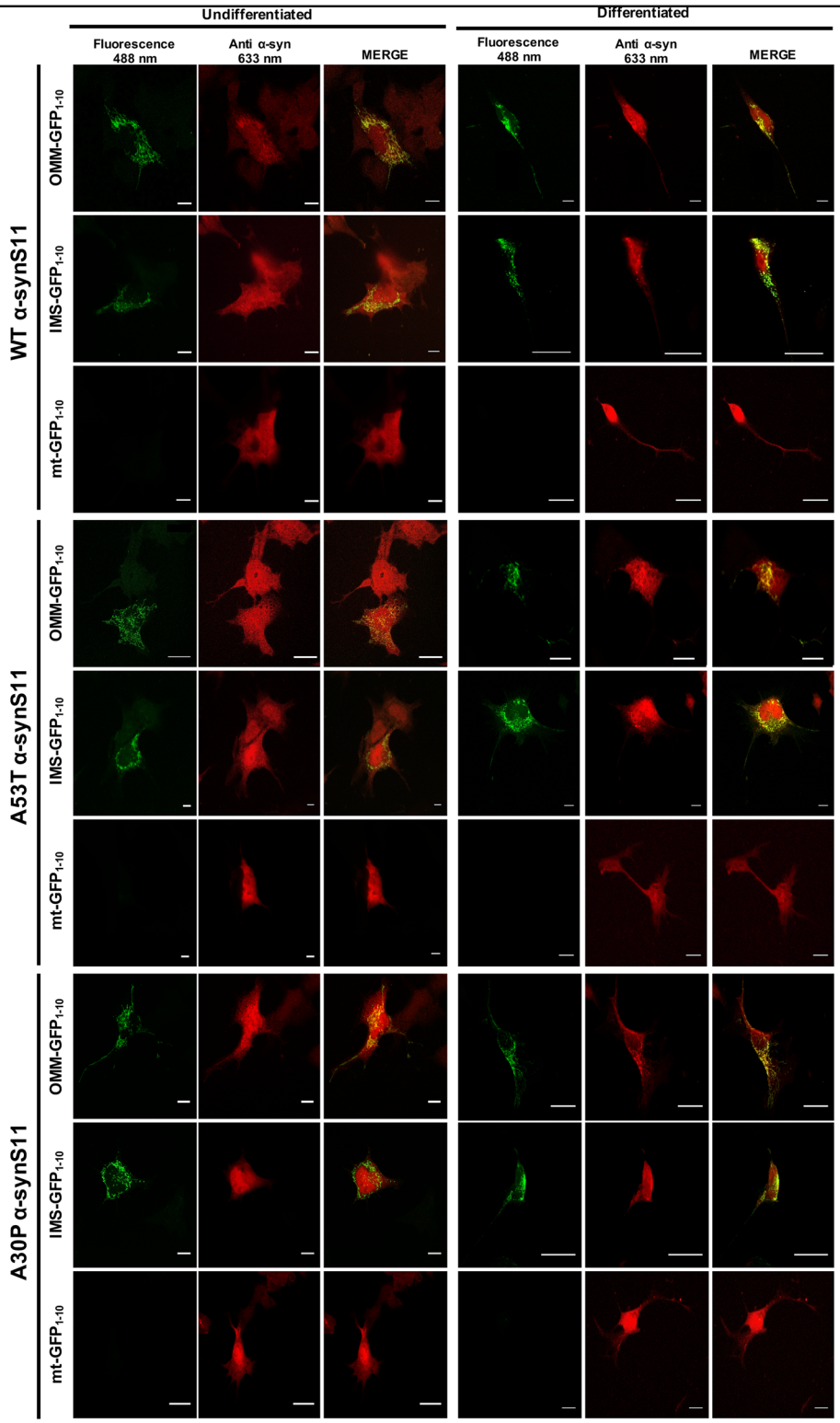

Fig. 2 Sub-mitochondrial localization of wild type and mutant α-syn was analyzed in undifferentiated. a and differentiated **b** BE(2)-M17 dopaminergic-like cells by the co-expression of the OMM, IMS and mitochondrial matrix targeted GFP_{1-10} non-fluorescent moiety and of the WT, A53T and A30P α-synS11. Confocal images were acquired at 488 and 594 nm excitation wavelength. Transfected cells were incubated with an anti α-syn primary antibody and stained with an Alexa 633 conjugated secondary antibody. Complementation of the GFP probes was revealed by fluorescent acquisition at 488 nm excitation wavelength. Scale bar is 20 µm

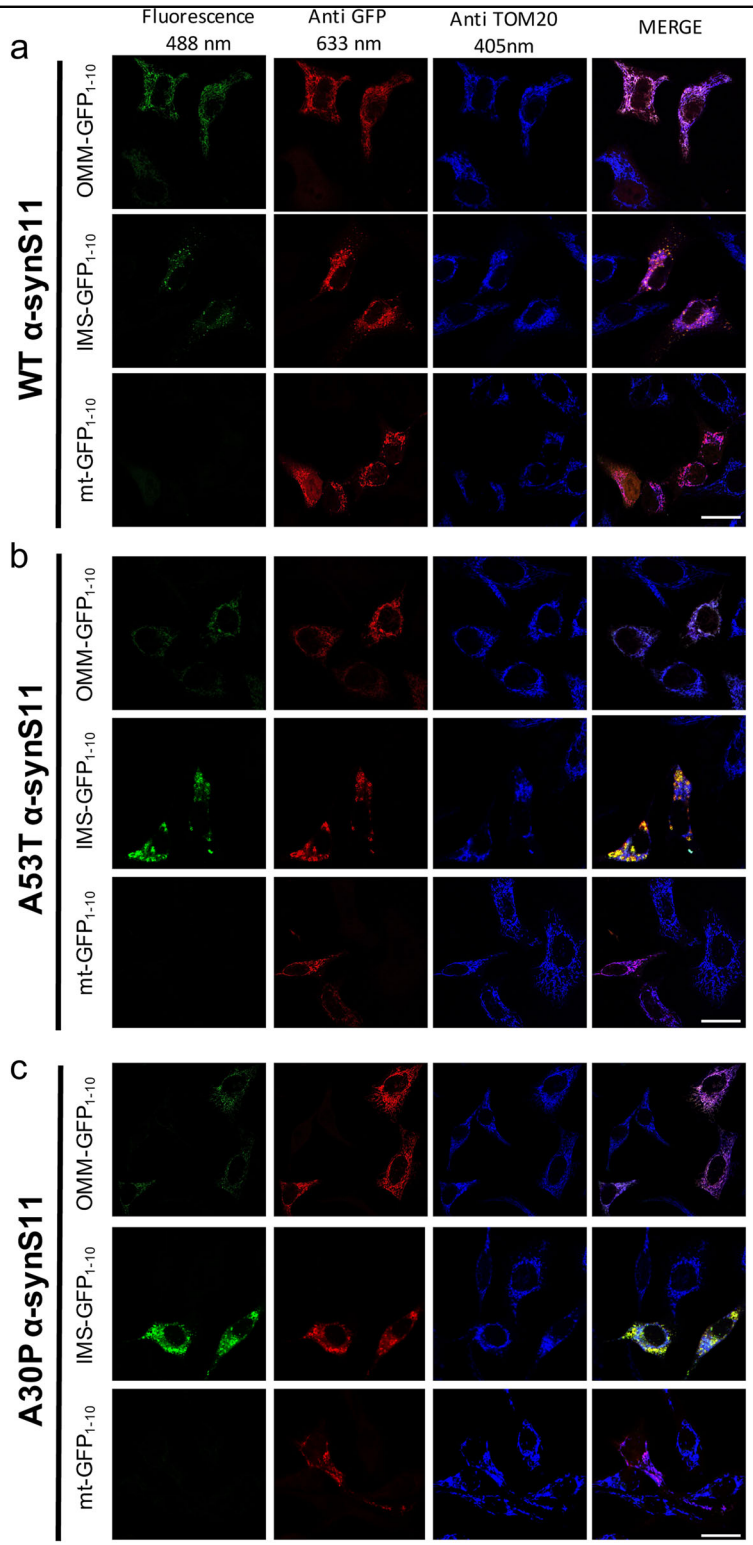

Fig. 3 Expression of the OMM, IMS and mitochondrial matrix targeted GFP_{1-10} non-fluorescent moiety and of the. a WT α-synS11, **b** A53T α-synS11, and **c** A30P α-synS11. Complementation of the GFP probes was revealed by fluorescent acquisition upon excitation at 488 nm wavelength. GFP was detected using a GFP primary antibody while mitochondria were stained using an anti TOM20 antibody. Confocal images were acquired at 633 and 405 nm excitation wavelength. Cells were stained with anti GFP and anti TOM20 antibodies and observed at a confocal microscope at 405, 488 and 633 nm excitation wavelength. Scale bar is 20 µm

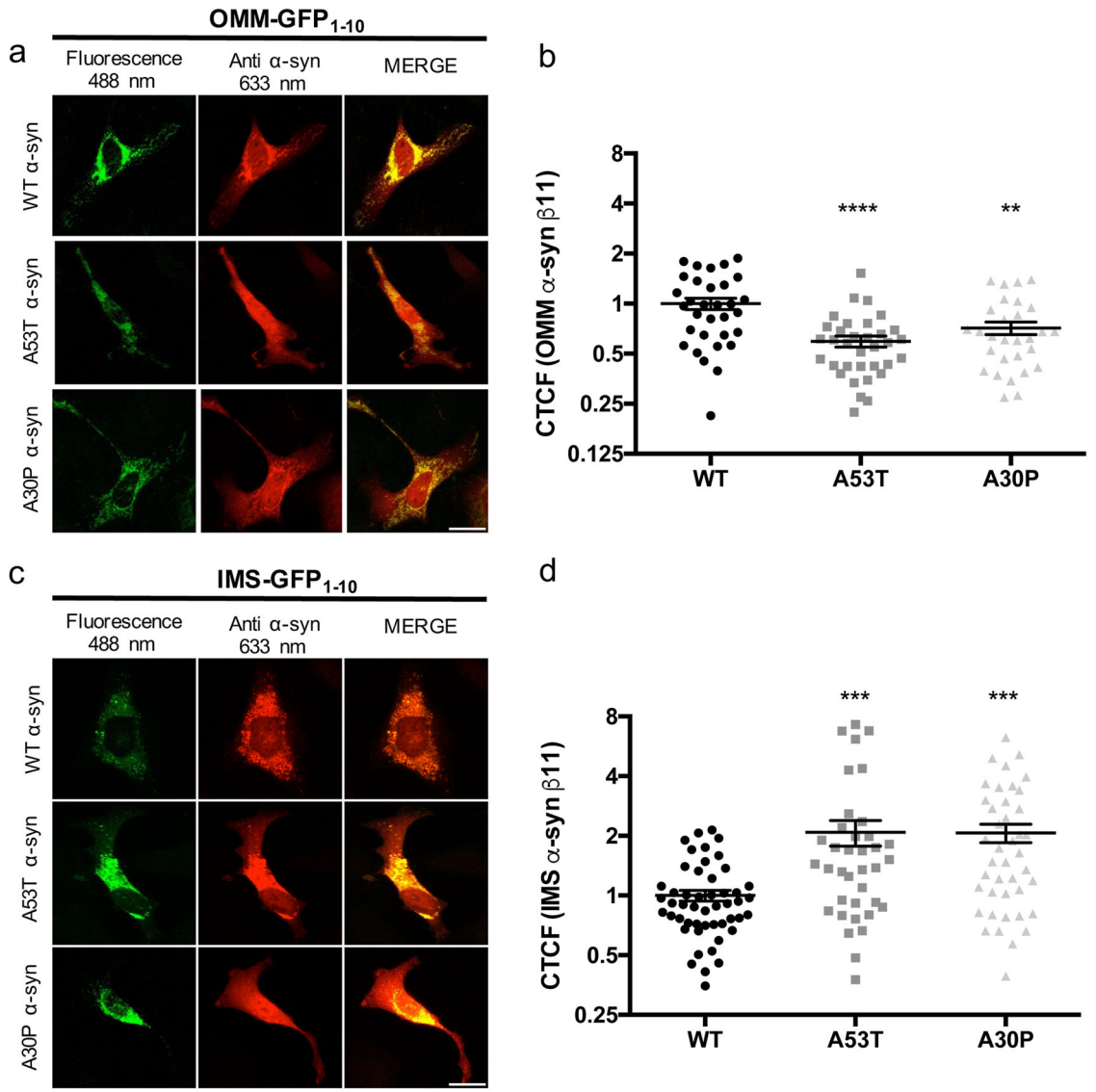

Fig. 4 Quantification of wild type and mutant α-syn distribution at the OMM and IMS. Expression of the OMM. a and IMS **c** targeted GFP_{1-10} non-fluorescent moiety and of the WT, A53T and A30P α-synS11. Transfected cells were incubated with an anti α-syn primary antibody and stained with an Alexa 633 conjugated secondary antibody. Complementation of the GFP probes was revealed by fluorescent acquisition at 488 nm excitation wavelength **a**, **c**. The corrected total cell fluorescence (CTCF) was quantified as described in the 'Materials and Methods' section and reported as normalized values with respect to WT α-syn **b**, **d** (****$p < 0.0001$, ***$p < 0.001$, **$p < 0.01$). One-way ANOVA retrieved a p value of 0.0001 for **b** and **d**. Dunnett's multiple comparison test retrieved a statistically significant difference between WT and A53T $p < 0.001$ and WT and A30P $p < 0.01$ **b** and between WT and A53T $p < 0.001$ and WT and A30P $p < 0.001$. Quantification of CTCF has been done on at least 29 cells from at least three independent experiments for each transfection condition. Scale bar is 20 µm

2.08 ± 0.31 $n = 37$; A30P α-syn 2.07 ± 0.22 $n = 42$) (Fig. 4d). To verify that the expression of α-synS11 constructs was similar among the different batches of transfected cells and that the same correlation exist between the immunoreactive α-synuclein signal and the fluorescence signal of reconstituted GFP we have quantified the red and the green fluorescence along the entire volume of the cells positive for reconstituted GFP_{1-10} and plotted them. As expected, a positive relationship is present for WT, A53T and A30P α-synS11 either at the OMM and at the IMS. However, a poor positive linear correlation is observed (Fig. S5) which is equivalent in all the batches of transfected cells (except for the A53T α-synS11 at the OMM, see the R^2 values for comparison), suggesting that cell specific differences in the expression level of α-synS11 do not affect the observed differences in fluorescence intensities among WT, A53T and A30P α-synS11 within the same sub-mitochondrial compartment.

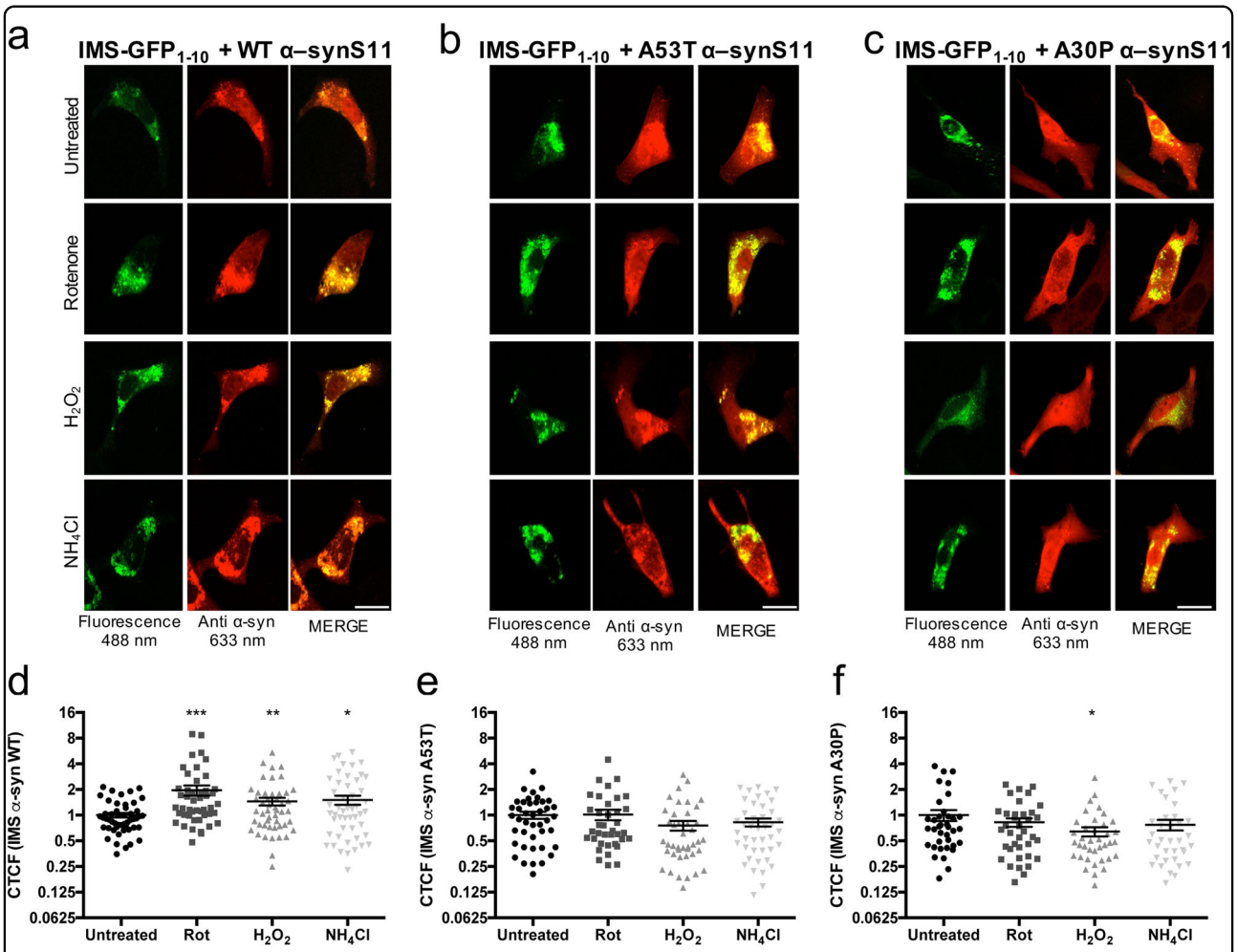

Fig. 5 α-syn distribution at the IMS upon inhibition of complex I inhibitor or oxidative stress or inhibition of endosome-lysosome system acidification. HeLa cells were co-transfected with wild type **a** and mutants **b**, **c** α-synS11 and IMS GFP_{1-10}, and treated with 10 μM rotenone for 12 h, 250 μM H_2O_2 for 12 h or 50 mM NH_4Cl for 2 h at 37 °C in a 5% CO_2 atmosphere, stained with an anti α-syn antibody and observed at a confocal microscope at 488 and 633 nm excitation wavelength. **d**–**f** CTCF was quantified as described in the 'Materials and Methods' section and reported as normalized values with respect to WT α-syn. (**d**, Student's *t*-test: ***$p < 0.001$, **$p < 0.01$, *$p < 0.05$; One-way ANOVA p=0.0037. Dunnett's multiple comparison test retrieved a statistically significant difference only for the Rot treated group, ***$p < 0.001$; **f** Student's *t*-test: *$p < 0.05$; One-way ANOVA and Dunnett's multiple comparison test retrieved no statistically significant differences between the groups). Quantification of CTCF has been done on at least 36 cells from at least three independent experiments for each condition. Scale bar is 20 μm

At the light of these results, we wanted to find specific cell conditions that may change α-syn distribution at the OMM or the IMS. We decided to evaluate this aspect by monitoring α-syn at the IMS. HeLa cells were transfected with IMS GFP_{1-10} and WT or mutant α-synS11 and treated with 10 μM rotenone for 12 h, 250 μM H_2O_2 for 12 h, or 50 mM NH_4Cl for 2 h at 37 °C in a 5% CO_2 atmosphere. As shown in Fig. 5a, d, there was a significant increase in WT α-syn in the IMS in treated HeLa cells compared to control (WT α-syn: control 1 ± 0.06 $n = 50$; rotenone 1.96 ± 0.27 $n = 48$; H_2O_2 1.45 ± 0.15 $n = 49$; NH_4Cl 1.51 ± 0.18 $n = 54$). Interestingly, upon the same stimuli, the IMS pool of α-synS11 mutants did not changed (Fig. 5b, c), as better appreciable from the quantitative analysis shown in Fig. 5e, f (for A53T α-syn: control 1 ± 0.10 $n = 42$; rotenone 1.02 ± 0.14 $n = 37$; H_2O_2 0.76 ± 0.10 $n = 42$; NH_4Cl 0.82 ± 0.09 $n = 42$ and for A30P α-syn: control 1 ± 0.15 $n = 37$; rotenone 0.82 ± 0.10 $n = 37$; H_2O_2 0.64 ± 0.08 $n = 38$; NH_4Cl 0.77 ± 0.11 $n = 36$).

At this point we were interested to assess whether the same conditions that favoured WT α-syn accumulation into IMS, may also lead to α-syn translocation into the mitochondrial matrix. Thus, we performed similar experiments using the mt GFP_{1-10} moiety: no fluorescence signal was detected for any of the α-synS11 constructs upon cells incubation with rotenone, H_2O_2 or NH_4Cl (data not shown), suggesting that these treatments, in our experimental conditions, do not induce WT

and mutant α-syn translocation into the mitochondrial matrix.

All together, these data suggest that the pathogenic mutations lead to α-syn accumulation in the IMS and that pharmacological treatments that impair complex I activity or increase oxidative stress or inhibit the endosome-lysosome system acidification mimic the same effect for WT α-syn.

The artificial targeting of WT α-syn, but not of its pathogenic mutants, to the mitochondrial matrix sustains ATP synthesis in a Complex III-dependent manner

Although we were not able to detect the presence of α-syn in the mitochondrial matrix (neither under basal nor under stress conditions), recent findings strongly supported the view that α-syn can indeed reach the mitochondrial matrix and modulate ATP production and/or mitochondrial membrane potential[33–35,38,48], indicating that in other cell types or under specific experimental conditions α-syn could translocate in the mitochondrial matrix.

Indeed, it has been shown that exogenous monomeric WT α-syn, but not its A30P mutant, is able to physically interact with the α subunit of the ATP synthase and to increase its activity in primary neuron/glia co-cultures from mice cerebral cortex[38]. Thus, we decided to directly investigate possible action on mitochondrial metabolism of α-syn artificially targeted to the mitochondrial matrix. To this end, we generated a mitochondrial matrix-targeted α-synS11 (mtα-synS11) by adding the same targeting sequence that we have fused to the GFP_{1-10} fragment. mt α-synS11 efficiently complemented $mtGFP_{1-10}$, as revealed by the mitochondrially localized green fluorescent signal observed following excitation at 488 nm wavelength (Fig. 6a). To evaluate its possible impact on mitochondria function, mitochondrial ATP production upon cells stimulation with histamine was measured in parallel both in cells overexpressing mt α-synS11 or untargeted α-synS11. As shown in Fig. 6b, while the overexpression of untargeted α-syn reduced mitochondrial ATP synthesis (as already shown in Fig. 1e), the mt α-synS11 was able to enhance ATP production (Mean values (% cps): mt Luc 100 ± 1.49 $n = 17$; mt α-syn 106.29 ± 1.28 $n = 19$; α-syn 94.27 ± 0.50 $n = 11$). Interestingly, mt α-synS11 still exerted this effect in the presence of complex I inhibitor rotenone (Mean values (% cps): mt Luc 94.45 ± 1.29 $n = 13$; mt α-syn 100.88 ± 1.83 $n = 10$; α-syn 88.48 ± 0.39 $n = 11$) (Fig. 6c), while the ability to promote ATP synthesis was lost in the presence of the complex III inhibitor antimycin, (Mean values (% cps): mt Luc 88.20 ± 0.86 $n = 12$; mt α-syn 87.24 ± 0.83 $n = 13$; α-syn 86.66 ± 0.58 $n = 11$) (Fig. 5d). Of notice, pathogenic mutants of α-syn artificially targeted to the mitochondrial matrix are not able to increase mitochondrial ATP synthesis upon cell stimulation, (Mean values (cps): mt Luc 100 ± 0.63 $n = 17$; mt A53T α-syn 99.20 ± 1.08 $n = 18$; mt A30P α-syn 101.13 ± 0.90 $n = 15$) (Fig. 6e).

To check whether the observed increases in ATP production could be related to possible effects of mt α-synS11 on mitochondrial Ca^{2+} uptake, as previously shown for untargeted cytosolic α-syn[32], mitochondrial Ca^{2+} measurements were performed using mitochondrially targeted photoprotein aequorin[49,50]. No alterations in mitochondrial Ca^{2+} levels were registered upon histamine stimulation in cells overexpressing the wt or the mutated mitochondrial matrix targeted α-syn constructs, indicating that the sustained ATP levels are not driven by an increase in mitochondrial Ca^{2+} transients that could stimulate the Krebs cycle (Peak values (μM): mtAEQ 124.19 ± 7.40 $n = 12$; mt WT α-syn 125.18 ± 5.34 $n = 14$; mt A53T α-syn 130.98 ± 6.35 $n = 13$; mt A30P α-syn 134.57 ± 4.77 $n = 13$) (Fig. 6f). These findings suggest that WT α-syn, resident in the mitochondria matrix, could play a direct role on ATP production by the modulation of the respiratory chain (possibly through complex III activity) and that the presence of pathogenic mutations compromises this function.

VDAC 1-3 are not responsible for α-syn translocation inside mitochondria

The evidence that a portion of α-syn resides at the IMS, requires the direct translocation of the protein from the cytosol across the outer mitochondrial membrane. Recent in vitro experiments using the Voltage Anion Channel (VDAC) reconstituted into planar lipid membranes suggested that α-syn is able to interact with/translocate through the VDAC1 to reach the IMS[51,52]. To verify the possibility that VDAC could represent a docking site for α-syn entry in IMS in living cells, we transfected mouse embryonic fibroblasts (MEF) WT and MEF VDAC 1-3 KO with IMS GFP_{1-10} and WT or mutant α-synS11: we could expect that the ablation of the channel could prevent α-syn translocation across the OMM. Surprisingly, we have found that VDAC 1–3 absence does not alter the ability of α-syn (WT and mutants) to translocate to the IMS, as revealed by the specific complementation of the fluorescent probe and the resulting green fluorescence emission (Fig. 7). These data clearly suggest that VDAC 1–3 are not essential for α-syn translocation inside mitochondria in intact cells. Whether this indicate that VDAC 1–3 proteins are not the only channels implicated in α-syn translocation or that α-syn takes completely different routes to reach the IMS (i.e., by TOM40 as previously suggested[14]) remains to be further elucidated.

In vivo localization of α-syn at the OMM and the IMS, but not the mitochondrial matrix

The above mentioned experiments suggested the existence of a mitochondrial pool of α-syn at the OMM and at

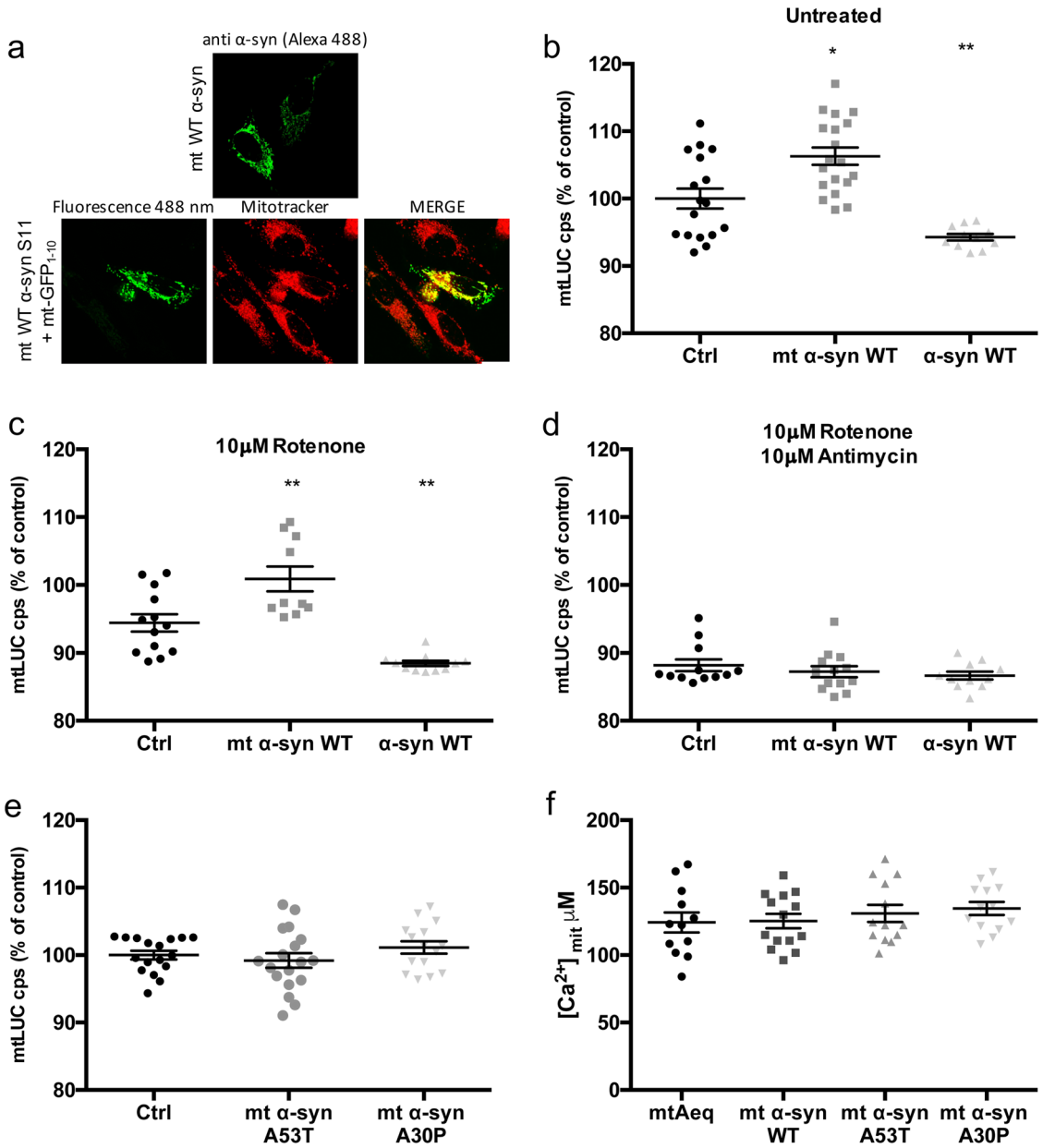

Fig. 6 WT and mutant α-syn targeting to the mitochondrial matrix differently affects mitochondrial ATP levels. a Complementation of the mitochondrial matrix targeted GFP_{1-10} non-fluorescent moiety upon co-expression of the targeted mt WT α-synS11. The mitochondrial localization was verified by mitotracker staining. Confocal images were acquired at 488 and 594 nm excitation wavelength. **b**, **c**, **d** Histograms showing mitochondrial ATP production upon histamine stimulation measured by mtLuc probe in HeLa cells overexpressing untargeted or mitochondrial matrix targeted α-syn in HeLa cells untreated **b** or treated with 10 μM rotenone **c** or **d** 10 μM rotenone + 10 μM antimycin for 12 h at 37 °C in a 5% CO_2 atmosphere. **e** Histograms showing mitochondrial ATP production upon histamine stimulation measured by mtLuc probe in HeLa cells overexpressing mitochondrial matrix targeted mt WT, mt A53T and mt A30P α-syn. Average values are shown as mean % calculated from the counts per second (cps) with respect to control cells. **f** Mitochondrial Ca^{2+} transients upon stimulation with 100 μM histamine were measured in HeLa cells by co-transfecting mtAEQ and empty vector, or mt WT, mt A53T and mt A30P α-syn. Bars represent mean Ca^{2+} peak values upon histamine stimulation. Data were collected from at least 10 coverslips/conditions from three independent experiments. (One-way ANOVA coupled with Dunnett's multiple comparison test retrieved a statistically significant difference between the groups: $^{**}p < 0.01$, $^{*}p < 0.05$). At least 10 independent measurements for three independent transfections have been done for each construct. Scale bar is 20 μm

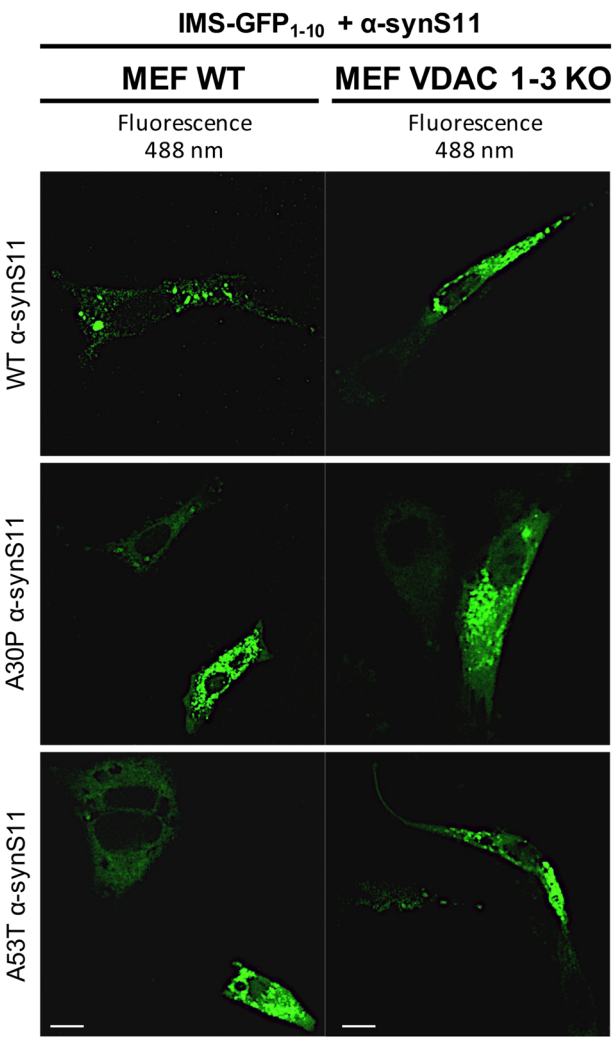

Fig. 7 α-syn mitochondrial import is not affected by VDAC 1-3 knock out in MEF cells. The IMS targeted GFP_{1-10} non-fluorescent moiety and of the WT, A53T and A30P α-synS11 were expressed in WT and VDAC 1-3 KO MEF. Complementation of the GFP probes was revealed by fluorescent acquisition at 488 nm excitation wavelength. Scale bar is 20 µm

the IMS while, under basal conditions we could never detect it within the mitochondrial matrix. To further validate these findings in a more complex system, we decided to test for the first time the possibility to follow the translocation of a protein of interest within mitochondrial sub compartments with our splitGFP system in the living vertebrate *Danio Rerio*. To this aim, fertilized oocytes at the stage of 1 cell have been microinjected with the plasmids encoding for α-synS11 (either WT, A53T or A30P) together with the OMM GFP_{1-10}, the IMS GFP_{1-10} or the mtGFP_{1-10} at the final concentration of 100ng/µl. Under these conditions, a mosaic expression is expected to take place. Injected embryos at 1dpf have been dechorionated, anesthetized and mounted in low melting agarose. Confocal z-stacks were acquired in vivo and, as shown in Fig. 8, a clear and strong signal can be detected with the OMM and the IMS GFP1-10 probes co-injected with either WT, A53T or A30P α-synS11, suggesting that a fraction of α-syn is indeed present at the OMM as well as the IMS in living zebrafish. On the other side, no mitochondrial signal could be detected by using the matrix targeted GFP_{1-10} supporting the idea that, under basal conditions, α-syn does not reach the mitochondrial matrix. These results have confirmed the findings we have obtained in HeLa and dopaminergic cells and, intriguingly, have also demonstrated that our splitGFP assay is suitable for in vivo settings.

Discussion

Mitochondrial dysfunctions and α-syn accumulation into Lewy bodies are both considered as key events in the progressive loss of dopaminergic neurons leading to PD manifestation. Although the precise role of α-syn in the neurodegenerative process is largely unknown, several lines of evidence have highlighted its possible involvement in the regulation of mitochondrial functions. For these reasons, numerous studies have focused their attention on α-syn contribution to the control of mitochondrial activities[53,54]. Nevertheless, whether mitochondrial dysfunctions represent a secondary event in α-syn-induced alterations or are directly triggered by α-syn at the mitochondrial level is still unclear. Moreover, the absence of techniques that allow to specifically monitor the protein's distribution inside organelles, further intricate the road to a complete understanding of α-syn physio/pathology inside mitochondria. Here, we employed a split-GFP based bimolecular fluorescence complementation (BiFC) tool[40,42] developed by our group to selectively monitor DJ-1 sub-mitochondrial distribution[43] and further improved with a novel non fluorescent GFP_{1-10} moiety targeted to the IMS[55] to selectively follow proteins translocation inside the inter membrane space. Our analyses revealed that a fraction of WT, A30P and A53T α-syn is localized at mitochondria both at the OMM and in the IMS, and that the overexpression of α-syn resulted in a decrease in mitochondrial ATP production upon cell stimulation, as reported by others[19]. This result was partially unexpected considering that we had previously shown that α-syn overexpression was able to enhance ER-mitochondria Ca^{2+} transfer[32], thus leading to the possibility that increased mitochondrial Ca^{2+} transients could augment ATP production. But it could be rationalized assuming that increased ER-mitochondria tethering may represent a compensatory response to cope with reduced mitochondrial ATP production in the presence of increased amount of α-syn and that in the absence of this compensatory response the deficit in ATP synthesis could be even greater. Interestingly, while the WT protein is

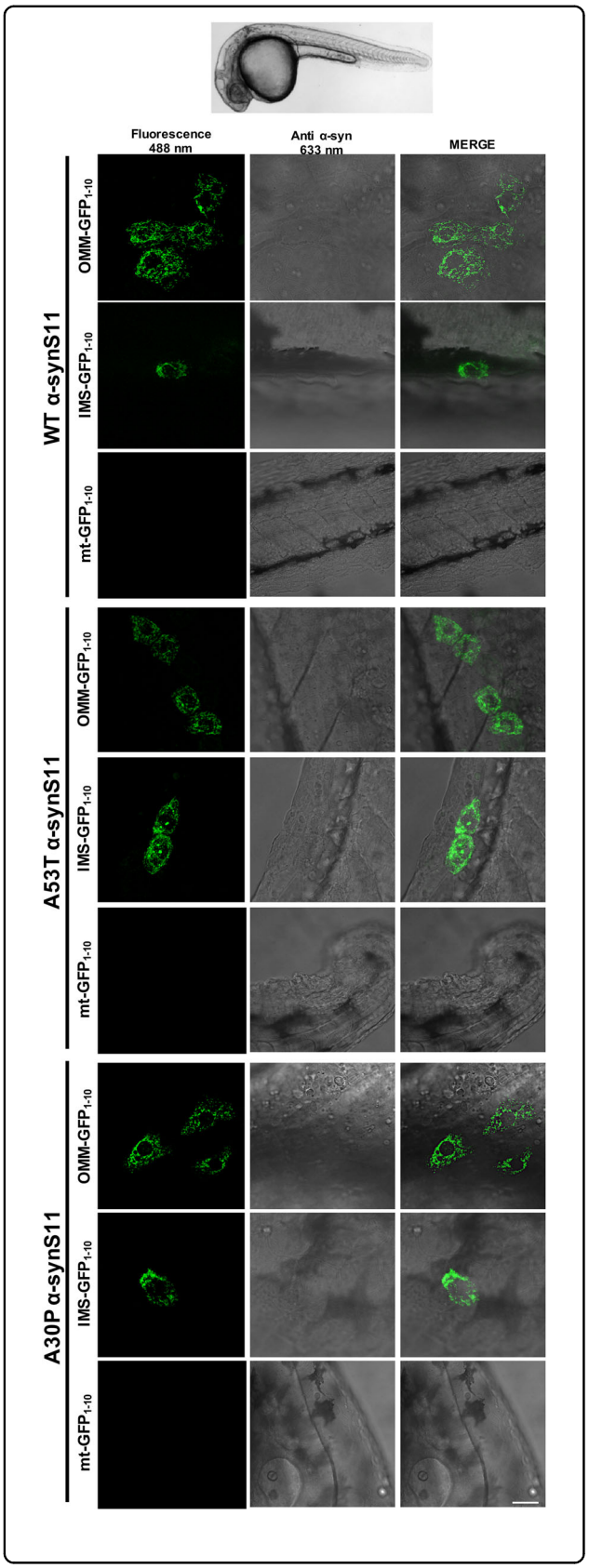

Fig. 8 Live imaging of SPLIT GFP reconstitution in 1 dpf zebrafish embryos. Wild type zebrafish embryos at 1-cell stage were injected with a plasmid expressing human WT or A53T and A30P mutants αsynS11 together with a plasmid expressing OMM-GFP$_{1-10}$, IMS-GFP$_{1-10}$ or mt-GFP$_{1-10}$. For the injections, the concentration of each plasmid was 50 ng/ul. After 1 day, images were collected. Each picture is the merge of several planes. Scale bar is 20 μm

prevalently localized at the OMM, the pathologic mutants show a major IMS distribution, in agreement with previous results showing a lower degree of localization of both mutant α-syn species to the endoplasmic reticulum-mitochondria interface compare with WT and a concomitantly higher degree of localization to the pure mitochondrial fraction[18]. Interestingly enough, we were able for the first time to test this system in a living vertebrate, i.e., the zebrafish *Danio Rerio* and confirm the presence of α-syn at the OMM and at the IMS, as well as its absence in the mitochondrial matrix under basal conditions. Our data indicate that conditions of cellular stresses promote the translocation of the WT protein to IMS, but not that of the mutant species, that are more abundant per se in this compartment, suggesting the possibility that the recruitment of α-syn from the OMM surface inside mitochondria, i.e., in the IMS and, possibly into the matrix where it enhances ATP production, could represent an initial step to counteract cell impairment and sustain bioenergetics. However, whenever α-syn accumulation become excessive, α-syn may fail to be imported in the mitochondrial matrix and stacked at the IMS where could be responsible for mitochondrial fragmentation, a mechanism of action previously suggested[29,30] and recently confirmed[56] to occur. Whether the different behavior of WT and mutant α-syn reflects possible role of α-syn inside mitochondria, i.e., in controlling mitochondrial dynamics[54] or ATP production[38], or is driven by a specific import of misfolded/aggregation prone proteins into mitochondria for their degradations, as recently suggested[57], deserves further investigation. Interestingly, Pozo Devoto and coworkers have recently shown that α-syn plays a direct physiological role in mitochondrial transport and morphology and that due to the different affinity for membrane lipids the association of WT and A53T or A30P α-syn with the mitochondria was different, thus suggesting that their effects on mitochondria are also dose-dependent[56].

Since recent evidence have shown that in primary neuron/glia co-cultures exogenous monomeric α-syn is able to physically interact with the α subunit of the ATP synthase[38], indicating a distinctive localization of the protein inside the mitochondrial matrix, we decided to evaluate phenotypes associated with this peculiar α-syn distribution by artificial targeting α-syn protein to the mitochondrial matrix. Interestingly, and in agreement

with previous studies[38], mitochondrial matrix-targeted WT α-syn is able to sustain mitochondrial ATP synthesis, while mutant species targeted to the mitochondrial matrix do not promote mitochondrial ATP production. We have found that this action is dependent on complex III activity, since it is prevented by the incubation with the complex III inhibitor antimycin. In this context, one may speculate that, in neurons, a pool of α-syn exerts a physiological role inside the mitochondrial matrix where it is able to increase ATP synthase activity ensuring mitochondrial health and synaptic functions and that another pool of α-syn may be recruited to this site upon stress condition to further sustain ATP production through the modulation of complex III activity. The occurrence of mutations may lead to a loss of function that causes energy depletion and neuronal cell toxicity, thus initiating the degenerative process in PD.

Materials and methods

DNA constructs

The full length α-syn WT, A53T and A30P -**β**11 construct have been generated by PCR using the following primers: α-syn-S11 (HindIII) For 5′- GTTCAAGCTTA TGGATGTATTCATGAAAGG -3′; α-syn-S11 (XhoI) Rev. 5′-ACTTCTCACTCGAGTTATGTGATGCCGGC GGCGTTCACGTA CTCGTGCAGCACCATGTGGTCC CGGCTGCCGCCGCCGCTGCCGCCGTCGCCGGCTT CAGGTTCGTAGTCTTG-3′ The DNA constructs encoding for the human α-syn WT, A30P and A53T used as a template are a kind gift of Prof. Alessandro Negro (Department of Biomedical Sciences, University of Padova). The C-terminus **β**11-tagged Cytochrome-c was produced by DNA synthesis (Thermo Scientific). Untargeted, mitochondrial matrix- and OMM-targeted humanized GFP 1–10 expressing vectors were generated by PCR amplification from the GPI-GFP1-10 template using forward primers containing the mitochondrial matrix presequence of the subunit VIII of cytochrome c oxidase and the N-terminal 33 amino acids sequence of TOM20 protein[43].

The GFP_{1-10} targeted to the intermembrane space (IMS) has been created by genetic fusion to the leader sequence of the IMS protein LACTB[44] and created by DNA synthesis (Thermo Scientific).

Cell cultures and transfection

HeLa, SHSY5Y cells and VDAC1/3$^{-/-}$ MEFs were grown in DMEM high glucose (Euroclone) containing 10% fetal bovine serum (FBS, Gibco), supplemented with 100 U/ml penicillin (Euroclone) and 100 µg/ml streptomycin (Euroclone), in a humidified atmosphere containing 5% CO_2. Undifferentiated BE(2)-M17 cells were maintained in a 1:1 mixture of Ham's F12 and Dulbecco's Modified Eagle's Medium (Gibco) supplemented with 10% fetal bovine serum and grown in a humidified incubator at 37 °C in the presence of 5% CO_2. The cell medium was replaced every 2 days, and the cells were subcultured once confluence was reached. In all of the experiments, the cells were used at early passages (P1-5 after purchase). Differences in morphology between proliferative and differentiated cells were evaluated by phase contrast light microscopy.

Cells were seeded onto 13 or 24 mm diameter glass coverslips and transfection was performed at 60–80% confluence using Lipofectamine TM 2000 Transfection Reagent (Life Technologies) for SHSY5Y, BE(2)-M17 and MEFs and the calcium-phosphate procedure for HeLa cells. To analyze the presence of α-syn in the mitochondrial sub-compartments after differentiation, BE(2)-M17 cells were seeded onto coverslips pre-coated with poly-D-lysine[58]. After 24 h, differentiation was induced by the addition of retinoic acid (RA) at concentrations of 5 µM. Fresh media containing RA was provided every 2 day and 7 days later the cells were transfected with the vectors containing the coding sequence for targeted GFP_{1-10} chimerae and WT, A53T or A30P α-syn. After 48h the samples were fixed and processed for immunocytochemistry. For Ca^{2+} measurement cells were co-transfected with aequorin construct targeted to the mitochondrial matrix[49]. Cells were generally analyzed 24–48 h after transfection.

Immunocytochemistry analysis

After 48 h of transfection, cells plated on 13 mm glass coverslips were washed twice with phosphate-buffered saline (PBS: 140 mM NaCl, 2 mM KCl, 1.5 mM KH_2PO_4, 8 mM Na_2HPO_4 pH 7.4) and fixed for 20 min with 3.7% formaldehyde in PBS. Cells permeabilization was performed by 20 min' incubation with 0.1% Triton X-100 in PBS, followed by 30 min' wash with 1% gelatin (type IV, from calf skin, Sigma) in PBS. The coverslips were then incubated for 90 min at 37 °C in a wet chamber with the specific primary antibody diluted in PBS: anti-GFP (Santa Cruz, sc-9996) anti-alpha synuclein (Santa Cruz, sc-12767), anti-TOM20 (Santa Cruz, sc-11415). Staining was revealed by the incubation with specific AlexaFluor 405, 488 or 633 secondary antibodies, 1:50 (Life technologies) for 45 min at room temperature. Fluorescence was detected with a Leica SP5 confocal microscope and analyzed by ImageJ software.

Quantification of BiFC at the OMM and IMS

To quantify fluorescence signals, the corrected total cell fluorescence (CTCF) was calculated according to the protocol described in[59]. Briefly, a complete z-stack of cells showing a clear fluorescence signal was acquired using a Leica SP5 confocal microscope. The total corrected cell fluorescence (CTCF) was calculated by selecting the cell using the freehand selection of Fiji in the drawing/selection

polygon tool and the area, the integrated density and the mean grey value are measured while the remaining signal coming from outside the cell was removed. Area, integrated density and mean grey value were then measured within the cells and three selected non-fluorescent area in the image were chosen as background. At least three additional selections from a non-fluorescent region next to the cell of interest were acquired and considered as background. The CTCF was calculated as follow: integrated density – (area of selected cell×mean fluorescence of background readings). The calculated CTCF was then normalised against the CTCF values of wt α-syn-expressing cells. The results are shown as fold change increase/decrease over wt α-syn expressing cells CTCF levels.

Luciferase assay

Luciferase luminescence was measured, as previously described[47]. HeLa cells co-transfected with a mitochondrial luciferase chimera (mtLuc[47]) were perfused at 37 °C with KRB (125 mM NaCl, 5 mM KCl, 1 mM Na_3PO_4, 1 mM $MgSO_4$, 20 mM HEPES, pH 7.4, 37 °C) containing 1 mM $CaCl_2$, 5.5 mM glucose and 20 μM luciferin. In total 100 μM histamine was added to the perfusion medium to induce mitochondrial ATP synthesis[47]. For each measurement, the light emission (cps, counts per second) after histamine application was normalized on cps emitted after luciferin addition. Where indicated, 10 μM rotenone and 10 μM antimycin were incubated for 12 h at 37 °C in a 5% CO_2 atmosphere.

Aequorin measurements

After 48 h of transfection mitochondrial low affinity aequorin (mtAEQ) was reconstituted by incubating cells for 1.5 h with 5 μM wt coelenterazine (Santacruz) in DMEM supplemented with 1% fetal bovine serum at 37 °C in a 5% CO_2 atmosphere. After reconstitution, cells were transferred to the chamber of a purpose-built luminometer, and Ca^{2+} measurements were started in Krebs-Ringer modified buffer (KRB,125 mM NaCl, 5 mM KCl, 1 mM Na_3PO_4, 1 mM $MgSO_4$, 5.5 mM glucose, 20 mM HEPES, pH 7.4, 37 °C) medium supplemented with 1 mM $CaCl_2$ by stimulating HeLa cells with 100 μM histamine. The experiments were terminated by cell permeabilization with 100 μM digitonin in a hypotonic Ca^{2+}-rich solution (10 mM $CaCl_2$ in H_2O) to discharge the remaining unused aequorin pool. The light signal was collected and calibrated off-line into Ca^{2+} concentration values using a computer algorithm based on the Ca^{2+} response curve of mitochondrial aequorin, as previously described[60].

Live imaging of αsyn sub mitochondrial localization in Zebrafish

The human WT, A53T or A30P mutant $\alpha syn S_{11}$ plasmids were injected into 1 cell stage WT eggs together with a plasmid expressing OMM-GFP_{1-10}, IMS-GFP_{1-10} or mt-GFP_{1-10}. For injections, all plasmids were diluted in Danieau solution (58 mM NaCl, 0.7 mM KCl, 0.4 mM MgSO4, 0.6 mM Ca (NO3)2, 5 mM HEPES pH 7.6) and 0.5% phenol red. For the injections, the concentration of each plasmid was 50 ng/ul. At 1dpf, about 30 embryos were screened for fluorescence, dechorionated and anesthetized. For in vivo imaging, about one third of the injected embryos showed fluorescent signal and half were anesthetised and mounted on 35 × 10 mm glass bottom Petri dishes (Ted Pella, INC. Prod. No. 14023-20) in low melting agarose (1.3%, Euro- Clone). Fish water containing tricaine methanesulfonate 0.61 mM (Sigma) was added in the Petri dishes, in order to keep fish anesthetized. Mounted fish were imaged at RT (20–23 °C) using a Leica TSC SP5 inverted confocal microscope, using a HCX PL APO ×63/numerical aperture 1.40–0.60. To image reconstituted GFP, a complete z-stack of the cell was acquired every 0.29 μm and shown as Z-projection of several planes.

Statistical analysis

All of the data are representative of at least three independent experiments unless otherwise indicated. The sample was chosen by considering a power of 80%, a two side alpha error of 0.05 and a beta error of 0.2. Values are expressed as mean ± SEM. Significant differences are determined by one-way ANOVA with Dunnett's multiple comparison test for multiparametric analysis of the different groups. Student's unpaired two-tailed t test was used for two experimental comparisons. All statistical analyses were performed using GraphPad Prism version 6.00 for Mac OS X, GraphPad Software, La Jolla California USA. A p value ≤0.05 was considered statistically significant.

Acknowledgements

The work is supported by grants from the Ministry of University and Research (Bando SIR 2014 no. RBSI14C65Z and PRIN2017 to T.C) and from the Università degli Studi di Padova (Progetto Giovani 2012 no. GRIC128SP0 to T.C., Progetto di Ateneo 2016 no. CALI_SID16_01 to T.C. and Progetto di Ateneo 2015 no. CPDA153402 to M.B.). We thank Prof. P. Pizzo (Department of Biomedical Sciences) for her support and Prof. F. Argenton and the Zebrafish Facility of the Department of Biology, University of Padova.

Author details

[1]Department of Biomedical Sciences, University of Padova, Padova, Italy. [2]Department of Biology, University of Padova, Padova, Italy. [3]Padova Neuroscience Center (PNC), University of Padova, Padova, Italy

Conflict of interest

The authors declare that they have no conflict of interest.

Supplementary Information accompanies this paper at (https://doi.org/10.1038/s41419-019-2092-1).

Received: 12 April 2019 Revised: 11 October 2019 Accepted: 28 October 2019
Published online: 12 November 2019

References

1. Hirsch, E. C. et al. Dopaminergic neurons degenerate by apoptosis in Parkinson's disease. *Mov. Disord.* **14**, 383–385 (1999).
2. Spillantini, M. G. et al. Alpha-synuclein in Lewy bodies. *Nature* **388**, 839–840 (1997). 10.1038/42166.
3. Hardy, J., Lewis, P., Revesz, T., Lees, A. & Paisan-Ruiz, C. The genetics of Parkinson's syndromes: a critical review. *Curr. Opin. Genet Dev.* **19**, 254–265 (2009). 10.1016/j.gde.2009.03.008.
4. Fusco, G. et al. Structural basis of synaptic vesicle assembly promoted by alpha-synuclein. *Nat. Commun.* **7**, 12563 (2016).
5. Burre, J. et al. Alpha-synuclein promotes SNARE-complex assembly in vivo and in vitro. *Science* **329**, 1663–1667 (2010).
6. Nemani, V. M. et al. Increased expression of alpha-synuclein reduces neurotransmitter release by inhibiting synaptic vesicle reclustering after endocytosis. *Neuron* **65**, 66–79 (2010).
7. Larsen, K. E. et al. Alpha-synuclein overexpression in PC12 and chromaffin cells impairs catecholamine release by interfering with a late step in exocytosis. *J. Neurosci.* **26**, 11915–11922 (2006).
8. Ma, K. L. et al. The nuclear accumulation of alpha-synuclein is mediated by importin alpha and promotes neurotoxicity by accelerating the cell cycle. *Neuropharmacology* **82**, 132–142 (2014).
9. Kontopoulos, E., Parvin, J. D. & Feany, M. B. Alpha-synuclein acts in the nucleus to inhibit histone acetylation and promote neurotoxicity. *Hum. Mol. Genet.* **15**, 3012–3023 (2006).
10. Schell, H., Hasegawa, T., Neumann, M. & Kahle, P. J. Nuclear and neuritic distribution of serine-129 phosphorylated alpha-synuclein in transgenic mice. *Neuroscience* **160**, 796–804 (2009).
11. Goers, J. et al. Nuclear localization of alpha-synuclein and its interaction with histones. *Biochemistry* **42**, 8465–8471 (2003).
12. Shavali, S., Brown-Borg, H. M., Ebadi, M. & Porter, J. Mitochondrial localization of alpha-synuclein protein in alpha-synuclein overexpressing cells. *Neurosci. Lett.* **439**, 125–128 (2008).
13. Cole, N. B., Dieuliis, D., Leo, P., Mitchell, D. C. & Nussbaum, R. L. Mitochondrial translocation of alpha-synuclein is promoted by intracellular acidification. *Exp. Cell Res.* **314**, 2076–2089 (2008).
14. Devi, L., Raghavendran, V., Prabhu, B. M., Avadhani, N. G. & Anandatheerthavarada, H. K. Mitochondrial import and accumulation of alpha-synuclein impair complex I in human dopaminergic neuronal cultures and Parkinson disease brain. *J. Biol. Chem.* **283**, 9089–9100 (2008).
15. Li, W. W. et al. Localization of alpha-synuclein to mitochondria within midbrain of mice. *Neuroreport* **18**, 1543–1546 (2007).
16. Parihar, M. S., Parihar, A., Fujita, M., Hashimoto, M. & Ghafourifar, P. Mitochondrial association of alpha-synuclein causes oxidative stress. *Cell Mol. Life Sci.* **65**, 1272–1284 (2008).
17. Devi, L. & Anandatheerthavarada, H. K. Mitochondrial trafficking of APP and alpha synuclein: Relevance to mitochondrial dysfunction in Alzheimer's and Parkinson's diseases. *Biochim Biophys. Acta* **1802**, 11–19 (2010).
18. Guardia-Laguarta, C. et al. alpha-Synuclein Is Localized to Mitochondria-Associated ER Membranes. *J. Neurosci.* **34**, 249–259 (2014).
19. Paillusson, S. et al. alpha-Synuclein binds to the ER-mitochondria tethering protein VAPB to disrupt Ca2+ homeostasis and mitochondrial ATP production. *Acta Neuropathol*, 10.1007/s00401-017-1704-z (2017).
20. Chinta, S. J., Mallajosyula, J. K., Rane, A. & Andersen, J. K. Mitochondrial alpha-synuclein accumulation impairs complex I function in dopaminergic neurons and results in increased mitophagy in vivo. *Neurosci. Lett.* **486**, 235–239 (2010).
21. Loeb, V., Yakunin, E., Saada, A. & Sharon, R. The transgenic overexpression of alpha-synuclein and not its related pathology associates with complex I inhibition. *J. Biol. Chem.* **285**, 7334–7343 (2010).
22. Reeve, A. K. et al. Aggregated alpha-synuclein and complex I deficiency: exploration of their relationship in differentiated neurons. *Cell death Dis.* **6**, e1820 (2015).
23. Dauer, W. et al. Resistance of alpha -synuclein null mice to the parkinsonian neurotoxin MPTP. *Proc. Natl Acad. Sci. USA* **99**, 14524–14529 (2002).
24. Klivenyi, P. et al. Mice lacking alpha-synuclein are resistant to mitochondrial toxins. *Neurobiol. Dis.* **21**, 541–548 (2006).
25. Martin, L. J. et al. Parkinson's disease alpha-synuclein transgenic mice develop neuronal mitochondrial degeneration and cell death. *J. Neurosci.* **26**, 41–50 (2006).
26. Subramaniam, S. R., Vergnes, L., Franich, N. R., Reue, K. & Chesselet, M. F. Region specific mitochondrial impairment in mice with widespread overexpression of alpha-synuclein. *Neurobiol. Dis.* **70**, 204–213 (2014).
27. Ellis, C. E. et al. Mitochondrial lipid abnormality and electron transport chain impairment in mice lacking alpha-synuclein. *Mol. Cell Biol.* **25**, 10190–10201 (2005).
28. Hsu, L. J. et al. alpha-synuclein promotes mitochondrial deficit and oxidative stress. *Am. J. Pathol.* **157**, 401–410 (2000).
29. Guardia-Laguarta, C., Area-Gomez, E., Schon, E. A. & Przedborski, S. A new role for alpha-synuclein in Parkinson's disease: Alteration of ER-mitochondrial communication. *Mov. Disord.* **30**, 1026–1033 (2015).
30. Nakamura, K. et al. Direct membrane association drives mitochondrial fission by the Parkinson disease-associated protein alpha-synuclein. *J. Biol. Chem.* **286**, 20710–20726 (2011).
31. Winslow, A. R. et al. alpha-Synuclein impairs macroautophagy: implications for Parkinson's disease. *J. Cell Biol.* **190**, 1023–1037 (2010).
32. Calì, T., Ottolini, D., Negro, A. & Brini, M. alpha-Synuclein controls mitochondrial calcium homeostasis by enhancing endoplasmic reticulum-mitochondria interactions. *J. Biol. Chem.* **287**, 17914–17929 (2012).
33. Martinez, J. H. et al. Alpha-synuclein mitochondrial interaction leads to irreversible translocation and complex I impairment. *Arch. Biochem. Biophys.* **651**, 1–12 (2018).
34. Grassi, D., Diaz-Perez, N., Volpicelli-Daley, L. A. & Lasmezas, C. I. Palpha-syn* mitotoxicity is linked to MAPK activation and involves tau phosphorylation and aggregation at the mitochondria. *Neurobiol. Dis.* **124**, 248–262 (2018).
35. Ding, H. et al. Asiatic acid prevents oxidative stress and apoptosis by inhibiting the translocation of alpha-synuclein into mitochondria. *Front Neurosci.* **12**, 431 (2018).
36. Zhang, L. et al. Semi-quantitative analysis of alpha-synuclein in subcellular pools of rat brain neurons: an immunogold electron microscopic study using a C-terminal specific monoclonal antibody. *Brain Res.* **1244**, 40–52 (2008).
37. Liu, G. et al. alpha-Synuclein is differentially expressed in mitochondria from different rat brain regions and dose-dependently down-regulates complex I activity. *Neurosci. Lett.* **454**, 187–192 (2009).
38. Ludtmann, M. H. et al. Monomeric Alpha-Synuclein Exerts a Physiological Role on Brain ATP Synthase. *J. Neurosci.* **36**, 10510–10521 (2016).
39. Amorim, I. S. et al. Sideroflexin 3 is an alpha-synuclein-dependent mitochondrial protein that regulates synaptic morphology. *J. Cell Sci.* **130**, 325–331 (2017).
40. Cabantous, S., Terwilliger, T. C. & Waldo, G. S. Protein tagging and detection with engineered self-assembling fragments of green fluorescent protein. *Nat. Biotechnol.* **23**, 102–107 (2005).
41. Cabantous, S. & Waldo, G. S. In vivo and in vitro protein solubility assays using split GFP. *Nat. Methods* **3**, 845–854 (2006).
42. Pedelacq, J. D., Cabantous, S., Tran, T., Terwilliger, T. C. & Waldo, G. S. Engineering and characterization of a superfolder green fluorescent protein. *Nat. Biotechnol.* **24**, 79–88 (2006).
43. Calì, T., Ottolini, D., Soriano, M. E. & Brini, M. A new split-GFP-based probe reveals DJ-1 translocation into the mitochondrial matrix to sustain ATP synthesis upon nutrient deprivation. *Hum. Mol. Genet.*, https://doi.org/10.1093/hmg/ddu519 (2014).
44. Cieri, D. et al. Tau localises within mitochondrial sub-compartments and its caspase cleavage affects ER-mitochondria interactions and cellular Ca(2+) handling. *Biochim. Biophys. Acta Mol. Basis Dis.* **1864**, 3247–3256 (2018).
45. Polianskyte, Z. et al. LACTB is a filament-forming protein localized in mitochondria. *Proc. Natl Acad. Sci. USA* **106**, 18960–18965 (2009).
46. Hung, V. et al. Proteomic mapping of the human mitochondrial intermembrane space in live cells via ratiometric APEX tagging. *Mol. Cell* **55**, 332–341 (2014).
47. Jouaville, L. S., Pinton, P., Bastianutto, C., Rutter, G. A. & Rizzuto, R. Regulation of mitochondrial ATP synthesis by calcium: evidence for a long-term metabolic priming. *Proc. Natl Acad. Sci. USA* **96**, 13807–13812 (1999).

48. Ludtmann, M. H. R. et al. alpha-synuclein oligomers interact with ATP synthase and open the permeability transition pore in Parkinson's disease. *Nat. Commun.* **9**, 2293 (2018).
49. Rizzuto, R., Simpson, A. W., Brini, M. & Pozzan, T. Rapid changes of mitochondrial Ca2+ revealed by specifically targeted recombinant aequorin. *Nature* **358**, 325–327 (1992).
50. Ottolini, D., Cali, T. & Brini, M. Methods to measure intracellular Ca(2+) fluxes with organelle-targeted aequorin-based probes. *Methods Enzymol.* **543**, 21–45 (2014).
51. Hoogerheide, D. P., Gurnev, P. A., Rostovtseva, T. K. & Bezrukov, S. M. Mechanism of alpha-synuclein translocation through a VDAC nanopore revealed by energy landscape modeling of escape time distributions. *Nanoscale* **9**, 183–192 (2017).
52. Rostovtseva, T. K. et al. alpha-Synuclein shows high affinity interaction with voltage-dependent anion channel, suggesting mechanisms of mitochondrial regulation and toxicity in Parkinson Disease. *J. Biol. Chem.* **290**, 18467–18477 (2015).
53. Abramov, A. Y., Berezhnov, A. V., Fedotova, E. I., Zinchenko, V. P. & Dolgacheva, L. P. Interaction of misfolded proteins and mitochondria in neurodegenerative disorders. *Biochem Soc. Trans*, https://doi.org/10.1042/BST20170024 (2017).
54. Pozo Devoto, V. M. & Falzone, T. L. Mitochondrial dynamics in Parkinson's disease: a role for alpha-synuclein? *Dis. models mechanisms* **10**, 1075–1087 (2017).
55. Cieri, D. et al. Tau localises within mitochondrial sub-compartments and its caspase cleavage affects ER-mitochondria interactions and cellular Ca(2+) handling. *Biochim. Biophys. Acta*, https://doi.org/10.1016/j.bbadis.2018.07.011 (2018).
56. Pozo Devoto, V. M. et al. alphaSynuclein control of mitochondrial homeostasis in human-derived neurons is disrupted by mutations associated with Parkinson's disease. *Sci. Rep.* **7**, 5042 (2017).
57. Ruan, Let al. Cytosolic proteostasis through importing of misfolded proteins into mitochondria. *Nature* **543**, 443–446 (2017). https://doi.org/10.1038/nature21695.
58. Filograna, R. et al. Analysis of the catecholaminergic phenotype in human SH-SY5Y and BE(2)-M17 Neuroblastoma Cell Lines upon Differentiation. *PLoS ONE* **10**, e0136769 (2015).
59. Gavet, O. & Pines, J. Progressive activation of CyclinB1-Cdk1 coordinates entry to mitosis. *Dev. Cell* **18**, 533–543 (2010).
60. Brini, M. et al. Transfected aequorin in the measurement of cytosolic Ca2+ concentration ([Ca2+]c). A critical evaluation. *J. Biol. Chem.* **270**, 9896–9903 (1995).